UNIWERSYTET
MIKOŁAJA KOPERNIKA
W TORUNIU
Wydział Nauk o Zdrowiu
Collegium Medicum w Bydgoszczy

Sanling Zuo

Metabolic signatures of probiotic and prebiotic functions in the intestine cells

This research was part of the OVOBIOM Project, financed by NCN under the grant agreement UMO-2019/35/B/NZ9/03186

Dissertation for PhD Candidates in Health Sciences

Supervisor:
dr hab. inż., Katarzyna Stadnicka, prof. UMK

Co-Supervisor:
dr hab., Przemysław Kosobucki, prof. PBS

Bydgoszcz 2025

Dedication

I would like to express my sincere gratitude to Professor Katarzyna Stadnicka for all her kind support, understanding and help, which really supported me in my scientific journey during this period.

I am grateful for the support of Professor Przemysław Kosobucki and Dr. Waldemar Studziński during my studies at the Faculty of Chemical Technology and Engineering in Bydgoszcz University of Science and Technology.

I am also grateful for all the invaluable help and support from Professor Krzysztof Skowron, Dr. Katarzyna Grudlewska-Buda, Dr. Anna Budzyńska and Dr. Natalia Wiktorczyk-Kapischke during my time at the Microbiology Laboratory in UMK Collegium Medicum, and I will always remember the days we spent together in the laboratory.

To my loving and devoting friends– they truly are the source of motivation and support for me to keep going.

Always and forever.

Contents

Abstract

Background: Gut health has an important impact on maintaining host health. Probiotics and prebiotics have an direct or indirect impact on gut health by modulating gut microbiota profiles and their metabolism. The novel predictive in vitro models are required to efficiently design prebiotic and probiotic formulations with proven bioactivity, for in vivo applications.

Objective: This study aimed to investigate as to how the two selected probiotics and prebiotics regulate the gut health of the host at the systemic level by identifying the metabolic signatures of these bioactive compounds using the animal and human *in vitro* and *in ovo* models.

Methods: This study consisted of three parts: **1/** Analysis of the metabolic footprint of the selected candidate probiotics cultivated with supplementation of the selected prebiotics: fish protein hydrolysate (F466Q022) and liquid seaweed extract (A114P252). **2/** *In vitro* characterization of the intestinal cells interacting with *Bifidobacterium lactis* NCC2818 (or its supernatant) and *Bacillus* strain (or its supernatant) **3/** Metabolic footprint and fingerprint of probiotic function in the synbiotic culture. *Bifidobacterium lactis* NCC2818 and *Bacillus* strain were cultivated in a medium containing 2% [v/v] of the two pre-selected prebiotic compounds (prebiotic fish protein hydrolysate and liquid seaweed extract) at 37°C for 24 h.

Results: Metabolite analysis of the supernatant samples was performed by gas chromatography-mass spectrometry (GC-MS). Differential metabolite analysis showed changes in the profiles of specific organic acids: lactic acid, citric acid, acetic acid, phosphoric acid ($p<0.05$). The metabolic pathway enrichment analysis showed that metabolic pathways such as amino acid metabolism, energy metabolism, and two-component signal transduction system were activated. Moreover, the dual species *in vitro* intestinal epithelial cell monolayer model was established to simulate responses of the host intestinal epithelial cells: the new chicken cell line Chick8E11 and the human cell line Caco-2 were co-cultivated with *Bifidobacterium lactis* NCC2818 (or its supernatant) and *Bacillus* strain (or its supernatant) at a ratio of 10:2 (bacteria: cells) for 24 hours. The observed changes in the gene and protein expression levels of tight junction cytokines Villin, Cytokeratin 18, Zonula Occludens 1, and

Occludin indicate that *Bifidobacterium lactis* NCC2818 can enhance the tight junction of the intestinal barrier in the *in vitro* intestinal cell co-culture and ensure the normal physiological regulation process of the cells. The identified effect of *Bacillus* strain on intestinal health was apparent by the enhanced adherence of the beneficial species to the intestinal cells. The differential and enrichment analyses showed, that *Bifidobacterium lactis* had a positive effect on the barrier function of intestinal cells, and supported the normal intestinal cells function by regulating amino acid metabolism, protein digestion and absorption.

Conclusion: This study developed a basis to explore the predictive value of *in vitro* intestinal models in metabolomics and microbiology to track the functional footprint and define the potential of novel candidate probiotics and prebiotics separately and in their synergistic combination. Moreover, the results of this thesis have been used for the further *in vivo* (*in ovo*) application, as the part of a vaster research project Ovobiom- National Science Centre ***UMO-2019/35/B/NZ9/03186***: Probiotics and prebiotics- their effect on the chicken intestine health and organism performance, from the pre-hatch period to the mature animal, to elucidate the mechanisms of their mode of action through early microbiome modulation.

Streszczenie

Wstęp: Zdrowie jelit ma istotny wpływ na utrzymanie homeostazy organizmu gospodarza. Probiotyki i prebiotyki mogą bezpośrednio lub pośrednio wpływać na zdrowie jelit poprzez modulację mikroflory i metabolizmu układu jelitowego.

Cel: Celem badań było zrozumienie mechanizmów regulacji zdrowia jelit gospodarza przez dwa probiotyki (*Bifidobacterium lactis NCC2818* i *Bacillus altitudinis*) oraz ich wpływu na poziomie ogólnoustrojowym poprzez identyfikację charakterystyki metabolicznej tych szczepów w modelach *in vitro* oraz *in ovo* oraz pogłębienie wiedzy dotyczącej funkcji związków bioaktywnych w zdrowiu jelit i rozwoju odporności przez całe życie.

Metody: Badanie składało się z trzech etapów: 1) Analiza profilu metabolicznego wybranych probiotyków-kandydatów podczas hodowli *in vitro* uzupełnionej wybranymi prebiotykami – prebiotycznym hydrolizatem białka rybnego (F466Q022) i płynnym ekstraktem z alg (A114P252). 2) Charakterystyka *in vitro* interakcji *Bifidobacterium lactis* NCC2818 (lub jego supernatantu) i szczepu *Bacillus* (lub jego supernatantu) z ustalonymi liniami komórkowymi Caco-2 i Chic-8E11 w modelu współhodowli jelitowej *in vitro*. 3) Analiza profilu metabolicznego i funkcji probiotycznej w komórkach jelitowych *in vitro* w tych samych warunkach współhodowli. *Bifidobacterium lactis* NCC2818 hodowano w pożywce zawierającej 2% [v/v] dwóch wstępnie wybranych związków prebiotycznych w temperaturze 37°C przez 24 godziny.

Wyniki: Analizę metabolitów próbek supernatantu przeprowadzono metodą chromatografii gazowej ze spektrometrią mas (GC-MS). Analiza różnicowa metabolitów wykazała istotne zmiany w zawartości poszczególnych kwasów organicznych: kwasu mlekowego, kwasu cytrynowego, kwasu octowego i kwasu fosforowego ($p<0.05$). Analiza wzbogacenia szlaków metabolicznych wykazała aktywację takich szlaków jak metabolizm aminokwasów, metabolizm energetyczny i dwuskładnikowy system przekazywania sygnałów. Ustanowiono jednowarstwowy model komórek nabłonka jelit *in vitro* poprzez symulację komórek nabłonka jelit gospodarza, wykorzystując nową linię komórek kurczaka izolowanych z zarodka kury (Chick8E11) oraz referencyjną linię komórek ludzkich Caco-2 hodowanych we

współhodowli z *Bifidobacterium lactis* NCC2818 (lub jego supernatantem) i *Bacillus altitudinis* (lub jego supernatantem) w stosunku 10:2 (bakterie:komórki) przez 24 godziny. Zmiany w poziomach ekspresji genów i białek połączeń ścisłych (Villin, Cytokeratyna 18, Zonula Occludens 1 i Occludin) wskazują, że *Bifidobacterium lactis* NCC2818 może wzmacniać ścisłe połączenia bariery jelitowej we współhodowli komórek jelitowych *in vitro* i wspierać prawidłowe procesy regulacji fizjologicznej komórek. Wpływ *Bacillus altitudinis* na zdrowie jelit odbywa się głównie poprzez wzmacnianie połączeń międzykomórkowych i adhezję do komórek jelitowych, modulując w ten sposób obfitość mikroflory jelitowej i poprawę zdrowia jelit. Poprzez różnicową analizę i wzbogacanie metabolitów stwierdzono, że *Bifidobacterium lactis* ma pozytywny wpływ na funkcję barierową komórek jelitowych i utrzymuje prawidłową czynność jelit poprzez regulację metabolizmu aminokwasów oraz trawienia i wchłaniania białek.

Wnioski: W niniejszym badaniu zaproponowano śledzenie profilu probiotyków *in vitro* oraz analizę i scharakteryzowanie interakcji i charakterystyki metabolicznej komórek jelitowych. Metabolomika i modele komórkowe *in vitro* mogą być wykorzystywane do przewidywania, badania i oceny wartości oraz dawkowania potencjalnych probiotyków, a także do zbadania możliwości predyktywnych badań prowadzonych w modelach *in vitro* i przekładania ich wyników na badania *in vivo*.

1. INTRODUCTION

Animal immunity and performance can be managed by optimization of gut health. The intestine not only plays an important role in the process of digesting and absorbing nutrients, but also serves as an important immune barrier for the body. Natural bioactive ingredients have been emerging as sustainable and effective modulators of gut health. Among them, probiotics and prebiotics have a scientifically proven potential to directly or indirectly influence the host intestine health, function and structure, by modifications of the intestinal metabolism through microbial and host cell-microbiota interactions. Complex nature of interactions between the intestinal microbiota and the host gastrointestinal environment require a holistic exploratory methodology (involving metabolomics, transcriptomics, metagenomics), in order to understand as to how probiotics and synbiotics modulate host intestinal health at a systemic level. The approach taken in this work is based on identification of metabolic profiles of probiotics and prebiotics function using the *in vitro* cellular models. The results of this study will be further explored *in vivo*, using the prenatal *in ovo* animal model, therefore the selection of the probiotic, prebiotic, phytoextracts compounds and cell models in this thesis was driven by the prospective investigation goals with the *in ovo research* model. The avian embryo is the only higher vertebrate, such easily accessible to research analyses. The manipulations can be straightforwardly performed prenatally, at various developmental stages, without any discomfort applied to the organism. Therefore, the chicken model is gaining increasing attention as the alternative pre-clinical model (Beacon et al., 2021; Garcia et al., 2021).

Introduction to this work is therefore divided into two major parts: part **a/** describing the applied *in vitro* model of intestinal cells, and part **b/** providing the applicable metabolomic methods to study the function of probiotics and prebiotics.

a/ The intestinal study models

The intestine is a highly selective barrier for anti-nutrients and external factors in the host health, and communication organ between the intestinal microenvironment and metabolism in the host body. We know that the main interface for communication between the host and the environment that enables homeostatic balance is the epithelial barrier of the skin, gastrointestinal system and airways. Epithelial barriers constitute the first line of physical, chemical and immunological defense and provide a protective wall against some adverse factors of the environment (Sözener et al., 2020). The gastrointestinal tract is one of the largest luminal interaction areas among these barriers (Odenwald et al., 2017). Among them, the intestinal epithelium is a semipermeable barrier that allows the absorption of nutrients and immune sensing while limiting the transport of potentially harmful antigens and microorganisms. This plays a key role in the regulation of the immune system and therefore in health (Vancamelbeke et al., 2017). The host ingests food, digests it through physical and chemical processes, and then absorbs the refined macro- and micronutrients. Absorption is mainly carried out by intestinal epithelial cells using active transporters, passive diffusion, paracellular transport in the intercellular space, and transcytosis (Satsu, H., 2017). During this process, nutrients are metabolized into forms suitable for transport to target organs.

The intestine is also an important part of the human immune system, known as gut-associated lymphoid tissue (GALT), which helps the host defend against bacteria, viruses, parasites, and food component antigens that persist in the intestinal lumen. The intestinal epithelium is composed of several cell types bound together by tight junctions to form a single layer, which prevents larger molecules and microorganisms from entering the intestinal lumen and into the underlying connective tissue, with a layer of mucus covering the apical cell membrane providing an additional physical and biochemical barrier (Fedi et al., 2021). This barrier plays a key role in maintaining body health and homeostasis. Moreover, the intestine is also the host of approximately trillions of microorganisms. The normal intestinal flora and the environment in which they coexist constitute the intestinal

microecosystem. Intestinal flora is the major component, and the structure and function of the intestinal mucosa have a major influence on the normal operability of the system.

Intestinal *in vitro* study platform

Due to the diverse and important physiological functions of the intestine, enterocyte models have great potential as *in vitro* platforms for preclinical research. Intestinal cell models are used to maximize simplicity in the study of bioavailability, adsorption and transport, food components, and interactions of probiotics or pathogens with the intestine in nutritional or toxicological settings (Costa et al., 2019).

Compared to animal models, which have limited screening capabilities and are expensive, intestinal cell models are simpler, more reliable, and more reproducible. Because cell line models can be a simpler and more manageable research platform for studying biological systems. Cell models are gaining more attention in the research community and are widely used. They are becoming increasingly realistic in *in vivo* physiological studies, thus providing a representative and suitable alternative to *in vivo* animal testing, and reducing the costs and ethical issues associated with the use of animal experiments. Cell culture models can support large-scale screening and are cost-effective. The intestinal cell models should be used as a substitute for the *in vivo* environment, reflecting the natural reactions of the intestine and the complex physiology of the intestine (Costa et al., 2019).

Currently, the most common *in vitro* intestinal cell models are cell lines isolated from cancer tissues. This is due to the establishment of *in vitro* models requiring long-term and stable research characteristics, while primary cell cultures have reproducibility limitations and short lifespans, which makes them rarely used for model establishment. In reports, commonly used cell lines, such as the human epithelial cell line Caco-2 (Sharma et al., 2020), human colon adenocarcinoma cell line HT-29 (Meng et al., 2017) and the intestinal epithelial cells (IEC)-6 (Xie et al., 2019). Among them, the Caco-2 cell line has been most widely studied and applied (Ding et al., 2021).

Caco-2 is the intestinal cell line derived from human colorectal cancer that differentiate spontaneously under standard culture conditions and are suitable for *in vitro* studies of the

human intestine due to their efficient intestinal transport process. Ding et al. described that the differentiated Caco-2 cell model has been used in a variety of intestinal studies, including intestinal absorption, intestinal transport, intestinal metabolism, intestinal barrier, intestinal immunity, and intestinal adhesion (Ding et al., 2021). The normal intestinal mucosal barrier consists of a physical barrier, chemical barrier, immune barrier and biological barrier. The physical barrier refers to the integrity of the intestinal mucosal epithelial structure of tight junctions (Branca et al., 2019). The physical barrier formed by intestinal epithelial cells and the connections between them is the first line of defense against pathogens and toxins from the external environment, and plays a key role in the intestinal barrier structure. Wang et al. drew a schematic diagram of the intestinal epithelial barrier is shown in Figure 1. The Intercellular junctions consist of adherens junctions (AJs), desmosomes and tight junctions (TJs) (Groschwitz et al., 2009), which are present on the surface of epithelial cells near the intestinal lumen. TJs are complex of multiple proteins and molecules, including four transmembrane proteins, namely occludin, claudins, zonula occludens (ZO) and junctional adhesion molecule (JAM) (Hu et al., 2015; Tsukita et al., 2019). TJs are regulated by numerous intracellular signaling pathways, such as myosin light chain kinase (MLCK), protein kinase C (PKC), and mitogen-activated protein kinase (MAPK) (Gonzalez-Mariscal et al., 2008). In addition, TJs are connected to the cytoskeleton that supports epithelial cells, and together they form a dynamic barrier system, permeability of which, determines the barrier function of the entire intestinal epithelium. Therefore, damages to intestinal TJs are associated with the occurrence of various diseases, such as inflammatory bowel disease (IBD) and irritable bowel syndrome (Lerner et al., 2015; Li et al., 2019).

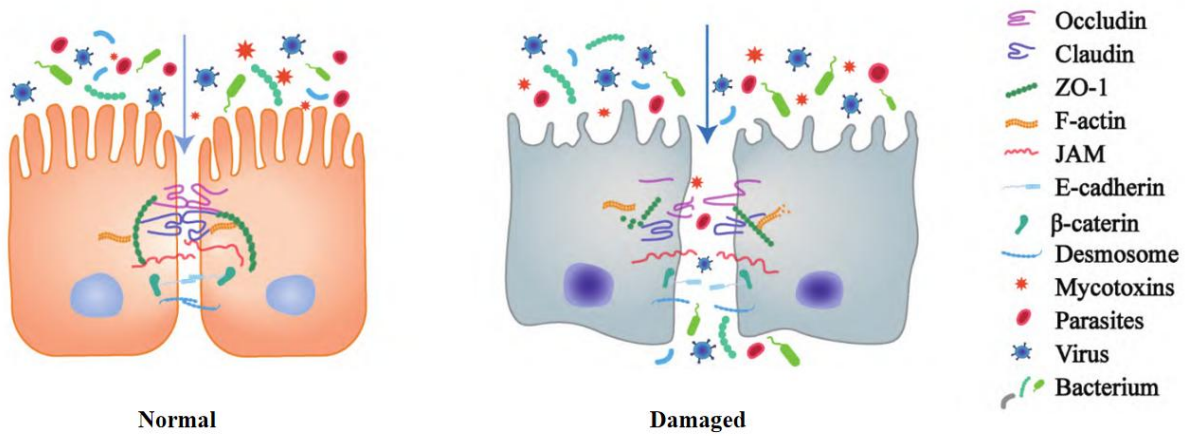

Figure 1. Schematic diagram of the intestinal epithelial barrier

(Wang et al., 2025)

***In ovo* study model**

The symbiosis between the host and the intestinal microbiota constitutes a microecosystem that plays an important role in maintaining intestinal homeostasis and regulating the host immune system. Industrially produced chickens have an incubation window where the potential for inoculation of the beneficial microbial community is suppressed, hindering the development of an appropriate microbiome, gastrointestinal system, and innate immunity. Delivery of prebiotics and probiotics into the air chamber on day 12 of egg incubation (12 embryo development day, EDD) or between 18-19 EDD stimulates the embryonic development and ensures an effective, optimal colonization of the embryonic microbiome with commensal microbial communities as early as during the perinatal period (Siwek et al., 2018, Maiorano et al. 2017). Numerous, recent in-house studies have proven life lasting benefits in the adult animal (increasing barriers to opportunistic pathogens, preventing myopathies), after modulating the gut microbiome *in ovo*, in chicken model (Stadnicka et al., 2020, Bogucka et al., 2022). In order to reduce number of experiments performed on life animals, adaptation of a chicken intestinal cell model for *in vitro* studies has a significant research potential. Secondly, the effects of bioactive ingredients followed at a simplified cellular and molecular (eg. metabolic) level,

allows to spot the potential mechanisms of their action and potentially extrapolate them to *in vivo* observations.

From a pragmatic standpoint, the multi-level opportunities of research performed using the *in ovo* model (prenatal injections, *in vivo* hatch and adult animal performance study, *in vitro* testing of selected physiological and biochemical aspects), allow to accelerate development of intestinal research platform (Bednarczyk et al., 2021; Ibrahim et al., 2025; Akhavan et al., 2023.)

In order to provide the translational research platform, and be able to translate the *in vitro* observation to *in vivo* mode, a compatible cell line to *in ovo* model is needed. Applying Chick-8E11 cell line combined with *in ovo* delivery system allows to complete this translational approach.Moreover, the Chick-8E11 was obtained from the chicken embryo at 18.5 day of development, making the compatibility of this *in vitro-in vivo* research platform even more relevant.

Currently,the development of an ileal explant culture model associated with an *in ovo* delivery system has been reported for studying short-term intestinal inflammation and secretory responses in an ex vivo environment. Researchers cultured ileal explants from 21-day-old broiler chickens *in vitro* for 6 hours. Based on the lactate dehydrogenase (LDH) release assay, the explants cultured for up to 2 hours still maintained more than 90% viability. The results demonstrate the potential usefulness of this intestinal explant culture model for short-term studies of biological factors in intestinal inflammation and secretory responses, but are insufficient for assessing tight junction reactivity (Zhang et al., 2017). It has also been reported that viable enterocyte aggregates were isolated from 19-day-old chicken embryos, which were able to expand and form a self-sustaining intestinal epithelial cell population that can survive for up to 12 days in culture. These cells were immunofluorescent positive for common intestinal epithelial markers, confirming that it is possible to isolate and maintain chicken intestinal epithelial cells in culture and their potential as an *in vitro* intestinal model for further studies (Ghiselli et al., 2021). However, the limitations of reproducibility of primary cell cultures still require long-term research on model establishment.

Currently, a promising Chick8E11 cell line, which was recently established by the Free University of Berlin (Kolenda et al. 2021) and provided by Tentamus Pharma & Med Deutschland GmbH for the research purpose. This new chicken cell line has not been widely characterized so far and has a potential to serve as a complementary monogastric model to the established human (e.g., Caco-2, HT-29) or porcine (e.g., IPEC-J1 and IPEC-J2) cell lines. Most importantly, it has the potential to be combined with an *in ovo* delivery system to complete this translational approach that can translate *in vitro* observations into *in vivo* models. Velge et al. described enterocyte differentiation markers in CHIC-8E11 applied it to study host adaptation to bacterial and parasitic infections (Velge et al., 2002). Kolenda et al. used CHIC-8E11 to the study pathogen-host cell interactions (Kolenda et al., 2021). In another study, Han et al. simulated viral transmission through the gastrointestinal tract by studying viral replication in CHIC-8E11 (Han et al., 2019). Avian pathogenic Escherichia coli (APEC) is a major bacterial pathogen of commercial poultry having potential threat to human. The contribution of APEC O-antigen synthesis, pseudouridine synthesis, sialic acid transport, putative fimbriae transcriptional regulators, and adhesin-related genes in adhesion to the CHIC-8E11 cell line and the human intestinal LoVo cell line has been reported (Ali et al., 2020). Kadekar et al. demonstrated the suitability of the CHIC-8E11 cell line for studying host-pathogen cell interactions in the context of necrotizing enteritis (NE) caused by *Clostridium perfringens* (Kadekar et al., 2024). In this work, the CHIC-8E11 cell line is for the first time applied to study probiotic, and synbiotic-host cell interactions with metabolomic approach. This thesis provides a step-wise knowledge that will be further used to follow *the* identified metabolic signatures *in vivo*. The same probiotic compounds as used in this study will be further investigated *in ovo*. The novel chicken intestinal cell line used in this thesis provides an excellent *in vitro* cell model to study the microecosystem of poultry intestinal cells and intestinal probiotics. In this study, the CHIC-8E11 cell line was used to evaluate the mechanism of action of potential probiotics and to analyze nutritional or microbial interactions affecting chicken intestinal epithelial homeostasis. This was combined with metabolic analysis of the *in ovo* delivery system to achieve a translational approach that translated *in vitro* observations into *in vivo* models.

Further exploration is needed to understand the potential functional signatures of probiotics and prebiotics to reveal the complexity of metabolic and physiological effects observed in the animal *in ovo* model and potentially translate them to human preclinical studies. These are not limited to nutritional research, but also to oncological investigations and applications, for which *in ovo* tumor xenografts gain increasing attention. such as INOVOTION (https://www.inovotion.com), which developed the Inovotion platform, an *in ovo* model for evaluating the activity of immuno-oncology drug candidates that induces a complete native chicken immune system after transplantation of human cancer cells (https://nc3rs.org.uk/crackit/ovo-model-immuno-oncology-screening). Also, several human recombinant proteins are produced in chickens and used in the clinics for rare diseases like Kanuma drug ,sebelipase alpha(Becker, R., 2015). Therefore, this thesis provides important input to health studies by providing metabolomic analysis pipeline to be extrapolated to other preclinical applications involving bioactive and microbiota- derived ingredients (Miebach et al., 2022; Kunz et al., 2019; Ghaffari-Tabrizi-Wizsy N., et al., 2019; Rovithi M., et al., 2017). Currently, *in vitro* studies complement *in vivo* research in this field, it allows to develop new predictive models and verify the existing ones, for the purpose of safe applications.

b/ Metabolomics in studying gut health

Gut health can be considered one of the major, manageable constituents of the host immunity and performance. The metabolomic approach to study functions of microbiota modulators was reviewed by the author of this thesis in Wu*, Zuo* et al. (2022). Metabolomics is an important part of systems biology/trans-omics. It is a systematic analytical science that studies the metabolites of biological samples or organs. Most of its metabolites are small molecules with a molecular weight of less than 1500Da. Analytical chemistry is a science that has both methodology and practical applications in various fields (Kosobucki et al., 2022). Modern analytical techniques can be used to conduct quantitative and qualitative diversified detection and analysis of metabolites of specific cells, blood, body fluids, etc. of organisms at specific periods (pathophysiological stimulation, different

developmental states, etc.) (Taylor et al., 2002). The life activities in cells are jointly constructed by genes, proteins and small molecule metabolites. The functionality of upstream macromolecules (genes, proteins) can eventually be reflected at the metabolic level, such as cell signal release, energy transfer, intercellular communication, receptor effects under changes in neurotransmitter release, and hormone regulation. Therefore, metabolomics is considered to be the ultimate analytical direction of "omics" research (German et al., 2004).

The metabolome is located downstream of the gene regulatory network and protein action network, providing terminal biological information. It can interact with upstream genes and proteins, and feedback the upstream life activity network to complete the various functional activities of the body. Compared with the genome and proteome, metabolomics has the following characteristics: 1/ Small changes in the expression of upstream functions such as genes and proteins are amplified in metabolites, making the detection easier; non-functional changes are therefore reflected at the metabolic level, which has the "noise filtering effect" in the process of transmitting upstream information to downstream; 2/ Metabolomics research does not require the establishment of a large number of databases of expression sequence tags; 3/ The types of metabolites are far less than the number of genes and proteins; 4/ The physiological/pathological state of the body can be understood through the analysis of metabolites in biological fluids; 5/ Metabolites are similar in different organisms, and the technology used in metabolomics is universal and general (Taylor et al., 2002).

According to the research purpose and the different metabolites detected, metabolomics can be divided into non-targeted metabolomics and targeted metabolomics (Johnson et al., 2016). Wu*, Zuo* et al. summarized the main strategies of metabolomics in Figure 2. (Wu*, Zuo* et al., 2022).

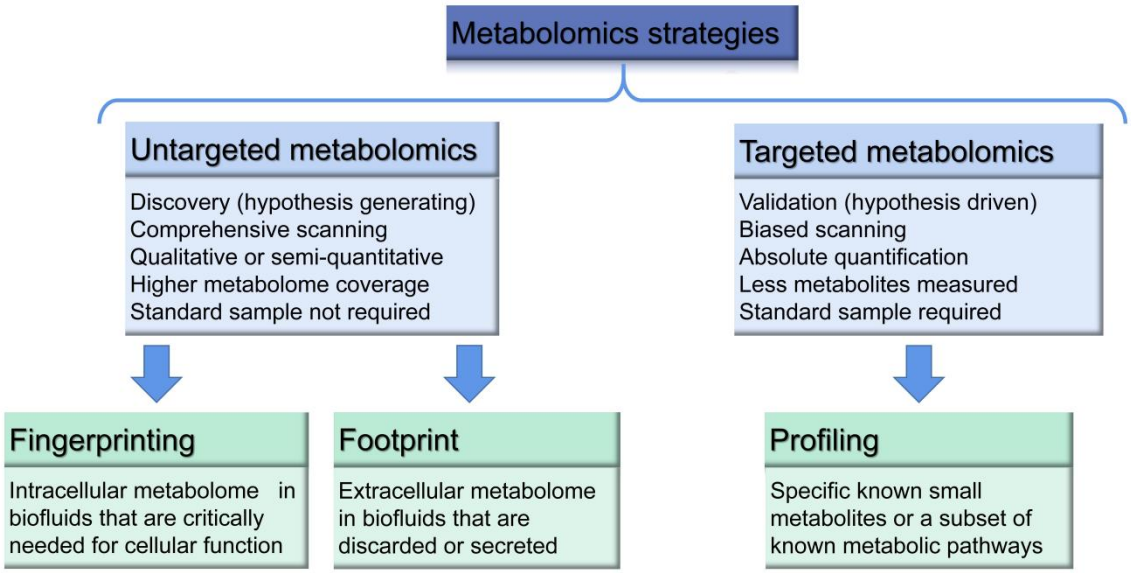

Figure 2. Main strategies of metabolomics

(Wu*, Zuo* et al., 2022)

Non-targeted metabolomics is a systematic and comprehensive analysis of endogenous metabolites in organisms (cells, body fluids or tissue samples), obtaining a large amount of metabolite data and processing it, aiming to find differential metabolites (Mamas et al., 2011), which is an unbiased metabolomics analysis. At present, non-targeted metabolomics analysis is widely used in biomarker discovery, disease diagnosis and mechanism research.

Targeted metabolomics analyzes a specific class of metabolites, selects specific detection methods and standards based on known metabolites, and is suitable for verifying the potential markers screened out. Among them, functional metabolomics is a deepening and extension of the concept of traditional metabolomics. It analyzes different biological samples (such as blood, urine, tissue, feces, etc.) to discover metabolite differences and metabolite pathway changes that are closely related to specific signal pathways and gene expression, and explores the mechanism of metabolite function (Stefely et al., 2016).

Intestinal microbes are microbial communities that live in the intestines. They are characterized by large numbers and complex classifications. They play an important role in host growth and development, nutritional metabolism, and healthy immunity. In the

long-term co-evolution, intestinal microbial flora and hosts adapt to each other, achieve dynamic balance, and form a mutually beneficial symbiotic state. The current research hotspot is to analyze the diversity of microorganisms in the intestine, and metagenomes are usually used to detect and analyze the types and numbers of microorganisms. As a unique microbial organ, the intestinal microbiome relies on the host's intestinal life and helps the host complete a variety of physiological and biochemical functions, such as participating in regulating the host's digestion and absorption, energy metabolism, maintaining intestinal homeostasis, regulating the proliferation and differentiation of epithelial cells, and preventing pathogenic microorganisms from colonizing on the mucosa (Markowiak-Kopeć et al., 2020). The host selectively colonizes certain microbial populations to provide them with a stable and nutritious living environment. In addition, intestinal microbes and their metabolites not only affect the development and stability of the host's neuroimmune system, maintain intestinal function and gastrointestinal barrier integrity, but also participate in the regulation of host nutritional metabolism (Qiao et al., 2014). The interaction between intestinal microbial communities, microorganisms, and hosts forms a dynamic balance and complex microbial environment in the intestine to maintain the normal functioning of the body (Dupont et al., 2020).

Intestinal microorganisms absorb and produce many metabolites, such as fatty acids, hormones, vitamins, etc. These metabolites are the products of upstream gene and protein expression (Markowiak-Kopeć et al., 2020). Intestinal microbial flora use undigested food residues in the upper digestive tract, digestive tract cell secretions, and apoptotic epithelial cells as metabolic substrates for metabolism and biosynthesis (Okumura et al., 2018). The metabolic activities of intestinal microbial flora affect the physiological metabolic characteristics of the host, and there are active metabolic exchange processes and common metabolic processes between the flora and the host (Zhou et al., 2020). The following metabolites are classified into the following main types:

1/ Carbohydrate metabolites: Intestinal microbial fermentation of carbohydrates is the core metabolic activity, mainly composed of oligofructose, xylitol, dietary fiber, etc., which are hydrolyzed by microorganisms to form short-chain fatty acids (SCFA), the final metabolic

product. Among them, butyrate can enhance the physical barrier function of intestinal epithelial cells by affecting the abundance of tight junction claudin protein and monocarboxylate transporter 1 (Mátis et al., 2022).

2/ Protein metabolites: Ingested protein and endogenous protein are mixed and digested in the small intestine and fermented by microorganisms in the large intestine. The energy produced by protein metabolism can be used as a partial energy source for a small amount of intestinal epithelial cells. After entering the body, protein is first hydrolyzed by proteases into small molecular amino acids and polypeptide substances, and enters bacteria and cells through cell membrane transport proteins. Some amino acids can affect the synthesis of proteins required by the host, such as intestinal bacterial metabolites derived from the essential amino acid tryptophan, which increase intestinal barrier function by maintaining the integrity of the apical junction complex and its related actin regulatory proteins. (Scott et al., 2020). Amino acids produced by intestinal microbial metabolism act as signal molecules, which can activate signal pathways and improve intestinal nutrition.

3/ Lipid metabolites: Intestinal microbial flora participate in the body's energy and fat metabolism through various pathways. Different sources of lipids affect the composition and quantity of intestinal microorganisms to influence the host's metabolism and health. Some of the lipid metabolic end products are SCFAs.

4/ Extracellular vesicles (EV): All bacteria release EVs as a mechanism for communication between species. Bacterial extracellular vesicles (BEV) are spherical lipid bilayer nanostructures that are natural carriers of bacterial molecules, including lipopolysaccharides (LPS), peptidoglycans, lipids, proteins, nucleic acids, as well as pathogens, toxins and virulence factors. They avoid direct cell-to-cell contact and deliver bacterial active compounds over long distances in a protected environment (Gilmore et al., 2019). Bacterial secreted vesicles mediate the function of the microbiota and intestinal homeostasis by transporting and delivering effector molecules into host cells that regulate host signaling pathways and cellular processes (Díaz-Garrido et al., 2021).

5/ Bacteriocin: These are interesting natural antimicrobial peptides that can modulate the microbiota and host immunity, affecting a variety of health-promoting functions in the

host (Anjana et al., 2022). Toxic proteins or peptides produced by bacteria that are active against related bacteria but do not harm the producing cells. In a crowded ecosystem, microorganisms must compete to survive. Bacteriocins play an important role in mediating inter- and intraspecific interactions between bacteria and shaping the diversity of bacterial communities. The interaction between microorganisms and hosts is influenced by various internal and external factors, and microbial communities also adapt, rearrange and evolve (Drider, D., 2021).

6/ Neurotransmitters: The synthesis and regulation of neurotransmitters by intestinal microbiota is an important part of the gut-brain axis, including secretion of synthetic neurotransmitters (such as GABA, dopamine, etc.), production of neurostimulatory metabolites that affect the immune system or generate substances that promote nerve growth (such as short-chain fatty acids, kynurenine, etc.) and other pathways (such as vagus nerve pathways or regulation of important dietary amino acids, etc.). These substances can directly or indirectly affect the nervous system (Dicks, L. M., 2022). However, the connection between the gut microbiota and neurotransmitters is a complex research area, although there are still many unknown areas that need further exploration.

7/ Postbiotics: functional bioactive compounds produced by microbiota, including bacterial metabolites, microbial cell components, functional proteins, extracellular polysaccharides (EPS), cell lysates, teichoic acid, peptidoglycan-derived peptides and pili-type structures (Roy et al., 2023). The concept of postbiotics was derived from food fermentation research. It has been reported that in *in vitro* and *in vivo* studies, the fermentation products of *Lactobacillus paracasei* CBA L74 acted by inhibiting the release of proinflammatory cytokines to protect the host from pathogens and enteric pathogens (Zagato et al., 2014). Intestinal microorganisms secrete EPS during their growth and metabolism, which protect intestinal probiotics from adverse conditions such as dehydration, toxin factors, and osmotic pressure, and play a role in adhesion and colonization, biofilm formation, and cell recognition. Extracellular polysaccharides are high molecular weight polysaccharide polymers. According to their bacterial attachment relationship, they can be divided into mucus polysaccharides and capsule polysaccharides (Gerwig G. J., 2019). They

have multiple biological functions such as antibacterial, antioxidant, anti-tumor, and immunomodulatory, and play an important role in maintaining the homeostasis of intestinal microecology. *Bifidobacterium* EPS has an inhibitory effect on the growth of enterococci and enterobacteriaceae (Biliavska et al., 2019); lactic acid bacteria EPS promotes the proliferation of potential probiotics, regulates the diversity of intestinal flora, and activates immune cells and lymphocytes through specific and nonspecific immune responses to adjust intestinal immunity (Surayot et al., 2014).

The intestinal microbial flora and the host are a steady-state environment. If the balance between microorganisms and the host is broken under the influence of the external environment, the intestinal flora structure changes from a physiological combination to a pathological combination, and the host will reduce its resistance to pathogens. This will lead to the occurrence of autoimmune diseases and inflammatory bowel disease (IBD). At present, through the analysis of the composition of intestinal microbial flora and microbial metabolomics, it is found that *Bifidobacterium* has a higher regulatory effect on intestinal homeostasis. It significantly improves the symptoms of intestinal inflammation, reduces the damage to the intestinal barrier, and increases the abundance and diversity of intestinal flora (*Muribaculaceae*, *Lactobacillus*, *Bacteroides*, and *Enterorhabdus*) (Han et al., 2024). The potential probiotics *Bifidobacterium lactis* NCC2818 and *Bacillus altitudinis* in this study have the potential to regulate the chicken microbiome, according to the stepwise testing and *in vitro* selection conducted by Akhavan et al. under the same project (Akhavan et al. 2023).

In order to optimize the use of probiotics and prebiotics, a more comprehensive and systematic understanding of their effects on intestinal function and microbial communities is needed. Since probiotics are living bacteria that have a great impact on the host through the production of their metabolites, the application of metabolomics is needed to analyze the mechanism of their metabolic footprint on the host's intestinal function. The evaluation of metabolic characteristics will help further clarify the biochemical mechanism by which probiotics and prebiotics play a role in intestinal health and provide guidance for subsequent clinical applications.

2. AIMS AND HYPOTHESIS

2.1. To study interaction of the selected probiotics, prebiotics and intestinal cells with the newly optimized gas chromatography mass spectrometry (GC-MS) protocol

Probiotics (and host intestinal cells) produce specific metabolic footprints and fingerprints that can be identified *in vitro* during culture. GC-MS technology was used to analyze the *in vitro* metabolite changes of the selected probiotics (*Bifidobacterium lactis* NCC2818 and *Bacillus strain*) cultivated with the addition of two *in vitro* selected prebiotics (prebiotic fish protein hydrolysate and liquid seaweed extract), and metabolite changes in the intestinal cells (Caco-2 and Chic-8E11) co-cultured with these probiotics. The changed metabolites were identified and their impact on the host intestine was estimated through the metabolic pathway database.

List of hypotheses:

H.1: The probiotic metabolism will be changed and identified at the pathways level, after stimulation with prebiotic

H.2: The intestinal cells metabolism will be changed and identified at the pathways level, as a result of the interaction with probiotic.

2.2. To characterize Caco2 and Chick8E11 intestinal cells in co-culture with probiotics, *in vitro*

In vivo, the probiotics influence intestinal health through regulating the host mucosal and systemic immune functions or modulating intestinal colonization by beneficial flora. Here, a novel chicken intestinal cell line, Chick8E11 cells was used to establish an *in vitro* intestinal co-culture cell model. Caco-2 cells are a widely used cell line in the intestinal research and serve as a reference cell line for this study. In this study, the colonization ability

of candidate probiotics to intestinal cells and their impact on the intestinal genes expression were evaluated.

List of hypotheses:

H.3: The optimal probiotic inoculation ratio to intestinal cells is required to maintain the intestinal epithelial cell monolayer in co-culture condition.

H.4: The same selected probiotics directly interact with chicken and human intestinal cells *in vitro*, and the ability of these probiotics to adhere to intestinal cells can be evaluated in chick8e11 and Caco-2 models.

H.5: Probiotics (*Bifidobacterium lactis* NCC2818 and *Bacillus altitudinis*) will affect intestinal marker genes expression in the Chick8E11 and Caco-2 intestinal cells, *in vitro*.

2.3. Metabolic footprint & fingerprint of probiotics and prebiotics function in chicken gut cells *in vitro* and *in ovo*

To co-culture intestinal cells with selected probiotics *in vitro*, apply the same probiotic and their combination with prebiotics (as synbiotic) *in ovo*, and study the changes of the types and quantities of endogenous small molecule metabolites in intestinal cells. By analyzing the characteristic changes of metabolites in cells (Metabolic Fingerprints) and metabolites secreted outside cells (Metabolic Footprints), the mechanism of action of probiotics on host intestinal cells can be comprehensively elucidating focusing on the intestinal function and health

List of hypotheses:

H.6: The metabolic fingerprint of probiotics (*Bifidobacterium lactis* NCC2818 and *Bacillus altitudinis*) will be obtained by their co-culture with intestinal cells.

H.7: Probiotic *Bifidobacterium lactis* NCC2818 will affect the metabolic characteristics related to the protein digestion and absorption metabolic pathways of Chick8E11 and Caco-2 cells *in vitro.*

3. MATERIAL & METHODS

3.1. Cell culture and probiotic culture

3.1.1. Cultivation of Caco-2 cells and CHIC 8E11 cells

The new chicken intestinal epithelial cell line CHIC 8E11 established from 18- day old chicken embryo Tentamus Pharma & Med Deutschland GmbH, Germany) was cultured in DMEM (Dulbecco's Modified Eagle Medium/F12, cat. D8437 Sigma-Aldrich, Merck Group Poland) supplemented with 10% FBS (fetal bovine serum, cat. F2442 Sigma-Aldrich, Poland). The human colon cell line Caco-2 (cat. 86010202, Sigma-Aldrich, Merck Group Poland)was cultured in MEM (Minimum Essential Medium Eagle, cat. M4655 Sigma-Aldrich, Merck Group Poland) supplemented with 10% FBS. Both cell lines were cultured at 37°C, 5% CO_2, 95% humidified incubator, with the addition of Penicillin- Streptomycin solution 100 U ml^{-1} (cat. P4333, Sigma-Aldrich, Merck Group Poland, and Amphotericin B solution 100 µgml^{-1} (cat. A2942 Sigma-Aldrich, Merck Group Poland) in 75 cm^2 cell culture flasks (cat. CLS354484, Corning, Merck Group Poland) to obtain appropriate density. The cells were then detached with trypsin- EDTA solution (cat. T4049- Sigma-Aldrich, Merck Group Poland) at 37˚C for 3-5 minutes. After the digestion reaction was completed with complete culture medium, the cells were collected by centrifuge at 300 g for 5 min, and counted. Next, the cells were diluted in the cell culture media appropriate for each of the cell lines, to obtain the desired cells concentration, then continue to culture the cells in cell culture flasks. For the subsequent experiments, the cells were inoculated into 6-well plates(cat. Z707767-72EA, TPP® tissue culture plates, Merck Group Poland) at a concentration of 1×10^5 cells/ per well, or into 96-well plates(cat. Z707902-108EA, TPP® tissue culture plates, Merck Group Poland) at a concentration of 5000 cells/ per well. Both cell lines were continuously maintained in the culture flasks with passaging and monitoring according to the producers instructions and standard subculture techniques.

To establish a cell bank of these two cells, their respective complete culture medium containing 10% DMSO (dimethyl sulfoxide, cat. D2650, Sigma-Aldrich, Merck Group Poland)

were used, following the cell freezing procedure, 1 × 10^6 cells per freezing flask using CoolCell™ LX Cell Freezing Container (cat. CLS432001-1EA, Corning®, Merck Group Poland) were stored at -80˚C overnight and then quickly transferred to liquid nitrogen humids (-196˚C) for long-term storage.

3.1.2. Bacteria and Growth Conditions

Bifidobacterium lactis NCC2818 was obtained from France L'institut Pasteur and grown in De Man, Rogosa and Sharpe GranCult broth (MRS, cat. 1106610500 Millipore Sigma-Aldrich, Merck Group Poland) at a temperature of 37˚C in CO_2 incubator according to the work of Akhavan et al. (Akhavan et al., 2023). *Bacillus strain* was provided by Teagasc Agriculture and Food Development Authority and South East Technological University, Ireland. The strain was grew in brain heart infusion broth NutriSelect Plus (BHI, cat. 53286 Millipore Sigma-Aldrich, Merck Group Poland) at a temperature of 30°C. After 24h incubation (without shaking), the cultures were centrifuged at 7000 rpm for 1 min and the cell-free supernatant (CFS) was collected. Then, the bacteria were suspended in the culture medium with an optical density of 0.5 at 600 nm (OD600 0.5), which is equivalent to a bacterial concentration of 2.9 × 10^7 CFU/mL, for the subsequent experiments of different determinations of probiotic-inoculated cell co-culture.

3.2. *In vitro* interaction studies between probiotics and prebiotic bioactive ingredients by GC-MS

3.2.1. Samples preparation

The bioactive ingredients: fish protein hydrolysate powder (F466Q022, BioAtlantis Ltd., Ireland) and liquid seaweed extract (A114P252, BioAtlantis Ltd., Ireland) were dissolved in the nutrient solutions MRS and BHI broths. The ingredients were added to the corresponding broth media at a final concentration of 2% (w/v) for powder prebiotic and 2% (v/v) for liquid prebiotic, and subsequently filtered with Titan3TM polyethersulfone (PES) Syringe filters

(0.22 micrometer; Alchem, Warsaw, Poland). Bacterial suspensions were prepared in 0.85% NaCl from the colonies growing in MRS, and adjusted to an optical density, OD = 1 read at 600 nm wavelength in SpectraMax® ID3 Multi-Mode Microplate Reader by Molecular Devices. Each prebiotic-probiotic culture well contained a 5% bacterial inoculum from the above described bacterial suspensions.

The MRS broth was used as the blank control. The probiotic positive control (MRS + Bifido) was the *Bifidobacterium lactis* cultured in MRS broth at 37°C (in 5% CO2). The bioactive ingredients fish protein hydrolysate and liquid seaweed extract, dissolved in MRS broth served as the prebiotics positive controls (MRS + fish protein hydrolysate, MRS + liquid seaweed extract). All the samples' abbreviations for the six groups analyzed for metabolites by GC-MS, are encoded with the capital letters A-F, as listed in Table 1.

Table 1. Names of the experimental groups analysed for metabolites by GC-MS

Groups	Code	Full name
A	MRS	MRS medium
B	MRS+*Bifido.*	MRS+*Bifidobacterium* lactis NCC2818
C	F466Q022+MRS	fish protein hydrolyzate+MRS
D	F466Q022+MRS+*Bifido.*.	fish protein hydrolyzate+MRS+*Bifidobacterium lactis* NCC2818
E	A114P252+MRS	liquid seaweed extract+MRS
F	A114P252+MRS+*Bifido.*.	liquid seaweed extract+MRS+*Bifidobacterium lactis* NCC2818

3.2.2. Sample pretreatment optimization

Short-Chain Fatty Acid (SCFA) determination was analyzed by gas chromatography – mass spectrometry (GC-MS). Briefly, 100 µl of supernatant was dried with a SpeedVac concentrator at -4°C overnight. The dried metabolite extracts were dissolved in 50 µl of the methoxyamine hydrochloride solution in pyridine (20 µg/µl) and vortex mixed for 2 min. Methoxymation was carried out at 70°C for 30 min. After the addition of 40 µl of

N-(tert-butyldimethylsilyl)-N methyltrifluoroacetamide (Figure 3) mixed with 1% tertbutyl-dimethylchlorosilane, derivatization was carried out at 70°C for 1 h.

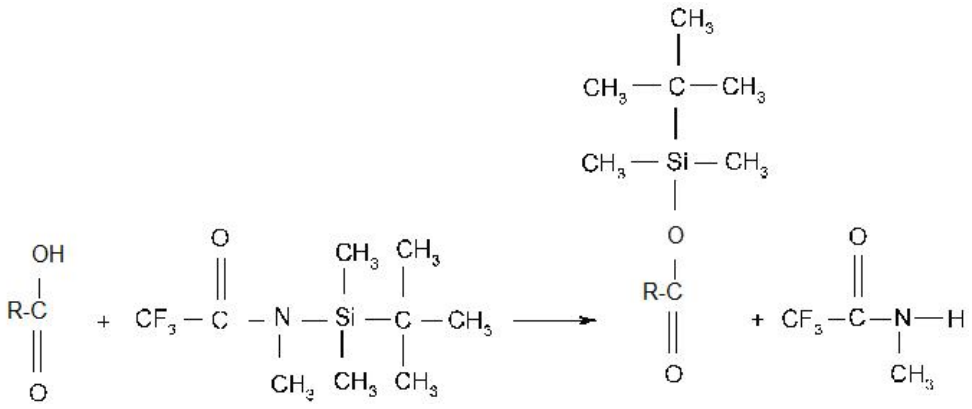

Figure 3. General derivatization mechanism for SCFA with MTBSTFA.

3.2.3. GC-MS working conditions

Gas chromatography (Agilent 7890B; Agilent, Santa Clara, CA) coupled with MS (Agilent 5977A; Agilent, Santa Clara, CA) was used for the analysis of the samples. The separation was achieved using an HP-5 MS column (30 m x 0.25 mm i.d. coated with 0.25 mm film thickness; Agilent, Santa Clara, CA). The gas chromatography temperature program (Table 2) was as follows: 50 °C held for 1.0 min, increased to 200 °C by 10 C/min, 200 °C held for 5.0 min, increased to 220 °C by 5 °C/min, 220 °C held for 10.0 min, and increased to 250 °C for 10 min by 15 °C/min. The inlet temperature was set at 250 °C. The mass range was set as 50 to 400 m/z. The ion source chamber was set at 230°C with the transfer line temperature set to 280 °C and the electron energy of 70 eV.

Table 2. The GC-MS temperature program

	Rate (°C/min)	Value (°C)	Hold Time (min)	Run Time (min)
(Initial)		50	1	1
Ramp 1	10	200	5	21
Ramp 2	5	220	10	35
Ramp 3	15	250	10	47

3.2.4. Metabolomics analysis of mass spectrometry data

All statistical analyses were performed using R software. Principal coordinate analysis (PCoA) was performed in R using the XCMS package (Domingo-Almenara et al., 2020). The heatmap was constructed using the 'pheatmap' package. The differential abundances of various profiles were tested with the Wilcoxon rank sum test and were considered significantly different at $p < 0.05$. The edges of the network were calculated by Spearman's rank correlation coefficient and visualized in Cytoscape (version 3.7.1).

The comparative analysis of metabolic differences involved multivariate statistical analysis and univariate statistical analysis to screen differential metabolites and conduct correlation analysis and pathway enrichment analysis. Multivariate statistical analysis was used for unsupervised principal component analysis (PCA) to observe the overall distribution between samples and the stability of the entire analysis process, and then use supervised partial least squares analysis (PLS-DA), and the orthogonal Partial least squares analysis (OPLS-DA) was used to distinguish overall differences in metabolic profiles between groups and to find differential metabolites between groups. One way Anova mainly focuses on the two aspects of univariate description and statistical inference. It was applies to extract the major information from a large number of sample data and describe the concentration or dispersion trend in the samples' data. One way Anova statistical inference was used to generate the general conclusions from the samples' data, by applying the interval estimation and statistical hypothesis testing. T test (Student's t test) and Fold change analysis were used

to compare metabolites between groups pairs.

A combination of multidimensional analysis and unidimensional analysis was used to screen differential metabolites between the groups. In OPLS-DA analysis, the variable weight value (Variable important in projection, VIP) was used to measure the influence strength and explanatory power of the expression pattern of each metabolite on the classification and discrimination of each group of samples, and to mine the biologically meaningful differential metabolites. Further, the T test was used to verify whether the difference between the metabolites was significant.

3.3. Establishment of intestinal co-culture model

3.3.1. Cell monolayer model

To form monolayers, experiments were performed on Chick-8E11 cells of chicken intestinal cell line and Caco-2 cells of human intestinal cell line grown under the conditions described in the chapter 3.1. Inoculate stably passaged cells into a 96-well microplate or 6-well plate, adjusted the appropriate cell seeding density, and cultured under the same conditions for about 48 hours to reach confluence to form a Chick-8E11 cell monolayer and Caco-2 cell monolayer. In order not to affect subsequent experiments, cells were washed three times with PBS and cultured as monolayers in antibiotic-free medium.

To observe the cell morphology and structure of two different intestinal cells, phalloidin cell actin-DAPI fluorescent staining was performed. A glass slide was placed flat in each well of 6-well plates, on top of which the cells were seeded at a seeding number of 1×10^5 cells per well. The culture medium was removes, the cells were gently washed twice with 1×PBS (pH 7.4, cat. D8537-6X500ML, Sigma-Aldrich, Merck Group Poland) preheated to 37°C, and fixed with 4% formaldehyde solution (pH 6.9, cat. 1004968350, Sigma-Aldrich, Merck Group Poland) dissolved in PBS for 30 minutes at room temperature. The cells were washed again twice with PBS, each wash for 5 min. The cells were permeabilized with 0.5% Triton X-100 solution (cat. T8787-100ML, Sigma-Aldrich, Merck Group Poland) for 5 min at room temperature, and again gently washed with PBS, twice. Then slowly add the prepared

TRITC-labeled phalloidin working solution (provided by Dr. Kazmierski Łukasz lab, Faculty of Medicine, UMK) to completely infiltrate and cover cells on the glass slide, incubated at room temperature in the dark for 30 minutes, and then gently washed the coverslip three times with PBS. The cell nuclei were counterstained with DAPI solution and the coverslips were washed with PBS. Finally, the cells were permanently sealed (cat. No producer of the sealing tape) and stored in the dark at 4°C. TRITC excitation/emission filter (Ex/Em=545/570 nm) and DAPI excitation/emission filter (Ex/Em=364/454 nm) were selected for fluorescence observation and image collection under a confocal microscope (model of the microscope is needed),supported by Dr. Kazmierski Łukasz lab, Faculty of Medicine, UMK

3.3.2. Intestinal cell spheroid model

A 3D *in vitro* culture model of chicken intestinal cells based on spheroids was established in a pilot experiment using ClinoStar (Celvivo, Odense Denmark) - modular CO2 incubator equipped with a set of bioreactors.

Firstly, the enterocyte spheroids were prepared using the microcavity culture plates (Celvivo, Denmark). Before application, the plates were washed twice with culture medium (DMEM/F12 or EMEM) to remove any residual air bubbles from the well surface, then plates were prefilled with 0.5 ml of culture medium and centrifuged at 3000 × g, for 3 min to let the medium fill the microcavities. Cells at a recommended seeding density of 5×10^6 (Chic-8E11) or 2.5×10^6 (Caco-2) were added to each well, and the plate was centrifuged again (100 × g, 3 min). The microwell plates were placed in incubator (37°C, 5% CO_2, humidified) for 24 hours, until the spheroids got formed in microcavities. After 14h, the cultured spheroids were transferred to the ClinoStar™ bioreactors according to the manufacturer's instruction. The detached spheroids were collected into a Petri dish and the quality of the spheroids was evaluated microscopically. The spheroids with a compact morphology(observed like Figure 4) were selected and transferred into the bioreactor. The spheroids (approximately n=300 per bioreactor) were cultured in a humidified incubator at 37°C, 5% CO2, 95% humidity for 12 days, with a careful adjustments of the rotation speed. The medium was refilled every 2-3 days, and the formation process and status of intestinal spheres were recorded.

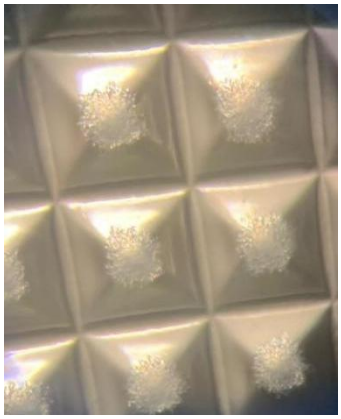

Figure 4. Images of cell spheroids with compact morphology on the microcavity culture plates under the microscope

3.4. *In vitro* characterization of the co-culture of the intestinal cells with probiotics

3.4.1. Optimization of the probiotics/to cells ratios in co-culture system

The probiotic bacteria *Bifidobacterium lactis* NCC2818 and *Bacillus strain* were collected during the exponential growth phase. The concentrations were assessed by measuring the optical density at 600 nm in a microplate reader and converting this value to the corresponding CFU/ml value by plate counting. Caco-2 cells and Chic-8E11 cells were incubated with *Bifidobacterium lactis* NCC2818 and *Bacillus strain* respectively at varying ratios (30:2; 15:2; 10:2; 5:2; 2:2; 1:2), bacteria (CFU): cells (n), in 96-well microplates for 0-24 hours (replicate number=3). Moreover, the collected probiotics were resuspended in the complete culture medium for Caco-2 cells and the complete culture medium for Chic-8E11 according to the required number of probiotics in the above different ratios and incubated for 24 hours. The probiotic supernatants from probiotic cultures in the intestinal cell culture medium, were collected by centrifugation at 10000 rpm, for 10 min. To ensure that the supernatant was free of probiotic bacteria, the supernatant was filtered through a 0.22 µm pore size filter prior to use. Next, the Caco-2 cells and Chic-8E11 cells were incubated with the above-mentioned probiotic supernatant for 24 hours.

The cell viability in co-culture systems at different ratios was determined by MTT

colorimetry (according to Mosmann T., 1983). For each different probiotic and cell co-culture combination at different ratios, minimum n=3 culture wells were used as technical repetitions in each biological replicate. The baseline absorbance for the control wells containing only confluent Chic-8E11 and Caco-2 cell cultures without any probiotic bacteria, was considered 1.0. The number of metabolically active cells treated with probiotics was calculated referring to that 1.0 baseline value, and the morphology of the treated cells was observed and recorded under a microscope.

3.4.2. Adhesion assays of probiotics to biological surfaces and intestinal cells

Assays of probiotic adhesion capabilities are performed to assess the probiotic properties associated with a potential to colonize the host gut. According to the previous studies of *Bifidobacterium* (Cronin et al., 2011) and the adhesion of *Bacillus* to colon cells (Prieto et al., 2014), the ability of the probiotic bacteria *Bifidobacterium lactis* NCC2818 and *Bacillus strain* to adhere to abiotic surfaces (bare polystyrene) were tested in 96-well microplates (flat bottom transparent polystyrene wells). The ability of both probiotic bacteria to adhere to biological surfaces was tested on mucin-coated 96-well plates. Mucin solution was first prepared by dissolving mucin from porcine stomach Type III (PGM) (cat. M1778-100G, Sigma Aldrich, Merck Group Poland) in PBS pH 7.4 to a final concentration of 10 mg x ml^{-1} according to the method of Sałański et al. (Sałański et al., 2022) with slight modifications. The amount of 100 µl of mucin solution was added to the wells of the 96-well microplate and the plate was washed twice with PBS to remove the excess mucin. Next, 100 µl of probiotic bacterial cell suspensions (at optical density of 1 at 600 nm) were seeded in each well of a bare plate (polystyrene) or a mucin-covered plate (PGM), and statically cultured aerobically at 37°C for 3 hours. Next, the wells were washed twice with 300 µl of PBS and once with 400 µl of sterile Milli-Q grade water to remove unbound bacteria. Bound bacteria were stained with 100 µl of crystal violet solution (cat. C0775-100G, Sigma-Aldrich, Merck Group Poland) per well for 10 min at room temperature and washed three times with water to remove excess stain. Finally, 200 µl of 96% ethanol was added to each well containing the probiotic bacteria., The adhesion was evaluated spectrophotometrically at

570 nm (OD 570) by stain intensity criterion. Three independent biological replicates were performed for each experiment. The bacterial adhesion levels were determined by taking the average of at least six measurements, and the results were expressed as standard deviation ± mean. Blank wells contained the PBS only.

The ability of probiotic bacteria to adhere to Caco-2 and Chic-8E11 cell layers was assesed. The indentical numbers of Caco-2 cells and Chic-8E11 cells, 2×10^5 cells per well, were seeded in 12-well plates (cat. Z707775-126EA, TPP® tissue culture plates, Merck Group Poland). The cells were cultured in the appropriate complete culture media with antibiotics at 37°C, 5% CO_2, and 95% humidity, reaching 90% confluency. The further culture steps were performed in the antibiotic-free medium Varying probiotic bacteria suspensions resuspended in antibiotic-free EMEM or DMEM/F12 medium were inoculates to the culture wells at a ratio of 10:1 (10 CFU of bacteria per 1 cell). The plates were incubated under the same conditions for 3 h followed by three times washes with PBS to remove the unbound bacteria. Caco-2 cells and Chic-8E11 cells that were having probiotics attached to them, were transferred to a PBS solution containing 0.1% TRITON X100 (cat. T8787-100ML, Sigma-Aldrich, Merck Group Poland) and gently lysed. The dilutions were spread on the corresponding agar plate (cat. 1465590020, Millipore, Merck Group Poland) and incubated at 30 or 37°C for 24 or 48 hours for the counts of viable bacteria. The adhesion was expressed as the number of viable adherent bacterial cells (CFU) per well for the same number of cells. Each experiment was performed in at least three independent biological replicates and three technical replicates.

3.4.3. qPCR detection of changes in the expression of selected genes in cells after co-culture with probiotics

To evaluate the changes in tight junction-related gene expression on epithelial intestinal cells co-cultured with probiotics, The following marker protein genes were tested: E-cadherin (CHD1), villin (VILL), cytokeratin 18 (CK18), cytokeratin 20 (CK20), zonula occludens-1 (ZO1), occludin (OCCL) and claudin-1 (CLDN), as well as the inflammation-related factor interleukin 18 (IL-18).

RNA samples preparation: Caco-2 and Chic-8E11 cells were co-cultured with probiotics *Bifidobacterium lactis* NCC2818 and *Bacillus* strain 6-well plates at the optimized probiotic (CFU) : cell (n) ratio, as according to the subchapter 3.4.1.. The confluent cell culture of each of the cell lines alone served as the blank control groups. The cultures were performed in 3 replicates, and 3 replicate samples were obtained per group.

The total RNA was extracted and purified using the GeneMATRIX Universal RNA Purification Kit (EURX®, Poland) according to the manufacturer's protocol. Due to the instability of RNA, agarose gel electrophoresis was used to determine the integrity of the extraction and preservation of RNA samples. The quantity and quality of RNA were determined spectrophotometrically by measuring absorbance at 260 and 280 nm. According to the manufacturer's instructions, iScript® cDNA Synthesis Kit (BIO-RAD, USA) was used to perform reverse transcription of RNA samples to generate more stable cDNA samples, which were stored at 4°C. The primer sequences are in Table 3, some of them were referenced, and the rest were designed using the Primer 6.0 software tool. To normalize cDNA amounts, the housekeeping genes GAPDH were used for Caco-2 cells and β-actin for Chic-8E11 cells. Finally, real-time PCR reactions were performed using the BIO-RAD CFX OPUS 96 Real-Time PCR Detection System and iTaq® Universal SYBR® Green Supermix (BIO-RAD, USA). Amplification consisted of 40 cycles of denaturation at 95°C for 30 s, annealing at 55°C for 30 s, elongation at 72°C for 45 s, and initial denaturation at 95°C for 3 min. Reactions for each sample were performed in triplicates. RNA-free water(Cat. no. E3598, EURX®, Poland) with the same volume as cDNA was added to the reaction system as a blank control. After the reaction was completed, the specificity was verified by melting curve analysis. Relative gene expression was calculated after normalization using the $2^{-\Delta\Delta CT}$ method according to Pfaffl (Pfaffl, M. W. 2001).

Table 3. List of Primer sequences used in the study

Cells	Gene	Primer sequence (5'- > 3')	Product length (bp)	NCBI Accession No.	Reference
Caco-2	E-cadherin	F: GAACGCATTGCCACATACAC R: AGCACCTTCCATGACAGACC	159	NM_001317185.2	(El-Ashmawy et al., 2019)
	Villin	F: GTCTTGCTGCTATCTATGGT R: TCTTCCTGTAGTCTCTTGGT	186	X12901.1	Designed
	Cytokeratin 18	F: CTGAGACCAATGACACCAA R: GACATCCAATGAACTCTGAAC	103	X12881.1	
	Cytokeratin 20	F: CTGTTTGTTGGCAATGAGAAAATGG R: GTATTCCTCTCTCAGTCTCATACT	304	NM_019010.3	(Van Eekelen et al., 2000)
	Zonula occludens-1	F: CAACATACAGTGACGCTTCACA R: CACTATTGACGTTTCCCCACTC	105	XM_054378717.1	(Ibrahim et al., 2020)

	Occludin	F: AGATGGACAGGTATGACAAG R: ACAGGCGAAGTTAATGGAA	271	U49184.1	Designed
	Claudin-1	F: GTGGAGGATTTACTCCTATGCCG R: TCAAGGCACGGGTTGCTT	164	NM_021101.5	(Gerardi et al., 2021)
	Interleukin 18	F: ATCGCTTCCTCTCGCAACAA R: CTTCTACTGGTTCAGCAGCCATCT	85	XM_054368670.1	(Sałański et al., 2022)
	GAPDH	F: TCACCAGGGCTGCTTTTAAC R: GACAAGCTTCCCGTTCTCAG	98	NM_001357943.2	(El-Ashmawy et al., 2019)
Chic8E11	Villin	F: GAACCTCTCGTGGCACCGC R: CTCATGTCCCTGCACCTCCC	152	XM_418521.5	(Ghiselli et al., 2021)
	Cytokeratin 18	F: CACAGATCCGGGAGAGCCTG R: CTCCACCGCGCTGTCATAGA	110	XM_025145666	
	Zonula occludens-1	F：CCACTGCCTACACCACCATCTC R：CGTGTCACTGGGGTCCTTCAT	138	XM_015278975.4	(Zhang et al., 2022)

Occludin	F：CGCAGATGTCCAGCGGTTACT R：CAGAGCAGGATGACGATGAGGAA	160	NM_205128.1	
β-actin	F: TTGTTGACAATGGCTCCGGT R: TCTGGGCTTCATCACCAACG	153	NM_205518.2	(Ma et al., 2023)

3.4.4. Immunofluorescence staining of intestinal cell markers in co-culture

The fluorescent staining of intestinal epithelial cells in co-cultures with probiotics was performed. The intercellular tight junction-related and skeleton structure-related proteins including E-cadherin (CHD1), cytokeratin 18 (CK18), zonula occludens-1 (ZO1), occludin (OCCL), claudin-1 (CLDN), desmoplakin (DMPK) and vimentin (VIM).

Cells fixation: the glass slides(cat.S8902-1PAK, Sigma-Aldrich, Merck Group Poland) were placed flat in each well of a 6-well plate. The Caco-2 and Chic-8E11 cells were co-cultured with probiotics *Bifidobacterium lactis* NCC2818 and *Bacillus* on the glass slides, at the ratios selected in accordance with subchapter 3.4.1. The blank control group contained the confluent cell cultures only. The experiment was repeated in triplicate to obtain three samples per group. All the medium was removed, when the cell confluence reached 80%, the adherent cells were gently washed twice with 1 mL of Dulbecco's phosphate buffered saline (DPBS, cat. D8537-6X500ML, Sigma-Aldrich, Merck Group Poland) and fixed with 4% paraformaldehyde (cat. AGR1026, Micro-Shop, Poland) for 20 min. After discarding all the liquid, 1.5mL DPBS was added to store the fixed cell samples at 4˚C. The antibodies used for immunofluorescence characterization are listed in Table 4. Antibody incubation and confocal fluorescence image acquisition were supported by Prof. Maciej Gagat lab, Department of Histology and Embryology.

Table 4. List of antibodies used for immunofluorescence characterization

Antibodies	Target Molecule	Function	Cat no.	Company&Country	Reference
Rabbit anti- ZO-1	Zonula Occludens 1	Primary antibody	33-9100	Thermofisher, USA	(Li et al., 2004)
Rabbit anti-claudin 1	Claudin-1		51-9000		
Rabbit anti-occludin	Occludin		71-1500		
Mouse Anti-E-Cadherin	E-cadherin		610181	BD Biosciences, USA	(Hardy et al., 2011)
Mouse anti-chicken vimentin	Vimentin		MA5-11883	Invitrogen, USA	(Ghiselli et al., 2021)
Mouse anti-chicken cytokeratin 18	Cytokeratin 18		MA1-06326		
Anti-Desmoplakin I+II antibody [DP2.15]	Desmoplakin		ab16434	Abcam plc, UK	(Acehan et al., 2008)
Goat anti-Mouse IgG (H+L) Cross-Adsorbed, Alexa Fluor™ 555	/	Secondary fluorescent antibody	A-21422	Thermofisher, USA	(Chen et al., 2015)
Goat anti-rabbit IgG (H+L) conjugated to Alexa Fluor™ 488	/		A-11001		

3.5. Metabolic footprint and fingerprint of probiotic function in co-culture with intestinal cells in the Caco-2 and Chic 8E11 models

Metabolomic samples preparation: Caco-2 and Chic-8E11 cells were co-cultured with *Bifidobacterium lactis* NCC2818 and *Bacillus* probiotics in 6-well plates at the probiotic (CFU): cells (n) ratios selected in accordance with subchapter 3.4.1. The blank control group contained the 80% confluent cell cultures only. Three replicates were obtained for each group.

The metabolic footprint samples: After 24 h of co-culture, the supernatant of the co-culture combination was collected by centrifugation at 10,000 rpm for 10 min.

The metabolic fingerprint samples: After the above metabolic footprint samples were collected, the supernatant was completely removed and, the cells were gently washed with PBS 3 times, followed by addition of 80% (v/v) methanol (cooled to -80˚C). Immediately after, the culture plates were placed in -20˚C for 20 min and kept on ice. The cells were scraped off with a cell scraper(cat. 99003, TPP®, GENOS in Poland) and collected into 2 ml conical tubes(cat. EP0030108078-250EA, Sigma-Aldrich, Merck Group Poland), followed by vortexing for 5 min, centrifuged at 10,000 × g for 5min at 4 - 8˚C. The metabolites-containing supernatants were transferred to the new conical tubes. All the samples were stored in -80˚C for subsequent analysis.

The analysis of metabolic footprints with the GC-MS protocol optimized in this thesis, including the samples pretreatment, GC-MS technical procedures and metabolomics mass spectrometry data analysis wasperformed as described in the Material and methods subchapter 3.2.

The metabolic fingerprint samples testing was performed by the Institute of Biocehmistry and Biophysics of Polish Academy of Sciences according to the targeted metabolomic analysis protocol of the MxP® Quant 500 kit (Biocrates, Austria). The polar small molecule classes were analyzed by liquid chromatography -tandem mass spectrometry (LC- MS/MS). The hexoses and lipid classes were analyzed by flow injection analysis- tandem mass spectrometry (FIA-MS/MS). The resulting data analysis was performed in this thesis

according to the Material and methods subchapter 3.2.

3.6. Metabolomic analysis of chicken intestinal contents after *in ovo* injection of candidate probiotics, prebiotics and synbiotics

Chicken intestinal contents were collected after *in ovo* injection of two candidate probiotics, prebiotics and synbiotics combination. The prebiotics and probiotics were selected based on conclusions from the previous in-house research (Akhavan et al. 2023).

Fresh fertilized eggs (Ross 308; n=928), originating from a flock in the peak of laying (30 wks old), were randomly divided into four experimental groups: (1) V/control (Phivax Vaccine Pahc, Phibro Animal Health Poland, Warsaw, injected alone), (2) V + PRO (Vaccine + 10^6 CFU probiotic), (3) V + PRE (Vaccine + 1mg prebiotic), (4) V + SYN [Vaccine + synbiotic (1 mg of prebiotic + 10^3 CFU probiotic)]. All eggs were incubated in the automated chicken egg incubators (Heka-Brutgeraete Favorit Olympia incubator Rietberg, Germany), according to the producer's manual. The incubation trial was performed in triplicate at three separate times.

The hatched chickens were placed in an automated chick nursery (Heka 4001/A Rietberg, Germany) with separated cages, directly after hatch. No invasive animal procedures were applied. The chickens were handled following local ethical commission decision no. WHiBZ/like.003/04/22 and Directive 2010/63/EU.

When the probiotic was injected alone, a dose of 10^6 CFU bacteria was used. When applied with the prebiotic, a dose of 10^3 CFU was used. Probiotic inocula were prepared under sterile conditions directly before the injections. The synbiotic formulation consisted of 25 µl prebiotic solution (vegetable protein hydrolysate or astragalus polysaccharides) combined with 2.5 µl probiotic suspension (10^3 CFU) and 22.5 µl vaccine carrier, yielding a total injection volume of 50 µl per embryonated egg. When administering the probiotic alone (probiotic *Bifidobacterium* strain group and probiotic *Bacillus* strain group), 2.5 µl of probiotic suspension (10^6 CFU) was diluted with a vaccine carrier to achieve the standard 50 µl total volume. For prebiotic-only delivery (prebiotic astragalus polysaccharide group and

prebiotic plant protein hydrolysate group), 25 µl of solution containing 1 mg prebiotic was supplemented with a vaccine carrier to the final 50 µl volume per embryonated egg.

The first control group was divided into: probiotic *Bifidobacterium* strains, prebiotic astragalus polysaccharide(APS) or synbiotics (10^3 CFU *Bifidobacterium* strains + 1 mg APS). The control groups were divided into: control group (BiA), probiotic *Bifidobacterium* strain group (BiB), prebiotic APS group (BiC) and synbiotic 10^3 CFU *Bifidobacterium* strains + 1 mg APS group (BiD).

The second comparative experimental groups were divided into: probiotic *Bacillus* strains, prebiotic plant protein hydrolysate-soy or synbiotic (10^3 CFU *Bacillus* strains + 1 mg protein hydrolysate) and the control group were compared as follows: control group (BaA), probiotic *Bacillus* strain group (BaB), prebiotic plant protein hydrolysate-soy group (BaC) and synbiotic 10^3 CFU *Bacillus* strains + 1 mg protein hydrolysate (BaD).

Inoculations were performed automatically into the amnion, using the Vinovo (Viscon Group, Gravendeel, The Netherlands) vaccination technology, at 18.5 days of incubation. The experiments were performed in accordance with the institutional guidelines concerning animal use and welfare, and according to the decision of the Local Ethical Committee WHiBZ/like.003/04/22.

The chickens (females only, for genetic homogeneity), were reared under standard broiler housing conditions, 4 replicates per group, 15 birds per pen, as part of larger experiment in the Ovobiom NCN project. Gut content for metabolome analysis was obtained from the ceca of 42-day-old broilers, deep frozen in dry ice and transported to -80 within 2 hours, stored until analysis.

3.7. Work flows

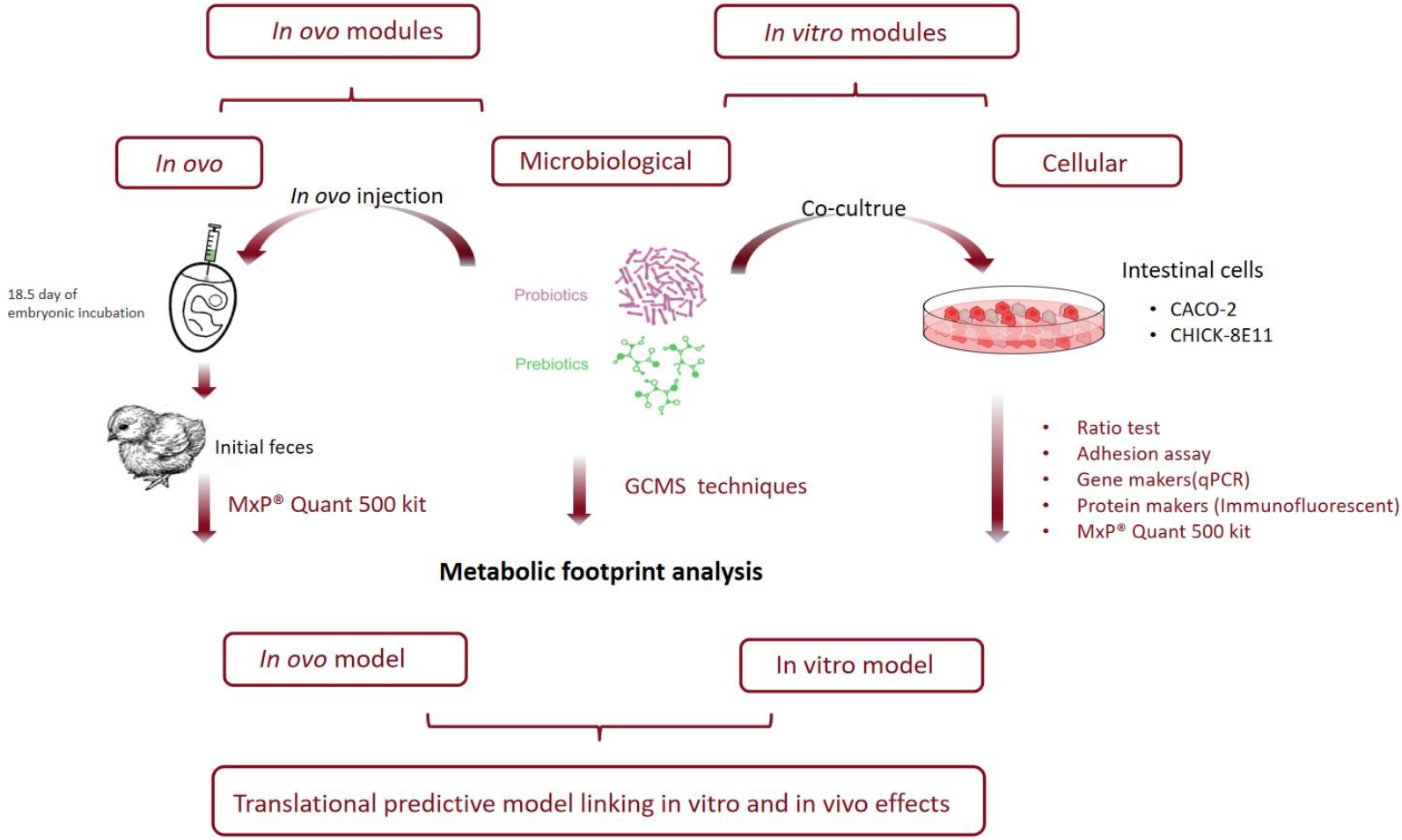

4. RESULTS

4.1. Metabolic footprint of the probiotics stimulated by prebiotic and protein hydrolysate *in vitro*

4.1.1. Total ion chromatograms (TICs) of the experimental groups obtained by gas chromatography-mass spectrometry (GC-MS) analysis

Examples of chromatograms from the study groups are listed below (Figure 5). Differences in the number and concentration of compounds between the test groups can be observed. For convenience of description, the group names are replaced from A to F (A: MRS; B: MRS + *Bifido.*; C: fish protein hydrolyzate + MRS; D: fish protein hydrolyzate + MRS + *Bifido.*; E: Liquid seaweed extract + MRS; F: Liquid seaweed extract + MRS + *Bifido.*) as showed in Table 1 above in the Methods 3.2.1. section.

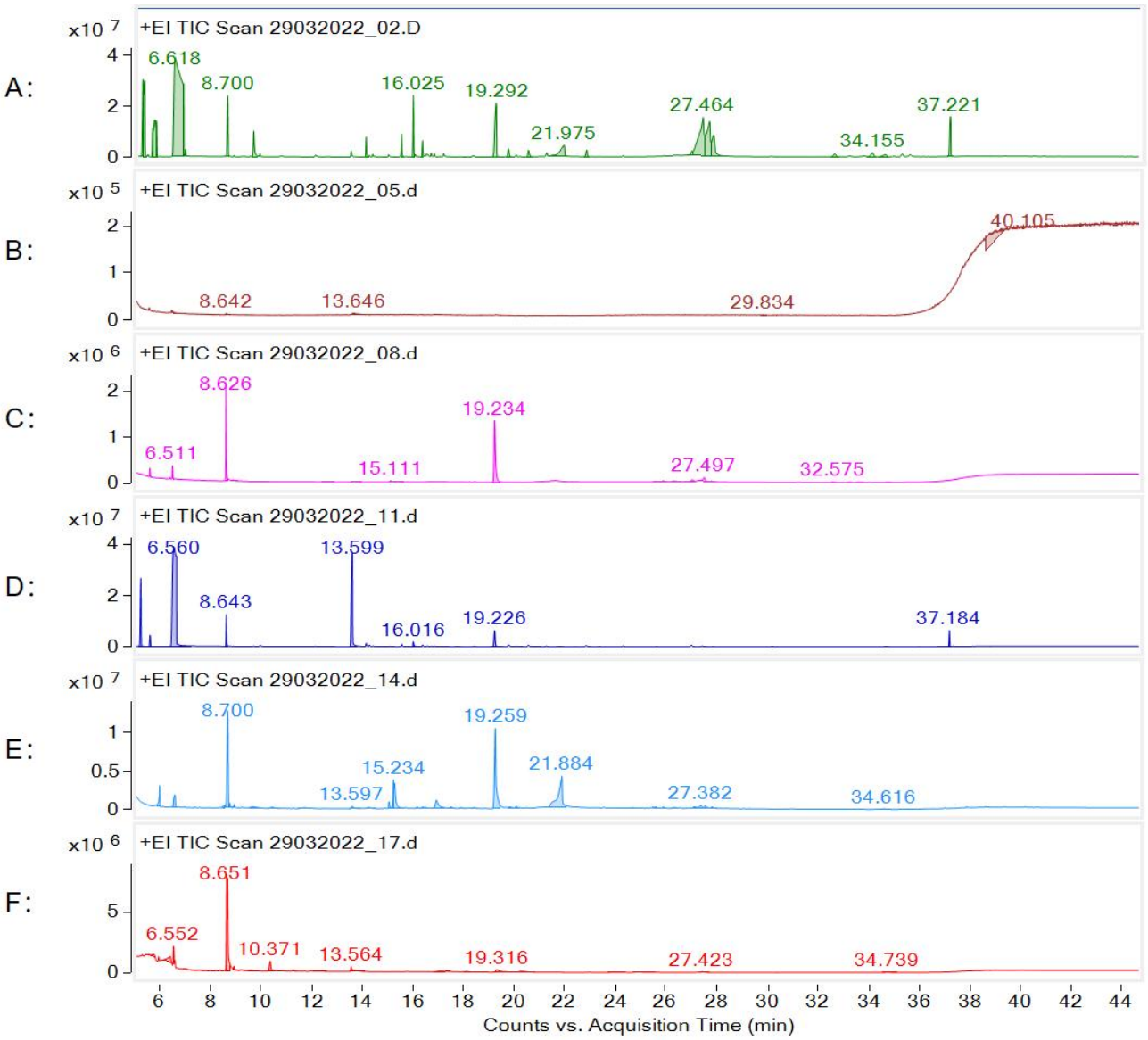

Figure 5. The representative mass chromatograms for the experimental groups: A: MRS; B: MRS + *Bifido.*; C: MRS + fish protein hydrolysate; D: MRS + fish protein hydrolysate + + *Bifido.*; E: MRS + seaweed extract; F: MRS + seaweed extract + *Bifido.*

Group A (MRS medium alone) contained a basic matrix being the source of nutrients for the bacteria used in the study. Based on the GC-MS analysis, the composition of the basic cultivation broth constituted mainly from organic acids including short chain fatty acids, non-essential amino acids, and benzoic acids (2-Butenedioic acid; 2-Methylpropanoic acid; 3,4-Dimethylbenzoic acid; Acetic acid; Butanedioic acid; Citric acid; Lactic acid;

L-Aspartic acid; L-Glutamic acid; L-Pyroglutamic acid; Oxalic acid; Pentanoic acid; Propanoic acid; Stearic acid), amino acids (Isoleucine; L-Alanine; L-Leucine; L-Methionine; l-Norvaline; L-Phenylalanine; L-Proline; L-Serine; L-Threonine; L-Valine). In the Group B (MRS + *Bifido.*), it was found that the compounds of the MRS medium were assimilated by bacteria. As a result, the following compounds were identified only: 2-Hydroxy-3-methylbutyric acid; Butanedioic acid; Glycine; Hexanoic acid; Isoleucine; Lactic acid; L-Alanine; L-Phenylalanine; L-Proline; L-Pyroglutamic acid; L-Valine; Palmitic Acid; Phosphoric acid; Stearic acid.

In order to identify the metabolic footprint of the probiotic growth stimulation, the effect of two selected bioactive ingredients: protein hydrolysate and seaweed extract prebiotic was analyzed in the subsequent experimental groups (C-F). Based on the chromatograms of the samples of group E (MRS + seaweed extract) and F (MRS + seaweed extract +*Bifido.*), it can be observed that the use of prebiotics had a positive effect on the metabolism of *Bifidobacterium*. As a result of probiotic metabolism in group F, the following additional metabolites were identified, among the others: 2-Methylpropanoic acid; Acetic acid; Boric acid; Cyclo(L-prolyl-L-valine); l-(+)-Lactic acid; Lactic acid; Methoxyacetic acid, Pentanoic acid; Phosphoric acid; Stearic acid. In turn, in group E (MRS enriched with seaweed extract), the largest spectrum of compounds was identified. The common compounds for groups E and F were: 2-Methylpropanoic acid; Acetic acid, Lactic acid; Phosphoric acid; Stearic acid. In addition, the following specific compounds were determined in the sample F with probiotic (MRS + seaweed extract + *Bifido.*): 1-Methoxy-2-propanol; 2-Butenedioic acid; 2-Hydroxy-3-methylbutyric acid; Butanedioic acid; Citric acid; Glycerol; Glycine; Hexanoic acid; Isoleucine; L-Alanine; L-Aspartic acid; L-Glutamic acid; L-Leucine; L-Methionine; L-Phenylalanine; L-Proline; L-Pyroglutamic acid; L-Serine; L-Threonine; L-Valine; Oxalic acid; Palmitic Acid; *p*-Isopropylbenzoic acid; Phthalic acid.

4.1.2. Principal Component Analysis (PCA) of metabolites identified with GC MS- stimulatory effect of fish protein hydrolysate and liquid seaweed extract o*n Bifidobacterium lactis*

Principal component analysis (PCA) of metabolites was applied to determine the variability between sample groups and within the experimental groups (A to F), the overall distribution trend between the samples, and evaluate the possible discrete points. The main parameters of the PCA model are the R-squared values R2X allowing to indicate the percentage of variance explained by the principal components. If there is a significant difference between the two samples, then the two coordinate points are relatively far away on the score map, and vice versa.

Each of the experimental groups was analyzed in 6 repetitions in order to verify the repeatability of the conducted research. Based on the PCA analysis (Figure 6), it can be concluded that all the analyzed study groups were reproducible.

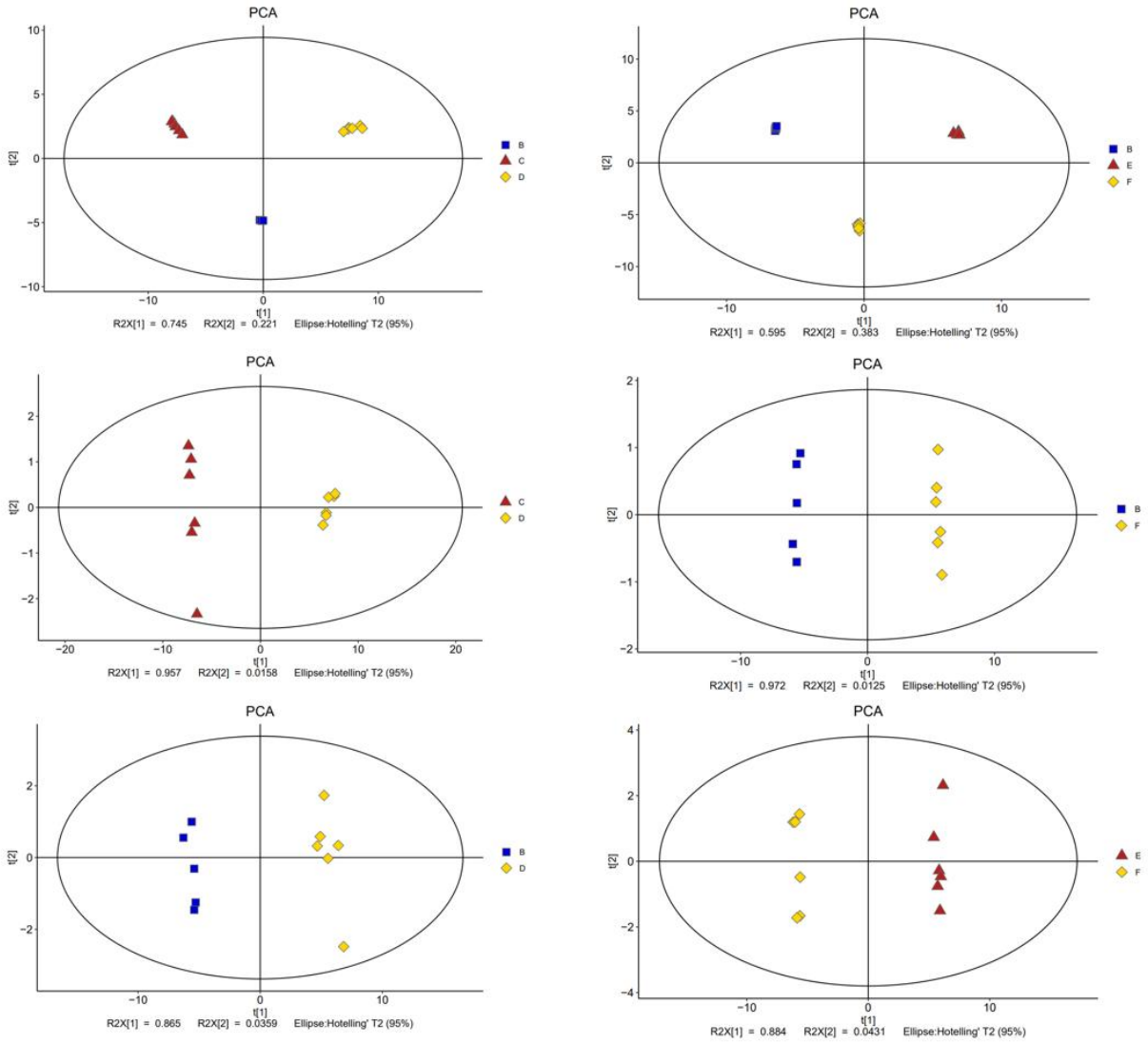

Figure 6. PCA (Principal Component Analysis) score plots of the metabolic profiles of the compared experimental groups: A-F

A: MRS; B: MRS + *Bifido.*; C: MRS + F466Q022 (fish protein hydrolysate); D: MRS + F466Q022 (fish protein hydrolysate) + *Bifido.*; E: MRS + A114P252 (seaweed extract); F: MRS + A114P252 (seaweed extract) + *Bifido.*

Tips: Different colors and shape combinations represent different sample groups (A-F), and the oval area represents the 95% confidence interval.

4.1.3. Orthogonal Partial Least Squares-Discriminant Analysis (OPLS-DA)

The Orthogonal Partial Least Squares-Discriminant Analysis OPLS-DA is a supervised discriminant analysis statistical method. This method is modified on the basis of PLS-DA to filter out noise irrelevant to classification information, improve the analysis ability and effectiveness of the model, and maximize the differences between different groups within the model. On the OPLS-DA score graph, there are two kinds of principal components, namely predictive principal components and orthogonal principal components. There is only one predictive principal component and there can be many orthogonal principal components. OPLS-DA maximizes the difference between groups and reflects it on a predictive component axis t[1] in the plot, so that the variation between groups can be directly identified at t[1], while the orthogonal principal component reflects the variation within the group. There are significant differences between the two groups of samples on the OPLS-DA score map.

On a basis of the OPLS-DA analysis, variability between 6 replicates for individual study groups was observed (Figure 7). It can be concluded that the variability for individual surface areas of individual compounds is within the confidence interval.

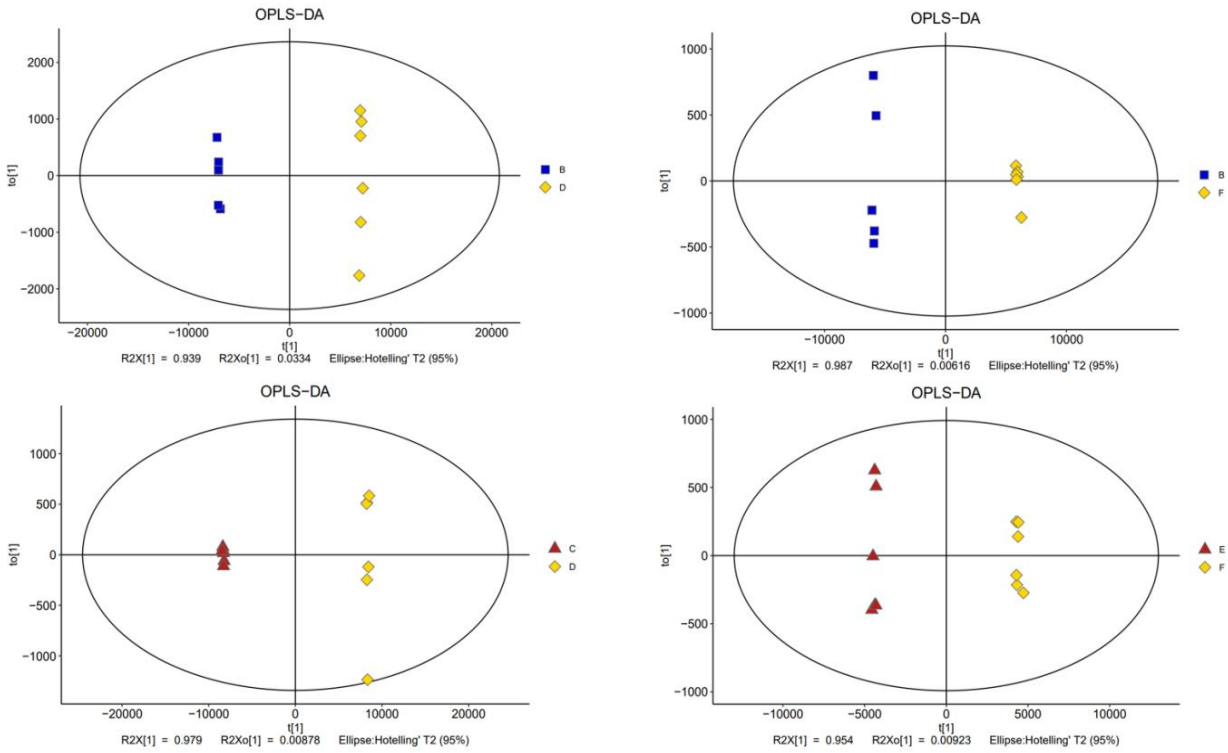

Figure 7. OPLS score plots of the metabolic profiles of the compared experimental groups: A-F

A: MRS; B: MRS + *Bifido.*; C: MRS + F466Q022 (fish protein hydrolysate); D: MRS + F466Q022 (fish protein hydrolysate) + *Bifido.*; E: MRS + A114P252 (seaweed extract); F: MRS + A114P252 (seaweed extract) + *Bifido.*

OPLS-DA maximizes the difference between the groups and reflects it on t[1] axis, so that the inter-group variation can be directly estimated at t[1], while the orthogonal principal component reflects the intra-group variation.

4.1.4. Permutation

In order to prevent the model from overfitting, seven-fold cross validation and 200 Response Permutation Testing (RPT) methods were used to examine the quality of the model. The response sorting test is a random sorting method used to evaluate the accuracy of the OPLS model. The results of the response sorting test of the OPLS-DA model were given. The OPLS-DA model was tested for 200 response rankings, that is, the X matrix was

fixed, and the variables (such as 0 or 1) of the previously defined classification Y matrix were randomly arranged n times (n=200) to establish the corresponding OPLS-DA model, and to calculate the R2 and Q2 values for the stochastic model. The regression line obtained by linear regression with R2Y and Q2Y of the original model has intercept values with the y-axis as R2 and Q2, which are used to measure whether the model is overfitting.

Based on the OPLS-DA analysis (Figure 8), it can be concluded that the selected model was a good fit as indicated by the green points positioned below the blue points. Moreover, the green regression lines of points intersect with the vertical axis below zero.

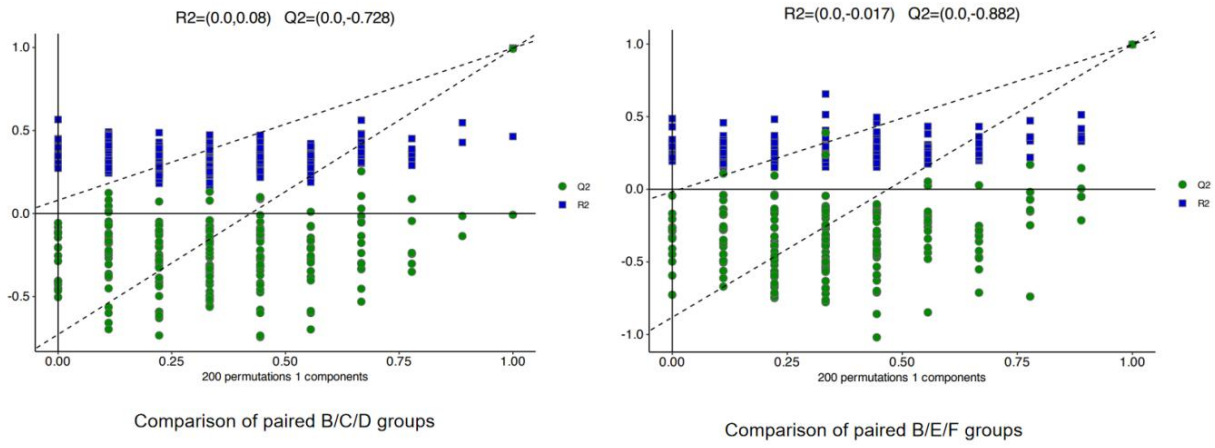

Figure 8. Permutation diagram of metabolic profiles of the compared experimental groups: B-F

B: MRS + *Bifido.*; C: F466Q022 (fish protein hydrolysate) + MRS; D: F466Q022 (fish protein hydrolysate) + MRS +*Bifido.*; E: A114P252 (seaweed extract) + MRS; F: A114P252 (seaweed extract) + MRS + *Bifido.*

The evaluation of model effectiveness is based on two criteria: 1/ All green Q2 values on the left are lower than the original points on the right; or 2/ The green regression line of Q2 points intersects with the vertical axis (left side) at or below zero.

4.1.5. One way Anova analysis

The One Way Anova analysis was applied to summarize samples with large amount of data and to statistically infer overall trends. T test (Student's t test) and Fold change analysis were used to compare the differences in metabolites between two groups.

The p-values and Fold change values in this study were visualized by using the volcano plots, which was helpful for screening differential metabolites, as shown in the figure below (Figure 8). The red spots represent the metabolites that were significantly up-regulated in the experimental group, and the blue spots indicate the metabolites that were significantly down-regulated. The grey points represent insignificant metabolites.

Based on the Figure 9, it can be observed that in the samples from group B (MRS + *Bifido.*) there was a lower concentration of the most of the analyzed chemical compounds (for example Citric acid, Acetic acid, Lactic acid, Phosphoric acid) than in the samples from group D in which the bioactive stimulant was added (MRS + fish protein hydrolysate + *Bifido.*). On the other hand, in the samples from group B there was a higher concentration of compounds such as Lactic acid and Phosphoric acid, compared to the samples from group F with the seaweed prebiotic added (MRS + seaweed extract + *Bifido.*). In the case of the metabolic compounds: Lactic acid, Citric acid in group C (MRS + fish protein hydrolysate) they were found at a lower concentration than in the samples of group D, in which the *Bifidobacterium lactis* was active (MRS + fish protein hydrolysate + *Bifido.*). Finally, when comparing the compounds of group E (MRS + seaweed extract) with the compounds of group F with probiotic (MRS + seaweed extract + *Bifido.*) , it can be observed that some compounds had a higher concentration in group E, and 4 compounds were lower.

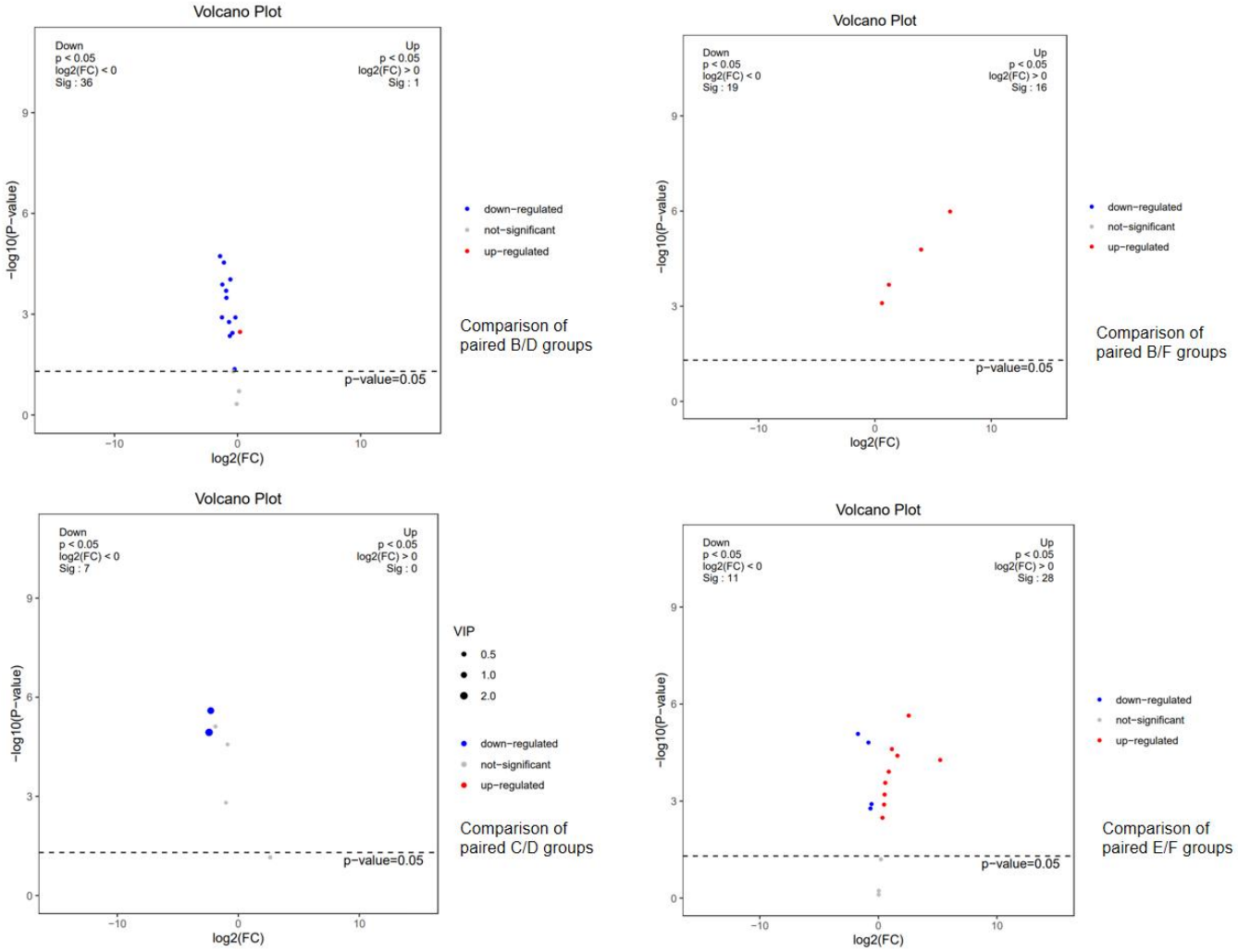

Figure 9. Volcano map of metabolic profiles of the compared experimental groups: B-F

B: MRS + *Bifido.*; C: MRS + F466Q022 (fish protein hydrolysate); D: MRS + F466Q022 (fish protein hydrolysate) + *Bifido.*; E: MRS + A114P252 (seaweed extract); F: MRS + A114P252 (seaweed extract) + *Bifido*

Each point in the figure represents a metabolite, the abscissa is the log2 (FC Fold Change) value of the two comparisons, the ordinate is the -log10 (*p*-value) value. Red dots represent differential metabolites with $p<0.05$ and FC>1, and blue dots represent differential metabolites with $p<0.05$ and FC<1.

4.1.6. Differential Metabolite Analysis

In order to more intuitively display the relationship between the samples and the expression differences of metabolites between different samples, the hierarchical clustering was performed on the expression of the total of significantly different metabolites and the top 20significantly different metabolites sorted by VIP (Hierarchical Clustering). These results are shown in the Figure 10. The abscissa indicates the sample name, and the ordinate indicates the differential metabolites. The color from blue to red indicates that the expression abundance of metabolites is from low to high, that is, the redder the color, the higher was the differential expression of the metabolites.

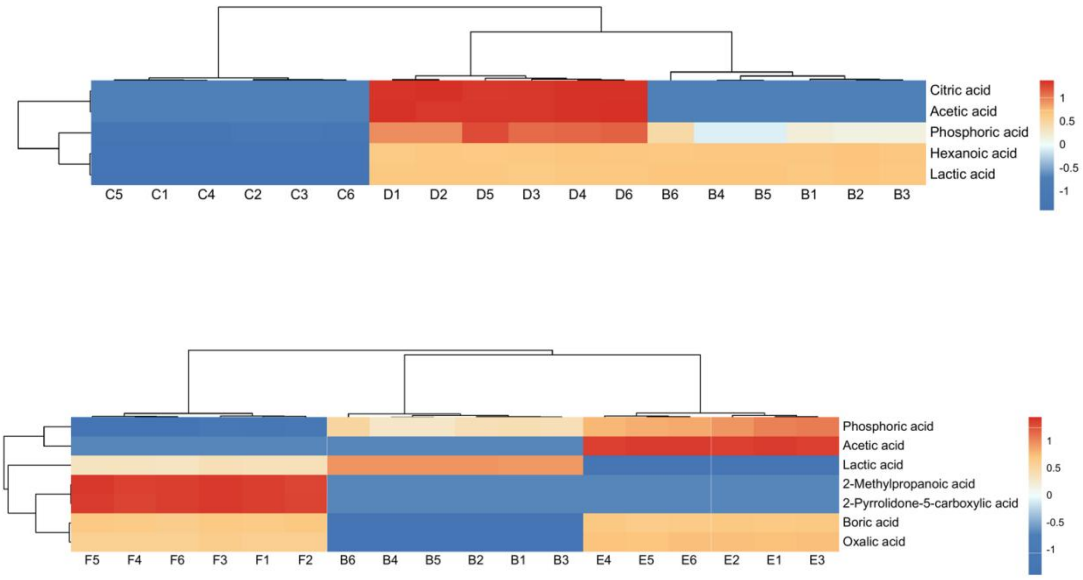

Figure 10. Differential metabolite clustering heatmap for different comparison groups: B/C/D and B/E/F： B: MRS + Bifido.; C: MRS + F466Q022 (fish protein hydrolysate); D: MRS + F466Q022 (fish protein hydrolysate) + Bifido.; E: MRS + A114P252 (seaweed extract); F: MRS + A114P252 (seaweed extract) + Bifido.

The horizontal axis represents the sample name, and the vertical axis represents the differential metabolites. The colors from blue to red represent the expression abundance of metabolites from low to high, that is, the redder the color, the higher the expression abundance of the differential metabolites.

When comparing groups B, C, D with each other, it was found that the highest concentration of metabolites was found in the samples from group D, in which the probiotic utilized fish prebiotic hydrolysate (MRS + fish protein hydrolysate + *Bifido.*). Only in the samples of group B (MRS + *Bifido.*), the lactic acid had a higher concentration. In turn, comparing the samples from groups B, E and F (MRS+seaweed extract + *Bifido.*), the concentration of latic acid was also the highest in group B (MRS + *Bifido.*), in which the probiotic utilized MRS as the only energy source. Whereas, the concentration of phosphoric acid and acetic acid increased in the samples of group E, in which the probiotic additionally utilized the liquid seaweed extract. For the other comparison variants it could be concluded that in general, the metabolites had higher concentrations in the F group samples: MRS + seaweed extract *Bifido.* (Figure 10)

A correlation on the top 20 significantly different metabolites sorted by VIP scoring was performed. The Pearson correlation coefficient was applied to measure the relationship between the two metabolites. Red color indicates positive correlation, and blue indicates the negative correlation. The larger the dot, the greater the correlation coefficient between the two variables is. The correlation point plot of differentially produced metabolites in groups B/C/D revealed that the major changes in the metabolites profile of *Bifidobacterium lactis* NCC2818 occurred when the prebiotic fish protein hydrolyzate (F466Q022) was added, as shown in Figure 11. The correlation point plot of differentially produced metabolites between the groups B/E/F showed that the main changes in metabolites produced by *Bifidobacterium lactis* NCC2818 were found when the liquid seaweed extract (A114P252) was added, as shown in Figure 12.

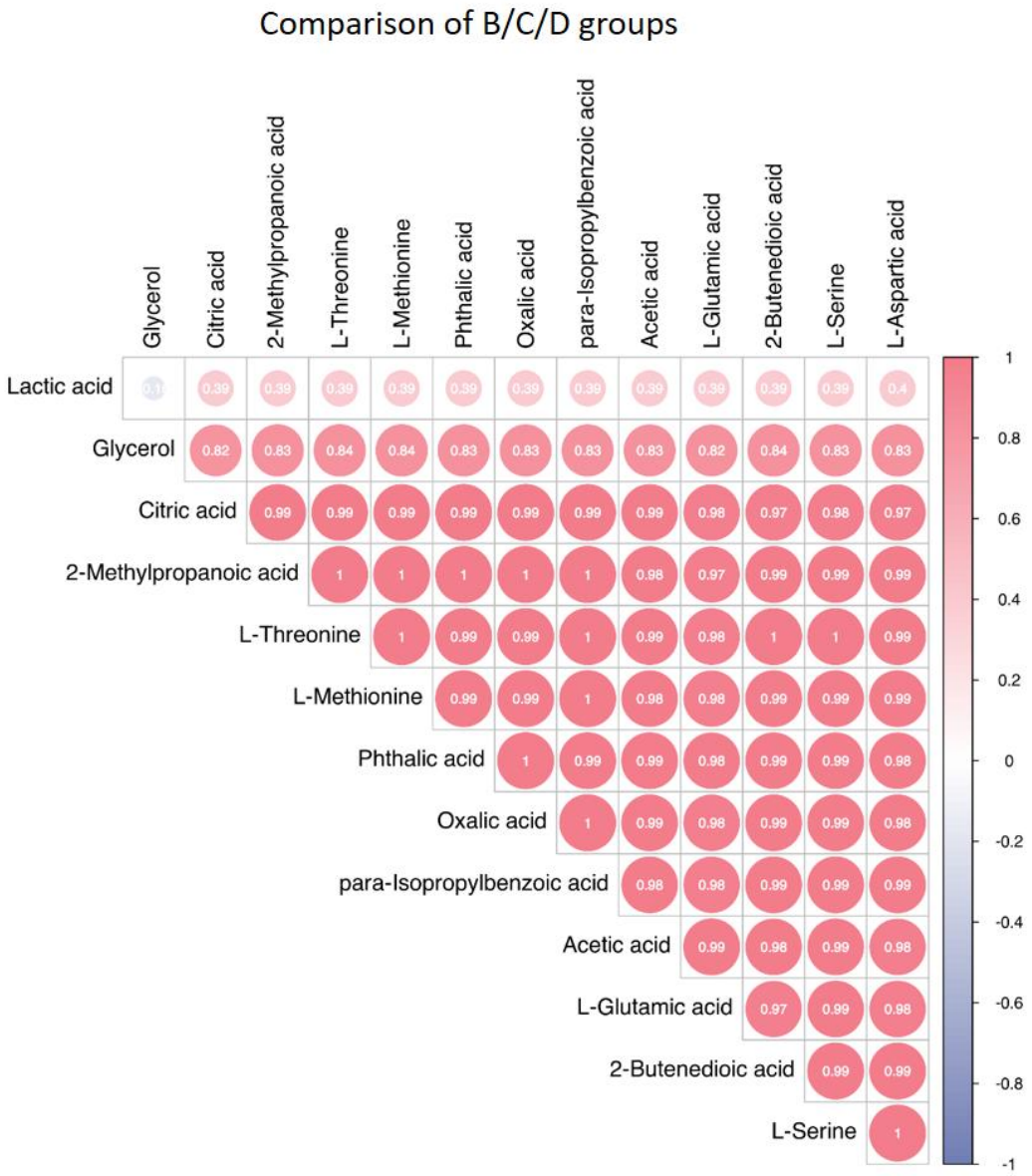

Figure 11. Correlation dot plot of differential metabolites in B/C/D groups: B (MRS + *Bifido.*), C (MRS + fish protein hydrolysate), D (MRS + fish protein hydrolysate + *Bifido.*)

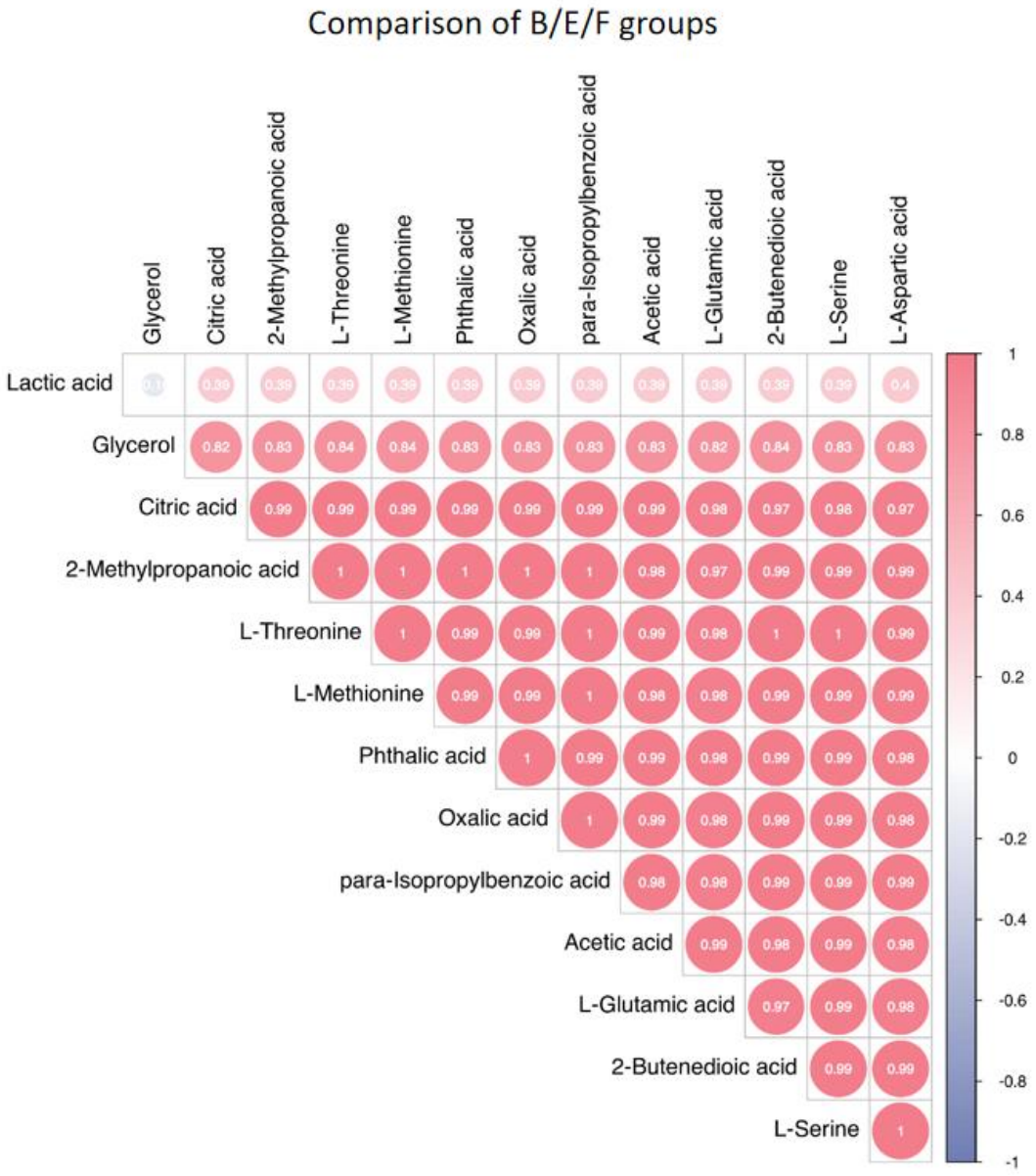

Figure 12. Correlation dot plot of differential metabolites in B/E/F groups: B (MRS + Bifido.), E (MRS + seaweed extract), F (MRS + seaweed extract + Bifido.)

According to the correlation analysis, almost all of the metabolites produced in B, C, and D groups were positively correlated with a high correlation coefficient. Therefore, the identified metabolites presented in the Figures 9-10 were correlated with the activity of the *Bifidobacterium lactis* probiotic depending on the energy source used by that probiotic (MRS medium only *versus* the supplementation with the fish hydrolysate protein prebiotic).

The metabolites of B, E, and F shown both positive and negative correlations. In particular, the lactic acid being negatively correlated with the rearrangement of probiotic metabolic activity due to addition of the liquid seaweed extract *in vitro*.

4.1.7. Metabolic pathway enrichment analysis

The pathway enrichment analysis of differentially produced metabolites allows to understand the mechanism of metabolic pathway changes. The KEGG ID enrichment results of metabolic pathways are presented in the Tables 5 and 6. A hypergeometric assay was used to identify pathway entries that were significantly enriched in metabolites with significantly differential expression compared to the overall background.

Table 5. Results of KEGG pathway enrichment analysis of the altered metabolites in B/C/D groups: B (MRS + *Bifido*.), C (MRS + fish protein hydrolysate), D (MRS + fish protein hydrolysate + *Bifido*.)

ID Annotation	Annotation	set	in background	background	RichFactor	p-value	-lg(p-value)	FDR correction
eco00190	Oxidative phosphorylation	2	16	3164	0,063	0,010	1,996	0,039
eco00010	Glycolysis / Gluconeogenesis	2	31	3164	0,032	0,020	1,710	0,039
eco00620	Pyruvate metabolism	2	31	3164	0,032	0,020	1,710	0,039
eco02020	Two-component system	2	41	3164	0,024	0,026	1,589	0,039
eco02024	Quorum sensing	2	42	3164	0,024	0,026	1,579	0,039
eco00640	Propanoate metabolism	2	48	3164	0,021	0,030	1,521	0,039
eco00051	Fructose and mannose metabolism	2	54	3164	0,019	0,034	1,470	0,039
eco02010	ABC transporters	2	93	3164	0,011	0,050	1,301	0,039

Table 6. Results of KEGG pathway enrichment analysis of the altered metabolites in B/E/F groups: B (MRS+*Bifido*.), E (MRS+seaweed extract), F (MRS+seaweed extract+*Bifido.*)

ID Annotation	Annotation	set	in background	background	RichFactor	*p*-value	-lg(p-value)	FDR correction
eco02020	Two-component system	3	41	3164	0,0488	0,0005	3,3120	0,0059
eco00190	Oxidative phosphorylation	3	16	3164	0,0625	0,0151	1,8211	0,0499
eco00020	Citrate cycle (TCA cycle)	3	20	3164	0,0500	0,0188	1,7247	0,0499
eco01053	Biosynthesis of siderophore group nonribosomal peptides	3	24	3164	0,0417	0,0226	1,6461	0,0499
eco00250	Alanine, aspartate and glutamate metabolism	3	28	3164	0,0357	0,0263	1,5797	0,0499
eco00010	Glycolysis / Gluconeogenesis	3	31	3164	0,0323	0,0291	1,5359	0,0499
eco00620	Pyruvate metabolism	3	31	3164	0,0323	0,0291	1,5359	0,0499
eco02024	Quorum sensing	3	42	3164	0,0238	0,0393	1,4055	0,0590
eco00640	Propanoate metabolism	3	48	3164	0,0208	0,0448	1,3483	0,0598
eco00051	Fructose and mannose metabolism	3	54	3164	0,0185	0,0503	1,2980	0,0604
eco00630	Glyoxylate and dicarboxylate metabolism	3	62	3164	0,0161	0,0500	1,3010	0,0629
eco02010	ABC transporters	3	93	3164	0,0108	0,0501	1,3002	0,0856

The descriptors of the parameters in the Tables 5-6 columns are as follows:

- ID Annotation: the ID number of the metabolic pathway
- Annotation: Metabolic pathway name (according to the KEGG)
- set: number of differential metabolites involved in all pathways
- in background: the total number of metabolites belonging to the model species in the pathway
- background: total number of metabolites belonging to the model species across all pathways
- RichFactor: enrichment factor, calculated as 'set' divided by 'in background'
- *p*-value: the hypergeometric test p-value of the metabolic pathway
- –lg(p-value): The logarithm of the p value based on 10, the smaller the *p* value, the larger the value
- FDR correction: FDR (False Discovery Rate) corrected p-value

Further, the *p*-value in the metabolic pathway is the significance of the enrichment of the metabolic pathway. The significant enrichment pathways were selected based on p-value to draw the bubble diagram (Figure 13 and 14). The ordinate indicates the name of the metabolic pathway; the abscissa indicates the enrichment factor (Rich factor = number of significantly different metabolites/total number of metabolites in this pathway). The larger the Rich factor, the greater the degree of enrichment was. The color gradually changing from green to red indicates that the p-value decreases. The larger the point (bubble), the more metabolites were enriched in the pathway.

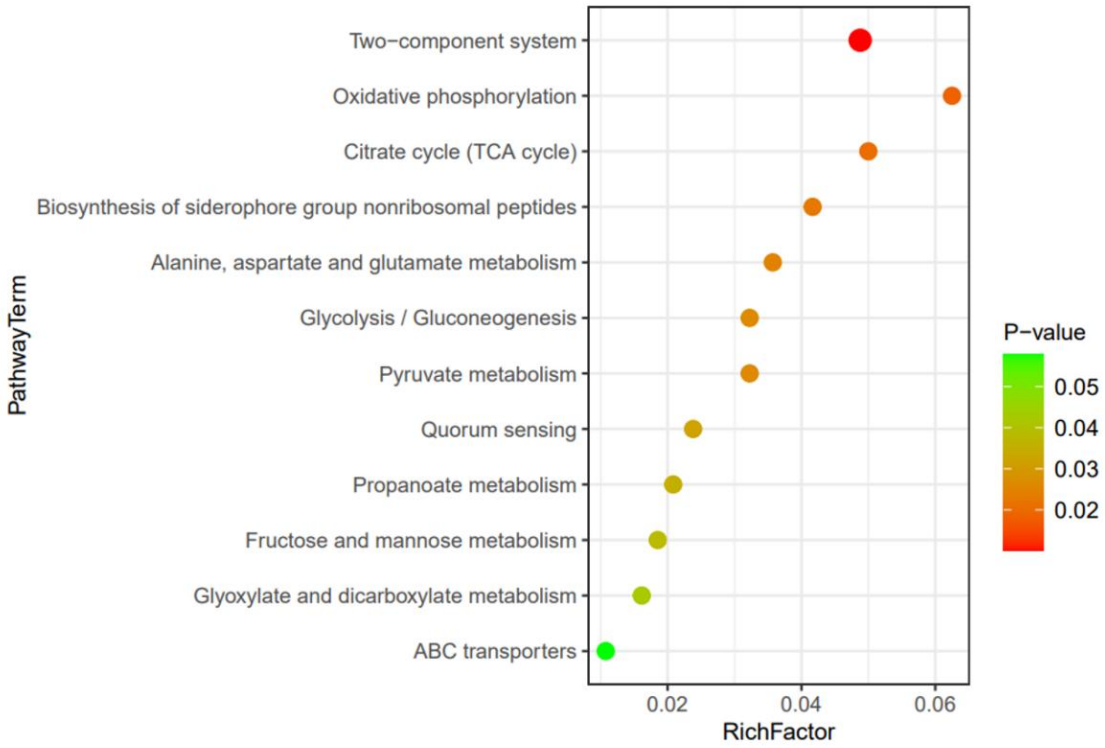

Figure 13. Significance bubble plots of enrichment of altered metabolic pathways in the B/C/D groups: B (MRS + *Bifido.*), C (MRS + fish protein hydrolysate), D (MRS + fish protein hydrolysate + *Bifido.*)

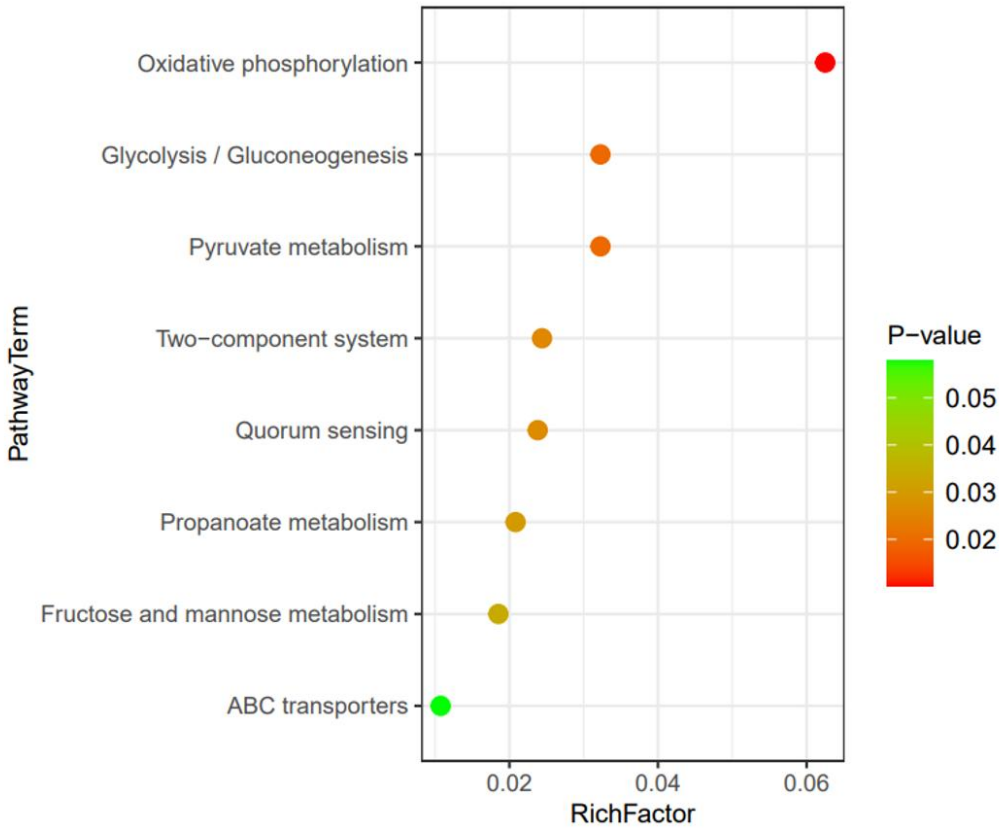

Figure 14. Significance bubble plots of enrichment of altered metabolic pathways in the B/E/F groups: B (MRS + *Bifido.*), E (MRS + seaweed extract), F (MRS + seaweed extract + *Bifido.*)

Based on the enrichment analysis of the differentially produced metabolites, top nine metabolic pathways with a p-value lower than 0.05 were found in the comparison of B (MRS +*Bifido.*), C (MRS + fish protein hydrolysate), and D (MRS + fish protein hydrolysate + *Bifido.*) groups, the most significant of which was the enrichment of the Two component system pathway. In the comparison of B (MRS + *Bifido.*), E (MRS+ seaweed extract), and F (MRS + seaweed extract + *Bifido.*) groups, 8 top metabolic pathways with a *p*-value lower than 0.05 were found, the most significant of which was the enrichment of Oxidative phosphorylation pathway.

4.2. Characterization of the intestinal co-culture model

4.2.1. Growth of intestinal cells in the monolayer model

a/ **The observation of the cell morphology and growth dynamics** of Chic-8E11 cells is represented in Figure 15. After the Chic-8E11 cells adhered to the bottom of the bottle (Figure 15. a), the heterogenic cytological morphology of epithelial (polygonal) and spindle-like (fibroblast-like) shapes was observed. The cell confluence reached approximately 40% after 4 days (Figure 15. b). After 8 days, the cells were fused to 100% confluency, forminga complete Chic-8E11 cell monolayer (Figure 15. c).

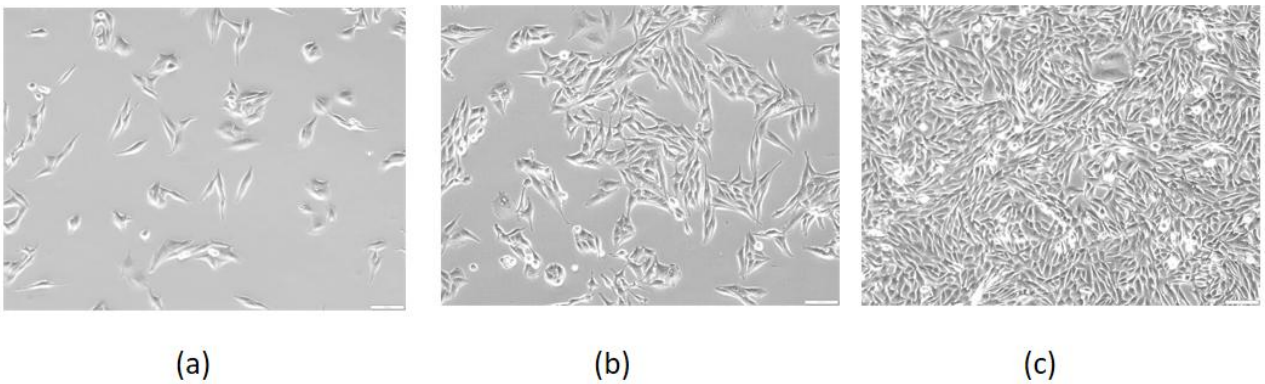

Figure 15. Microscopic images of Chic-8E11 cells, scale bar 100 µm, magnification x100.

(a) The cells have just begun to adhere to the plate; (b) The cells have grown to about 40% confluence; (c) The cells have grown to 100% confluence, forming a complete Cell monolayer.

Similarly, the *in vitro* adherence phases and growth process of Caco-2 cells was observed and recorded, as shown in Figure 16. After the Caco-2 cells adhered to the bottom of the bottle, the cytological morphology was epithelial and polygonal, reaching approximately 60% confluence after 4 days, and 100% confluence (Figure 16. c) within 7 days to form a uniformed homogenic Caco-2 cell monolayer.

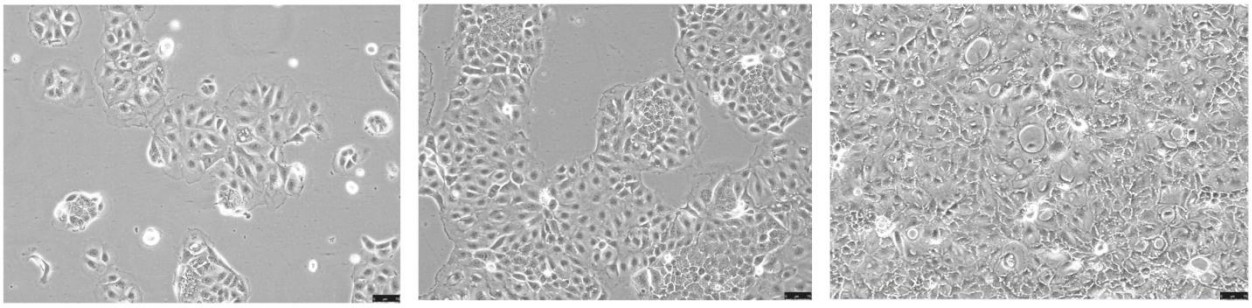

(a) (b) (c)

Figure 16. Microscopic images of Caco-2 cells growth *in vitro*, scale bar 75µm, magnification x130.

(a) The initial stage: static attachment of the cells; (b) The cells at about 60% confluence; (c) The cells after reaching 100% confluence, forming a complete of cell monolayer.

b/ **Staining with the epithelial markers.** As shown in Figure 17, the phalloidin-DAPI cell actin fluorescence staining showed the actin microfilaments appearing green in the cell structure (phalloidin fluorescence), and the cell nuclei appearing blue (DAPI fluorescence). The actin microfilaments of Chic-8E11 cells confirmed the spindle-like and polygonal shape documented in the light microscope. The adjacent cells were closely connected and there was a partial overlap and coverage observed between cells. Caco-2 cells had a homogenous cuboidal morphology. The actin microfilaments of Caco-2 cells reflected the polygonal shape of the cells. When Caco-2 cells adhere and grow on the plate, The attached Caco-2 cells were tightly connected with each other and showed a tendency to grow fast, forming almost completely flat monolayer, with no overlaps. Moreover, the edges of separate cell colonies were clearly distinguished with vibrant borders, indicating the progressing expansion.

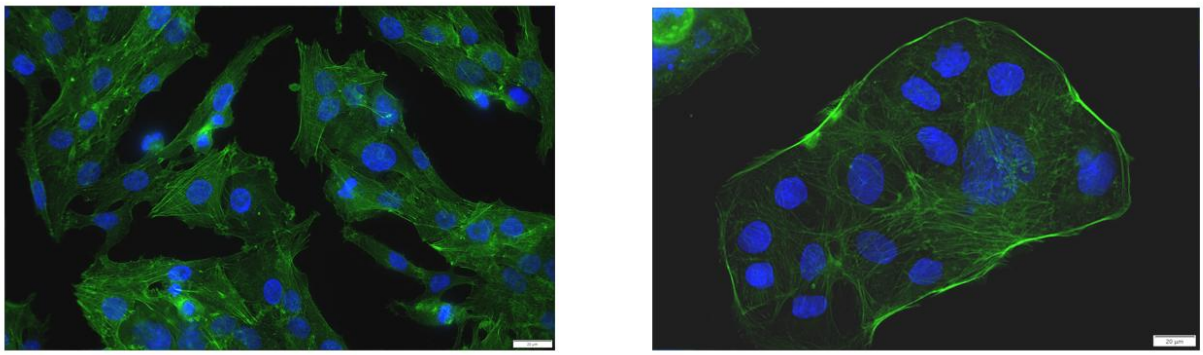

Chic-8E11 CACO-2

Figure 17. Confocal images of phalloidin-DAPI cell protein staining of Chic-8E11 and Caco-2 cells, scale bar 20µm, magnification x500.

4.2.2. Intestinal cells spheroid model

The separated microspheres formed in the microwell plate were introduced into the bioreactor, and were continuously rotated and cultured in the Spheroid culture in ClinoStar™ - CO_2 Incubator. Cell spheroids of different sizes were formed at different times to adjust the rotation speed.

The intestinal spheroids formed after 12 days varied in shape, and the size of the spheres was approximately 0.5 to 1.5 mm in diameter. The images of Chic-8E11 cell spheroids formation are shown in Figure 18. First, in the microwell plate , the Chic-8E11 cells formed numerous isolated microspheres with compact connections between the cells. After transfer to the rotating bioreactor vessel (10 rpm, slowly increasing from 1 rpm to 10 rpm, approximately 0.5 rpm/h) for one day, the Chic-8E11 cell spheroids began to grow rapidly, and the spheres volumes did become larger. The bioreactor rotation speed increased to 25 rpm. After 12 days, the bioreactor rotation speed reached 30 rpm, and the Chic-8E11 cell spheroids volume increased. When the volume of cell spheroids no longer increases, it can be observed that intestinal spheroids are basically formed. After two weeks of culture, the oblate intestinal spheroids were observed, irregular in shape, reorganizing, resembling the intestinal organoid early stages.

The images of Caco-2 cell spheroids during their formation are shown in Figure 19. Caco-2 cells formed microspheres with relatively loose connections between the cells in a microwell plate. Upon the transfer of the progenitor spheres to the bioreactor, it was rotated at a low speed of 5 rpm. The Caco-2 cell spheroids began to grow slowly, and as the bioreactor speed up approximately 1rpm per day to 15rpm, the volume of spheroid increased slowly. After 12 days of culture, the Caco-2 spheroids were considered as formed. In contrast with Chic-8E11 cells, the intestinal spheroids of Caco-2 cells were less compact, with a centralized shape in the center and loose sphere borders.

Figure 18. Images of Chic-8E11 cell spheroids at different times of culture in a rotating bioreactor, at 50x magnification. The speed of rotation was gradually increased to: (a) 10 rpm after 1 day; (b) 25 rpm after 6 days; (c) 30 rpm after 12 days.

Figure 19. Images of the Caco-2 cell spheroids at different times of culture in a rotating bioreactor, at 50x magnification. The speed of rotation was gradually increased to: (a) 5 rpm at day 1; (b) 10 rpm after 6 days; (c) 15 rpm after 12 days.

4.3. *In vitro* characterization of a direct interaction of probiotics (*Bifidobacterium lactis* and *Bacillus strain*) with the intestinal cells in co-culture model

4.3.1. Optimization of a probiotic ratio in a co-culture system

MTT colorimetry was used to determine intestinal cells viability in two different co-culture systems with different ratios of probiotic supplementation. The higher the absorbance value, the higher the viability of the cells was. The Caco-2 cells and Chic-8E11 cells were incubated with *Bifidobacterium lactis* NCC2818 (*Bifido.*) and *Bacillus* strain (*Bacilllus*), or with probiotic supernatants at different ratios bacteria (CFU) : cells (n): (30:2; 15:2; 10:2; 5:2; 2: 2; 1:2). All the ratios combinations were evaluated under the same conditions for 24 hours. The results are illustrated in the Figures 20-27. In total, there were four different co-culture systems of the tested intestinal cells and probiotics: a/ Chic-8E11 cells and *Bifido.* (or *Bifido.* supernatant), Figures 20-21; b/ Chic-8E11 cells and *Bacillus* (or *Bacillus* supernatant), Figures 22-23; c/ Caco-2 cells and *Bifido.* (or *Bifido.* supernatant), Figures 24-25; d/ Caco-2 cells and *Bacillus* (or *Bacillus* supernatant), Figures 26-27. Based on the MTT test results and the morphological microscopic assesment of the co-cultures, it was found that the ratio of 10:2 (bacteria (CFU): number of cells) was optimal. This ratio was applied in the subsequent experimental co-cultures.

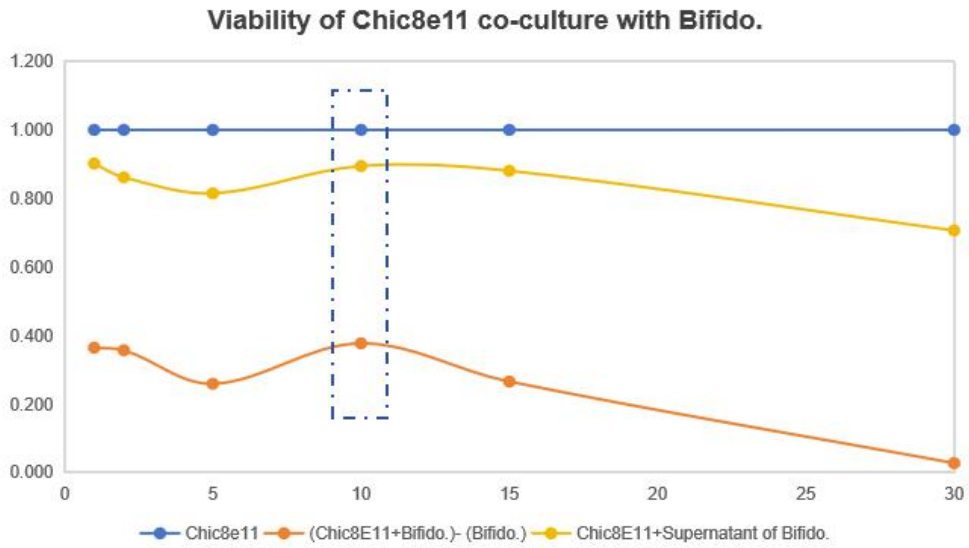

Figure 20. Viability trend of co-culture of Chic-8E11 cells and *Bifido.* (or *Bifido.* supernatant).

Blue line = Chic8E11: absorbance value of Chic8E11 cells alone; orange line = (Chic8E11 + *Bifido.*) - (*Bifido.*): absorbance value of Chic-8E11 cells co-cultured with *Bifido.* minus the absorbance value of probiotic *Bifido.*, eliminating the effect of probiotic *Bifido.* from the MTT absorbance value; yellow line = Chic8E11 + Supernatant of *Bifido.*: absorbance value of Chic-8E11 cells cultivated with the addition of *Bifido.* supernatant.

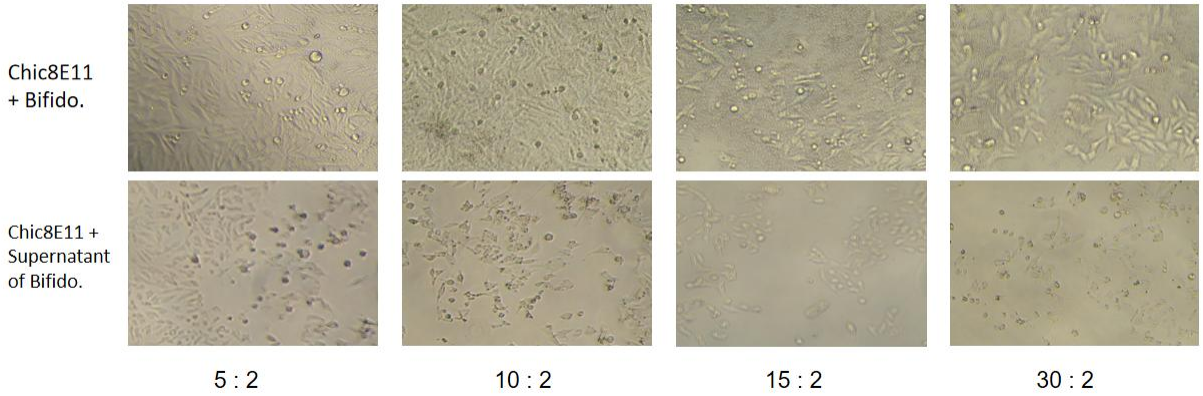

Figure 21. Light microscope images of Chic-8E11 cells co-cultured at different rations with *Bifido.* or addition of *Bifido.* supernatant.

Ratios are given for bacteria (CFU): cells (n), magnification x100.

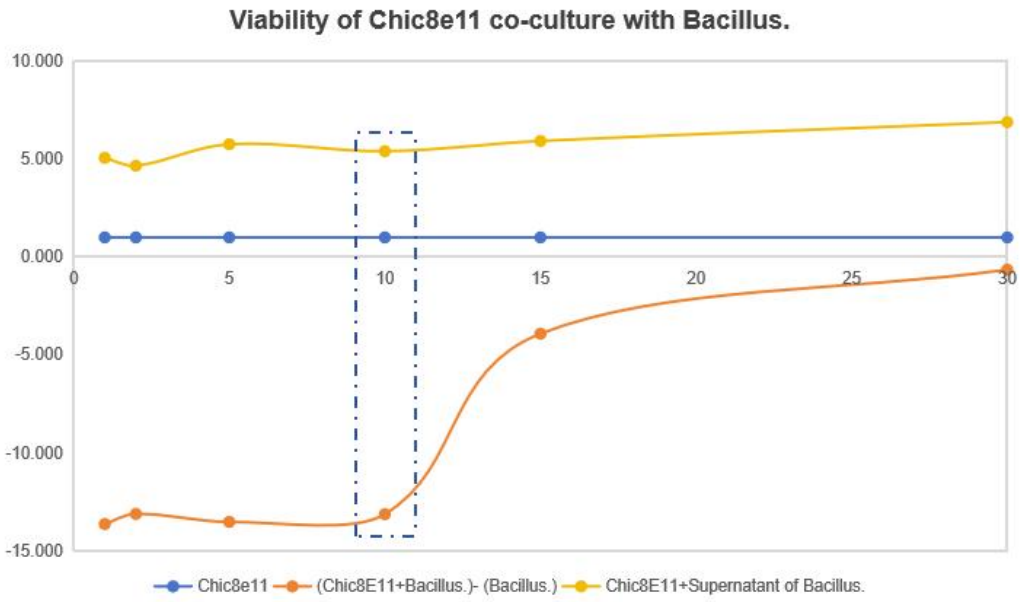

Figure 22. Viability trend of co-culture of Chic-8E11 cells and *Bacillus* or addition of *Bacillus* supernatant.

Blue line = Chic-8E11: absorbance of Chic8-E11 cells only; orange line = (Chic-8E11 + *Bacillus*) - (*Bacillus*): absorbance of Chic-8E11 cells co-cultured with *Bacillus* minus the absorbance of probiotic *Bacillus*, eliminating the effect of probiotic *Bacillus* from the MTT absorbance; yellow line = Chic8E11 + Supernatant of *Bacillus*: absorbance of Chic-8E11 cells cultured with the supernatant of *Bacillus* added.

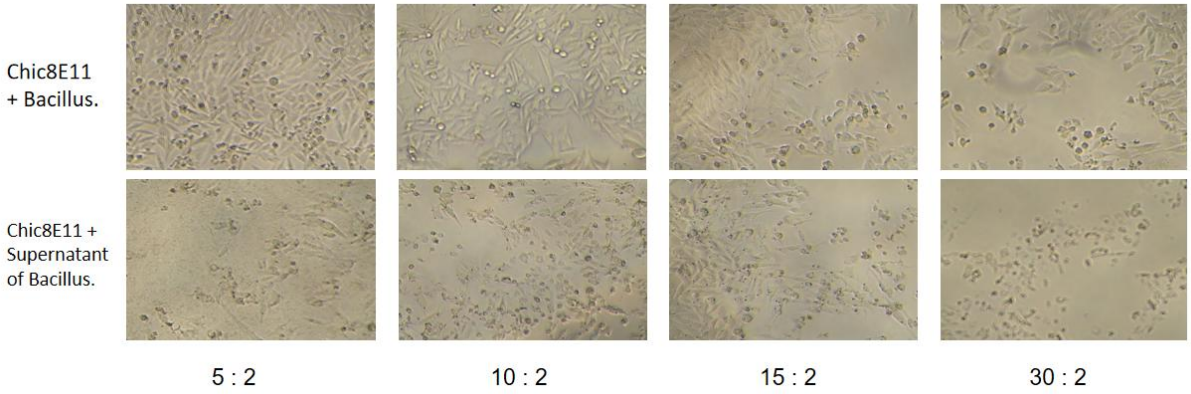

Figure 23. Light microscope images of Chic-8E11 cells co-cultured at different ratios with *Bacillus* or addition of *Bacillus* supernatant.

Ratios are given for bacteria (CFU): cells (n), magnification x100.

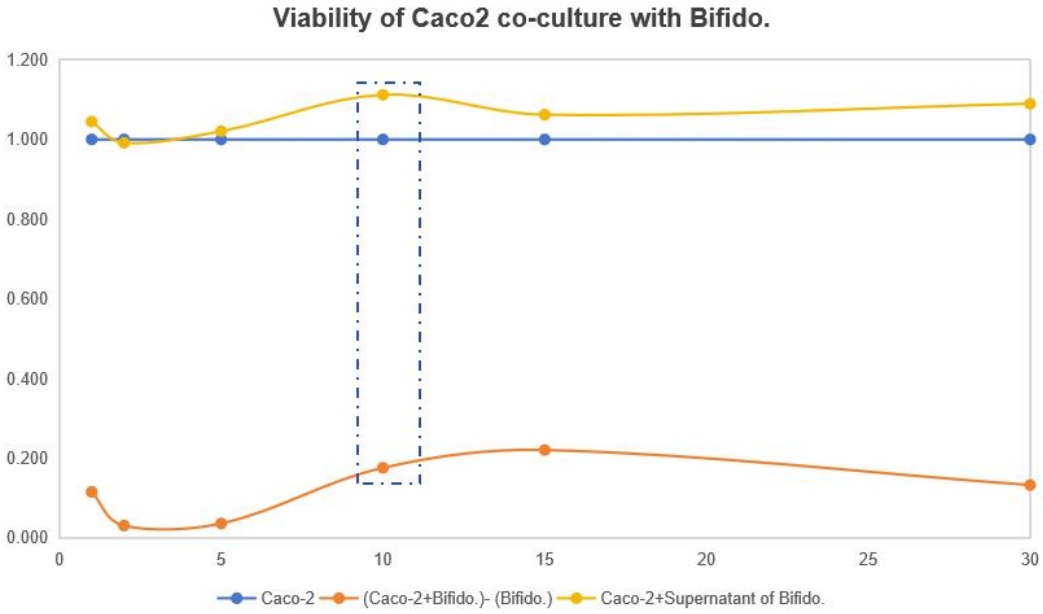

Figure 24. Viability trend of co-culture of Caco-2 cells with *Bifido.* or addition of *Bifido.* supernatant.

Blue line = Caco-2: absorbance of Caco-2 cells only; orange line = (Caco-2 + *Bifido.*) - (*Bifido.*): absorbance of Caco-2 cells co-cultured with *Bifido.* minus the absorbance of probiotic *Bifido.*, eliminating the effect of probiotic *Bifido.* from the MTT absorbance readout; yellow line = Caco-2 + Supernatant of *Bifido.*: absorbance of Caco-2 cells cultured with *Bifido.* supernatant added.

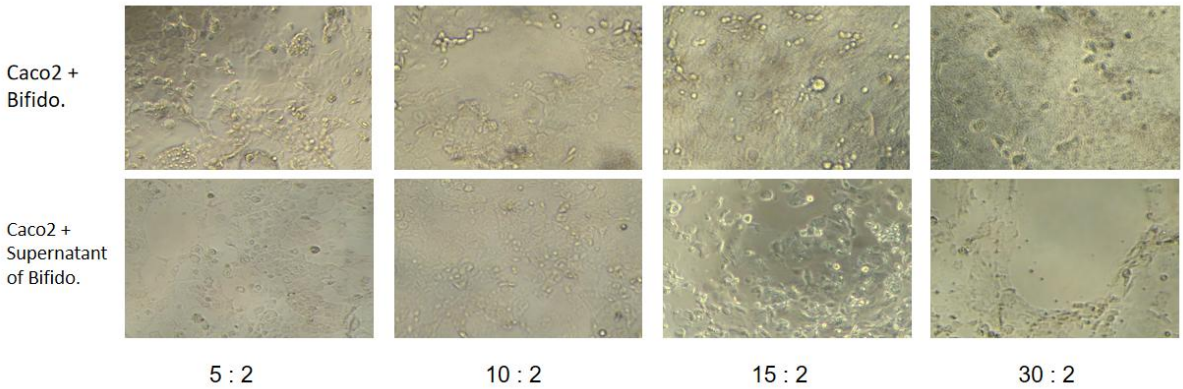

Figure 25. Light microscope images of Caco-2 cells co-cultured at different ratios with *Bifido.* or addition of *Bifido.* supernatant. at 100x magnification.

Ratios are given for bacteria (CFU): cells (n), magnification x100

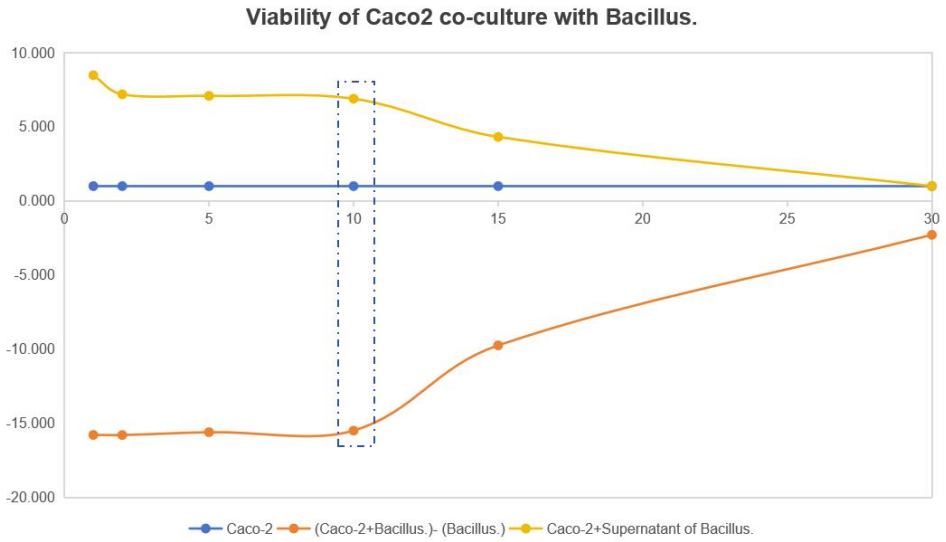

Figure 26. The viability trend of co-culture of Caco-2 cells with *Bacillus* or addition of *Bacillus* supernatant.

In the legend, the blue line Caco-2 represents the absorbance value of Caco-2 cells alone; the orange line (Caco-2 + *Bacillus*) - (*Bacillus*) represents the absorbance value of Caco-2 cells and *Bacillus* co-culture minus the absorbance value of probiotic *Bacillus* alone, eliminating the effect of probiotic *Bacillus* from the MTT absorbance value; the yellow line Caco-2 + Supernatant of *Bacillus* represents the absorbance value of Caco-2 cells cultured with the addition of supernatant of *Bacillus*.

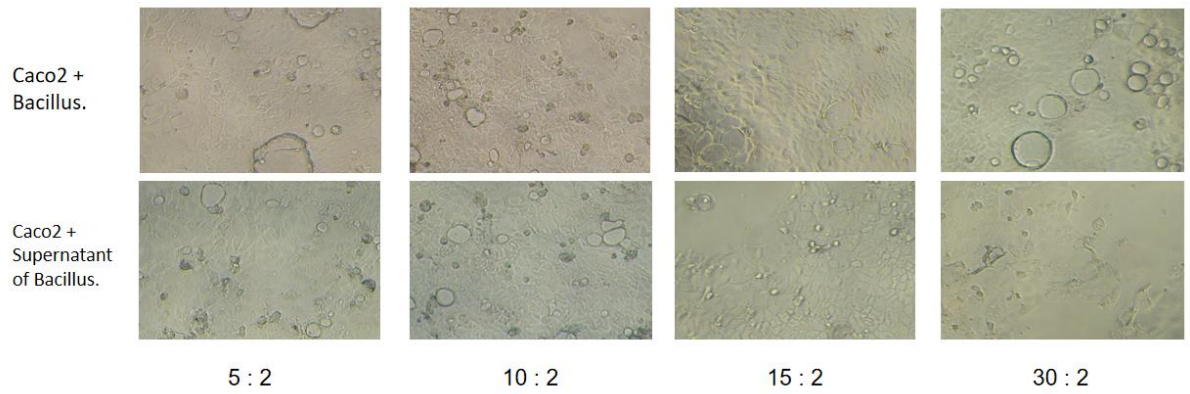

Figure 27. Light microscope images of Caco-2 cells co-cultured at different ratios with *Bacillus* or addition of *Bacillus* supernatant.

Ratios are given for bacteria (CFU): cells (n), magnification x100.

4.3.2. Probiotic adhesion assays to biological (non-biological) surfaces and to the intestinal cells

The adhesion of probiotics *Bacillus strain* and *Bifidobacterium lactis* NCC2818 on polystyrene (non-biological) and mucin (biological) surfaces was evaluated by spectrophotometric measurement of absorbance at 570 nm (OD570). As shown in Figure 28, the adhesion potential of *Bacillus strain* and *Bifidobacterium lactis* NCC2818 on polystyrene (non-biological) and mucin (biological) surfaces was demonstrated. The OD value of mucin alone was used as a negative control. *Bacillus strain* showed an increased adhesion to the mucin surface, and *Bifidobacterium lactis* NCC2818 showed stronger adhesion to the mucin surface. On the non-biological surface of polystyrene, both *Bacillus strain* and *Bifidobacterium lactis* NCC2818 showed low, but still detectable adhesion.

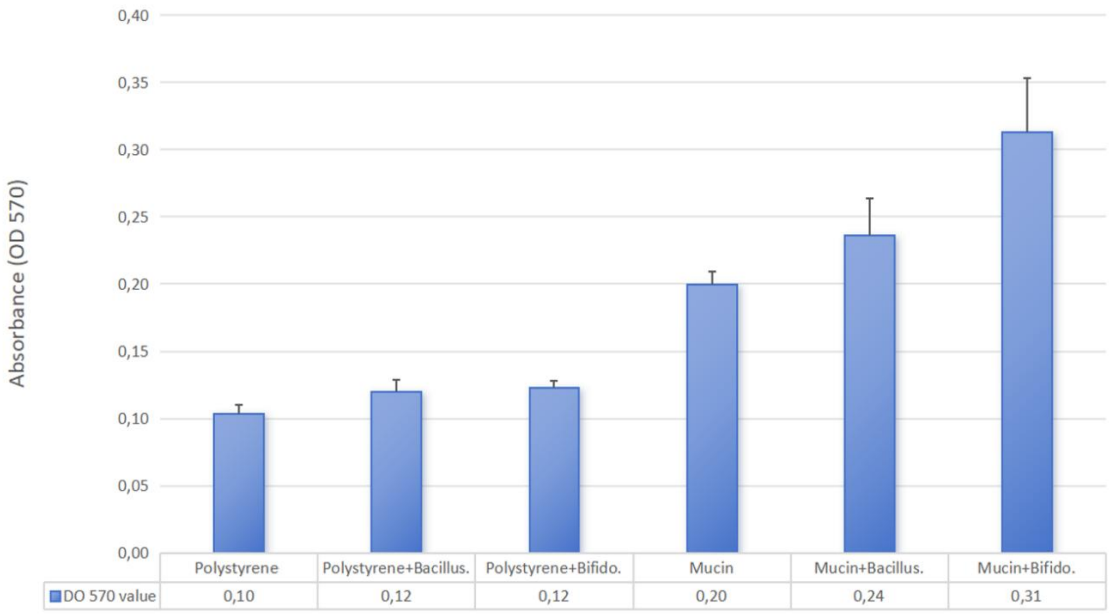

Figure 28. *In vitro* adhesion tests of the probiotics *Bacillus strain* and *Bifidobacterium lactis* NCC2818 to abiotic and biotic surfaces.

Polystyrene (abiotic) and mucin-coated polystyrene (biotic) microplates were stained and the absorbance results were expressed by optical density (OD). Mean ± SD of two independent experiments were shown.

The viable bacterial count method was applied to detect and analyze the adhesion ability of the investigated probiotics to intestinal cells. As it can be noted in the Figure 29, the adhesion force of *Bifidobacterium lactis* NCC2818 to both Caco-2 cells and Chic-8E11 cells was relatively high, and the adhesion force to Chic-8E11 cells appeared stronger than that to Caco-2 cells. In contrast, *Bacillus strain* showed a strong adhesion only to the Chic-8E11 cells. Moreover, the *Bacillus* adhesion to Chic-8E11 cells was stronger than *Bifidobacterium lactis* NCC2818.

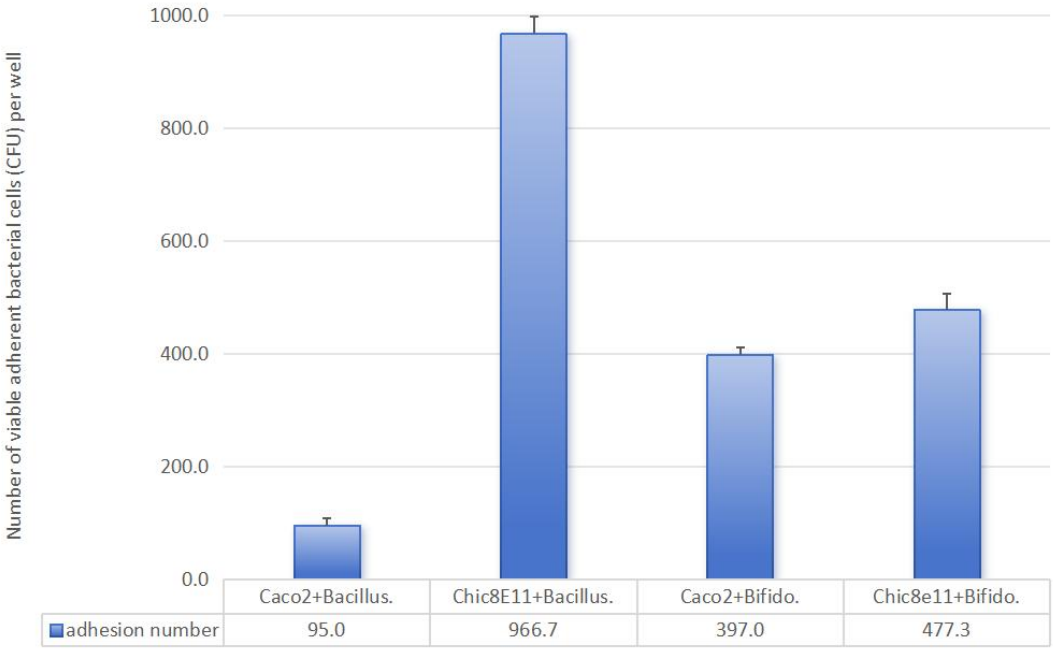

Figure 29. Number of viable, attached bacterial cells (CFU) in different co-culture combinations. The same numbers of probiotic cells were seeded in each testing well. The mean ± SD of the number of probiotic adhered in the four co-culture systems is shown.

4.3.3. qPCR detection of cell target gene expression

The Real-time quantitative PCR was used to detect changes in the expression of genes related to the intestinal cells and tight junctions under various co-culture systems. As shown in Figure 30, after Chic-8E11 cells were co-cultured with *Bifido.*, the supernatant of *Bifido.*, and Bacillus or supplemented with the supernatant of *Bacillus*, the expressions of villin, cytokeratin 18, zonula occludens-1 and occludin genes were up-regulated or

down-regulated to varying degrees. Among them, after co-culture with *Bifidobacterium lactis* NCC2818, the villin gene [VIL1] of Chic-8E11 cells was significantly up-regulated ($p < 0.05$), and the occludin gene was significantly up-regulated ($p < 0.01$). In addition, the cytokeratin 18 gene was significantly up-regulated ($p < 0.01$) and the occludin gene was also extremely significantly upregulated ($p < 0.01$) under the action of supernatant. After co-culture with *Bacillus altitudinis*, the Zonula occludens-1 gene of Chic-8E11 cells was significantly downregulated ($p < 0.01$). As shown in Figure 31, after Caco-2 cells were co-cultured with *Bifido.* (or the supernatant of *Bifido.*) and *Bacillus* (or the supernatant of *Bacillus*), E-cadherin, villin, cytokeratin 18, cytokeratin 20, zonula occludens-1, occludin, claudin-1 and interleukin 18 genes expressions were all up-regulated or down-regulated to varying degrees. Among them, after co-culture with *Bacillus altitudinis*, the cytokeratin 18 gene of Caco-2 cells was significantly up-regulated ($p < 0.01$), and the cytokeratin 20 gene was significantly up-regulated ($p < 0.01$), while the E-cadherin and interleukin 18 genes were significantly down-regulated ($p < 0.01$). Under the action of its supernatant, the cytokeratin 20 gene of Caco-2 cells was also significantly up-regulated ($p < 0.05$), and the claudin-1 gene was significantly up-regulated ($p < 0.01$). After co-culture with *Bifidobacterium lactis* NCC2818, the E-cadherin, zonula occludens-1, occludin, claudin-1, and interleukin 18 genes of Caco-2 cells were significantly up-regulated ($p < 0.01$). Under the action of *Bifido.* supernatant, the zonula occludens-1 gene of Caco-2 cells was significantly up-regulated ($p < 0.05$), and the occludin and claudin-1 genes were also significantly high up-regulated ($p < 0.01$).

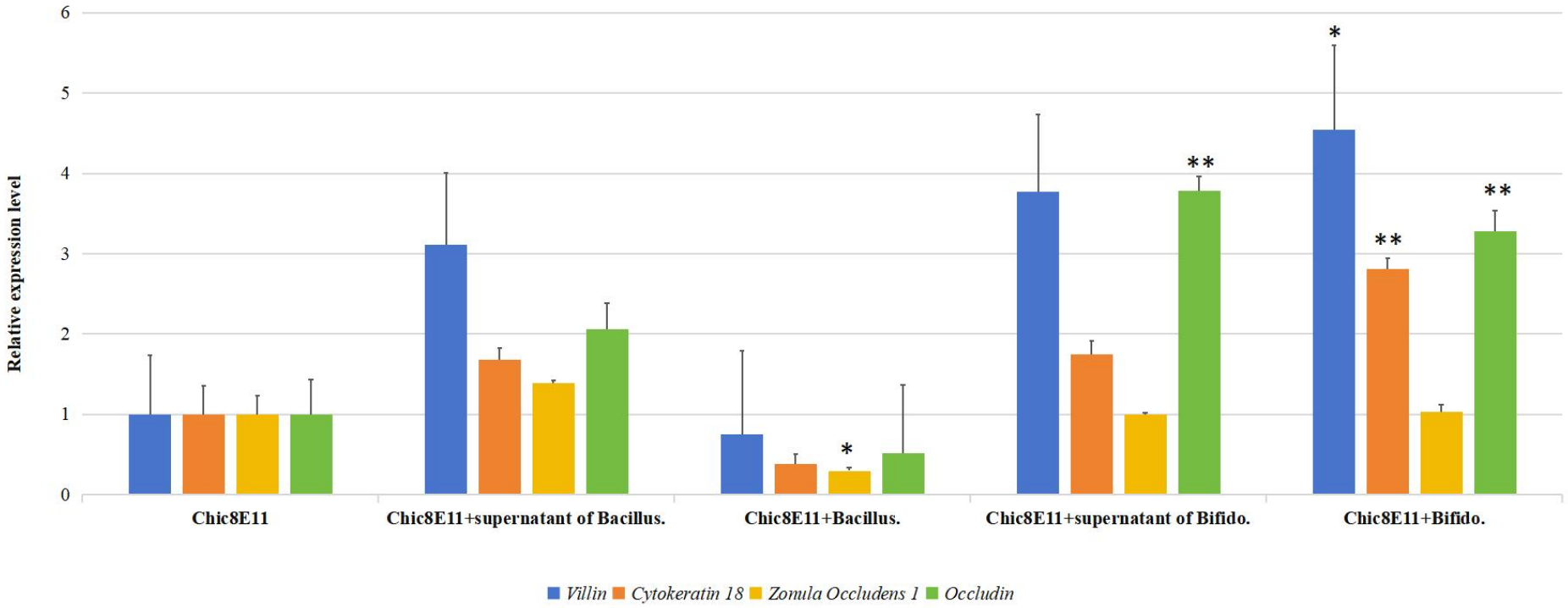

Figure 30. Relative expression levels of villin, cytokeratin 18, zonula occludens-1 and occludin genes in Chic-8E11 cells after co-culture with *Bifido.* or addition of *Bifido.* supernatant and *Bacillus* or addition of *Bacillus* supernatant.

* indicates $p<0.05$, ** indicates $p<0.01$

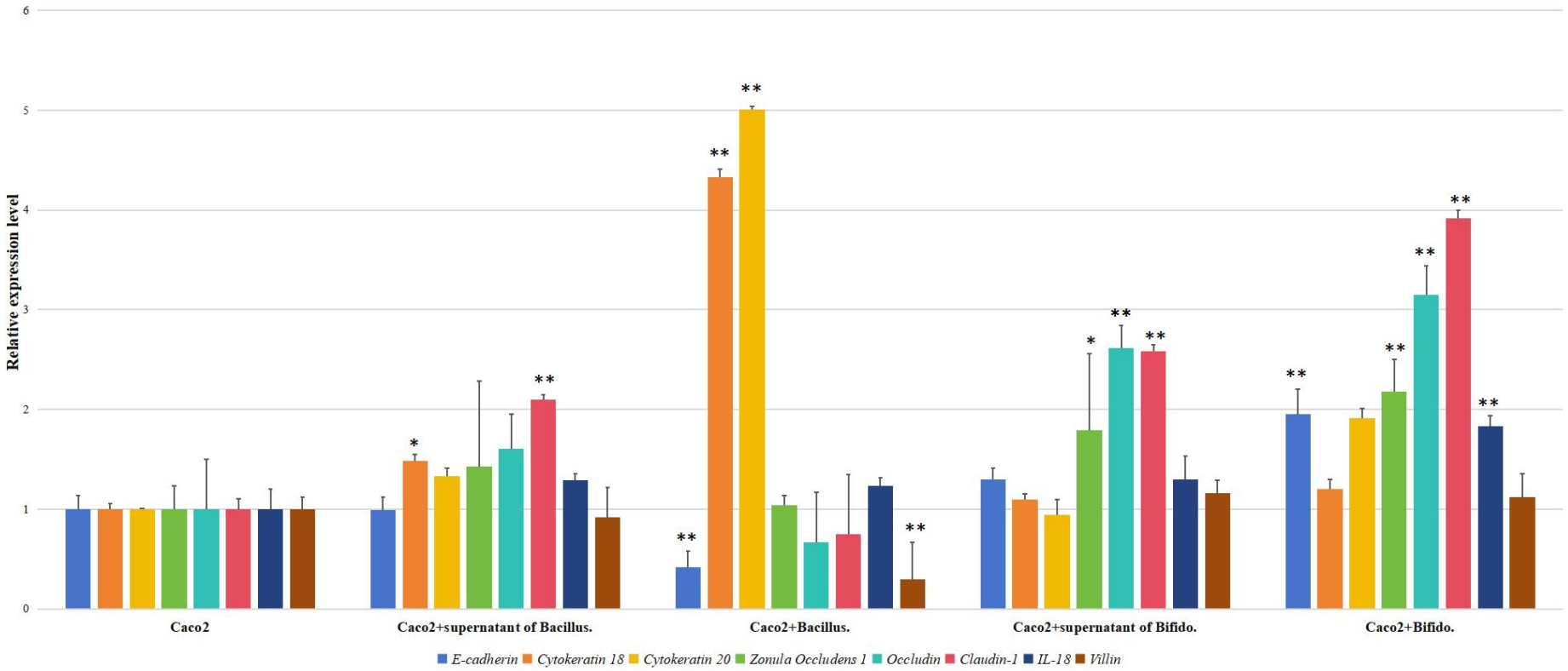

Figure 31. Relative expression levels of E-cadherin, villin, cytokeratin 18, cytokeratin 20, zonula occludens-1, occludin, claudin-1 and interleukin 18 genes in Caco-2 cells after co-culture with *Bifido.* or addition of *Bifido.* supernatant, and with *Bacillus* or addition of *Bacillus* supernatant.

* indicates $p<0.05$, ** indicates $p<0.01$.

4.3.4. Immunofluorescent staining of cell markers

Caco-2 and Chic-8E11 cells were co-cultured with the probiotics *Bifidobacterium lactis* NCC2818 *and Bacillus* strain*,* and their supernatants, respectively. Fluorescent staining of protein markers related with tight cell-cell junctions and cytoskeleton structure of enterocytes, was performed in four different cell-probiotic co-culture systems: a/ Chic-8E11 cells with *Bifido.* or addtion of *Bifido.* supernatant; b/ Chic-8E11 cells with *Bacillus* or addtion of *Bacillus* supernatant; c/ Caco-2 cells with *Bifido.* or addtion of *Bifido.* supernatant; d/ Caco-2 cells with *Bacillus* or addtion of *Bacillus* supernatant. The Caco-2 and Chic-8E11 cell culture alone, were set as blank control groups. The following proteins were analyzed: CHD1, CK18, ZO1, OCCL, CLDN, desmoplakin (DMPK) and vimentin (VIM)

The immunofluorescent images were organized into a matrix according to the classification of different protein markers to facilitate the comparison of the groups under the above different co-culture systems, as shown in Figures 32 - 42. The fluorescent protein markers of CHD1, CK18, ZO1, OCCL, CLDN, DMPK and VIM bind to cells' proteins, which can be presented as red fluorescence signals of Alexa Fluor 555 or green fluorescence signals of Alexa Fluor 488 dye. DAPI fluorescent dye penetrates the intact cell membrane and strongly binds to DNA to show dark blue fluorescence signals, which can locate the position of cells under the microscope fluorescence mode.

As shown in Figure 32, the ZO1 (red) protein marker is expressed at the edge of the Chic8E11 cell monolayer. After the co-culture with *Bacillus*, the ZO1 protein fluorescence signal of Chic8E11 cells was not significantly different from that of the control group. Similarly, after Chic-8E11 cells were co-cultured with *Bifido.* or the supernatant of *Bifido.*, there was no significant difference in the ZO1 protein fluorescence signal. However, when the supernatant of *Bacillus* was added, the ZO1 protein fluorescence signal of Chic8E11 cells was enhanced.

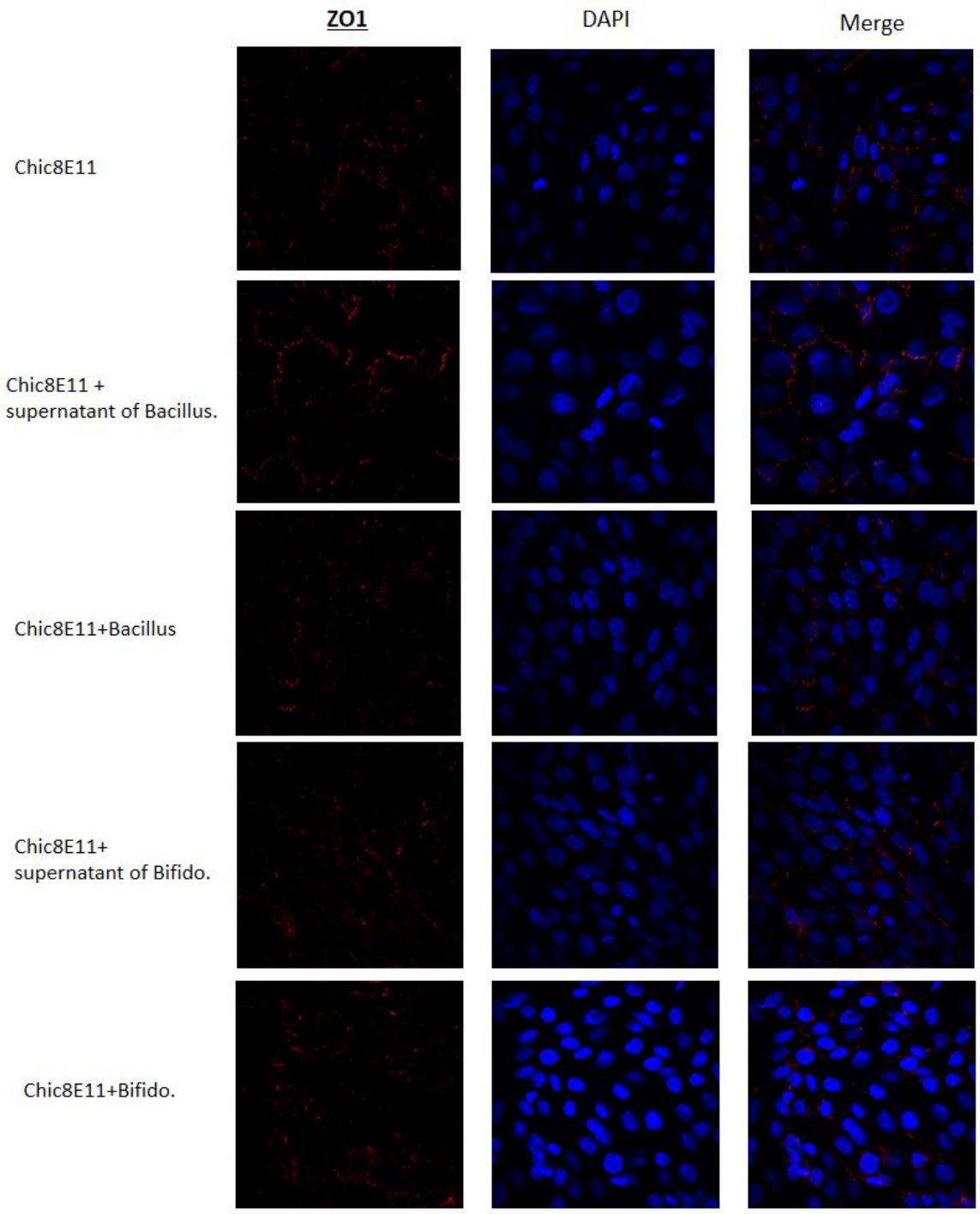

Figure 32. Matrix diagram of the localization and immunofluorescence changes of Zonula occludens-1 protein in Chic8E11 cells after their co-culture with *Bifido.* or the supernatant of *Bifido.* and *Bacillus* or the supernatant of *Bacillus*, scale bar 50μm, 200x magnification.

As shown in the Figure 33, the occludin (green) protein marker was dispersedly expressed in Chic8E11 cells. The fluorescence signal of the occludin protein was enhanced after the Chic-8E11 cells were co-cultured with *Bacillus* (or the supernatant of *Bacillus*), and the fluorescence signal of the occludin protein in Chic-8E11 cells was enhanced even more, when the supernatant of *Bacillus* was added. The fluorescence signal of the occludin protein was also enhanced after the Chic-8E11 cells were co-cultured with *Bifido.* or the supernatant of *Bifido.*. In comparison, the fluorescence signal of the occludin protein in Chic-8E11 cells was enhanced after their co-culture with *Bifido.*. After a comprehensive comparison, it was found that the fluorescence signal of the occludin protein in Chic-8E11 cells was the highest when the supernatant of *Bacillus* was added.

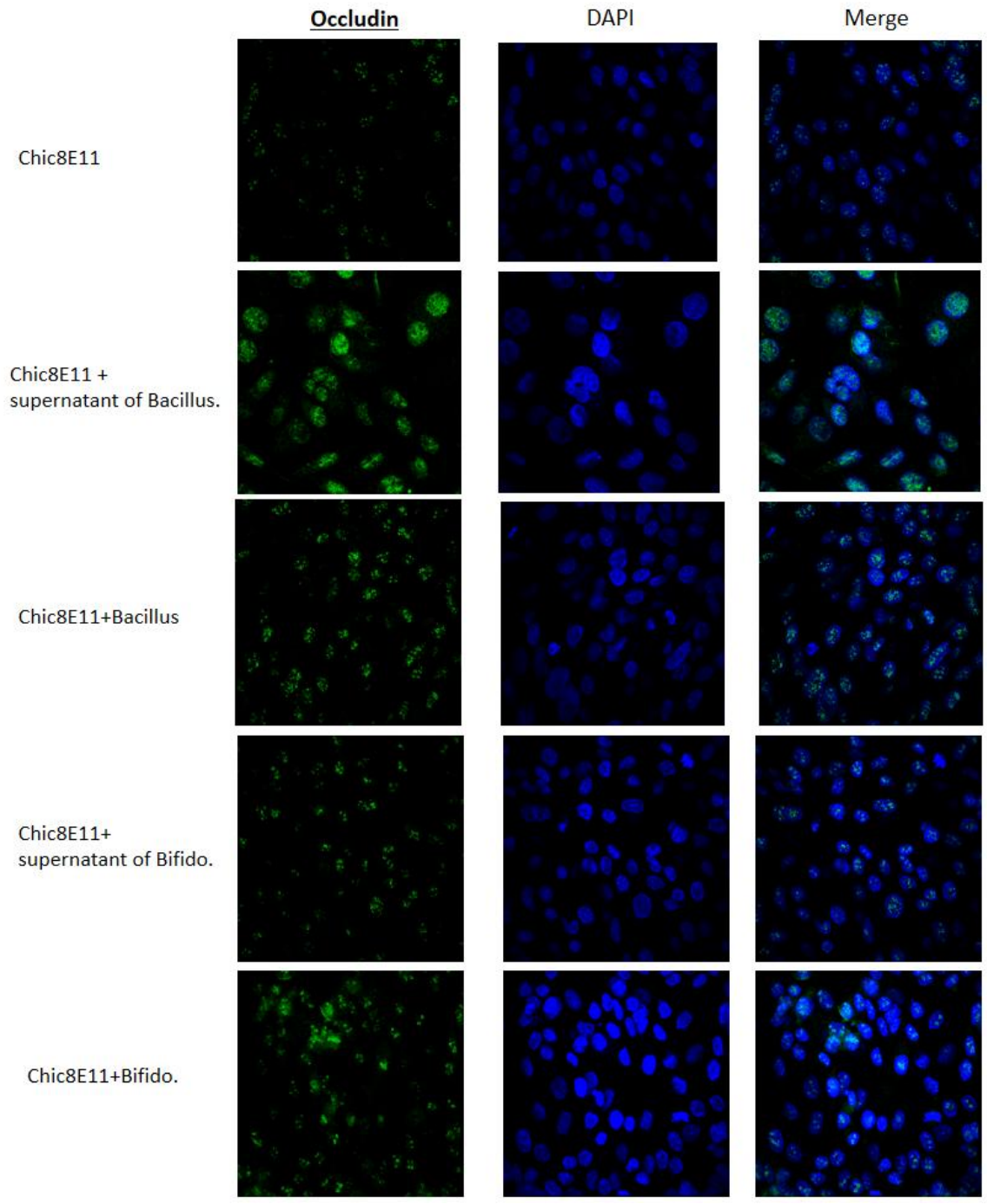

Figure 33. Matrix diagram of the localization and immunofluorescence changes of occludin protein on Chic8E11 cells after co-culture with *Bifido.* or the supernatant of *Bifido.*, and *Bacillus* or the supernatant of *Bacillus*, scale bar 50μm, 200x magnification.

As shown in Figure 34, the E-cadherin (red) protein marker was strongly expressed in Chic8E11 cells. The fluorescence signal of E-cadherin protein in Chic-8E11 cells was enhanced after their co-culture with *Bacillus* or the supernatant of *Bacillus*, and the fluorescence signal of E-cadherin protein in Chic-8E11 cells was enhanced even more when the supernatant of *Bacillus* was added. However, the fluorescence signal of E-cadherin protein in Chic-8E11 cells was not significantly enhanced after co-culture with *Bifido.* or the supernatant of *Bifido.*. After a comprehensive comparison, it was found that the fluorescence signal of E-cadherin protein in Chic-8E11 cells was enhanced the most when the supernatant of *Bacillus*was added.

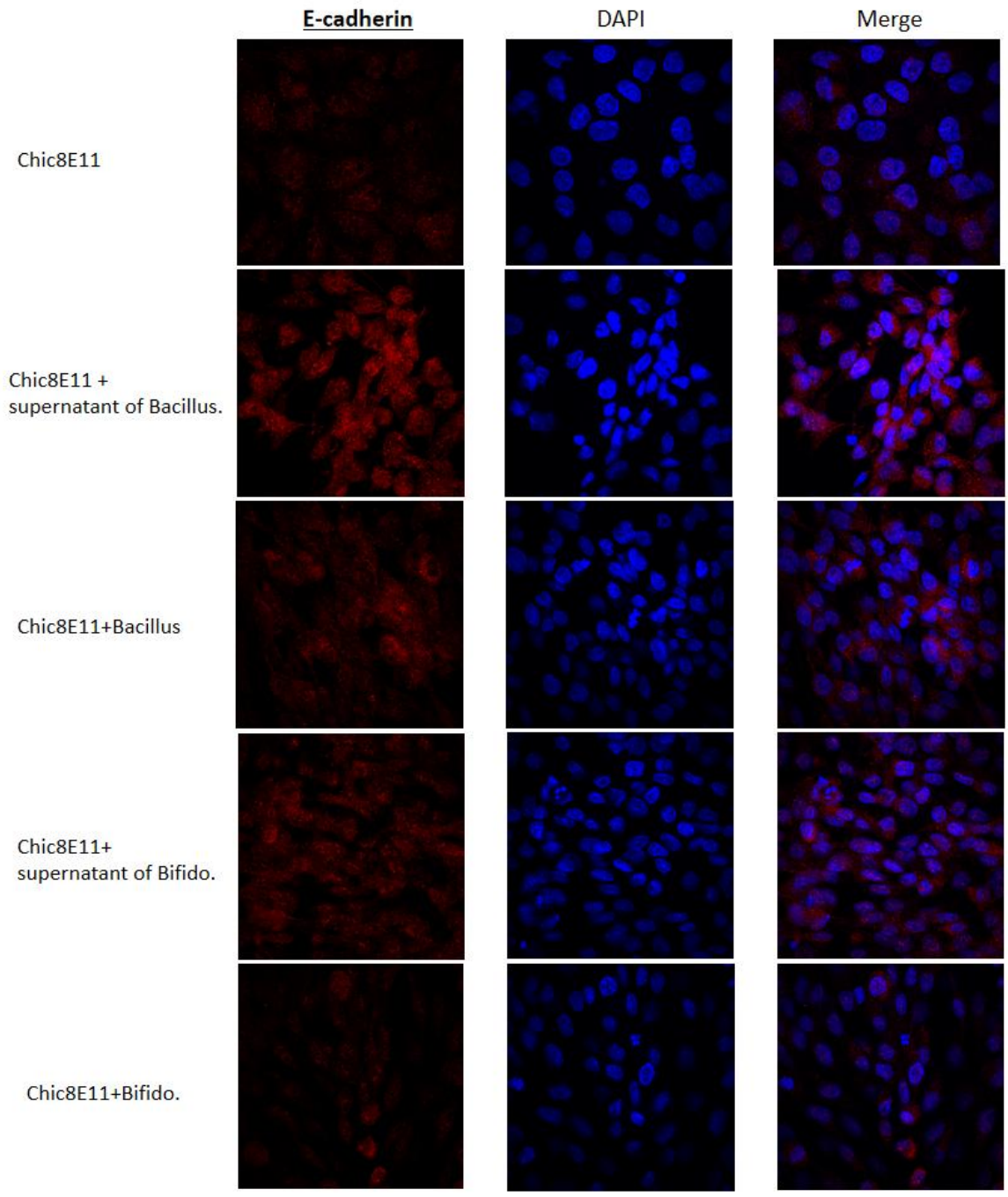

Figure 34. Matrix diagram of the localization and immunofluorescence changes of E-cadherin protein on Chic8E11 cells after co-culture with *Bifido.* or the supernatant of *Bifido.* and *Bacillus* or the supernatant of *Bacillus*, scale bar 50μm, 200x magnification

As shown in Figure 35, the vimentin (red) protein marker was dispersedly expressed on Chic8E11 cells. After co-culture with *Bacillus* or the supernatant of *Bacillus* cultured alone, the fluorescence signal of vimentin protein in Chic-8E11 cells was weakened. In contrast, after co-culture with *Bifido.* (or the supernatant of *Bifido.*), the fluorescence signal of vimentin protein in Chic-8E11 cells was significantly enhanced.

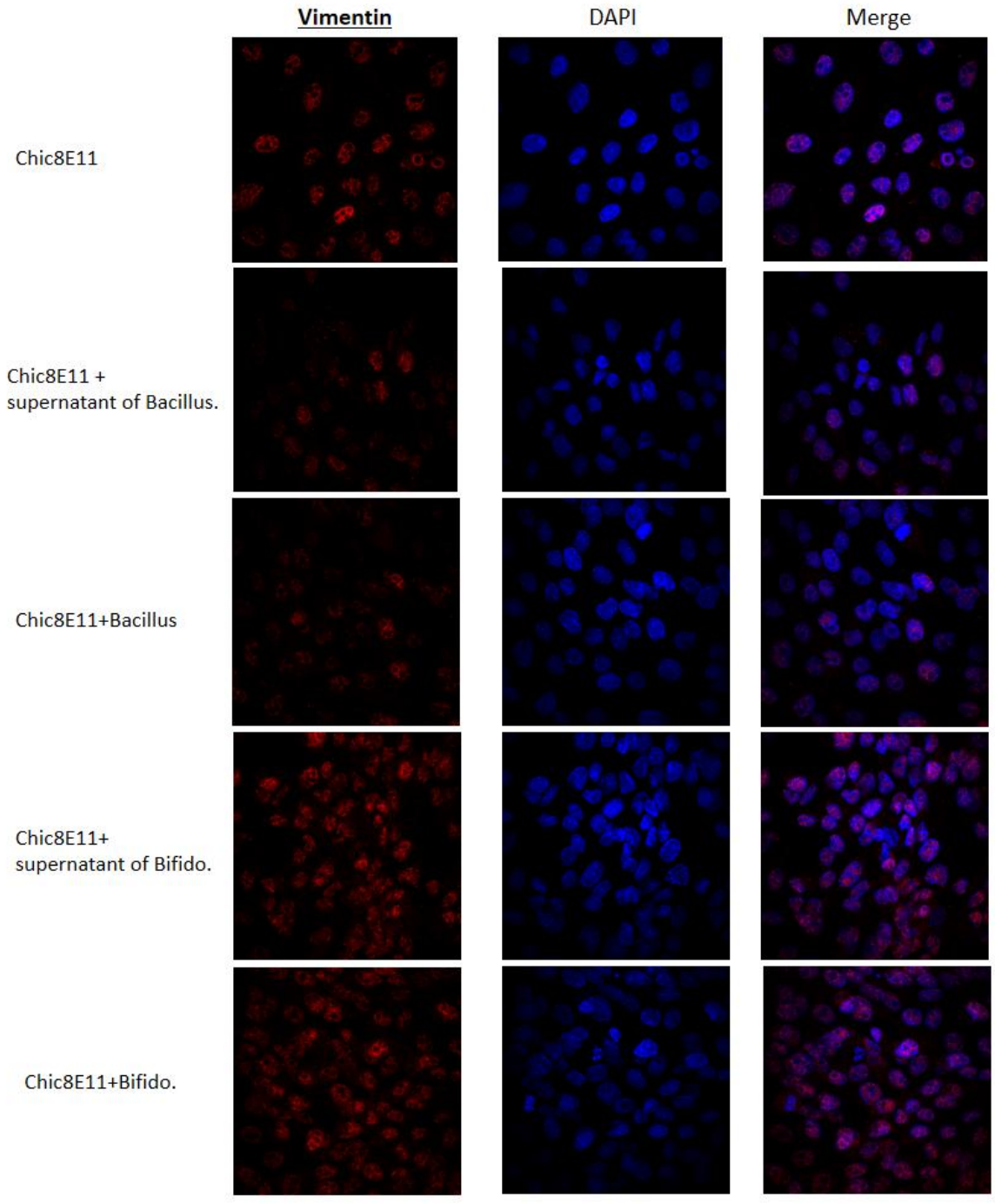

Figure 35. Matrix diagram of the localization and immunofluorescence changes of vimentin protein in Chic-8E11 cells after co-culture with *Bifido.* or the supernatant of *Bifido.* and *Bacillus*,or the supernatant of *Bacillus*, scale bar 50μm, 200x magnification

As shown in Figure 36, the cytokeratin 18 (red) protein marker is fully expressed on Chic-8E11 cells. After co-culture with *Bacillus* or *Bifido.*, or the supernatant of *Bifido.*, there was no significant difference in the fluorescence signal of cytokeratin 18 protein in Chic-8E11 cells. However, under the condition of adding the supernatant of *Bacillus*, the fluorescence signal of cytokeratin 18 protein in Chic-8E11 cells was significantly enhanced.

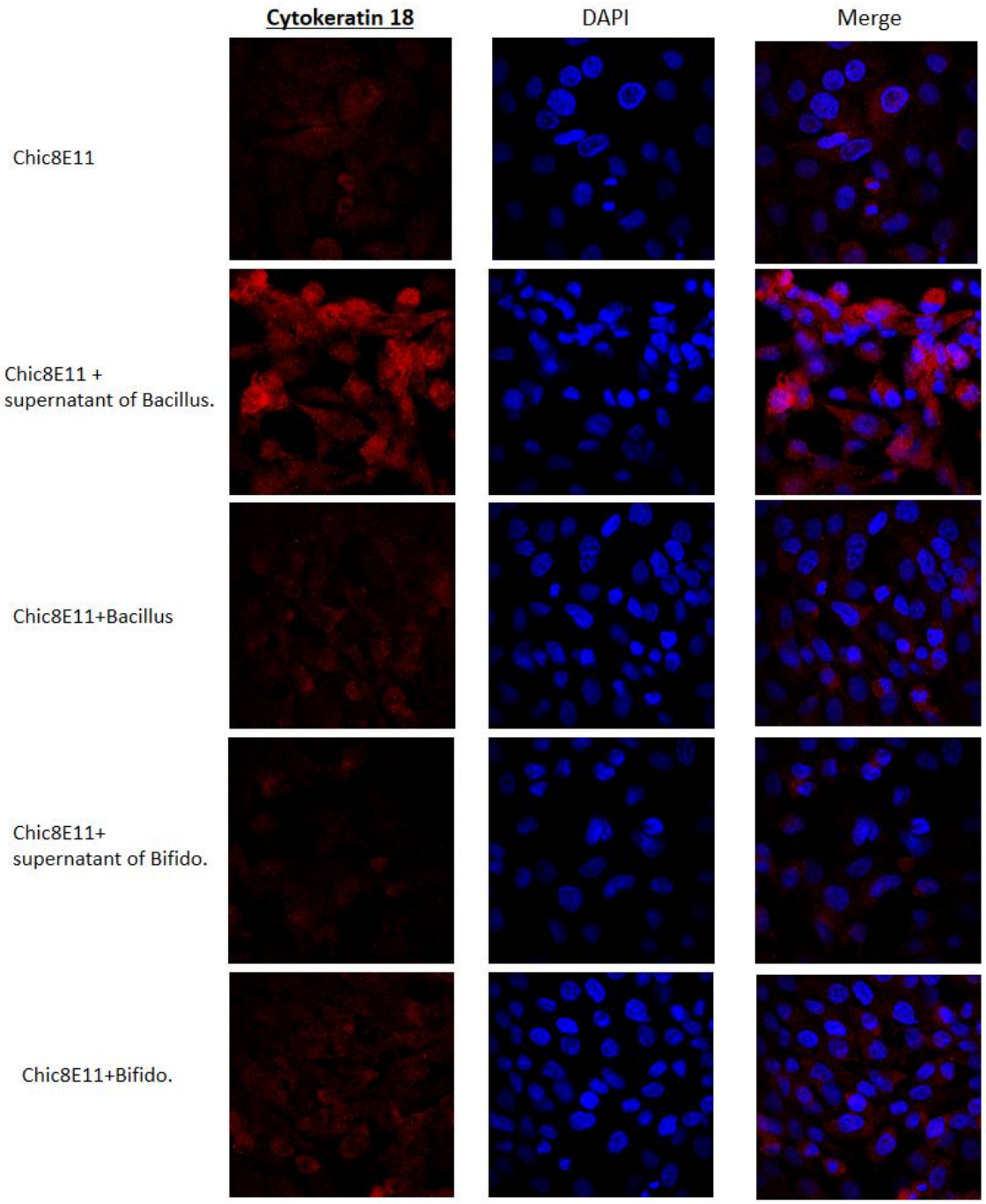

Figure 36. Matrix diagram of the localization and immunofluorescence changes of cytokeratin 18 protein on Chic-8E11 cells after co-culture with *Bifido.* or the supernatant of *Bifido.*, and *Bacillus* or the supernatant of *Bacillus*, scale bar 50μm, 200x magnification

As shown in Figure 37, the desmoplakin (red) protein marker was expressed in the Chic-8E11 cells and tended to be expressed in aggregates. After co-culture with *Bacillus* or the supernatant of *Bacillus*, or *Bifido.*, the fluorescence signal of desmoplakin protein in Chic-8E11 cells was weakened to varying degrees. However, under the condition of adding the supernatant of *Bifido.*, the fluorescence signal of desmoplakin protein in Chic-8E11 cells was significantly enhanced.

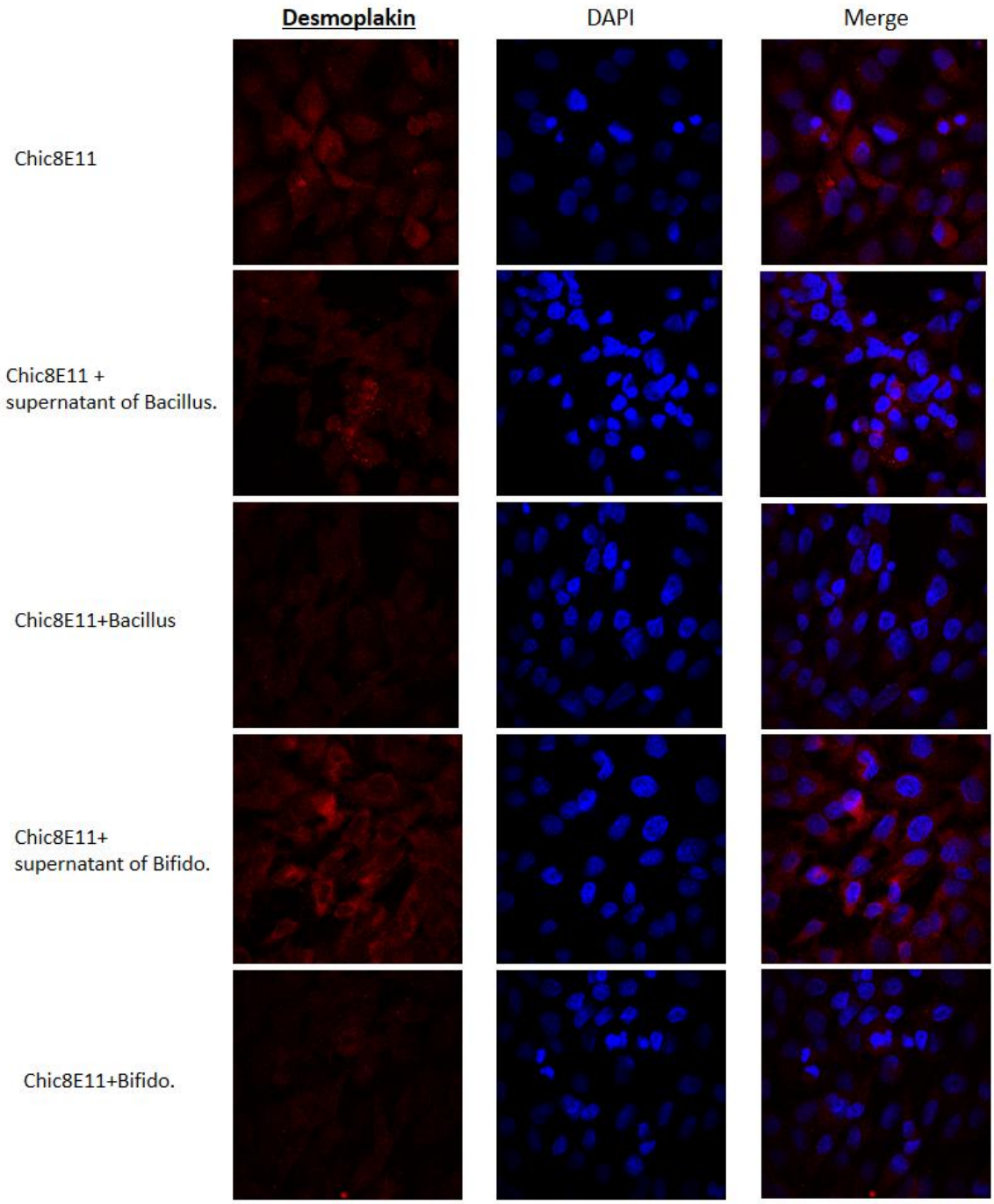

Figure 37. Matrix diagram of the localization and immunofluorescence changes of desmoplakin protein on Chic-8E11 cells after co-culture with *Bifido.* or the supernatant of *Bifido.*, and *Bacillus* or the supernatant of *Bacillus*, scale bar 50μm, 200x magnification

As shown in Figure 38, the ZO-1 (red) protein marker was clearly expressed at the edges and cell-to-cell junction of each Caco-2 cell. There was no significant difference in the fluorescence signal of Zonula occludens-1 protein in Caco-2 cells after co-culture with *Bacillus* or *Bifido.*, or the supernatant of *Bifido.*. However, when the supernatant of *Bacillus* was added, the fluorescence signal of zonula occludens-1 protein in Caco-2 cells was enhanced, especially at the cell-cell junctions.

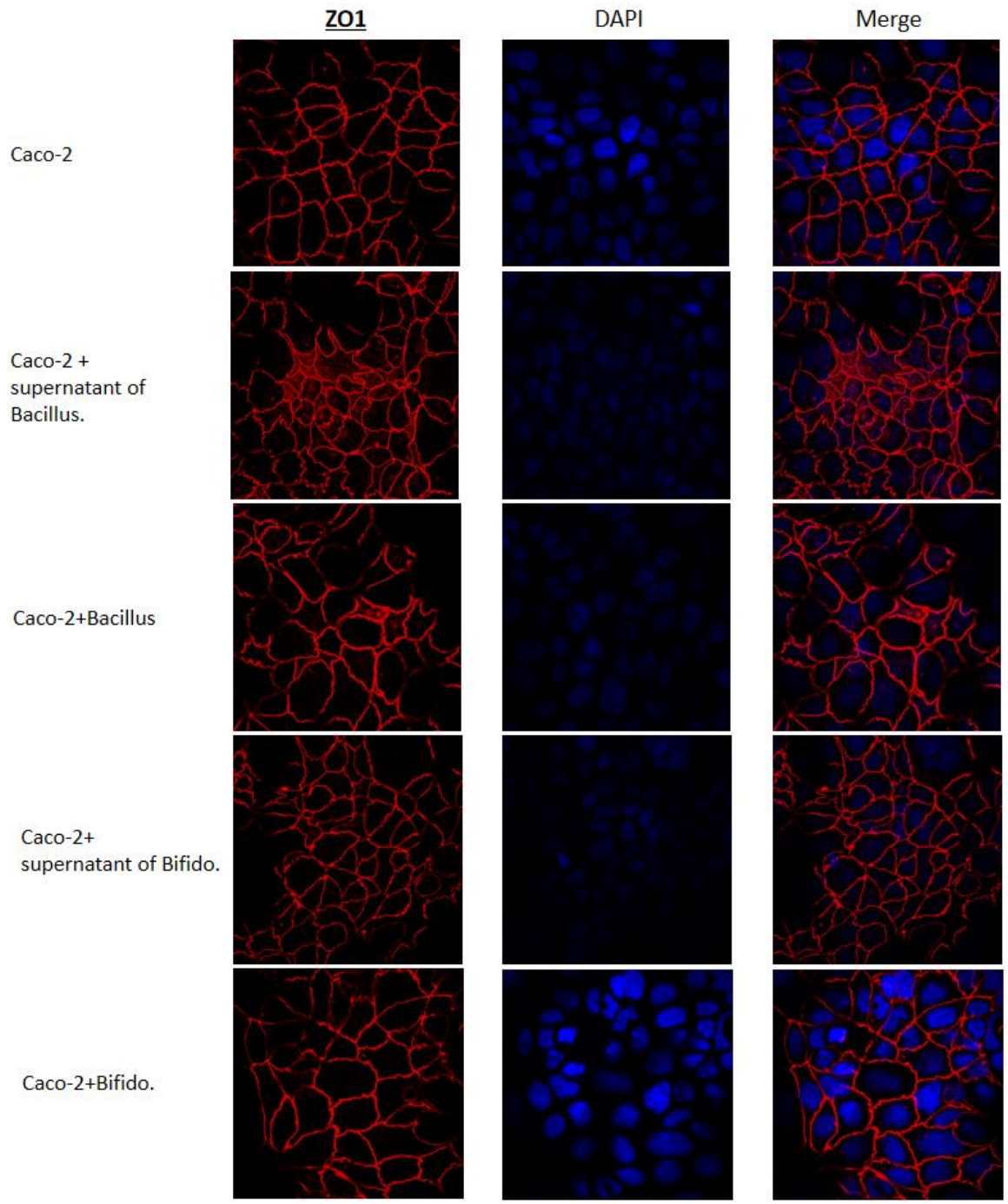

Figure 38. Matrix diagram of the localization and immunofluorescence changes of zonula occludens-1 protein on Caco-2 cells after co-culture with *Bifido.* or the supernatant of *Bifido.*, and *Bacillus* or the supernatant of *Bacillus*, scale bar 50μm, 200x magnification

As shown in Figure 39, the occludin (green) protein marker is expressed in Caco-2 cells, and the cell edge is more clearly expressed. After co-culture with *Bifido.* or the supernatant of *Bifido.*, or the supernatant of *Bacillus*, the fluorescence signal of occludin protein in Caco-2 cells at the cell-cell junction and cell surface was significantly enhanced. Only after co-culture with *Bacillus* there was no significant difference in the fluorescence signal of occludin protein in Caco-2 cells.

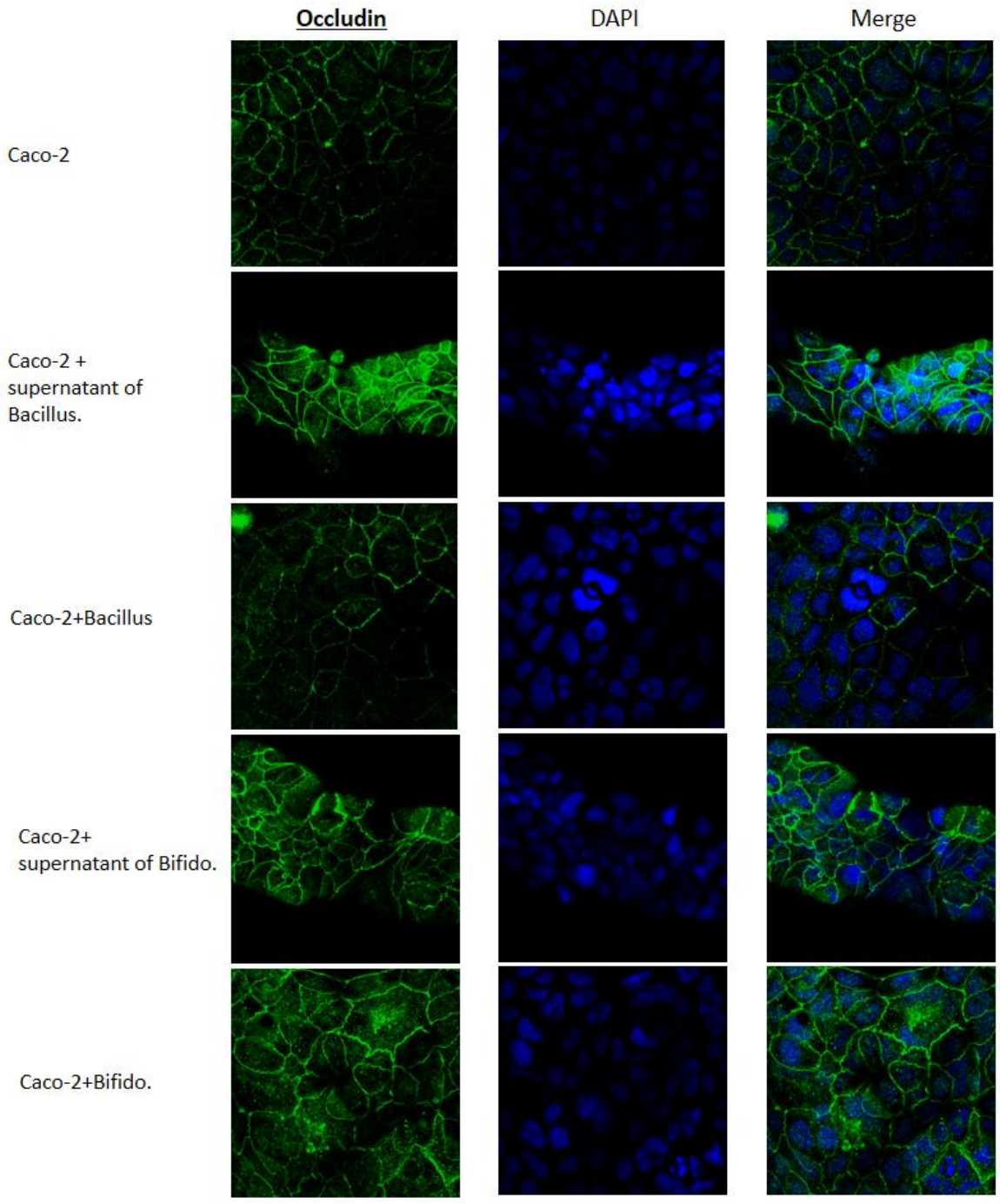

Figure 39. Matrix diagram showing the localization and immunofluorescence changes of occludin protein on Caco-2 cells after co-culture with Bifid or the supernatant of *Bifido.*, and *Bacillus* or the supernatant of *Bacillus*, scale bar 50μm, 200x magnification.

As shown in Figure 40, the E-cadherin (red) protein marker is more expressed near the edge of the cell on Caco-2 cells. After co-culture with *Bacillus* or the supernatant of *Bacillus*, the fluorescence signal of E-cadherin protein in Caco-2 cells was weakened, especially near the cells' edges. In contrast, after co-culture with *Bifido.* or the supernatant of *Bifido.*, the fluorescence signal of E-cadherin protein of Caco-2 cells was slightly enhanced. After the co-culture with *Bacillus*, the fluorescence signal almost disappeared.

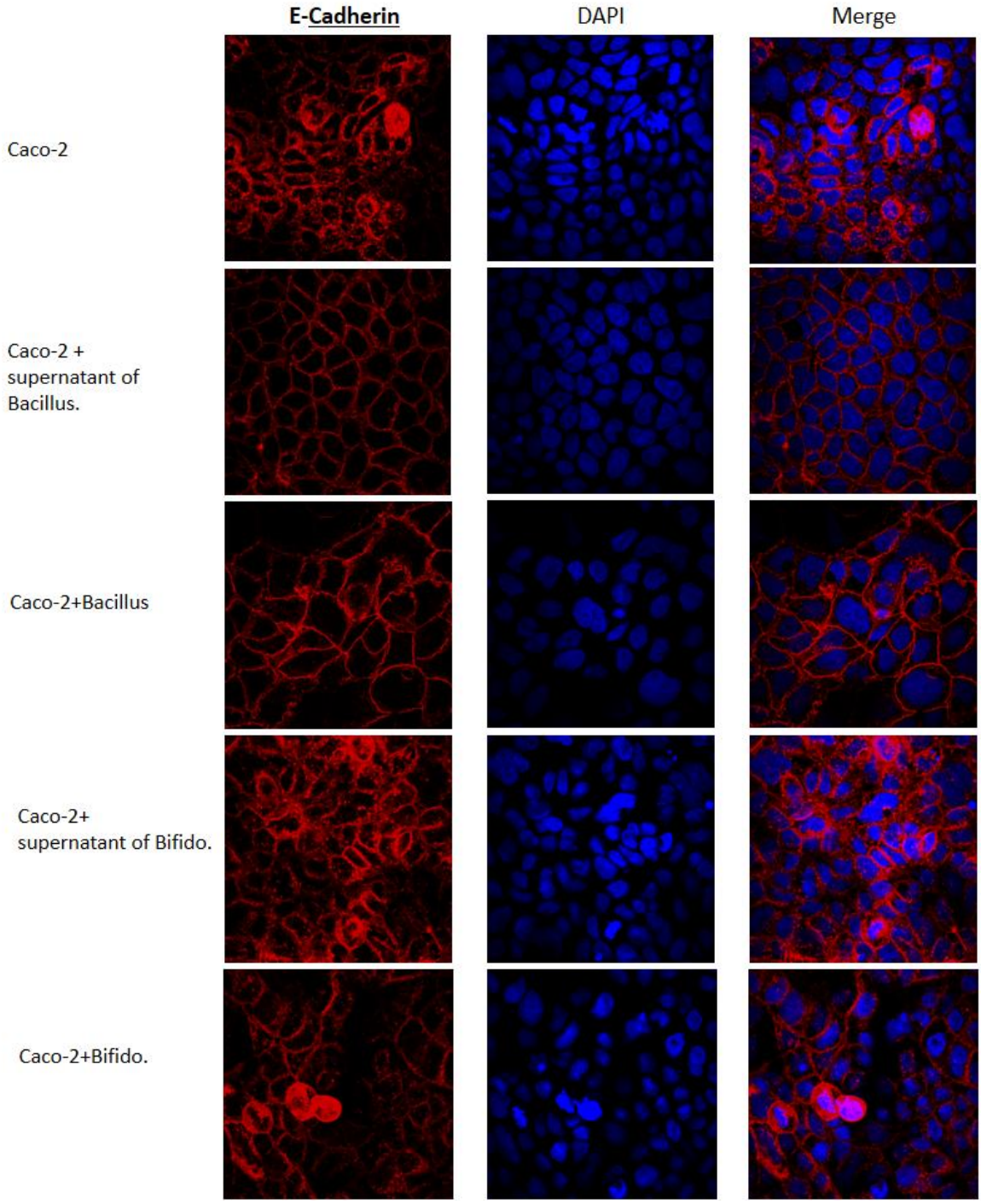

Figure 40. Matrix diagram of the localization and immunofluorescence changes of E-cadherin protein on Caco-2 cells after co-culture with *Bifido.* or the supernatant of *Bifido.*, and *Bacillus* or the supernatant of *Bacillus*, scale bar 50µm, 200x magnification

As shown in Figure 41, the claudin-1 (green) protein marker was dispersedly expressed in Caco-2 cells. Compared with the blank group of Caco-2 cells, the claudin-1 protein fluorescence signal of Caco-2 cells decreased to varying degrees after co-culture with *Bacillus* or the supernatant of *Bacillus*, and *Bifido.* or the supernatant of *Bifido.*. In particular, after co-culture with *Bacillus*, the Claudin-1 protein fluorescence signal of Caco-2 cells almost disappeared.

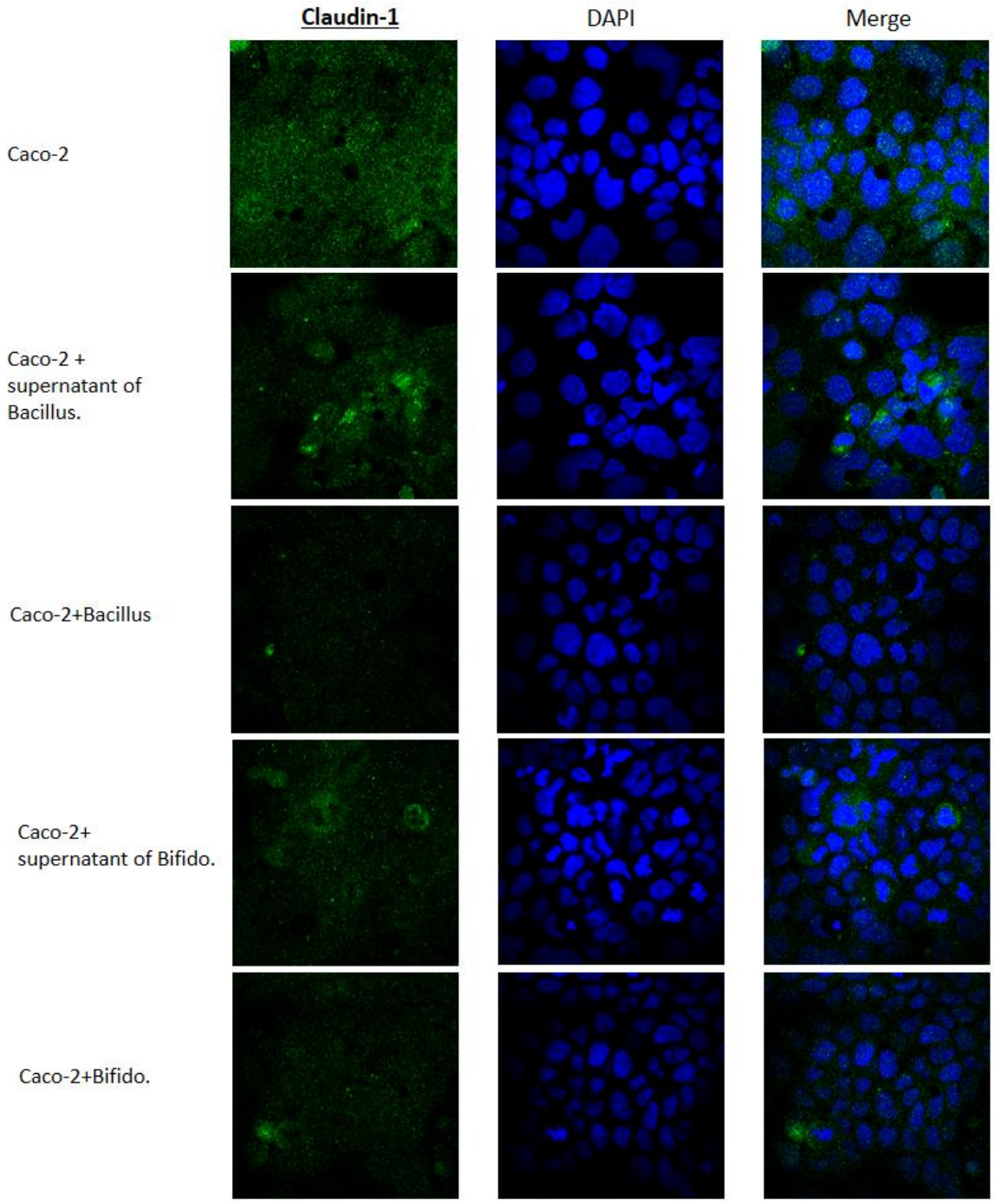

Figure 41. Matrix diagram showing the localization and immunofluorescence changes of claudin-1 protein in Caco-2 cells after co-culture with *Bifido.* or the supernatant of *Bifido.*, and *Bacillus* or the supernatant of *Bacillus*, scale bar 50μm, 200x magnification.

As shown in Figure 42, the desmoplakin (red) protein marker was dispersedly expressed in Caco-2 cells. After the co-culture with Bacillu, there was no significant difference in the fluorescence signal of desmoplakin protein in the Caco-2 cells. When the supernatant of *Bifido.* was added, the fluorescence signal of desmoplakin protein of Caco-2 was enhanced.

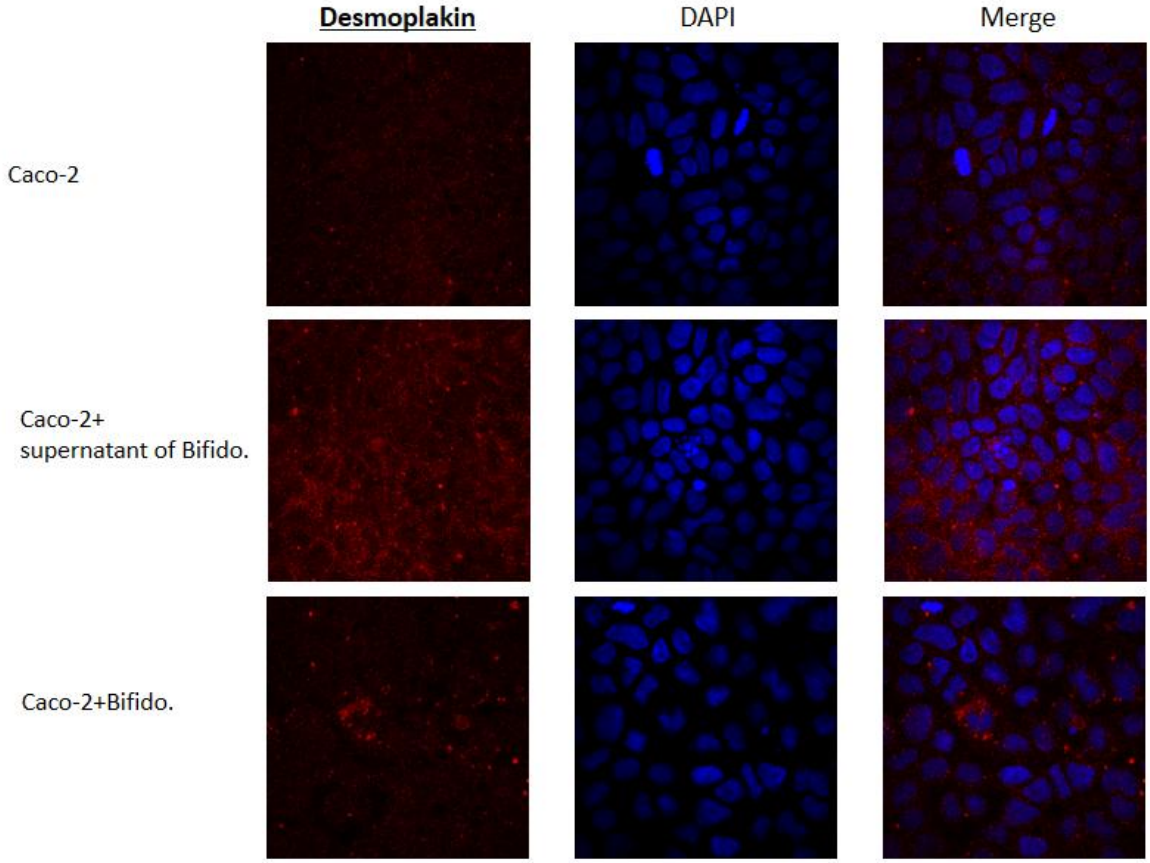

Figure 42. Matrix diagram of the localization and immunofluorescence changes of desmoplakin protein on Caco-2 cells after co-culture with *Bifido.* or the supernatant of *Bifido.*, scale bar 50μm, 200x magnification.

4.4. Metabolic footprint and fingerprint of probiotic activity in the intestinal cells *in vitro*

4.4.1. Metabolic footprint analysis

The metabolites in the supernatants of Caco-2 culture (B), *Bifidobacterium lactis* NCC2818 (C), and Caco-2 co-cultured with *Bifidobacterium lactis* NCC2818 (D) were compared.

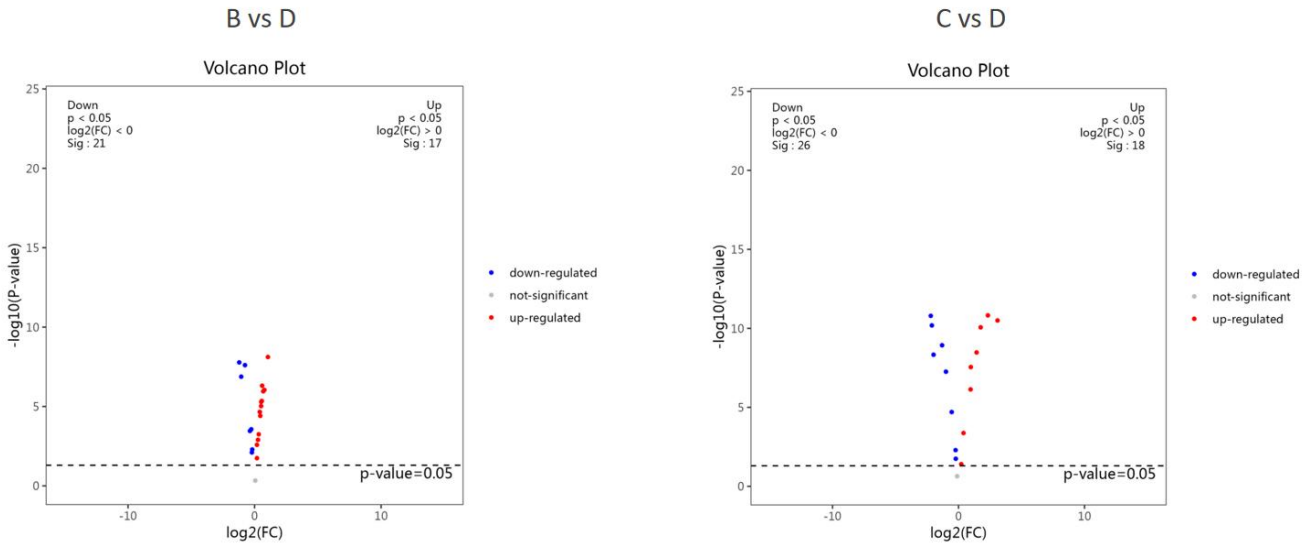

Figure 43. Volcano map of metabolic profiles of the compared groups: B vs D and C vs D: the supernatants of Caco-2 culture (B), *Bifidobacterium lactis* NCC2818 (C), and Caco-2 co-cultured with *Bifidobacterium lactis* NCC2818 (D)

Each point in the figure represents a metabolite, the abscissa is the log2 (FC) value of the two comparisons, the ordinate is the -log10 (*p*-value) value, and the red point is $p < 0.05$ and FC > 1 Metabolites, blue dots are metabolites changed with $p < 0.05$ and FC < 1.

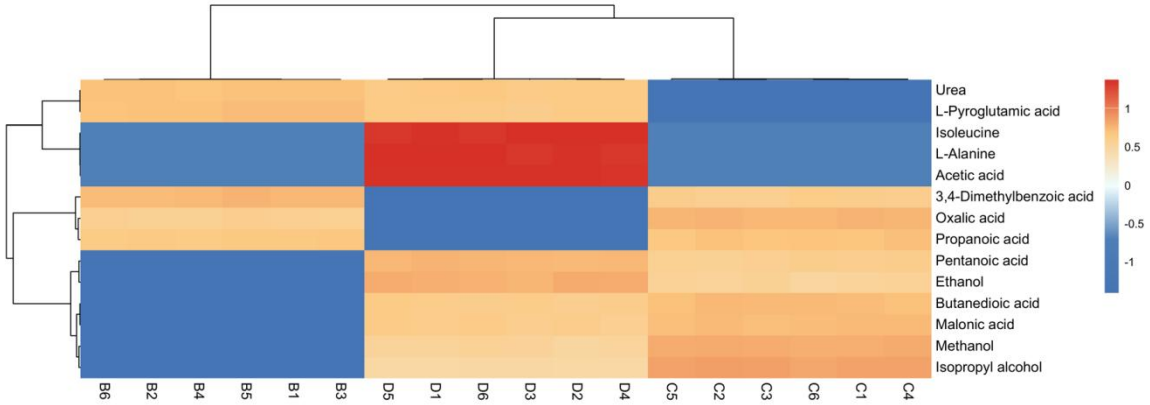

Figure 44. Differential metabolite clustering heatmap for comparison B/C/D groups : the supernatants of Caco-2 culture (B), *Bifidobacterium lactis* NCC2818 (C), and Caco-2 co-cultured with *Bifidobacterium lactis* NCC2818 (D)

The horizontal axis represents the sample name, and the vertical axis represents the differential metabolites. The colors from blue to red represent the expression abundance of metabolites from low to high, that is, the redder the color, the higher the expression abundance of the differential metabolites.

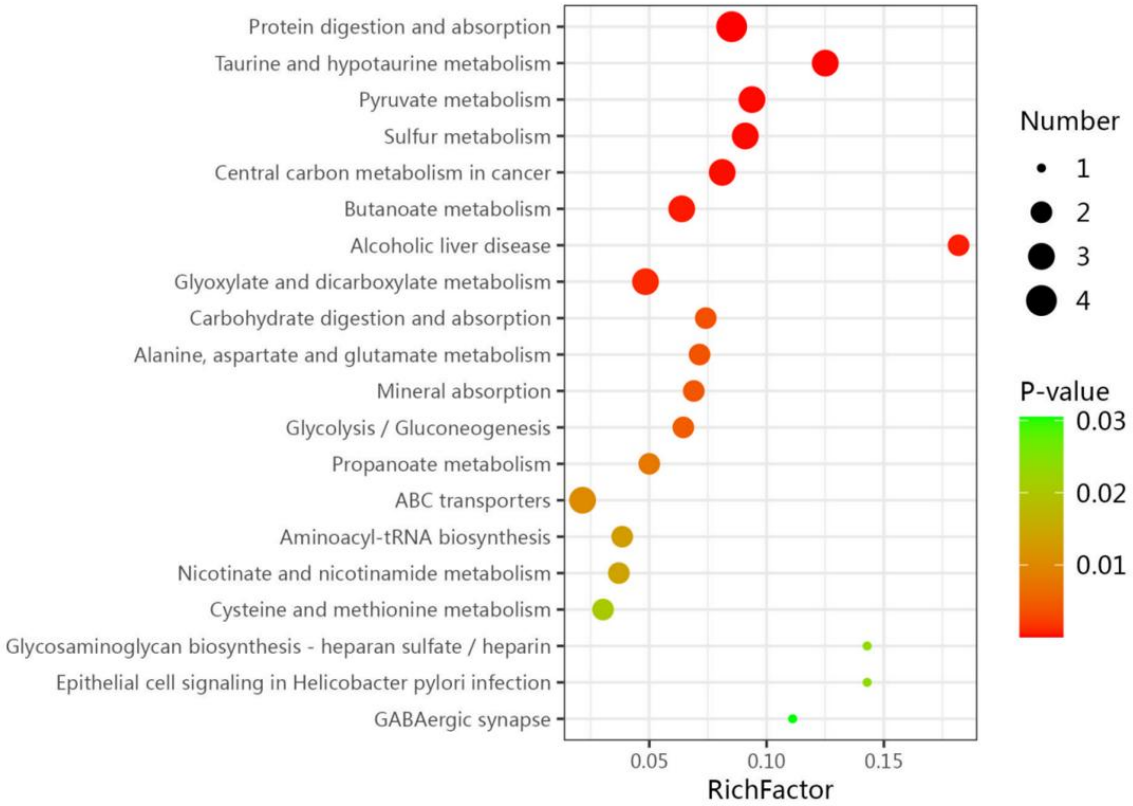

Figure 45. Significance bubble plots of enrichment of the altered metabolic pathways in the experimental B/C/D groups: the supernatants of Caco-2 culture (B), *Bifidobacterium lactis* NCC2818 (C), and Caco-2 co-cultured with *Bifidobacterium lactis* NCC2818 (D)

The metabolites in the supernatants of Chic-8E11 (b), *Bifidobacterium lactis* NCC2818 (c), and Chic-8E11 co-cultured with *Bifidobacterium lactis* NCC2818 (d) were compared.

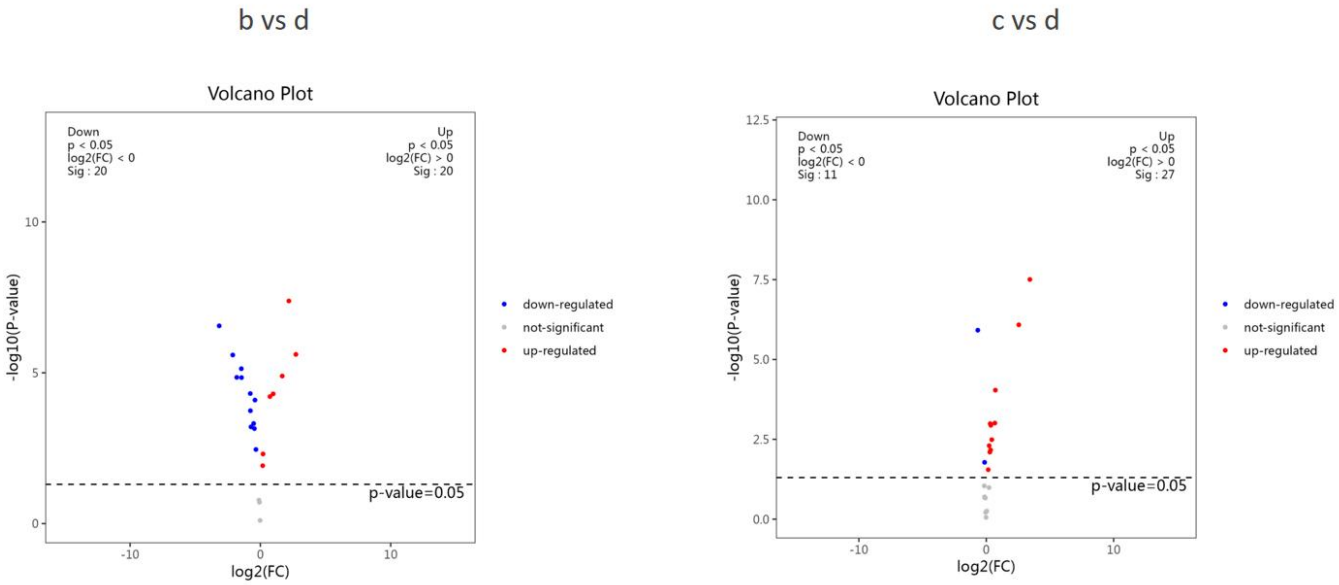

Figure 46. Volcano map of metabolic profiles of the comparison b/c/d groups : the supernatants of Chic-8E11 culture (b), *Bifidobacterium lactis* NCC2818 (c), and Chic-8E11 co-cultured with *Bifidobacterium lactis* NCC2818 (d)

Each point in the figure represents a metabolite, the abscissa is the log2 (FC) value of the two comparisons, the ordinate is the -log10 (*p*-value) value, and the red point is $p < 0.05$ and FC > 1 metabolites, blue dots are metabolites with $p < 0.05$ and FC < 1.

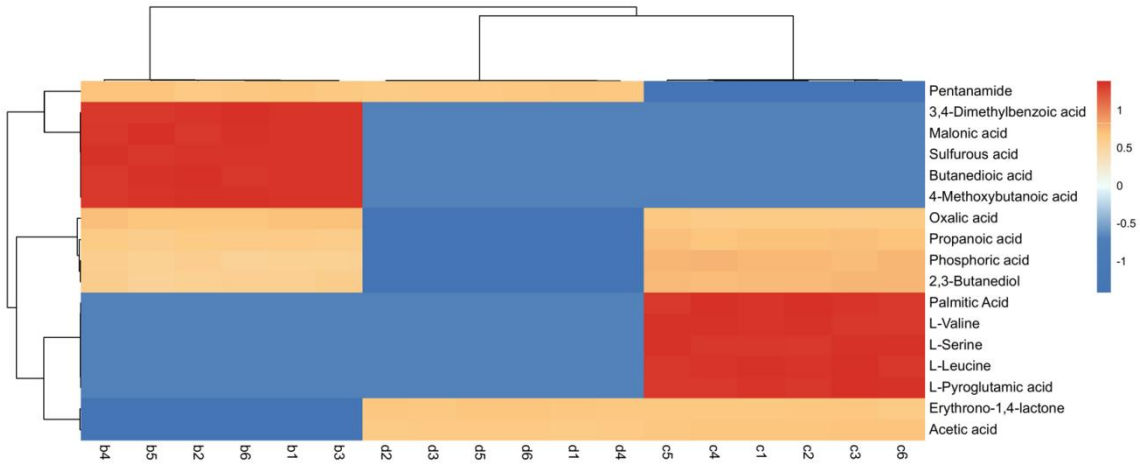

Figure 47. Differential metabolite clustering heatmap for experimental b/c/d groups : the supernatants of Chic-8E11 culture (b), *Bifidobacterium lactis* NCC2818 (c), and Chic-8E11 co-cultured with *Bifidobacterium lactis* NCC2818 (d)

The horizontal axis represents the sample name, and the vertical axis represents the differential metabolites. The colors from blue to red represent the expression abundance of metabolites from low to high, that is, the redder the color, the higher the expression abundance of the differential metabolites.

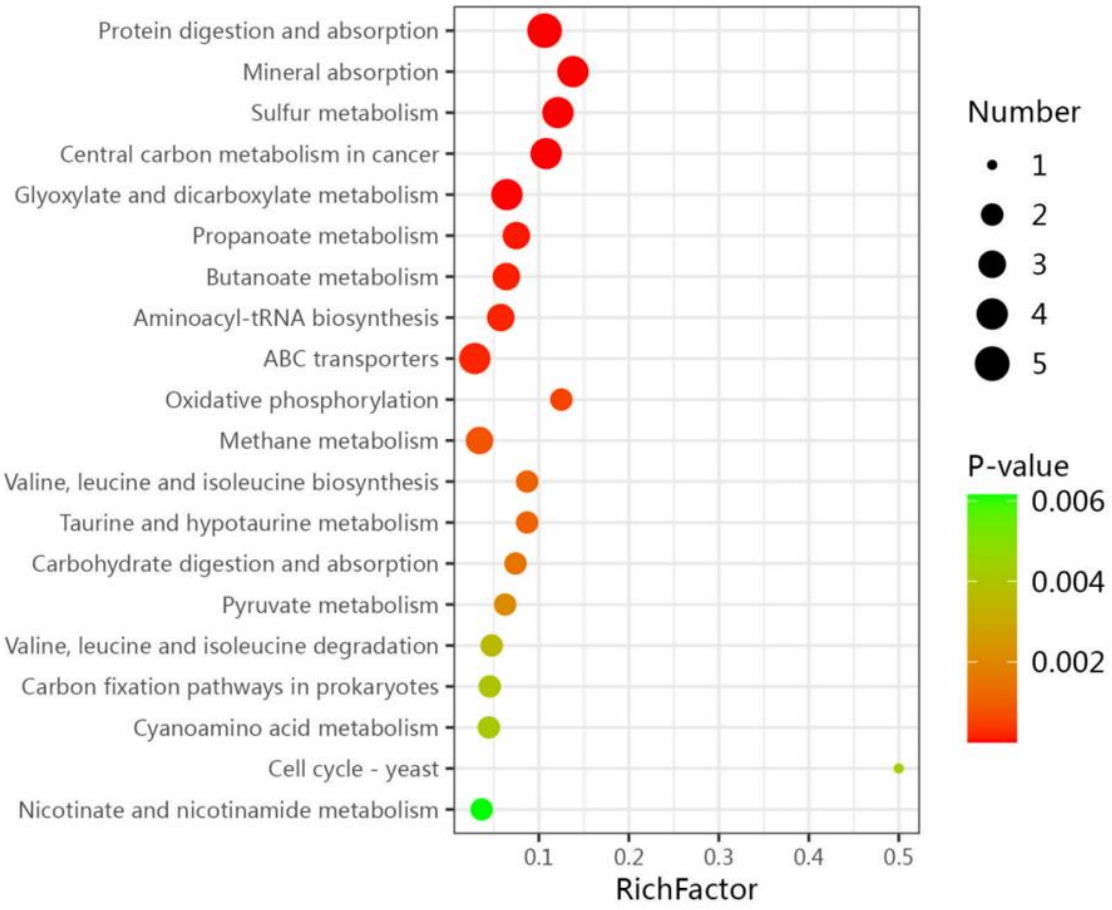

Figure 48. Significance bubble plots of enrichment of altered metabolic pathways in the experimental b/c/d groups : the supernatants of Chic-8E11 culture (b), *Bifidobacterium lactis* NCC2818 (c), and Chic-8E11 co-cultured with *Bifidobacterium lactis* NCC2818 (d).

4.4.2. Metabolic fingerprint analysis

The metabolite differences in the Caco-2 cells interacting with *Bacillus strain* or it's culture supernatant, were compared as: Caco-2 cells (C1), Caco-2 cells with the supernatant of *Bacillus* (C1SB1), and Caco-2 cells co-cultured with *Bacillus* (C1B1).

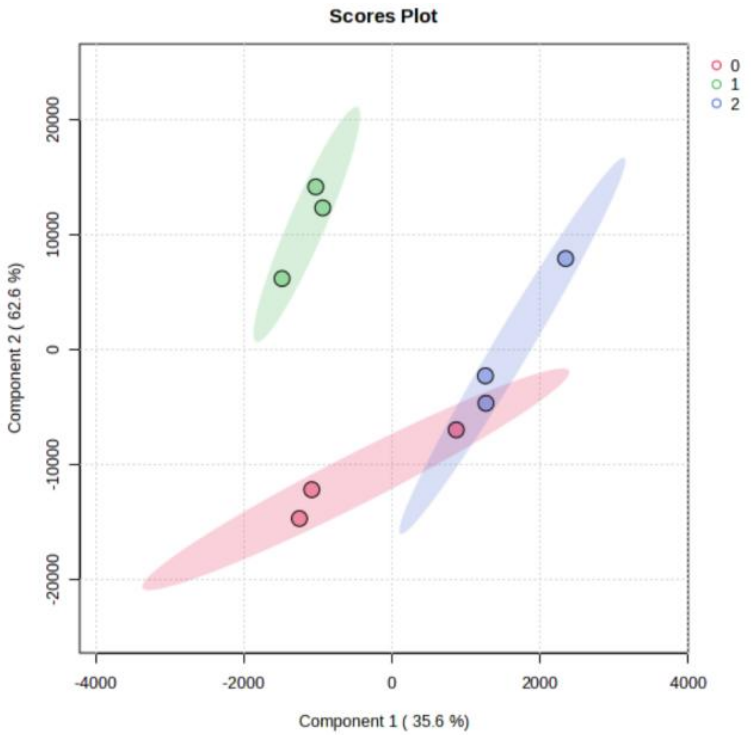

Figure 49. Partial Least Squares Discriminant Analysis (PLS-DA) of metabolic profiles of the compared experimental groups C1/C1SB1/CIB1: Red dots represent Caco-2 cells (0), green dots represent Caco-2 cells with the supernatant of *Bacillus* (1), and blue dots represent Caco-2 cells co-cultured with *Bacillus* (2)

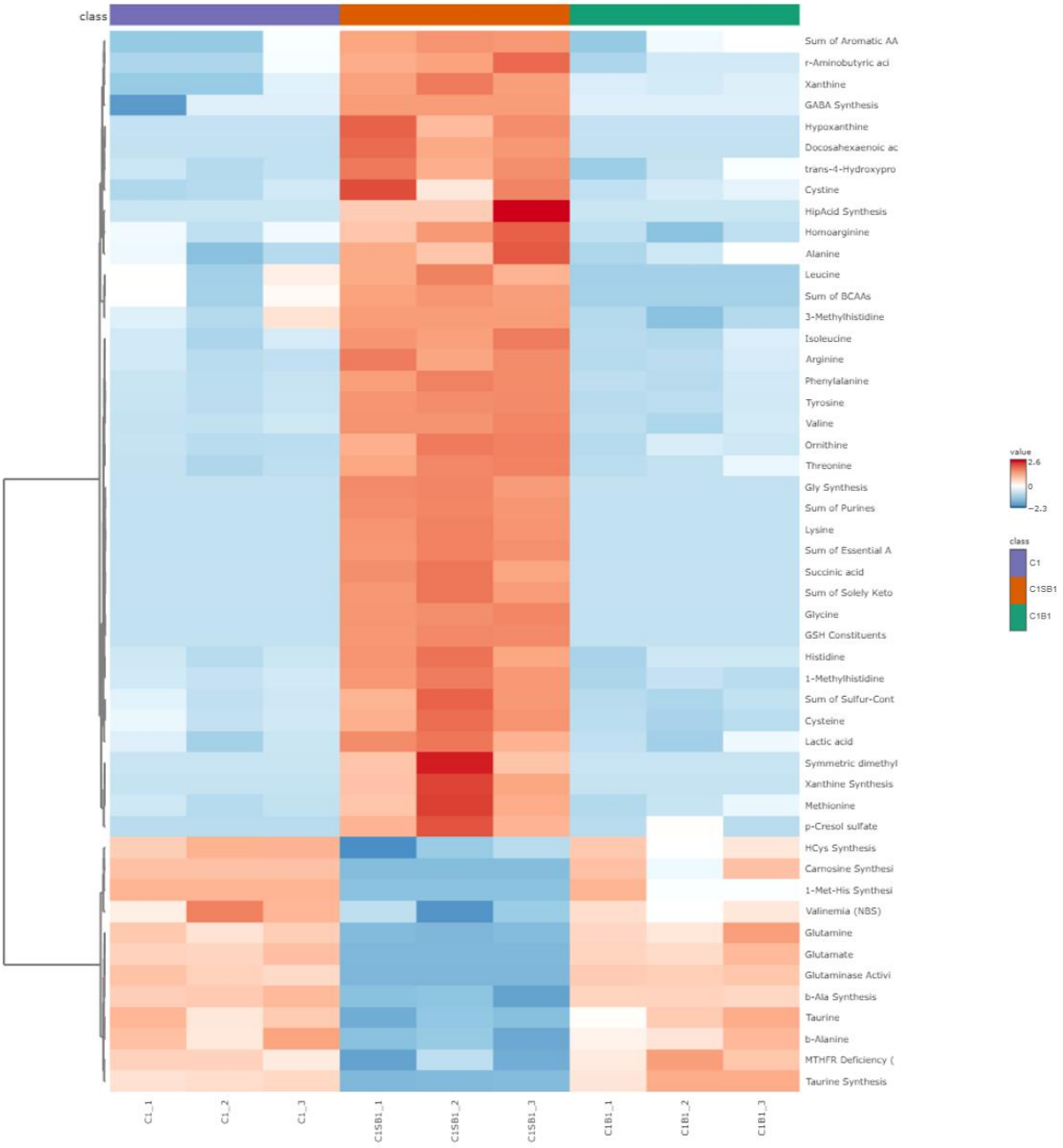

Figure 50. The differential metabolite clustering heatmap for comparisons in experimental groups C1/C1SB1/CIB1: Purple in class represents Caco-2 cells (C1), orange in class represents Caco-2 cells with the supernatant of *Bacillus* (C1SB1), and green in class represents Caco-2 cells co-cultured with *Bacillus* (C1B1)

The horizontal axis represents the sample name, and the vertical axis represents the differential metabolites. The colors from blue to red represent the expression abundance of metabolites from low to high, that is, the redder the color, the higher the expression abundance of the differential metabolites.

KEGG enrichment analysis of differential metabolites in the control group, Caco-2 cells (C1), and the two experimental groups, Caco-2 cells with the supernatant of *Bacillus* (C1SB1), and Caco-2 cells co-cultured with *Bacillus* (C1B1), was performed respectively, and the scatter plot of the top 25 metabolic pathways ranked by significance and the corresponding metabolic pathways were obtained.

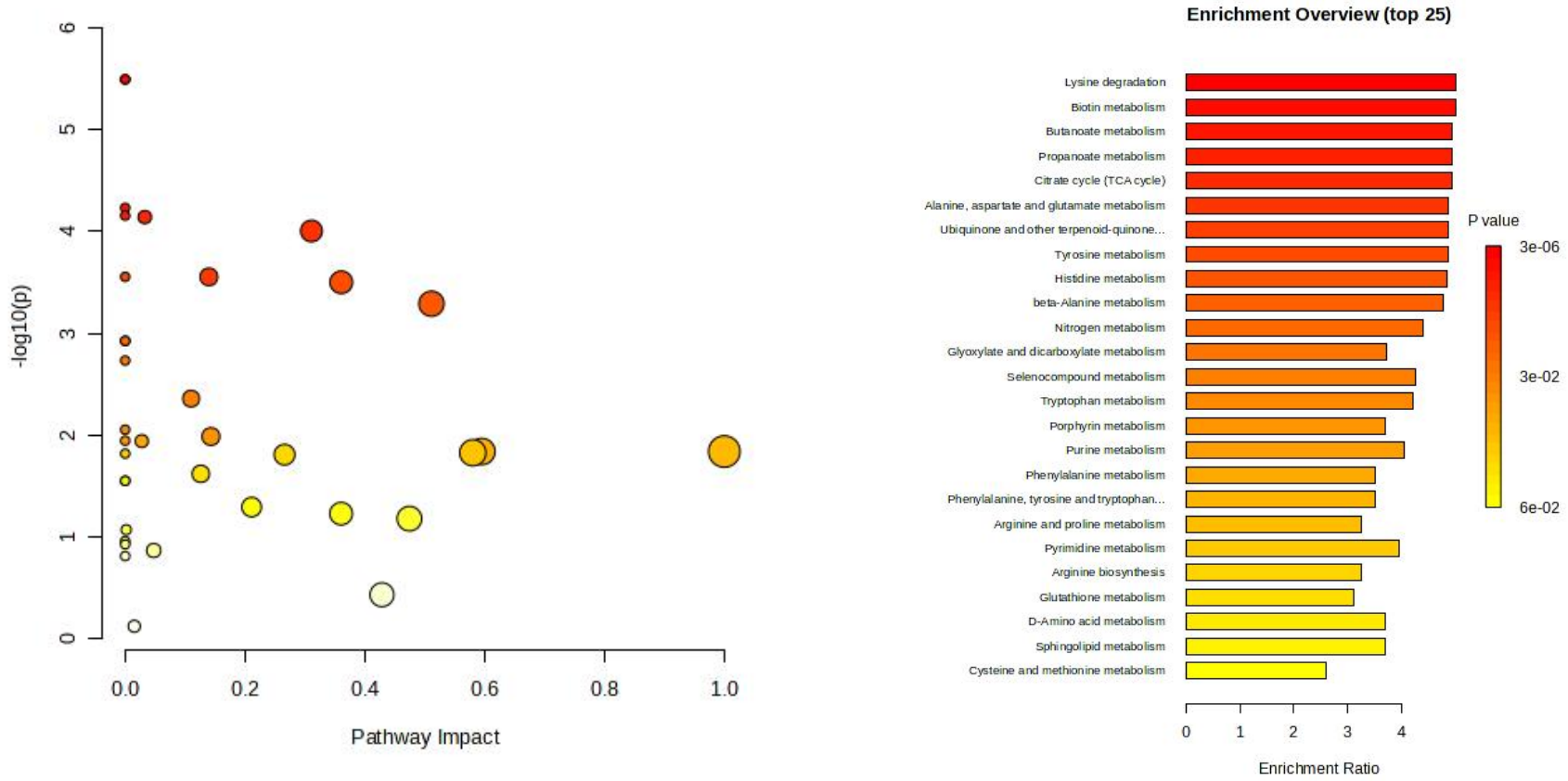

Figure 51. Scatter plot of metabolic pathways affected by differential metabolite enrichment in the experimental groups C1/C1SB1 and the corresponding metabolic pathway overview: the control group, Caco-2 cells (C1), and the experimental groups, Caco-2 cells with the supernatant of *Bacillus* (C1SB1). The redder the color, the smaller the p-value and the higher the significance.

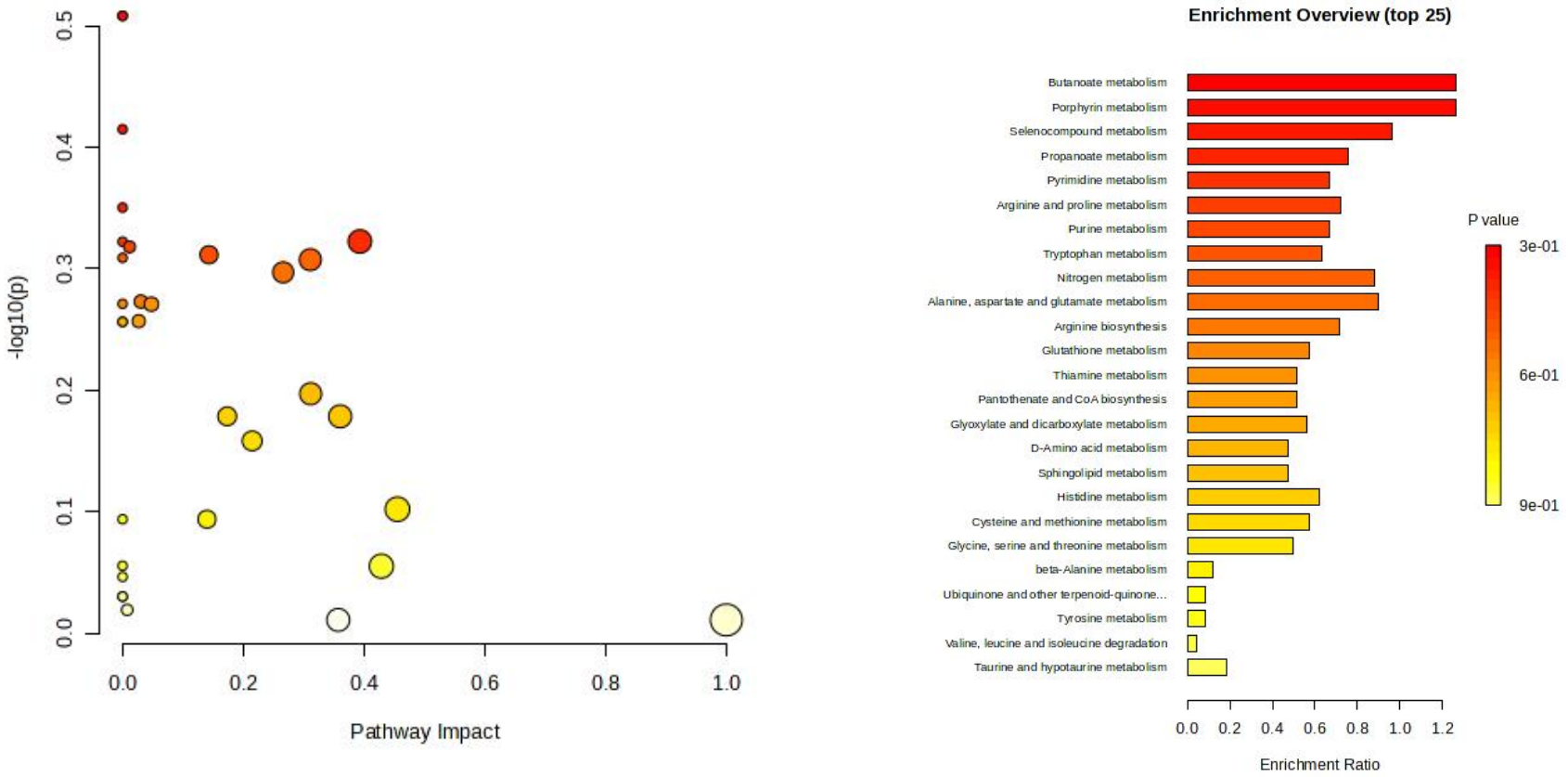

Figure 52. Scatter plot of metabolic pathways affected by differential metabolite enrichment in the experimental groups C1/C1B1 and the corresponding metabolic pathway overview: the control group, Caco-2 cells (C1), and the experimental groups, Caco-2 cells co-cultured with *Bacillus* (C1B1). The redder the color, the smaller the p-value and the higher the significance

The metabolite differences in the Caco-2 cells interacting with *Bifidobacterium lactis* NCC2818 or it's culture supernatant, were compared as: Caco-2 cells (C1), Caco-2 cells with the supernatant of *Bifido.* (C1SB2), and Caco-2 cells co-cultured with *Bifido.* (C1B2).

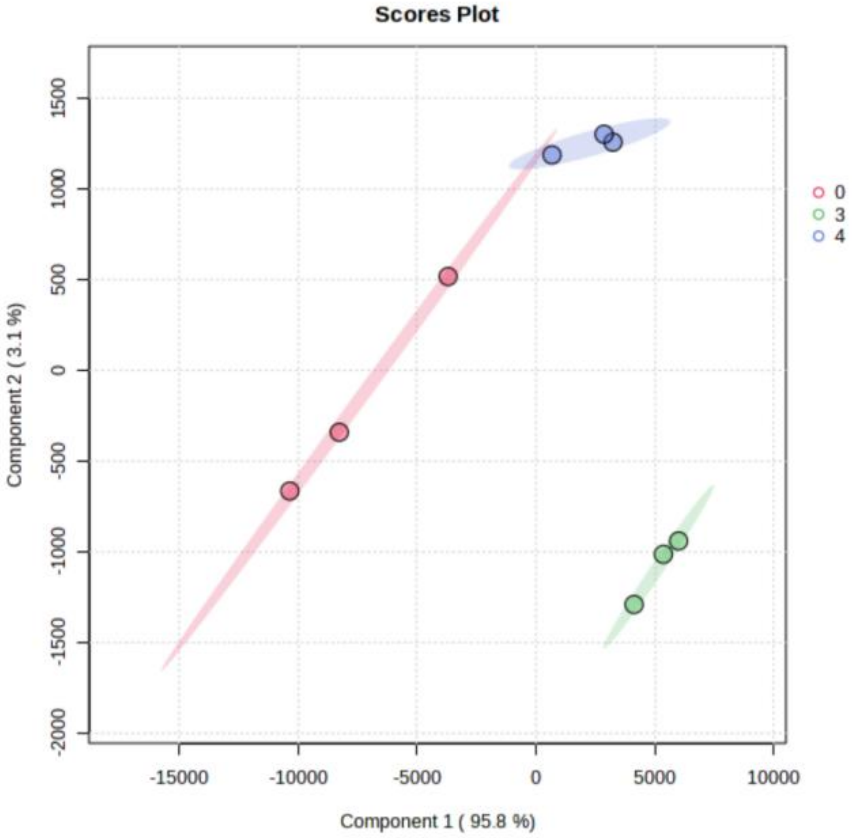

Figure 53. Partial Least Squares Discriminant Analysis (PLS-DA) of metabolic profiles of the compared experimental groups C1/C1SB2/C1B2: Red dots represent Caco-2 cells (0), green dots represent Caco-2 cells with the supernatant of *Bifido.* (3), and blue dots represent Caco-2 cells co-cultured with *Bifido*. (4)

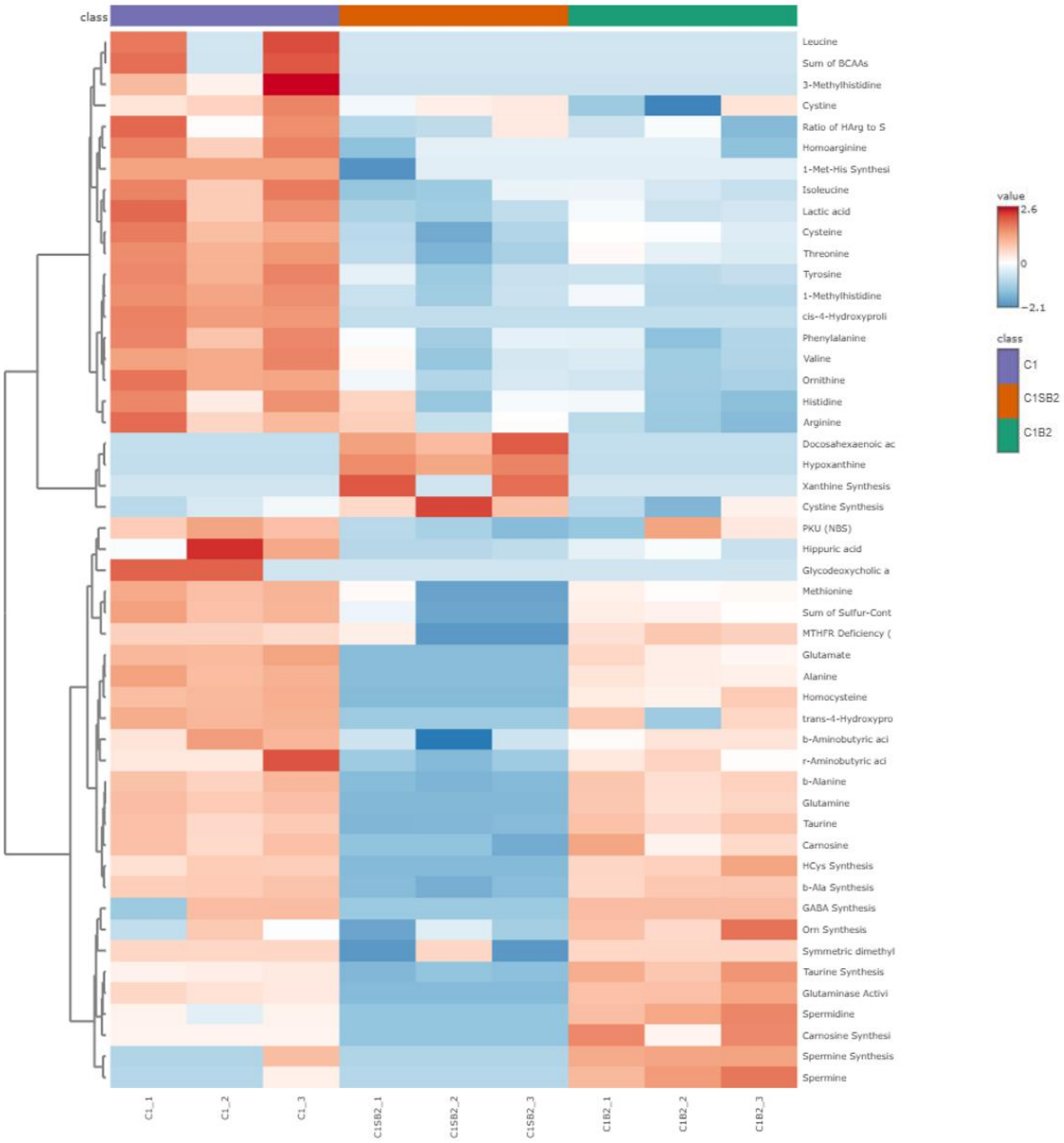

Figure 54. Differential metabolite clustering heatmap for different experimental groups C1/C1SB2/C1B2: Purple in class represents Caco-2 cells (C1), orange in class represents Caco-2 cells with the supernatant of *Bifido.* (C1SB2), and green in class represents Caco-2 cells co-cultured with *Bifido.* (C1B2)

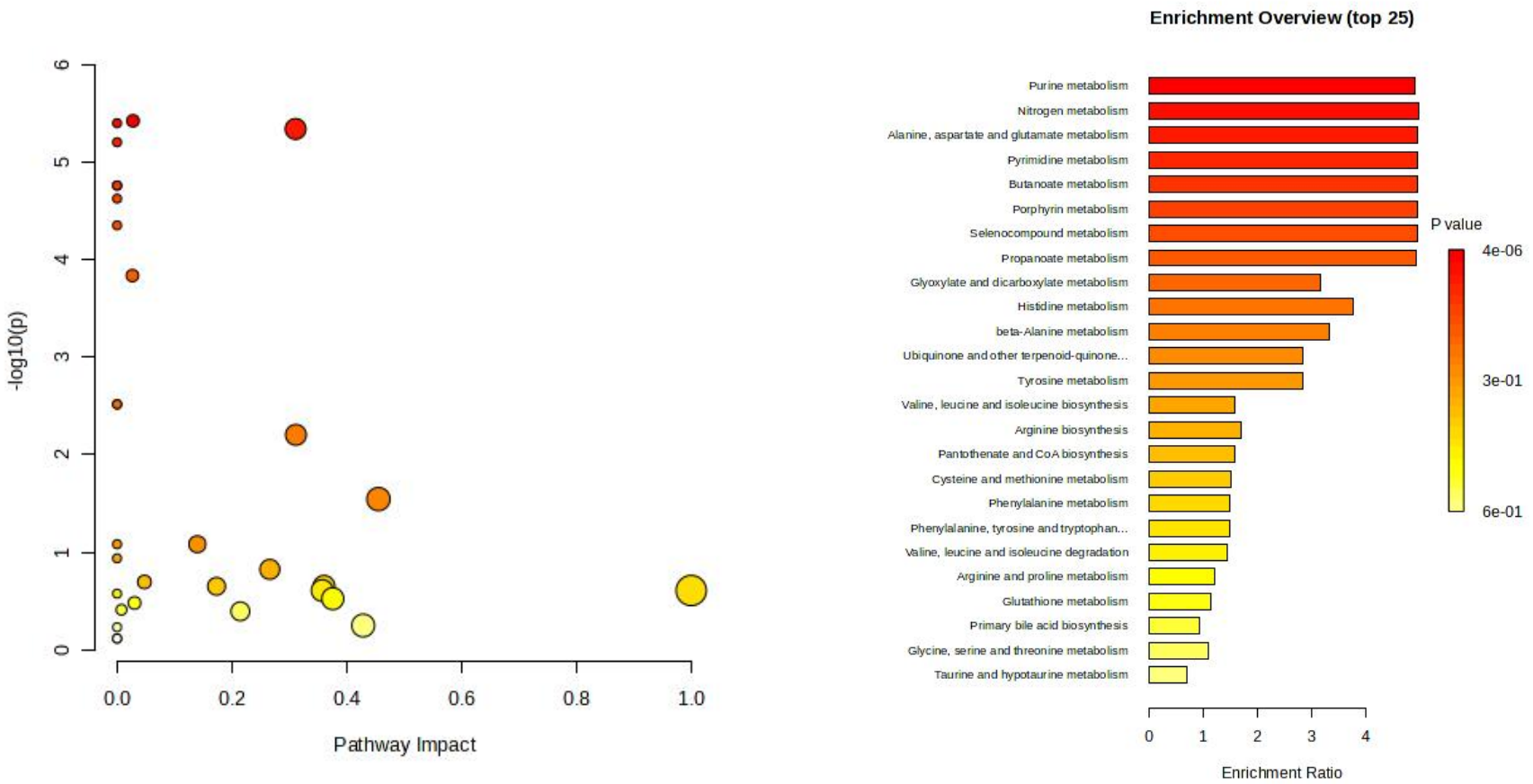

Figure 55. Scatter plot of metabolic pathways affected by differential metabolite enrichment in the experimental groups C1/C1SB2 and the corresponding metabolic pathway overview: the control group, Caco-2 cells (C1), and the experimental groups, Caco-2 cells with the supernatant of *Bifido.* (C1SB2). The redder the color, the smaller the p-value and the higher the significance.

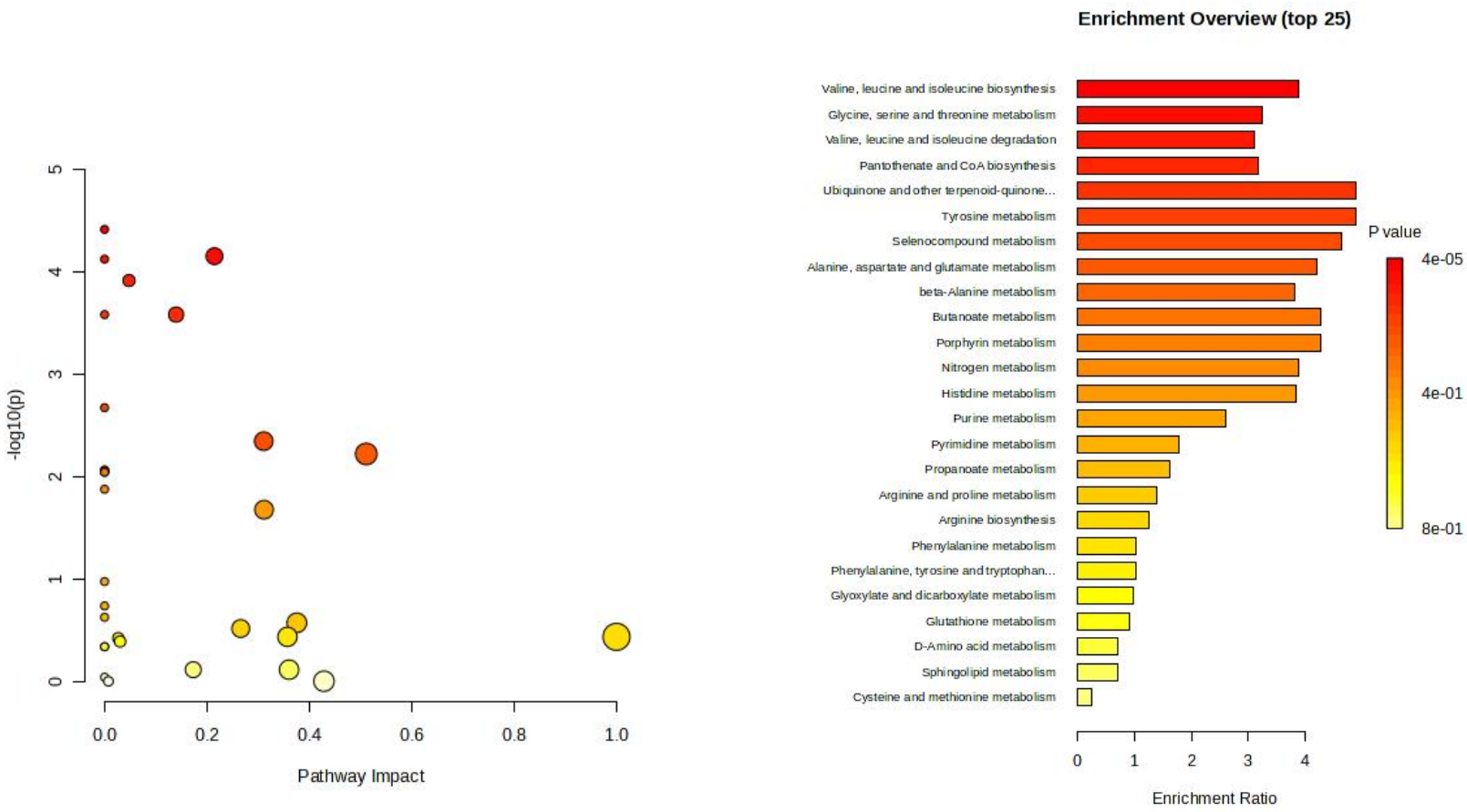

Figure 56. Scatter plot of metabolic pathways affected by differential metabolite enrichment in the experimental groups C1/C1SB2 and the corresponding metabolic pathway overview: the control group, Caco-2 cells (C1), and the experimental groups, Caco-2 cells co-cultured with *Bifido.* (C1B2). The redder the color, the smaller the p-value and the higher the significance.

The metabolite differences in the Chic-8E11 cells interacting with *Bacillus strain* or it's culture supernatant, were compared as: Chic-8E11 cells (C2), Chic8E11 cells with the supernatant of *Bacillus* (C2SB1), and Chic-8E11 cells co-cultured with *Bacillus* (C2B1).

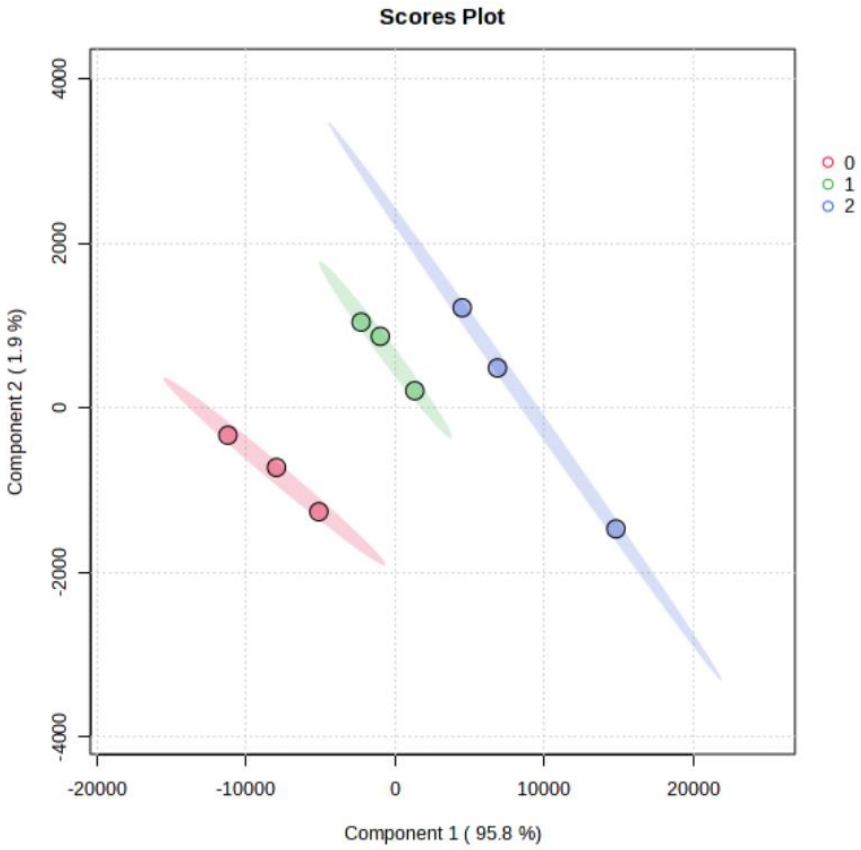

Figure 57. Partial Least Squares Discriminant Analysis (PLS-DA) of metabolic profiles of the compared experimental groups C2/C2SB1/CIB1: Red dots represent Chic-8E11 cells (0), green dots represent Chic-8E11 cells with the supernatant of *Bacillus* (1), and blue dots represent Chic-8E11 cells co-cultured with *Bacillus* (2)

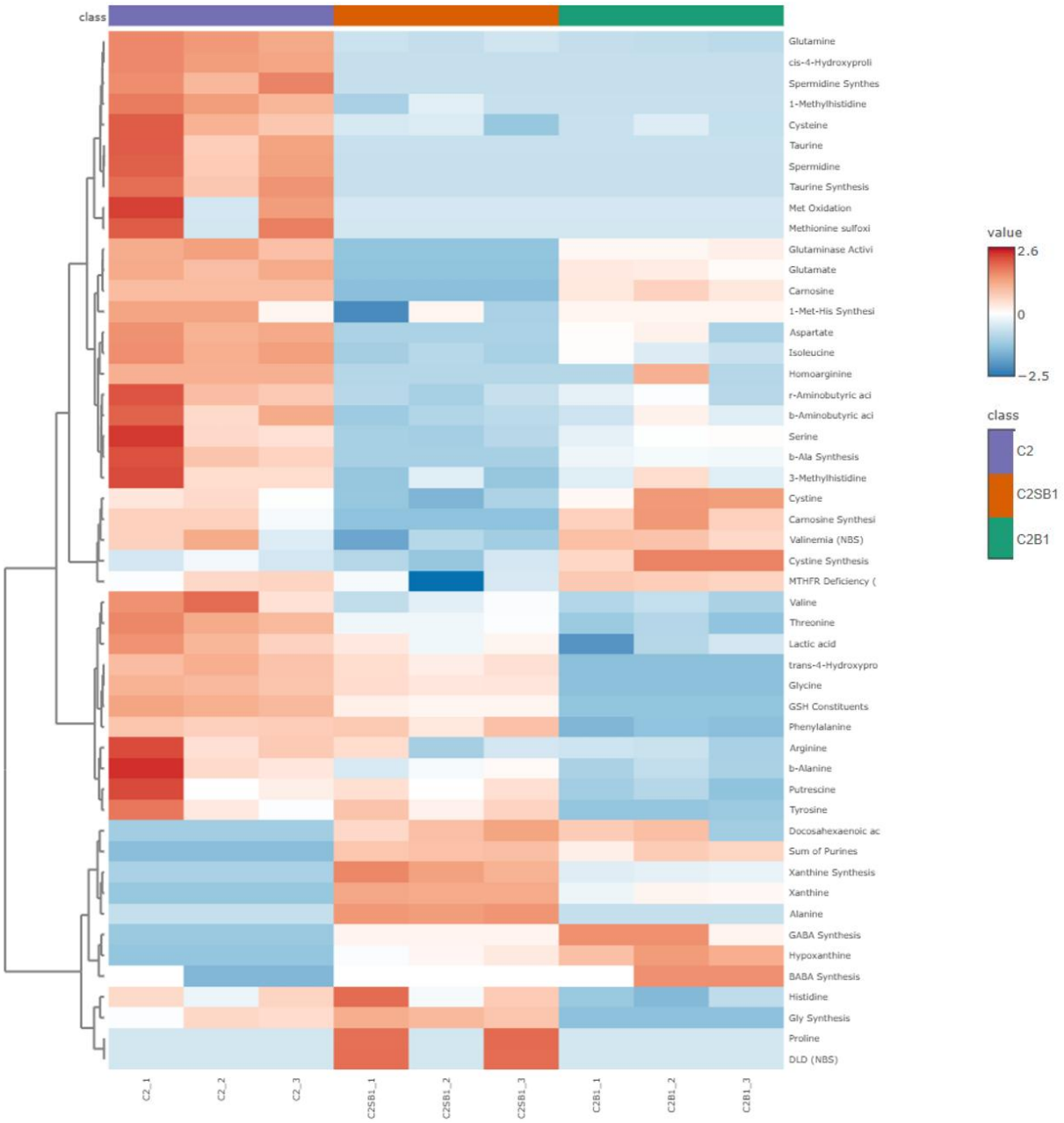

Figure 58. The differential metabolite clustering heatmap for different comparison experimental groups C2/C2SB1/CIB1: Purple in class represents Chic-8E11 cells (C2), orange in class represents Chic-8E11 cells with the supernatant of *Bacillus* (C2SB1), and green in class represents Chic-8E11 cells co-cultured with *Bacillus* (C2B1)

The horizontal axis represents the sample name, and the vertical axis represents the differential metabolites. The colors from blue to red represent the expression abundance of metabolites from low to high, that is, the redder the color, the higher the expression abundance of the differential metabolites.

KEGG enrichment analysis of differential metabolites in the control group, Chic-8E11 cells (C2), and the two experimental groups, Chic8E11 cells with the supernatant of *Bacillus* (C2SB1), and Chic-8E11 cells co-cultured with *Bacillus* (C2B1), was performed respectively, and the scatter plot of the top 25 metabolic pathways ranked by significance and the corresponding metabolic pathways were obtained.

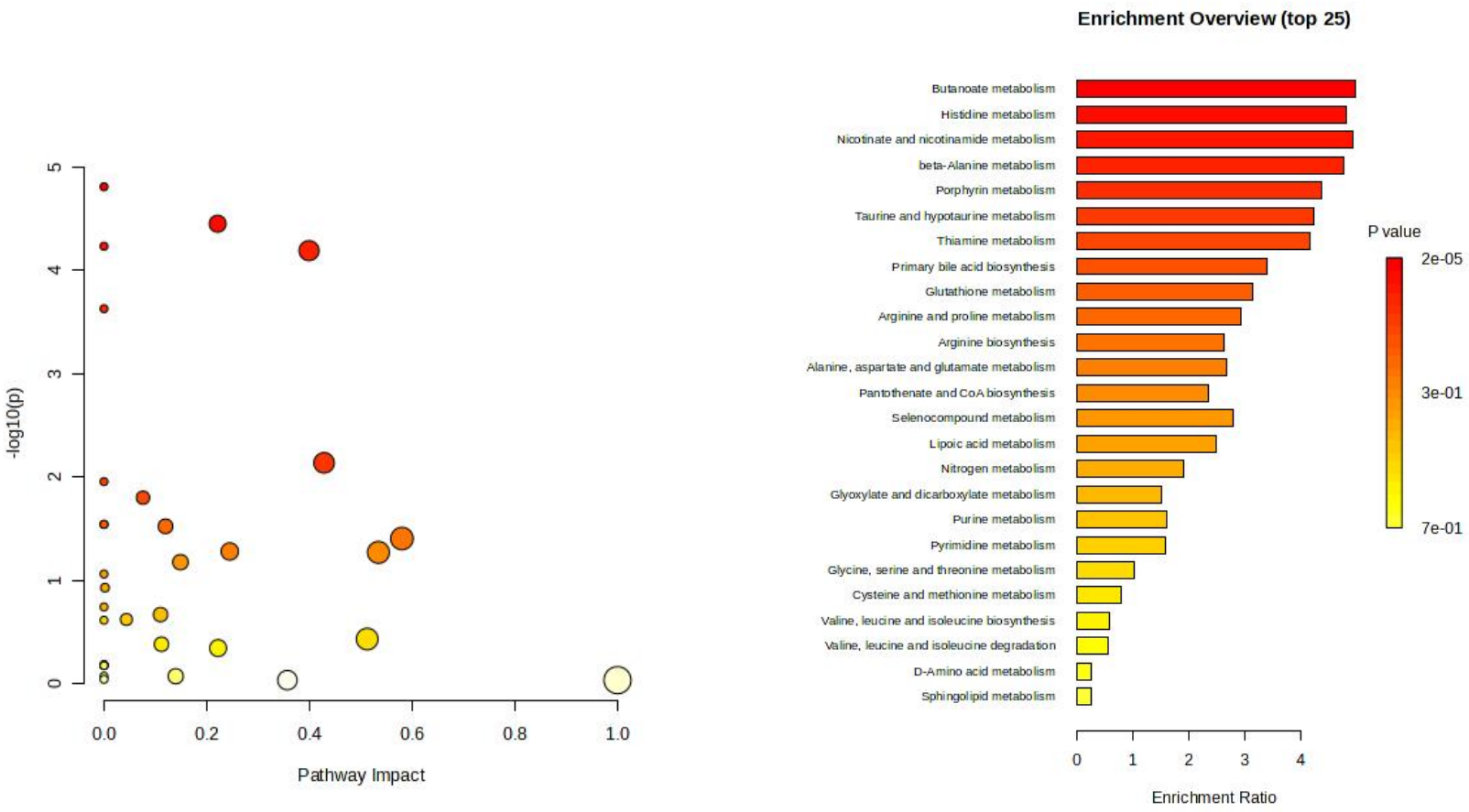

Figure 59. Scatter plot of metabolic pathways affected by differential metabolite enrichment in the experimental groups C2/C2SB1 and the corresponding metabolic pathway overview: the control group, Chic-8E11 cells (C2), and the experimental group, Chic8E11 cells with the supernatant of *Bacillus* (C2SB1). The redder the color, the smaller the p-value and the higher the significance.

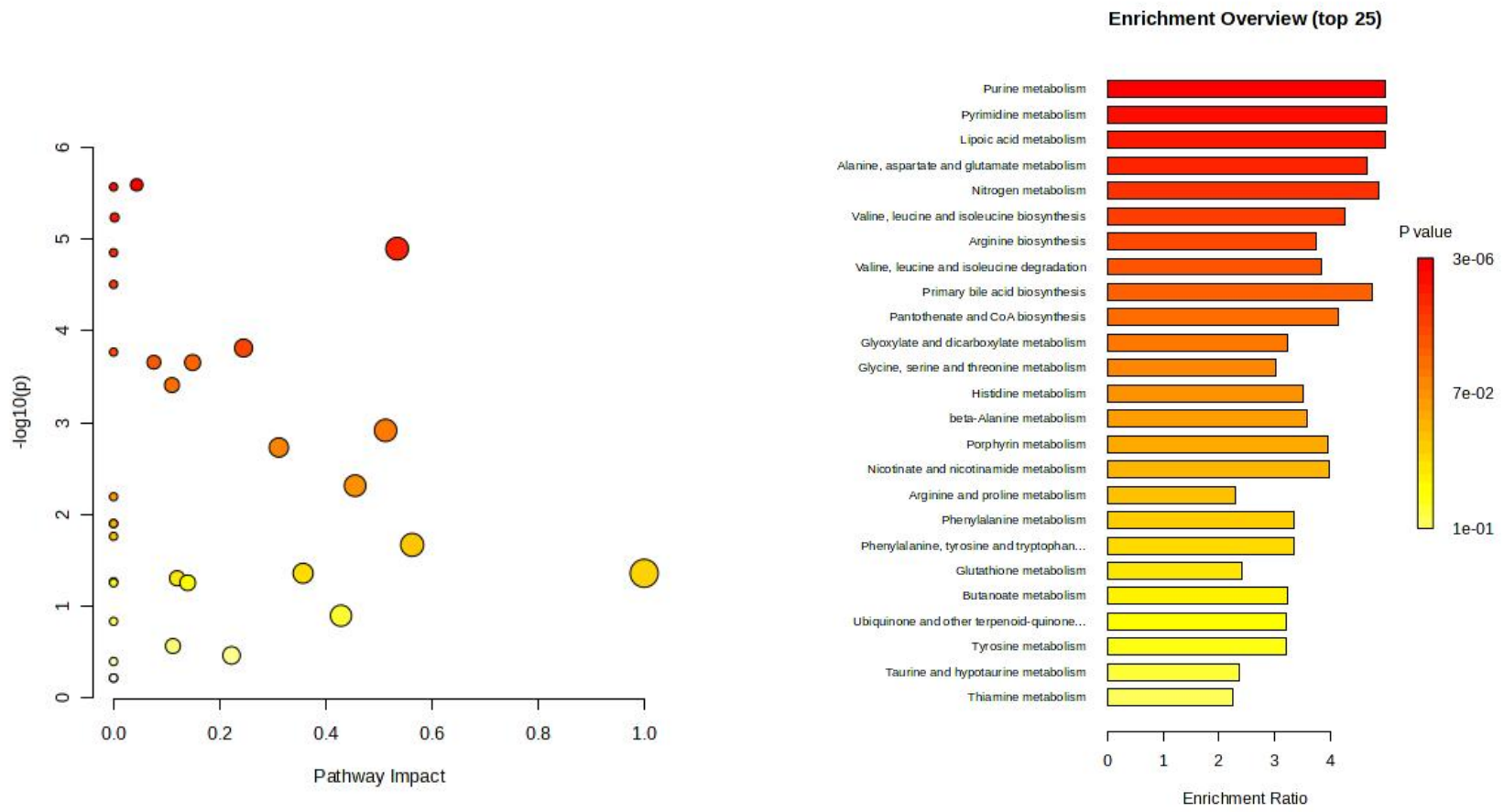

Figure 60. Scatter plot of metabolic pathways affected by differential metabolite enrichment in the experimental groups C2/C2B1 and the corresponding metabolic pathway overview: the control group, Chic-8E11 cells (C2), and the experimental group, Chic-8E11 cells co-cultured with *Bacillus* (C2B1). The redder the color, the smaller the p-value and the higher the significance.

The metabolite differences in the Chic-8E11 cells interacting with *Bifidobacterium lactis* NCC2818 or it's culture supernatant, were compared as: Chic-8E11 cells (C2), Chic-8E11 cells with the supernatant of *Bifido.* (C2SB2), and Chic-8E11 cells co-cultured with *Bifido.* (C2B2).

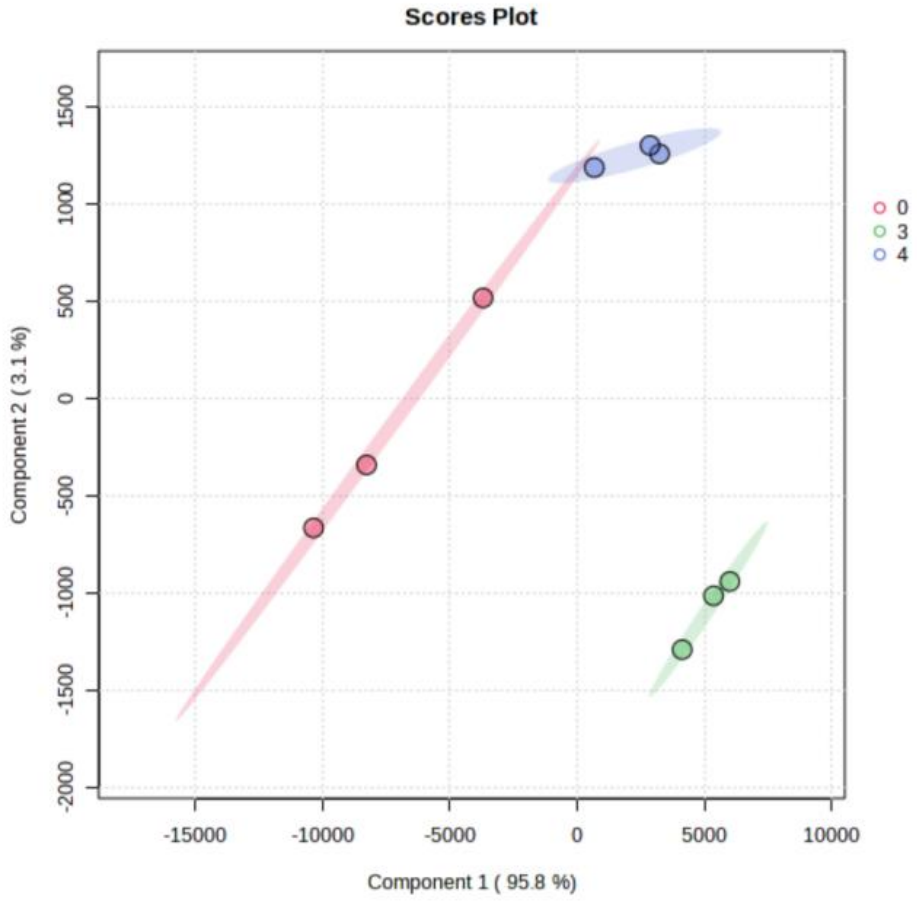

Figure 61. Partial Least Squares Discriminant Analysis (PLS-DA) of metabolic profiles of the compared experimental groups C2/C2SB2/C2B2: Red dots represent Chic-8E11 cells (C2), green dots represent Chic-8E11 cells with the supernatant of *Bifido.* (C2SB2), and blue dots represent Chic-8E11 cells co-cultured with *Bifido.* (C2B2)

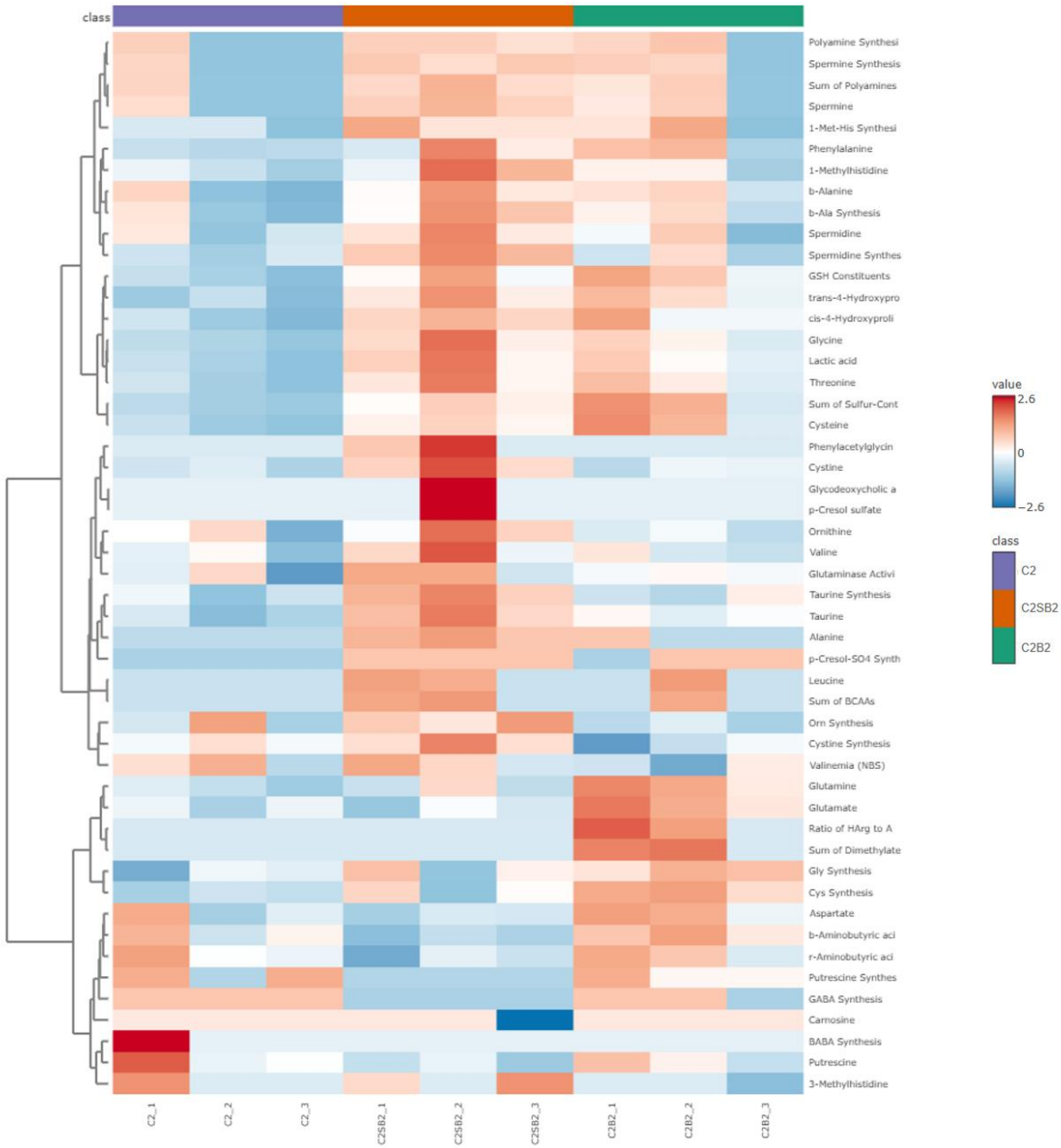

Figure 62. Differential metabolite clustering heatmap for different experimental groups C2/C2SB2/C2B2: Purple in class represents Chic-8E11 cells (C2), orange in class represents Chic-8E11 cells with the supernatant of *Bifido.* (C2SB2), and green in class represents Chic-8E11 cells co-cultured with *Bifido.* (C2B2)

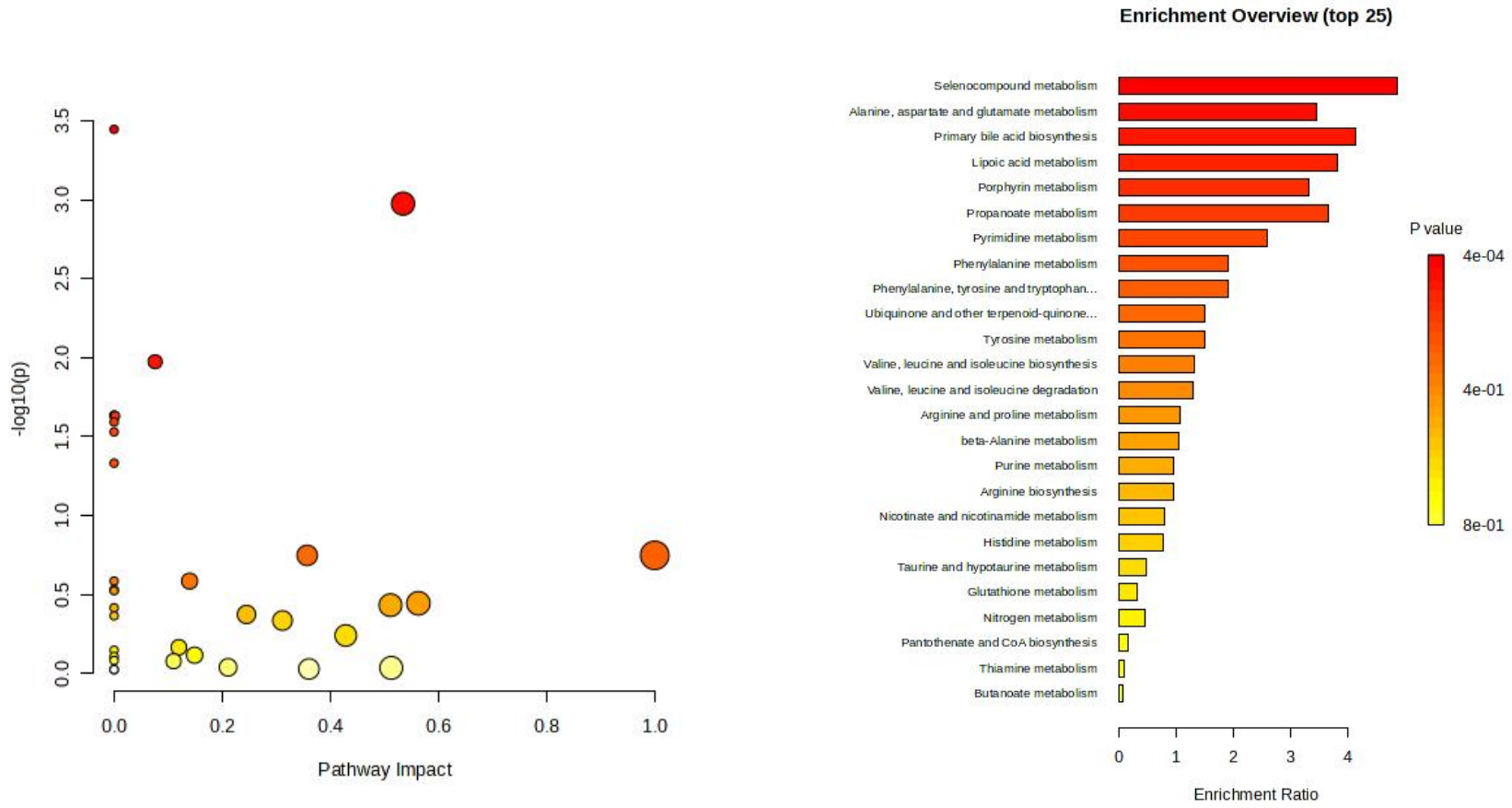

Figure 63. Scatter plot of metabolic pathways affected by differential metabolite enrichment in the experimental groups C2/C2SB2 and the corresponding metabolic pathway overview: the control group, Chic-8E11 cells (C2), and the experimental group, Chic-8E11 cells with the supernatant of *Bifido.*(C2SB2). The redder the color, the smaller the p-value and the higher the significance.

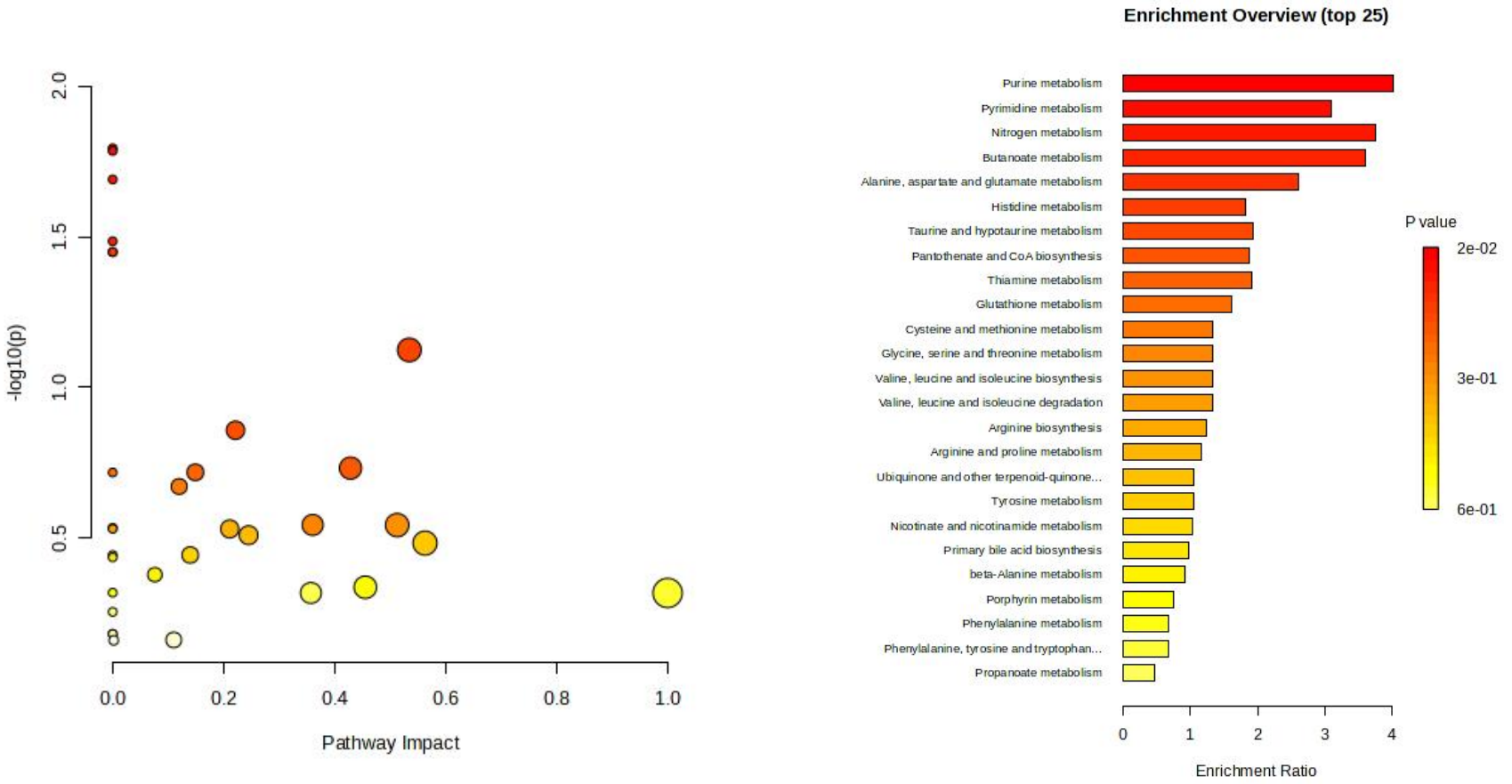

Figure 64. Scatter plot of metabolic pathways affected by differential metabolite enrichment in the experimental groups C2/C2B2 and the corresponding metabolic pathway overview: the control group, Chic-8E11 cells (C2), and the experimental group, Chic-8E11 cells co-cultured with *Bifido.* (C2B2). The redder the color, the smaller the p-value and the higher the significance.

4.5. Metabolomic analysis of chicken intestinal contents after *in ovo* injection of candidate probiotics, prebiotics and synbiotics

The metabolite differences between the *in ovo* injection of probiotic *Bifidobacterium* strain, prebiotic Astragalus polysaccharides or synbiotic (10^3 *Bifidobacterium* strain + 1 mg Astragalus polysaccharides) and the control group were compared as follows: control group (BiA), probiotic *Bifidobacterium* strain group (BiB), prebiotic Astragalus polysaccharides group (BiC) and synbiotic 10^3 *Bifidobacterium* strain + 1 mg Astragalus polysaccharides group (BiD).

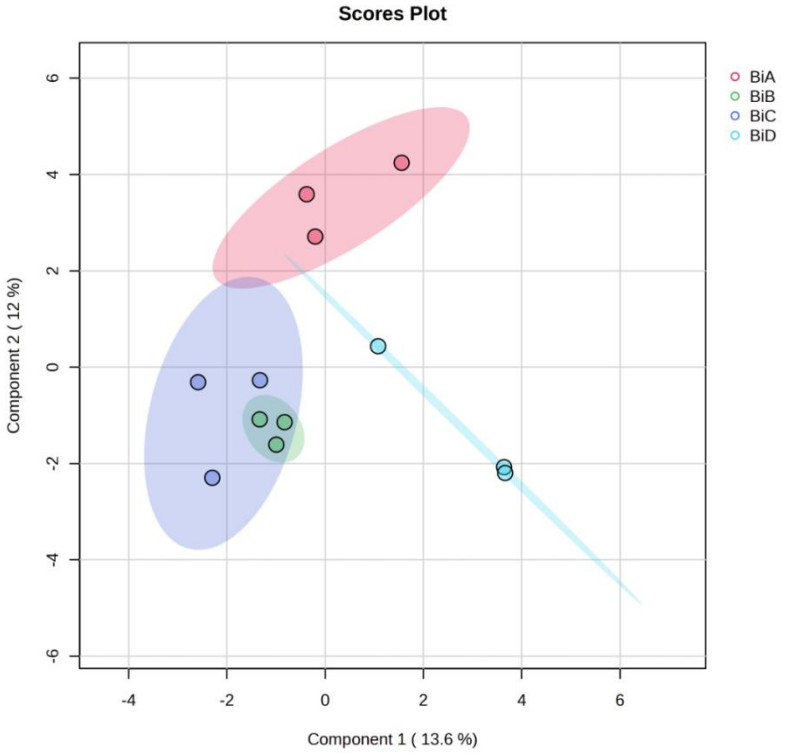

Figure 65. sparse Partial Least Squares Discriminant Analysis (sPLS-DA) of metabolic profiles of the compared experimental groups BiA/BiB/BiC/BiD: Red dots represent control group (BiA), green dots represent probiotic *Bifidobacterium* strain group (BiB), purple dots represent prebiotic Astragalus polysaccharides group (BiC), and blue dots represent synbiotic 10^3 *Bifidobacterium* strain + 1 mg Astragalus polysaccharides group (BiD)

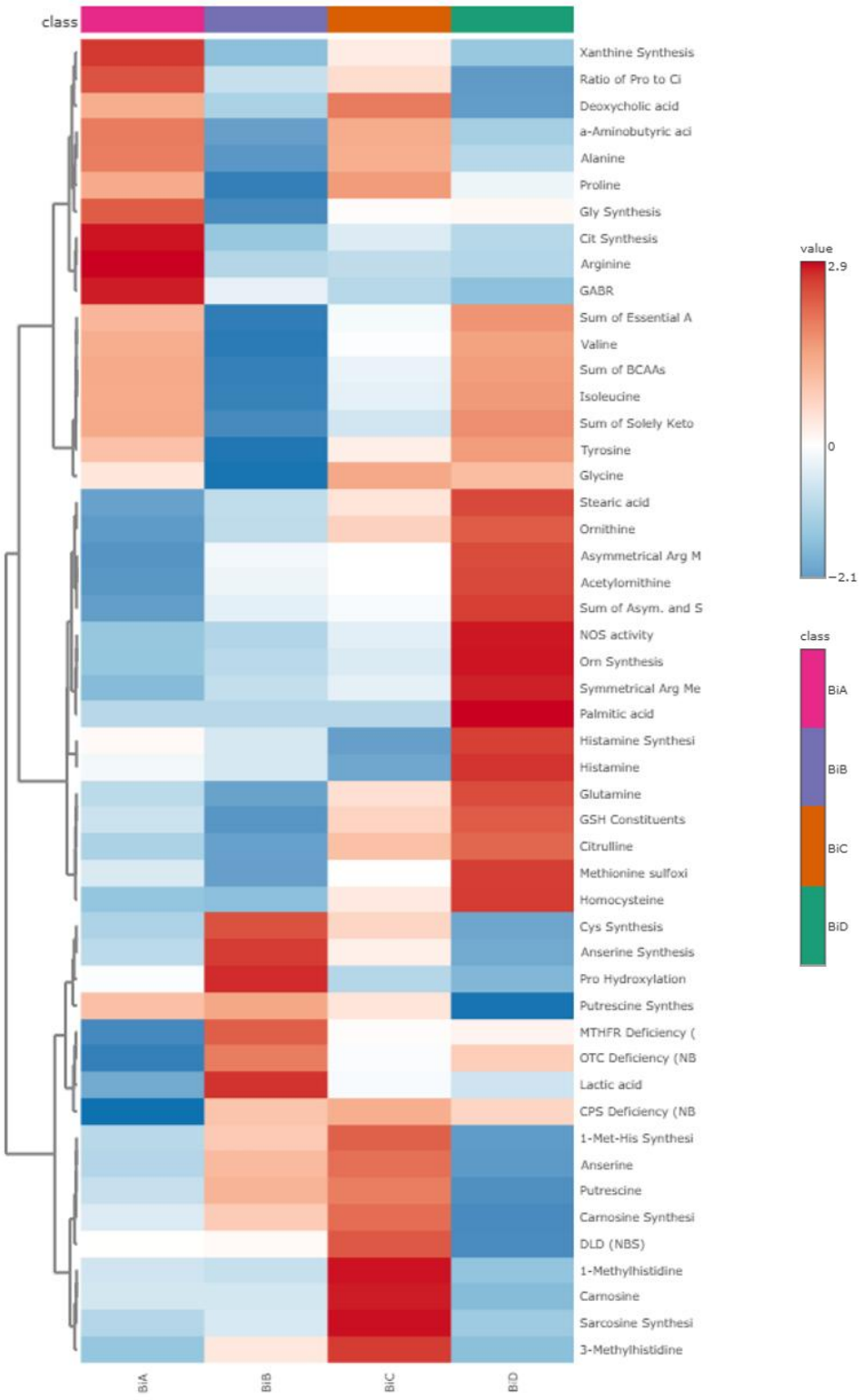

Figure 66. Differential clustering heat map of the average metabolite values of BiA/BiB/BiC/BiD in different experimental groups: Purple in class represents control group (BiA), blue in class represents probiotic *Bifidobacterium* strain group (BiB), orange in class

represents prebiotic Astragalus polysaccharides group (BiC), and green in class represents synbiotic 10^3 *Bifidobacterium* strain + 1 mg Astragalus polysaccharides group (BiD)

KEGG enrichment analysis of differential metabolites in the control group with probiotic *Bifidobacterium* strain, prebiotic Astragalus polysaccharides and synbiotic (10^3 *Bifidobacterium* strain + 1 mg Astragalus polysaccharides) was performed respectively, and the scatter plot of the top 25 metabolic pathways ranked by significance and the corresponding metabolic pathways were obtained.

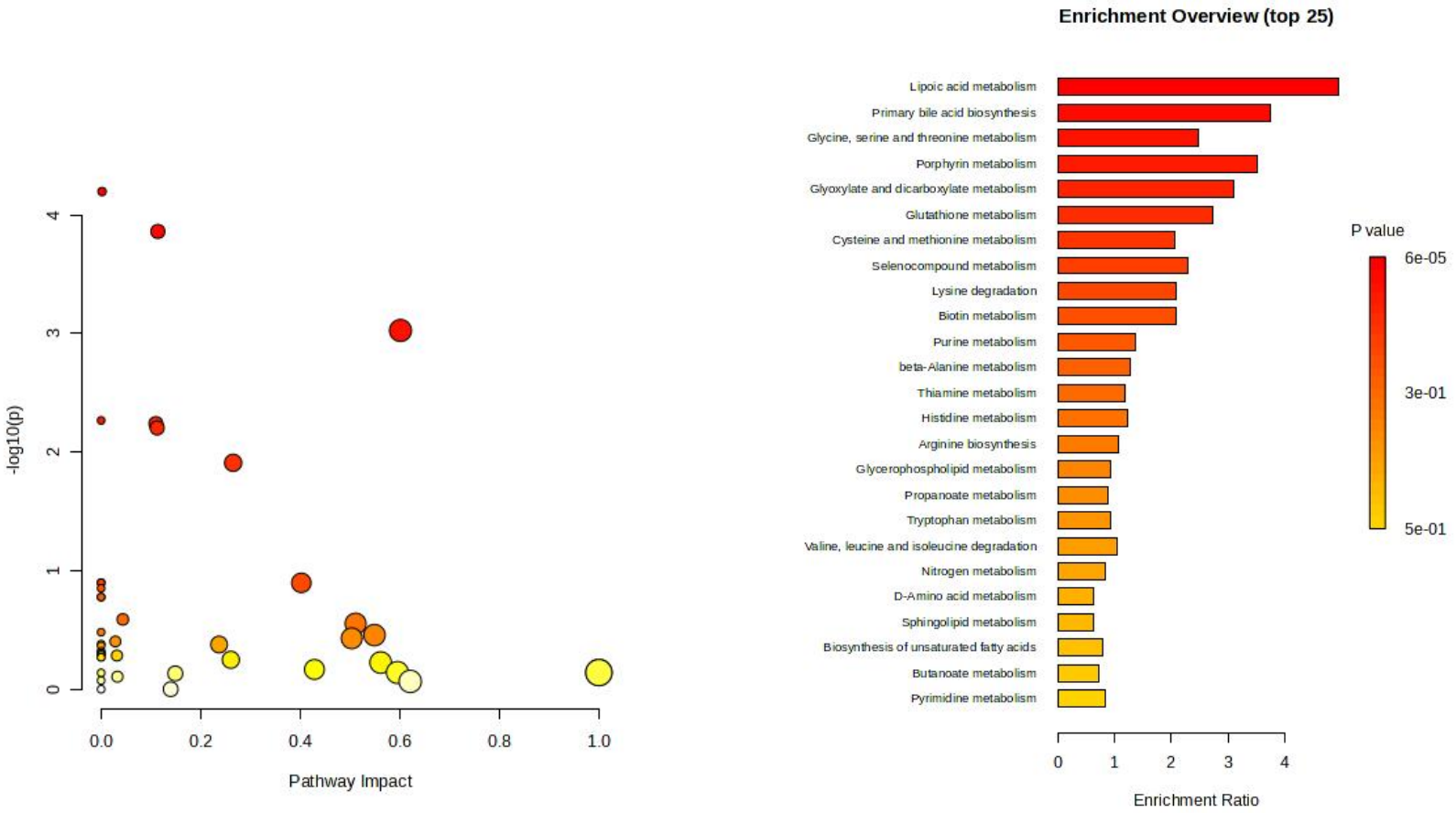

Figure 67. Scatter plot of metabolic pathways affected by differential metabolite enrichment in the experimental groups BiA/BiB and the corresponding metabolic pathway overview: control group (BiA), and the experimental group probiotic *Bifidobacterium* strain group (BiB). The redder the color, the smaller the *p*-value and the higher the significance.

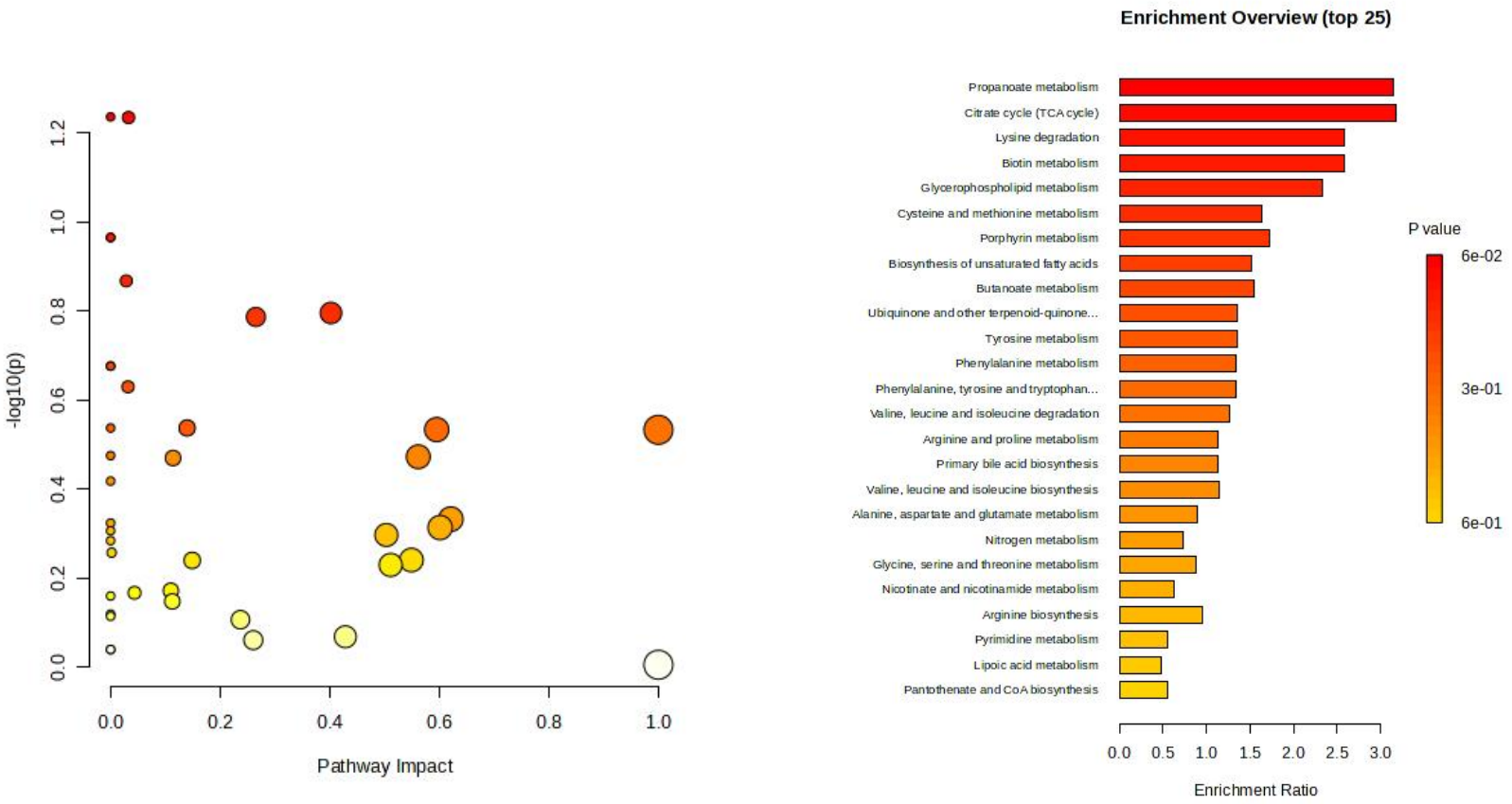

Figure 68. Scatter plot of metabolic pathways affected by differential metabolite enrichment in the experimental groups BiA/BiB and the corresponding metabolic pathway overview: control group (BiA), and the experimental group prebiotic Astragalus polysaccharides group (BiC). The redder the color, the smaller the *p*-value and the higher the significance.

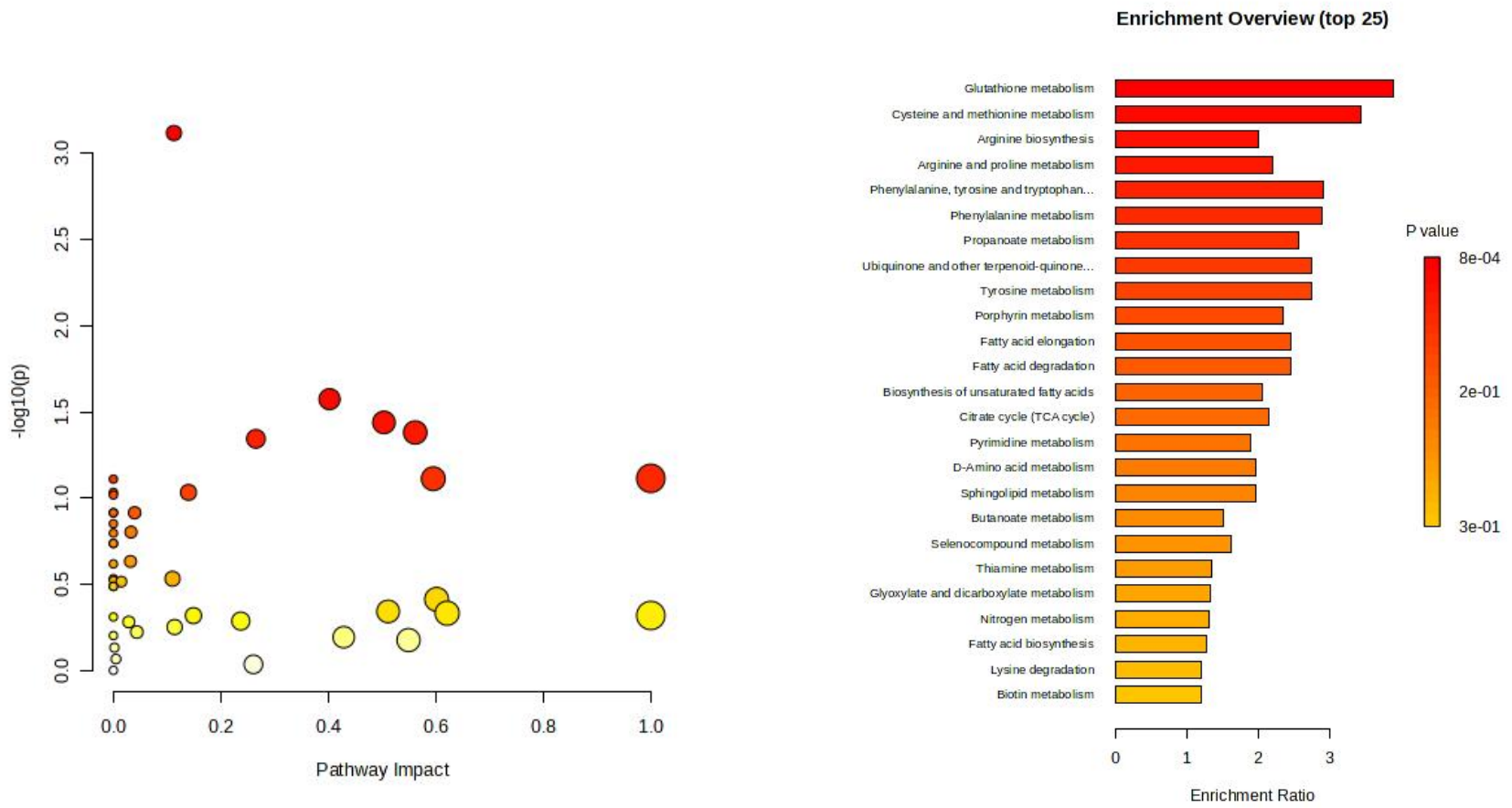

Figure 69. Scatter plot of metabolic pathways affected by differential metabolite enrichment in the experimental groups BiA/BiB and the corresponding metabolic pathway overview: control group (BiA), and the experimental group synbiotic 10^3 *Bifidobacterium* strain + 1 mg Astragalus polysaccharides group (BiD). The redder the color, the smaller the *p*-value and the higher the significance.

The metabolite differences between the *in ovo* injection of probiotic *Bacillus* strain, prebiotic vegetable protein hydrolysate-soya or synbiotic (10^3 *Bacillus* strain + 1 mg protein hydrolysate) and the control group were compared as follows: control group (BaA), probiotic *Bacillus* strain group (BaB), prebiotic vegetable protein hydrolysate-soya group (BaC) and synbiotic 10^3 *Bacillus* strain + 1 mg protein hydrolysate (BaD).

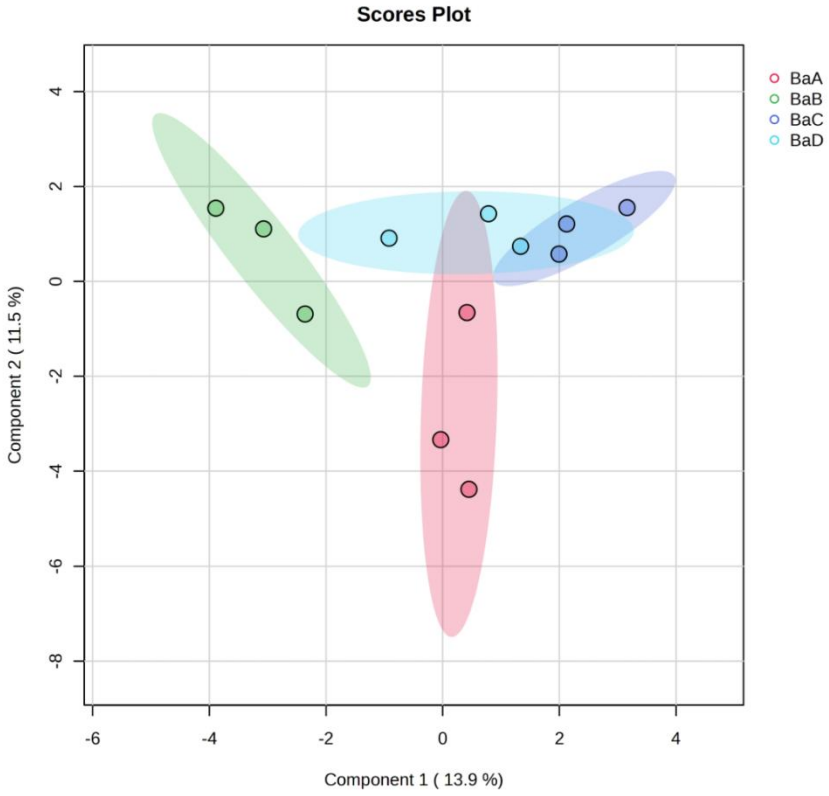

Figure 70. sparse Partial Least Squares Discriminant Analysis (sPLS-DA) of metabolic profiles of the compared experimental groups BaA/BaB/BaC/BaD: Red dots represent control group (BaA), green dots represent probiotic *Bacillus* strain group (BaB), purple dots representprebiotic vegetable protein hydrolysate-soya group (BaC), and blue dots represent synbiotic 10^3 *Bacillus* strain + 1 mg protein hydrolysate (BaD)

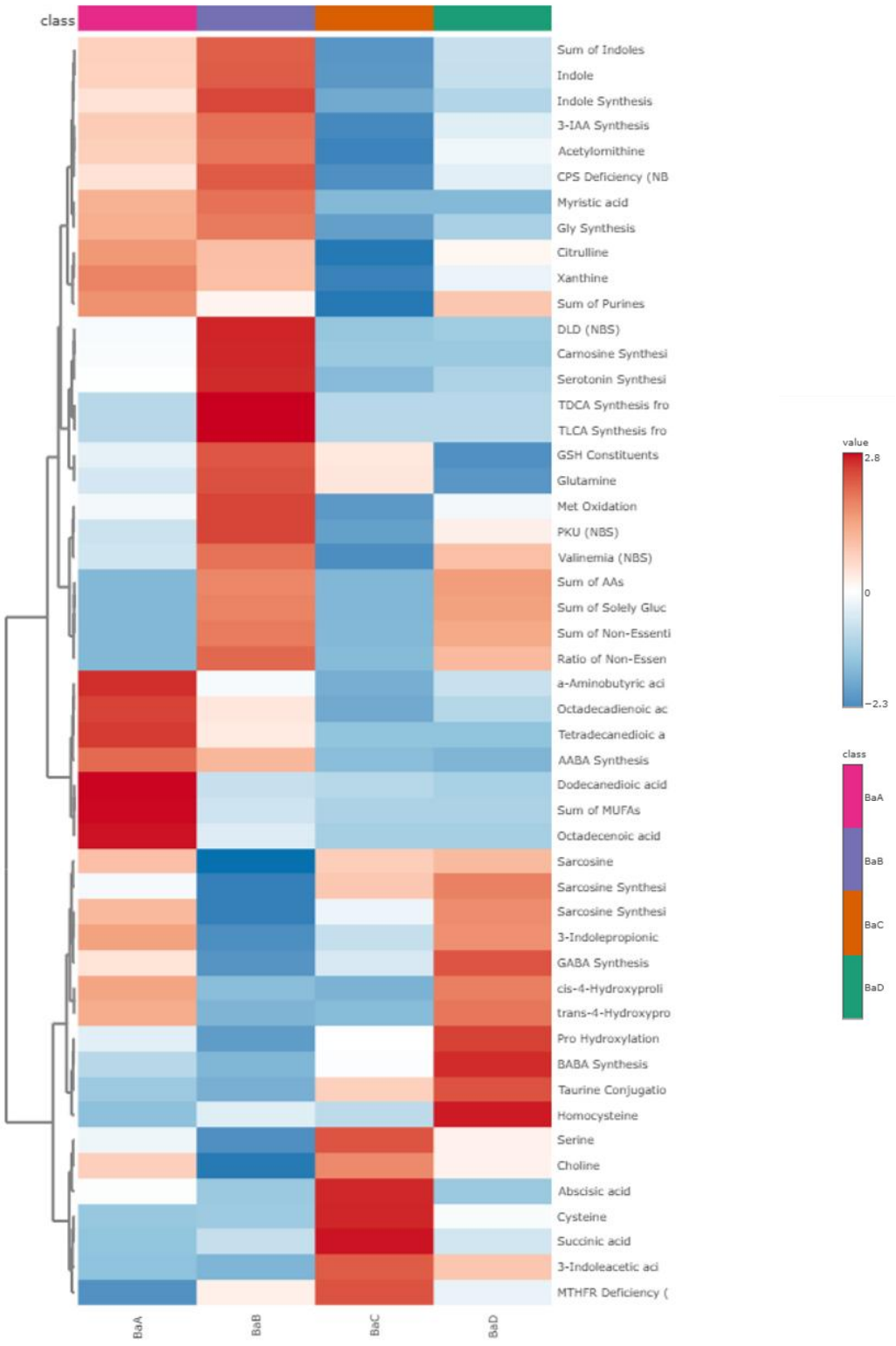

Figure 71. Differential clustering heat map of the average metabolite values of BaA/BaB/BaC/BaD in different experimental groups: Purple in class represents control group (BaA), blue in class represents probiotic *Bacillus* strain group (BaB), orange in class

represents prebiotic vegetable protein hydrolysate-soya group (BaC), and green in class represents synbiotic 10^3 *Bacillus* strain + 1 mg protein hydrolysate (BaD)

KEGG enrichment analysis of differential metabolites in the control group with probiotic *Bacillus* strain, prebiotic vegetable protein hydrolysate-soya and synbiotic (10^3 *Bacillus* strain + 1 mg protein hydrolysate) was performed respectively, and the scatter plot of the top 25 metabolic pathways ranked by significance and the corresponding metabolic pathways were obtained.

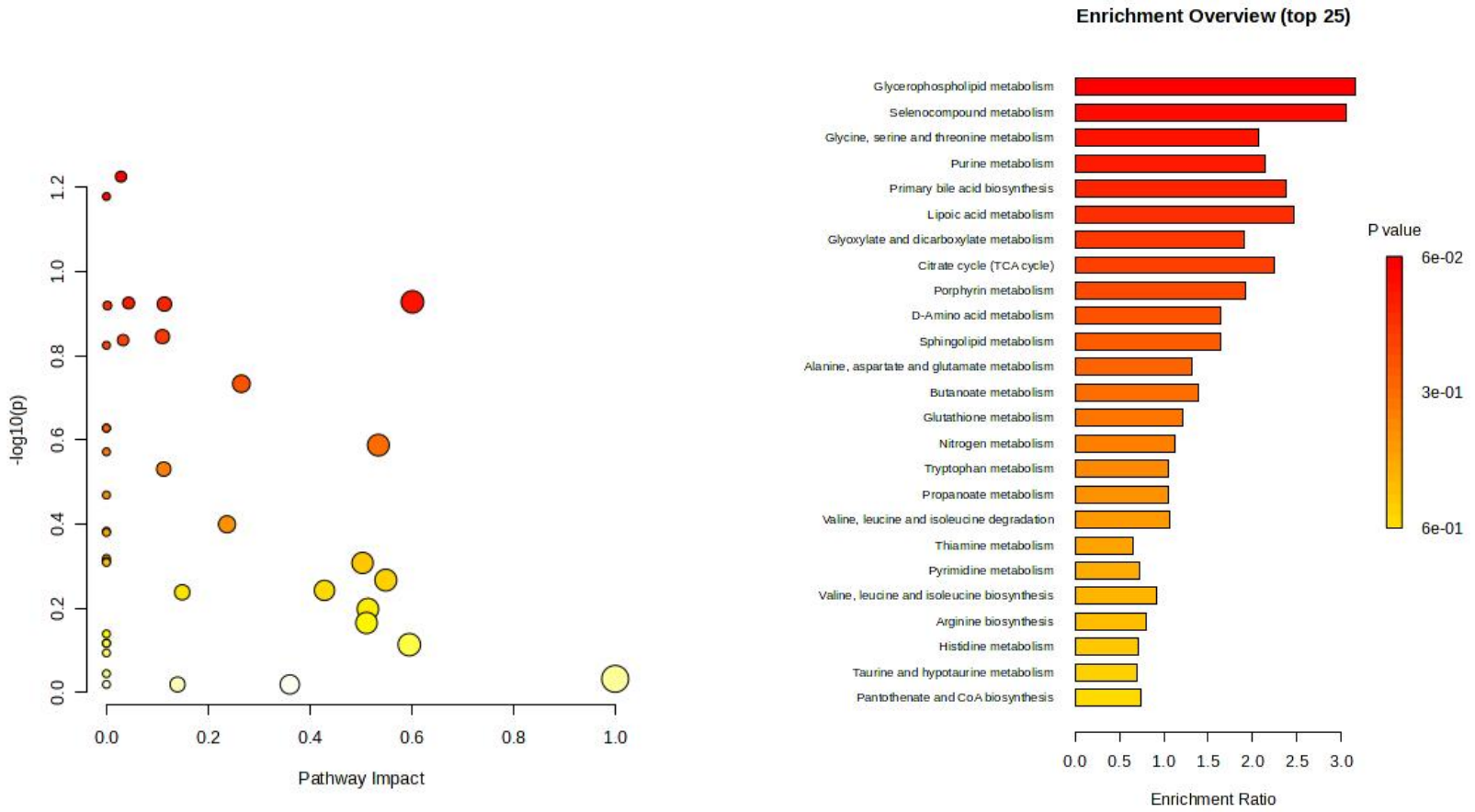

Figure 72. Scatter plot of metabolic pathways affected by differential metabolite enrichment in the experimental groups BaA/BaB and the corresponding metabolic pathway overview: control group (BaA), and the experimental group probiotic *Bacillus* strain group (BaB). The redder the color, the smaller the *p*-value and the higher the significance.

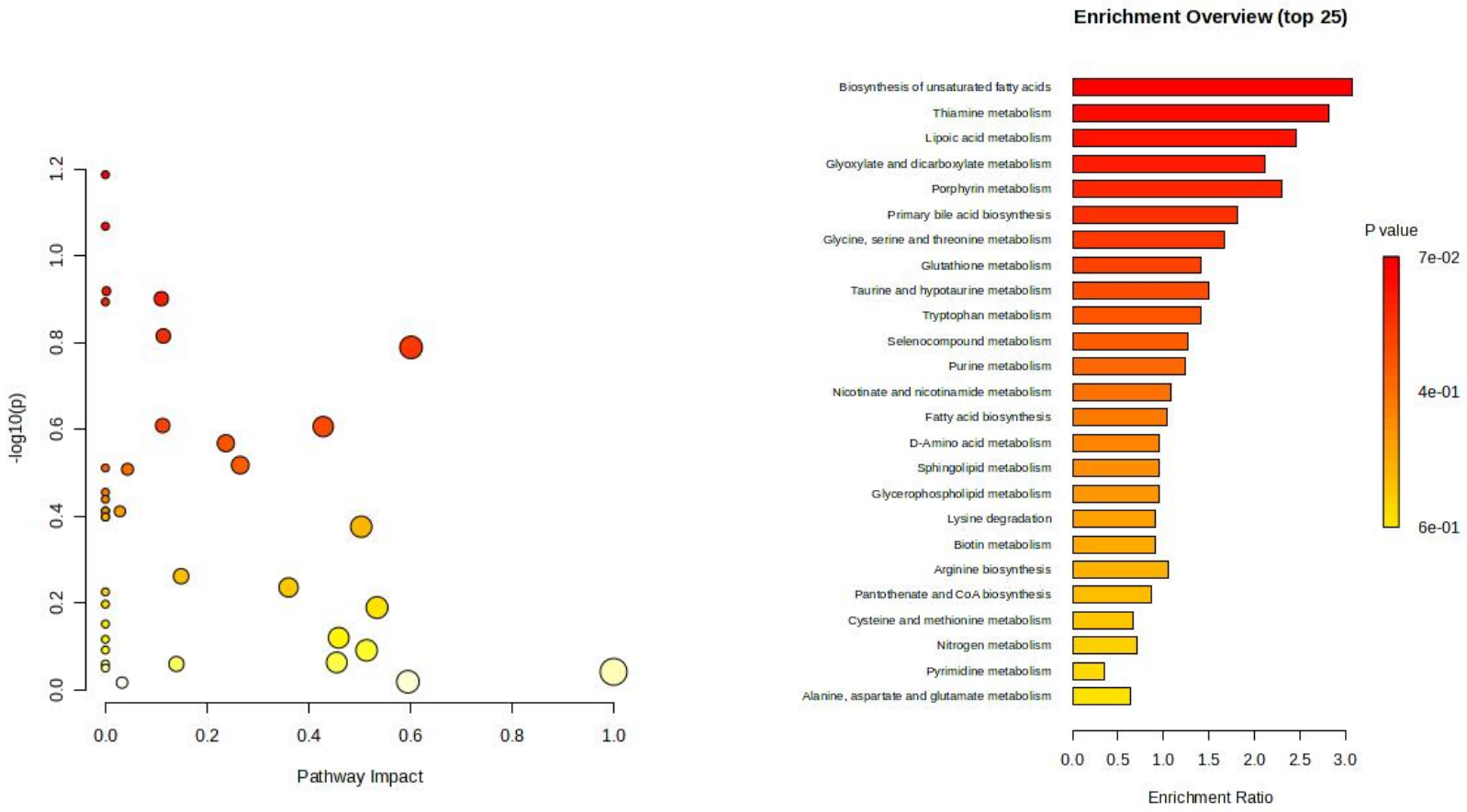

Figure 73. Scatter plot of metabolic pathways affected by differential metabolite enrichment in the experimental groups BaA/BaC and the corresponding metabolic pathway overview: control group (BaA), and the experimental group prebiotic vegetable protein hydrolysate-soya group (BaC). The redder the color, the smaller the *p*-value and the higher the significance.

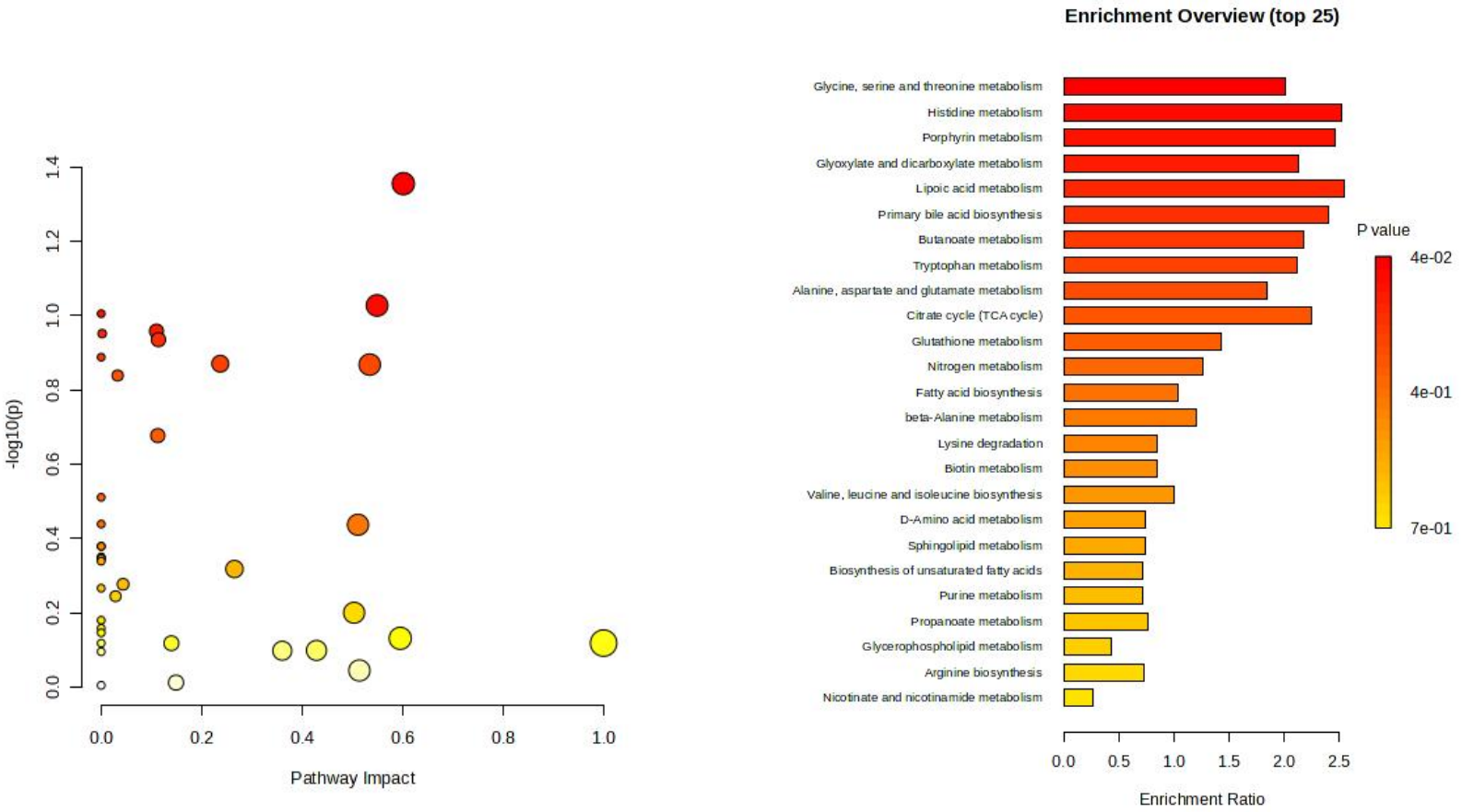

Figure 74. Scatter plot of metabolic pathways affected by differential metabolite enrichment in the experimental groups BaA/BaD and the corresponding metabolic pathway overview: control group (BaA), and the experimental group synbiotic 10^3 *Bacillus* strain + 1 mg protein hydrolysate (BaD). The redder the color, the smaller the *p*-value and the higher the significance.

5. DISCUSSION

5.1. Characterization of Caco2 and Chick8E11 cells in an *in vitro* intestinal co-culture model with the probiotics *Bifidobacterium lactis* NCC2818 and *Bacillus* strain

Intestinal barrier plays an important role in maintaining the gut health and appropriate level of defense. It is mainly composed of epithelial cells and intercellular junctions, which are the apical junctional complex (AJC) composed of tight junctions (TJ), adherens junctions (AJ), gap junctions (GJ) and desmosomes (DES) (Garcia et al., 2018).

Tight junctions are mainly composed of transmembrane protein complexes (such as claudins and occludins) and cytoplasmic protein ZO-1 (Hu et al., 2012), among which occludin is involved in regulating the intermembrane diffusion and paracellular diffusion of small molecules; ZO1 is a plaque protein that can act as a connector to connect transmembrane proteins to the actomyosin ring around the junction. Plaque proteins play a core role in TJ regulation and cause reorganization of the cytoskeleton; Claudin-1 is the structural skeleton of TJ and can regulate intestinal permeability (Ibrahim et al., 2020). Adherence junctions (AJs) mainly maintain cell-to-cell adhesion, regulate the actin-organized cytoskeleton, and establish a hub for cell signaling and gene transcription regulation (Takeichi, M., 2014); E-cadherin is the main transmembrane protein of AJ, which strengthens cell-to-cell adhesion by connecting to the actin cytoskeleton. Desmoplakin is a member of the plakin family that directly binds to cytokeratin intermediate filaments, giving epithelial cells stronger intercellular adhesion (Garcia et al., 2018). These proteins together, functionally constitute the intestinal barrier which is essential for maintaining an individual's health and acts as a physical key line of defense against foreign antigens from the environment.

In order to understand the effects of selected probiotics on the intestinal barrier, the results of ZO-1, claudin, occludin, E-cadherin, and desmoplakin gene/protein expression levels were determined in this study. There were new evidences on the role of microbiota, and probiotics in particular, in regulation of intestinal barrier function. Some metabolites

produced by probiotics enhance the expression of tight junctions, and promote mucus secretion (Liu et al., 2020).

The human intestinal cell model Caco-2 and the novel cell line model chicken intestinal cell Chic-8E11 can be used as stable monolayer cell models for subsequent studies. Among them, the Caco-2 cell line is derived from the human colon adenocarcinoma model and is one of the most widely studied and applied intestinal cell models to date (Ding et al., 2021). Chic-8E11 cells are derived from chicken intestinal epithelial cells, a clone of MM-CHIC 8E11, as a novel avian cell line model. Cell culture is very important for the examination of cell biology and specific cell mechanisms of bioactive substances *in vitro*.

Two-dimensional (2D) monolayer is currently the most stable and popular cell culture model. Since many cell lines have the ability to self-assemble, there is a 3D culture method to produce spheroids (Białkowska et al., 2020). Culturing cells into spheroids has significant advantages, and a better *in vitro* model is three-dimensional (3D) culture. Since spheroids are composed of complex cell networks, this allows the culture to use its structure to establish cell-to-cell contacts and communication. Compared with traditional standard 2D monolayer cell culture, spheroids can improve the performance and function of key biological components that simulate the complex crosstalk between cells in the intestinal microenvironment (Beamer et al., 2023).

Moreover, it was observed that compared with Caco-2 cells, Chic-8E11 cells grew more closely, and the intestinal spheroids formed by Chic8E11 were more compact, showing a microscopic intestinal morphology, which can be used as a potential *in vitro* 3D culture model. The potential value of these two intestinal cells has been observed, but in-depth development and research have not yet been conducted to establish stable and reproducible 3D culture models of Caco-2 cells or Chic-8E11 cells for research applications. Therefore, current *in vitro* research is still being carried out using reliable and highly reproducible cell monolayer models.

In this study, under the stimulation of two probiotics or their supernatants, the occludin gene of Chic-8E11 cells was significantly up-regulated ($p < 0.01$) or there was an up-regulation trend, as shown in Figure 33, indicating that under the action of

Bifidobacterium lactis NCC2818 (or its supernatant) and *Bacillus strain* supernatant, the tight junction intestinal barrier of chicken intestinal cells Chic-8E11 and human intestinal cells Caco-2 was strengthened through the expression of occludin. According to literature, this mode of probiotic function supports normal regulation of physiological processes in the cells (Belardi et al., 2020; Haas et al., 2022). At the protein expression level, the occludin protein gene expression of chic-8E11 cells showed up-regulation trend, similar to its gene expression changes, further indicating that under the action of *Bifidobacterium lactis* NCC2818 (or its supernatant) and *Bacillus* strain (or its supernatant), intestinal cells function was improved and strengthened. In the study by Huang et al., it was found that the expression levels of ZO-1 and occludin genes in the midgut of tilapia were increased after feeding the basal diet (CT) and supplementing with some potential probiotics from the genus *Bacillus* (Huang et al., 2024). And in the study of Zhang et al., it was shown that the expression level of tight junction protein occludin was significantly increased when *Bacillus* subtilis was supplemented in the basal diet of laying hens (Zhang et al., 2021).

In addition, there was no significant trend in the expression of ZO-1 gene and protein in Chic-8E11 cells, indicating that the effect of *Bifidobacterium lactis* NCC2818 (or its supernatant) was not correlated with the ZO-1-related tight junction protein of Chic-8E11 cells. It has been reported in the literature that the probiotic *Bifidobacterium breve* JCM1192 competitively reduces the abundance of Salmonella typhimurium in broilers by adhering to intestinal epithelial cells, improving the colonization of beneficial intestinal bacteria; *Bifidobacterium infantis* BL2416 improves the weight gain and food conversion rate of broilers. Both of them can be used as alternative therapies for Salmonella typhimurium infection in broilers. However, *Bifidobacterium longum* Ncc2785 neither attaches to epithelial cells nor induces cytokine release, and therefore cannot prevent the colonization of harmful bacteria in broilers (El-Sharkawy et al., 2020). *Bifidobacterium lactis* Bb12 completely inhibited the growth of avian pathogenic Escherichia coli (APEC) at 24 h to control APEC infection in chickens, and can be used as a new antibiotic alternative therapy (Kathayat et al., 2022). The mechanisms of action of *Bifidobacterium* probiotics on poultry intestinal health are different, and there are currently few studies on the relationship between *Bifidobacterium* probiotics and tight junctions in the chicken intestine. However,

the expression of the ZO-1 gene in Caco-2 cells was significantly upregulated ($p < 0.01$), indicating that *Bifidobacterium lactis* NCC2818 (or its supernatant) acts on the ZO-1-related tight junction proteins of Caco-2 cells to enhance the tight junction barrier of the human intestine. It has been reported that in an *in vitro* study, pretreatment with *Bifidobacterium* significantly upregulated the expression of occludin, claudin-3, and ZO-1 in LPS-induced barrier damage in Caco-2 monolayer intestinal epithelial cells ($p < 0.01$), thereby regulating the normalization of the expression of tight junction proteins in intestinal cells. In an *in vivo* study, feeding with *Bifidobacterium* reduced the incidence of necrotizing enterocolitis (NEC) in rats ($P < 0.05$) and reduced the severity of the NEC model (Ling et al., 2016).

After *Bacillus* treatment, the ZO-1 gene was down-regulated, which suggests that the addition of this probiotic in a direct contact with Chic-8E11 cells did not stimulate formation of the tight junction. In contrast, the *Bacillus* supernatant increased the expression of the ZO-1 gene and protein, indicating that *Bacillus* metabolites have a regulatory (enhancing) effect on the cellular intestinal barrier. Zhu La et al. found that the probiotic properties of the six strains of *Bacillus* were different. Among them, the dietary supplementation of *Bacillus* CML532 strain significantly improved the gene expression of occludin, claudin-2, claudin-3 and ZO-1 on day 42 ($p < 0.05$). Such a modulation can promote the animal growth and improve intestinal barrier and absorption function (Zhu La et al., 2024). It can be concluded that *Bacillus* acts on intestinal tight junctions by regulating the expression of ZO-1 genes and proteins, indicating that its metabolites may have the effect of improving intestinal barrier function.

Immunofluorescence staining showed that after Chic-8E11 cells were stimulated with *Bacillus* (or its supernatant), the expression of E-cadherin protein was high, and the cell adhesion and the cytoskeleton between actin elements were intact, indicating that the polarity of epithelial cells was well maintained and the function was stable. Xu et al. found that endophytic *Bacillus* (*Bacillus altitudinis*) has been identified as an inducer for ginsenoside production in the study of ginsenosides, improving intestinal epithelial cells by restoring the production of E-cadherin and N-cadherin. (Xu et al., 2023)

The expression of desmoplakin protein in Chic-8E11 cells was down-regulated, indicating that the probiotics *Bacillus* stain (or its supernatant) and *Bifidobacterium lactis* NCC2818 in this study inhibited the adhesion ability of Chic-8E11 cells by desmoplakin function. However, a study found that dietary supplementation with *Bacillus subtilis* had no significant effect on the total egg production of 28-week-old Hy-line Brown laying hens, and there was no significant change in average egg weight and intestinal morphology, while inducing a healthier microbiota composition and inducing the expression of other higher tight junction proteins to enhance the physical barrier function of the intestine (Zhang et al., 2021). It appears that the probiotic *Bacillus* strains do not regulate the intestinal barrier function through desmoplakin protein. However, after adding the supernatant of *Bifidobacterium lactis* NCC2818, the expression of desmoplakin protein in Chic-8E11 cells and Caco-2 cells was upregulated, and the adhesion ability remained normal. In the study of the effects of *Bifidobacterium* on intestinal flora, barrier function and bacterial translocation (BT) in a mouse model of ischemia and reperfusion (I/R) injury, Wang et al. found that pretreatment with *Bifidobacterium* alleviated the destruction of TJ in the ileum induced by I/R (Wang et al., 2013). This suggests that metabolites of *Bifidobacterium* play an important regulatory role in barrier function by improving tight junction morphology through desmoplakin proteins.

The polarized intestinal epithelial Caco-2 cell line is a well established research model to study the effects of novel probiotics and anti-inflammatory agents and gut barrier function (Fusco et al., 2023). Moreover, the findings in Caco-2 can be extrapolated to human research. This cell line has been used to test anti cancer antiproliferative effect of novel *Lactobacilli* strains (Sałański et al., 2022). In the study, Caco-2 was applied as the referential cell line used in this thesis in parallel with the novel intestinal Chic 8E11 cell line. Here, in Caco-2 the ZO-1, occludin, and claudin-1 genes were significantly upregulated, which explains the strengthening modulatory function of *Bifidobacterium lactis* NCC2818 (or its supernatant) and *Bacillus* supernatant on the intestinal barrier in Caco-2. The intestinal barrier promoting mechanisms involve the role in cell sealing and reducing permeability, as well as closing the intercellular gaps, and strengthening the TJ barrier, so that the physical defense is

established against exogenous factors including the pathogens. These effects were confirmed by the immunofluorescence staining of ZO-1 and occludin in figure 38 and 39.

In the results of immunofluorescence staining, the addition of probiotics caused slightly different expressions of E-cadherin protein. As the effect of the treatment with *Bifidobacterium lactis* NCC2818 (or its supernatant), the production of E-cadherin increased, but addition of *Bacillus* (or its supernatant weakened the E-cadherin fluorescence signal in Caco-2 cells. Lewis et al. found that the addition of *Bifidobacterium lactis* NCC2818 to diet increased the expression of E-cadherin in the epithelium of early neonatal piglets (Lewis et al., 2017). This suggests that *Bifidobacterium lactis* NCC2818 (or its supernatant) helps improve intestinal health by improving epithelial barrier integrity. Another worth exploring observation was that the claudin-1 fluorescence signal was weakened after stimulation of Caco-2 cells with both probiotics: *Bacillus* (or its supernatant) and *Bifidobacterium lactis* NCC2818 (or its supernatant). Diao et al. reported the increase of the mRNA abundance of occludin (OCLN) and claudin-1 (CLDN1) in weaned piglets by infusing short-chain fatty acids (SCFA) into the stomach, highlighting that SCFA play a key role to improve barrier function (Diao et al., 2019). Varrying observations may be due to the difference in the environment of *in vivo* and *in vitro* cell studies of the mechanism of action of probiotics on the intestine. These results and models need a further exploration.

Villin is the major modulating protein associated with the microvilli actin. It is located on the apical surface of intestinal epithelial cells and regulates epithelial cell morphology, actin reorganization and cell movement. It regulates cell viability by maintaining actin dynamics homeostasis (O'Reilly et al., 2016); it can also affect cytoskeleton remodeling by controlling epithelial cell-specific apoptosis (Wang et al., 2008). The adjustment of epithelial cell morphology and the maintenance of actin dynamics ensure the maintenance of normal intestinal cell function. In order to clarify the effects of selected probiotics on intestinal cell morphology, the results of Villin gene expression levels were determined in this study.

In this study, the significant up-regulation ($p < 0.05$) and up-regulation trend of the Villin gene in Chic-8E11 cells (Figure 30) suggests that the morphology of Chic-8E11 epithelial cells could be modulated by *Bifidobacterium lactis* NCC2818 (its supernatant) and *Bacillus*

altitudinis supernatant, leading to the enrichment of the cytoskeleton structure and decreasing the cell apoptosis rate. Earlier it was confirmed supplementation with Enterococcus faecium affects the abundance of villi in broiler chickens and can maintain the balance between cell proliferation and apoptosis, which is of fundamental significance to the function of the intestinal barrier (Luo et al., 2013). On a contrary, the direct co-culture of Chic-8E11 with *Bacillus* caused the downregulation trend of the Villin gene therefore inhibiting the normal function of Chic-8E11 cells barrier upon suboptimal probiotic treatment. Similarly, in the experiment with Caco-2 cells, the Villin gene was significantly down-regulated ($p < 0.01$) and had a down-regulation trend, after *Bacillus* treatment. For the second probiotic, both *Bifidobacterium lactis* NCC2818 and its supernatant leaded to up-regulation trend of Villin gene indicating the beneficial potential on enhancing the structure and maintenance of Caco-2 cell barrier function. The results observed with *Bacillus* and its supernatant showed both positive and negative effects. Therefore, it is most likely that suboptimal treatment is responsible for the disruption of the intestinal barrier rather than the probiotic itself. It can be further concluded that the use of this sensitive cell model could allow the development of safe and effective *in vivo* probiotic treatment doses. Based on pilot observations in this thesis, a further development of both co-culture and spheroids models are suggested.

Cytokeratin is the major structural protein in epithelial cells, forming a cytoskeleton of intermediate filament protein type (Banwell B. L., 2001). The intermediate filaments are composed of a large number of nuclear proteins and cytoplasmic proteins. CK18 is the most common and typical member of the large intermediate filament gene family; the known function of CK18 is to provide intracellular scaffolds to build cytoplasm and resist external stress (Coulombe et al., 2004), and it can also participate in regulating signal pathways such as cell growth and apoptosis to maintain the basic metabolic process of the cells. CK20 is also a member of the intermediate filament protein family, and CK20 plays an additive and compensatory role with CK18 in maintaining the intestinal keratin filament organization (Zhou et al., 2003). Vimentin belongs to the type III intermediate filament protein family, a specific component of the cytoskeletal network (Banwell B. L., 2001). The composition of intermediate filaments changes with the inhibition of keratin CK18 and 20 and the activation

of vimentin (Vim), thereby affecting the cytoskeletal remodeling of epithelial cells (Jing et al., 2020). The intermediate filament protein family occupies an important position in the skeletal structure of epithelial cells, and also responds to external stress. In order to analyze the changes of selected probiotics on the intestinal cytoskeleton, the CK18, CK20, and vimentin gene/protein expression levels were measured in this study.

In Chic-8E11 cells, the CK18 gene was significantly upregulated and showed an upregulation trend, suggesting the stimulatory effect of *Bifidobacterium lactis* NCC2818 (its supernatant) and *Bacillus* supernatant on the cytoskeleton proteins. The presence of the CK18 gene is widely used to identify epithelial cells (Zhang et al., 2019), which indicates that after probiotic treatment, Chic-8E11 epithelial cells are intact, cell growth and apoptosis pathways operate in a balanced manner, and the normal metabolic level of the cells is maintained. In the immunofluorescence staining experiment, the enhanced expression of CK18 after co-culture of *Bacillus* supernatant with Chic-8E11 cells also confirmed this result.

The expression of Vimentin protein in Chic-8E11 cells was different after different probiotic treatments (or their supernatants). It has been reported in brain endothelial-related studies that the surface antigen I/II protein BspC interacts with the C-terminal domain of cell surface vimentin to promote bacterial attachment to brain endothelial cells, and purified BspC protein can induce immune signaling pathways (Deng et al., 2019). The protein expression was downregulated after addition of *Bacillus altitudinis* (and its supernatant), and the protein expression was upregulated after the addition of *Bifidobacterium lactis* NCC2818 (and its supernatant). In this study *Bifidobacterium lactis* NCC2818 (and its supernatant) supported the integrity of the cytoskeleton by regulating the expression of vimentin and may promote the attachment of probiotics. Vimentin has been reported to be an important factor in protecting intestinal epithelial cells from inflammation and tumorigenesis.

In Caco-2 cell line, CK18 and CK20 genes were significantly up-regulated after both probiotic treatments suggesting that various probiotics, with dose tolerance, can maintain or strengthen the integrity of the cytoskeleton network, and play an active role in regulating

signaling pathways such as cell growth and apoptosis, and maintaining the basic metabolic process of cells.

IL-18 is a type of immunomodulatory cytokine with strong IFN-γ inducing activity, which plays an important role in Th1-mediated chronic inflammatory diseases and a range of regulatory functions outlined as follows: 1/ activates NK cells, which accelerates the elimination of pathogens and malignant tumor cells (Boraschi et al., 2006); 2/ IL-18 stimulates T lymphocyte activation, promotes T cells to stimulate specific immune responses, and resist external infections and stress (Tsutsui et al., 2012); 3/ stimulates immune cells to produce interferon γ (IFN-γ), and modulates immune cell activity In addition to exploring the intestinal barrier, this study explored the inflammatory and immune response of the cells after co-culture with probiotics, by determination of IL-18 gene expression levels.

In Caco-2, the IL-18 gene was significantly upregulated indicating that the immunomodulatory effect could be triggered by the addition of *Bifidobacterium lactis* NCC2818 (and its supernatant) and *Bacillus* (and its supernatant). The upregulation of the pro-inflammatory gene IL-18 may be resulting from the activation of the signaling pathway of cells in response to exogenous bacteria strains, likewise the mechanisms for anti-pathogens defence (Sałański et al., 2022). Interleukin 18 is an important cytokine for maintaining intestinal epithelial cell homeostasis and preventing the progression of colorectal cancer CRC (Mager et al., 2016). It has been reported that probiotics induce immune responses in the intestine and activate pro-inflammatory and regulatory cytokines, such as IL-10, IL-12, TNF-α, IL-18 (Zhong et al., 2014), and probiotic *Lactobacillus* strains can increase interleukin-18 levels in colorectal cancer (CRC) cells (Hradicka et al., 2020).

Probiotics are live microorganisms that, when administered in adequate amounts, confer a health benefit on the host. *Lactobacillus*, along with species of *Bifidobacterium*, have historically been common probiotics. Among them, *Bifidobacterium lactis* NCC2818 was used as a probiotic supplement. In animal models, intervention with *Bifidobacterium lactis* NCC2818 led to a decrease in IgA in the mucosa-associated lymphoid tissue, increasing the barrier function between the lumen and the intestinal lamina propria. Subsequently, it was shown to improve gut barrier function and have a marked effect on the developmental and

metabolic functions of the mucosal immune system (Lewis et al., 2017). In *in vivo* feeding experiments, *Bacillus* can improve the growth performance and carcass weight of pig offspring by improving the absorption capacity of the small intestine (Crespo-Piazuelo et al., 2022). In addition, supplementation of *Bacillus plateauensis* in sow and/or after weaning has a significant effect on sow colostrum and feces, as well as offspring digestion and fecal flora abundance, among which the increase in fecal *lactic acid bacteria* abundance was associated with the previously reported improvement in growth performance (Rattigan et al., 2023).

In this thesis, the studied probiotics were step-wise selected based on *in vitro* experiments reported by Akhavan et al. (2023) as a part of a larger project . Assessing the further potential of the studied probiotics requires measurement of health benefits as part of *in vivo* trial.

5.2. Analysis of *in vitro* metabolite changes of selected probiotics (*Bifidobacterium lactis* NCC2818 and *Bacillus strain*) cultured with fish protein hydrolysate and seaweed liquid extract

The advanced protocol using high-sensitivity GC-MS, principal component analysis, and univariate and multivariate statistical analysis methods was used to investigate the effects of the probiotic *Bifidobacterium lactis* NCC2818 in combination with two different bioactive stimulants fish protein hydrolysates (and a liquid seaweed extract to identify changes in metabolites in the main metabolic pathways, as shown below.

Intestinal bacteria or bacterial communities (microbiota) use AA from food or the host to synthesize the proteins they need, or further metabolize these nutrients through conversion or fermentation to produce various metabolites in the small and large intestines, such as ammonia, hydrogen sulfide (H2S), nitric oxide (NO), polyamines, phenols and indole compounds (Macfarlane et al., 2012). The role of amino acids in the body includes the synthesis of proteins and peptides and conversion into sugars, lipids, etc., or oxidation to produce carbon dioxide and water to release energy. Amino acids have also immunomodulatory effects, such as L-arginine, which can increase the formation of nitric oxide (NO) and stimulate the formation of peroxynitrite. It is a central metabolite of multiple cellular processes in macrophages and other cells, thereby regulating the host's cellular immunity (McKell et al., 2021). Compared with the control group (MRS), the levels of amino acids such as valine, L-arginine, valine and citrulline produced by the probiotic *Bifidobacterium lactis* NCC2818 were significantly increased after administration of fish protein hydrolysate and liquid seaweed extract ($p < 0.05$). This suggests that fish protein hydrolysate and liquid seaweed extract may influence the utilization of amino acids (AA) in *Bifidobacterium lactis* NCC2818, Therefore, for the *in vivo* situation the improved energy management could be hypothesized.

The importance of amino acid metabolism in intestinal bacteria has been reported. Dietary intervention with functional AA, probiotics and prebiotics to change the abundance and activity of intestinal bacteria can improve or prevent the development of metabolic syndrome (Dai et al., 2015).

The differential metabolites of fish protein hydrolysate acting on *Bifidobacterium lactis* NCC2818 were enriched in the Citrate cycle (TCA cycle) pathway (Figure 13), which is related to energy metabolism. Acetyl CoA is a product of glucose, fatty acid and amino acid catabolism. Glucose is converted into pyruvate by glycolysis, and pyruvate is decarboxylated by enzymatic oxidation to generate acetyl CoA. Acetyl CoA is enzymatically converted into citric acid in mitochondria, and citric acid is oxidized by tricarboxylic acid cycle (TCA). Therefore, acetyl CoA is a basic indicator of cell metabolism. Moreover, pyruvate can convert sugar, amino acids and fats into each other through acetyl CoA and TCA cycle to generate energy. In the study on the effects of probiotic combined with prebiotic supplementation on the metabolism of weaned rats, it was found that after intragastric supplementation of probiotics (*Lactobacillus acidophilus* NCFM and *Bifidobacterium lactis* Bi-07) and prebiotics (Lycium barbarum polysaccharides, Poria cocos polysaccharides and lentinan), fecal metabolites such as caproate, valerate, butyrate, propionate, lactate, acetate, succinate, methanol, threonine and methionine increased significantly, which were related to short-chain fatty acid (SCFA) metabolism and TCA cycle metabolism (Wang et al., 2018), and can regulate common systemic metabolic processes, including energy metabolism, amino acid metabolism, lipid metabolism, nucleic acid metabolism and intestinal flora-related metabolism. In this experiment, after the fish protein hydrolysate stimulated *Bifidobacterium lactis* NCC2818 metabolism to modulate the Citrate cycle (TCA cycle) pathway which in turn was significantly upregulated ($p < 0.05$). Therefore the activity of the stimulated probiotic was shown to be associated with the promotion of cellular energy metabolism.

The differential metabolites produced by *Bifidobacterium lactis* NCC2818 after stimulation with fish protein hydrolysate or seaweed extract, were enriched in the two-component signal transduction system (Figure 13 and 14). The two-component signal transduction system enables bacteria to sense, respond and adapt to various environments, stressors and growth conditions(Wolanin et al., 2002). This pathway has been adjusted in response to various stimuli, including nutrients, cellular redox state, osmotic pressure changes, antibiotics, temperature, chemotactic agents, pH, etc. (Attwood et al., 2007). The identification and molecular characterization of the two-component regulatory system (2CRS)

was reported and found to control the response to inorganic phosphate starvation in *Bifidobacterium breve* UCC2003, allowing for an adaptive response that increases fitness and survival under adverse conditions (Alvarez-Martin et al., 2012). This suggests that the bioactive stimulants fish protein hydrolysate and liquid seaweed extract may act to increase the adaptability of *Bifidobacterium lactis* NCC2818 to the environment.

Upon such a stimulation, the differential metabolites of *Bifidobacterium lactis* NCC2818 were also enriched in the oxidative phosphorylation pathway (Figure 13 and 14). Oxidative phosphorylation is a metabolic pathway involving electron transfer-related phosphorylation or terminal oxidation. Through this pathway, cells use enzymes to oxidize nutrients, thereby releasing chemical energy to produce adenosine triphosphate (ATP). Cells release the energy stored in glucose chemical bonds in the citric acid cycle, producing carbon dioxide and high-energy electron donors NADH and FADH. Oxidative phosphorylation uses these molecules and oxygen to produce ATP, which is used by the entire cell when energy is needed. It has been reported that in the study of the probiotic effects of *Lactobacillus gasseri* LA39, activation of the oxidative phosphorylation pathway increased energy production in porcine intestinal epithelial cells, indicating that this probiotic may be a potential probiotic candidate for promoting intestinal energy production (Hu et al., 2018).

5.3. Metabolic footprints and metabolic fingerprints of probiotic functions in intestinal cells *in vitro*

In the co-culture of cells and probiotics, acetate levels changed in the Caco-2 co-culture system, while acetate and propionate levels changed in the Chic-8E11 system. In addition, there were significant differences in the levels of organic acids (succinate and L-alanine) and essential and non-essential amino acids (glutamate and isoleucine) ($p < 0.05$). Among the top 20 significantly enriched pathways shown in Figures 45 and 48, the most enriched were the pathways of protein digestion and absorption. Since peptide transporter 1 (PEPT1) is the only oligopeptide transporter in the intestinal brush border, it helps absorb small peptides into intestinal cells, and a large amount of SCFA are produced during protein digestion and absorption (Balakrishnan et al., 2012). It has been reported that the supernatant of *Bifidobacterium* upregulated the expression of serotonin transporter (SERT), which is responsible for catabolism, in HT-29 and Caco-2 cells (Cao et al., 2018). SCFAs are essential for colon function and can regulate colon growth, differentiation, motility, blood flow, barrier integrity, being also the main source of metabolic fuel with health maintenance properties, for the colon (Xie et al., 2021). The observed metabolite changes indicate that the probiotic *Bifidobacterium lactis* NCC2818 enhances the absorption and transport mechanisms of intestinal cells. Similarly, studies have reported that from the metabolome analysis of the placenta, the mechanism by which *Bifidobacterium* regulates placental structure and nutrient transporter capacity is to promote cell metabolism, growth, and function by changing the metabolic characteristics of the cecum and using metabolic acetate. The effect of acetate on fetal metabolism after being transported to the fetus through the placenta (Lopez-Tello et al., 2022).

It was found that after stimulation by different prebiotics, the metabolic profiles of probiotics were different. In the cell co-culture system treated with different probiotics, the lactic acid level changed significantly ($p < 0.05$). The acetic acid level in Caco-2 cells increased, accompanied by increased propionic acid and lactic acid levels ($p < 0.05$). Acetic acid and propionic acid changed significantly also in Chic-8E11 cells ($p < 0.05$). The production of organic acids such as succinic acid and alanine, as well as essential and non-essential amino

acids such as leucine, phenylalanine, and serine changed significantly ($p < 0.05$). SCFAs are the end products of dietary fiber fermented by intestinal flora and play an important role in maintaining normal intestinal function (Martin-Gallausiaux et al., 2021). Various organic acids and amino acids are closely related to metabolic pathways such as cellular sugar metabolism, TCA cycle, and G protein-coupled receptors, and the mechanisms induced by these interactions play a key role in maintaining the homeostasis of the intestine and other organs (Koh et al., 2016; Sivaprakasam et al., 2016).

Changes in these metabolites stimulated by novel bioactive ingredients (probiotics and prebiotics) reflect the metabolic status of host cells and explain the relationship between the metabolic signatures of prebiotic and probiotic function in the physiological responses of the host at a systemic level. The results of these *in vitro* studies can be used to predict the effects of novel ingredients in the host, developing metabolomics strategies for future *in vivo* applications to specifically modulate gut health. Gut health modulation is a promising, strategic preventive measure for sustainable regulation of animal health to eliminate outbreaks of foodborne pathogens that pose a threat to public health. The application of sensitive and responsive cell models such as Caco-2 and Chic-8E11 contributes to the development of safe and effective combinations and doses for *in vivo* probiotic-based treatments.

5.4. Metabolic footprints of probiotic functions in intestinal cells *in ovo*

This study explored the significant effects of probiotics, prebiotics and synbiotics on intestinal metabolic footprint after intraocular injection through metabolomics analysis. Principal Component Analysis (PCA) showed significant differences in the response values of the main metabolites. The results in Figure 65 showed that there were significant differences in the metabolite categories between the control group and the three experimental groups (probiotic *Bifidobacterium* strain group, prebiotic APS group and synbiotic 10^3 CFU *Bifidobacterium* strain + 1 mg APS group), and the stability of the model was good. The results of the heat map of the differential metabolite screening results in Figure 66 showed that the differential metabolites in the probiotic *Bifidobacterium* strain group and the prebiotic APS group were significant, and the number of differential metabolites increased in the synbiotic 10^3 CFU *Bifidobacterium* strain + 1 mg APS group was more, including Stearic acid, Ornithine, Asymmetrical Arg M, Acetylomithine, Palmitic acid, Glutamine, GSH Constituents, Citrulline, Homocysteine, etc. At the same time, the KEGG pathway enrichment analysis results of the three experimental groups compared with the control group (Figures 67 - 69) showed that they have significant effects and differences on multiple metabolic pathways in the intestine.

Among the significantly enriched pathways in the comparative analysis of the probiotic *Bifidobacterium* strain group, the most enriched is lipoic acid metabolism. Lipoic acid is an antioxidant that protects cells from oxidative stress and is an important cofactor in mitochondrial metabolism. These cofactors of key enzyme complexes are important in the synthesis of acetyl-CoA. Acetyl-CoA is a key step in the citric acid cycle (TCA cycle) to generate energy in the form of ATP to provide energy forAuthority life activities in the body (Rei Yan SL, et al., 2021). Oxidative stress (OS) is the negative effect of reactive oxygen species (ROS) free radicals produced in the body and is considered to be one of the important factors leading to aging and disease. Currently, many *in vitro* and *in vivo* studies have shown that probiotic Bifidobacterium is a new source of natural antioxidants (Averina et al., 2021).

Among the significantly enriched pathways in the comparative analysis of the prebiotic APS group, the most enriched are propionate metabolism and citric acid cycle (TCA cycle). Propionate is one of the short-chain fatty acids produced by the intestinal microbiota through the fermentation of dietary fiber. It can be converted into propionyl-CoA, and after carboxylation and isomerization, it enters the tricarboxylic acid (TCA) cycle in the form of succinyl-CoA to provide energy sources for other metabolic processes (Gomes et al., 2022). Propionate metabolism is involved in maintaining metabolic balance and may be affected by factors such as diet, intestinal microbiota and aging (Shafer et al., 2025). Propionate metabolism plays a vital role in energy metabolism, metabolic homeostasis and overall health. Currently, polysaccharides are considered to be important natural ingredients that can replace antibiotics to improve intestinal health. There have been many reports that astragalus polysaccharides (APS) are widely used in intestinal health (Liang et al., 2024). Li, S. et al. found that APS has a protective effect on the immune development of cyclophosphamide-induced immunosuppression in the small intestinal mucosa (Li et al., 2019). This shows that prebiotic APS can promote intestinal metabolism and strengthen intestinal metabolic homeostasis.

Here it can be found that both the prebiotic APS group and the probiotic *Bifidobacterium* strain group have significant direct or indirect effects on the metabolism of the citric acid cycle (TCA cycle). This shows that both have the effect of promoting the metabolism and energy metabolism of intestinal cells.

Among the significantly enriched pathways in the comparative analysis of synbiotics (*Bifidobacterium* strain + APS group), the most enriched are glutathione metabolism, cysteine and methionine metabolism, phenylalanine metabolism, and propionate metabolism. Glutathione exists as a cellular antioxidant, which can prevent reactive oxygen species (ROS) and other harmful molecules from damaging cells (Wu et al. 2004). Therefore, glutathione can be very important in detoxification when some drugs or exogenous substances are ingested (Hristov B. D., 2022). Moreover, glutathione can be converted into cysteine and glutamate in metabolism (Tang, L., et al., 2015) to maintain cell health. This also significantly affects cysteine and methionine metabolism, cysteine produced in glutathione

metabolism, and cysteine synthesized from methionine, which means that it is closely related to their metabolism.

From the most significantly enriched pathways in the comparison between each treatment group and the control group, it can be seen that the probiotic *bifidobacterium* strain group, the prebiotic APS group and their synbiotic group all have significant effects on energy metabolism and amino acid metabolism, and each treatment group has different metabolic characteristics and obvious distinctions. Table 7 here summarizes the relative levels of key metabolites of probiotic *Bifidobacterium* strains, prebiotic APS and their synbiotic combinations, and classifies them by functional categories, briefly describing the significance of related metabolic pathways. Among them, "+" indicates relative level, and the more "+" indicates the higher the level. It was found that the commonly affected metabolic pathways include propionate metabolism, cysteine and methionine metabolism, synthesis of unsaturated fatty acids, butyrate metabolism, primary bile acid biosynthesis, etc. Among them, bile acid is essential for the digestion and absorption of dietary fat, and also plays a role in cholesterol homeostasis and the excretion of toxic substances (Vaz et al., 2017).

Table 7. Metabolic characteristics of probiotic *Bifidobacterium* strains, prebiotic APS (Astragalus pokysaccharides) and their synbiotic combination

Metabolite Class	Metabolite	Probiotic (*Bifido*.)	Prebiotic (APS)	Synbiotic (*Bifido*.+APS)	Functional significance
Antioxidants	GSH constituents	++	++	+++	Cellular protection, detoxification
	Cysteine synthesis	+++	+	++	Supports antioxidant production
Amino Acids	Citrulline	+	++	+++	Nitric oxide (NO) cycle, mucosal barrier regulation
	Ornithine	+	++	+++	Ammonia detoxification
Energy metabolism	Lactic acid	+++	+	++	Antimicrobial, energy substrate
	Glutamine	+	++	+++	Primary enterocyte fuel
Lipid metabolism	Fatty acids	+	++	+++	Membrane integrity, signaling
Bile Acids	Deoxyholic acid	+	++	+	Reduced inflammation

From the common significant difference metabolites and enriched metabolic pathways, it can be observed that each treatment group has different metabolic characteristics, but

importantly, the synbiotic group provides the most balanced metabolic characteristics. Some metabolic changes showed that the synbiotics are the superposition of the metabolic effects of the probiotic *Bifidobacterium* strains and prebiotic APS, such as energy metabolism, antioxidant capacity, amino acid metabolism, and fatty acid metabolism. Some metabolic changes showed the effects of metabolic adaptation, such as bile acid metabolism, rather than simple "beneficial" or "harmful" effects. The most obvious ones are amino acid metabolism and energy metabolism. The glutathione (GSH) component is slightly increased in the probiotic group and prebiotic group, but the content is the highest in the synbiotic group, highlighting its enhanced cell protection and detoxification ability.

This study explored the metabolomics analysis in Figure 70. The PCA analysis shows the significant differences in the response values of the main metabolites between the control group and the three experimental groups, the probiotic *Bacillus* strain group, the prebiotic vegetable protein hydrolysate-soya group and its synbiotic (*Bacillus* strain + vegetable protein hydrolysate-soya) group. There are significant differences in the metabolite categories between the groups, and the model is stable. The results of the heat map of the differential metabolite screening results in Figure 71 showed that the probiotic *Bacillus* strain group, the prebiotic vegetable protein hydrolysate-soya group and its synbiotics have significant differential metabolites, including Indole, acetylguanine, glycine, citrulline, total purine, total glutamine, methionine and other amino acids, homocysteine, succinic acid, etc. Figure 72 - 74 showed the KEGG pathway enrichment analysis results of the three experimental groups compared with the control group.

Among the significantly enriched pathways in the comparative analysis of the probiotic *Bacillus* strain group, the most enriched ones are glutamate/cholephospholipid metabolism, selenocompound metabolism, and glycine, serine, and threonine metabolism. Among them, glutamate is a participant in the TCA cycle and is related to energy production. And glutamate can maintain the balance of redox in cells and has the effect of preventing oxidative stress (Zhang D et al., 2024). Therefore, glutamate metabolism plays a central hub role in various metabolic pathways, including nitrogen metabolism, amino acid biosynthesis, and energy production. Glutamate not only provides nitrogen as a nitrogen donor for purine

and pyrimidine synthesis, but also provides amino groups for all amino acids. Transaminases catalyze the transfer of amines from glutamate to precursors of serine, aspartate, alanine, leucine, isoleucine, phenylalanine, and tyrosine. All other amino acids are synthesized from these amino acids, so they indirectly obtain their amine nitrogen from glutamate (Walker et al., 2016). In selenium compound metabolism, selenium is a key component of selenoproteins, which are involved in various metabolic processes, antioxidant defense, etc. (Kang et al., 2020). Therefore, it can be observed that the probiotic *Bacillus* strain group significantly enhanced the intestinal protein and amino acid metabolism, including glutamate metabolism and glycine, serine and threonine metabolism.

Among the significantly enriched pathways in the comparative analysis of the prebiotic vegetable protein hydrolysate-soya group, the most enriched were the biosynthesis of unsaturated fatty acids, thiamine metabolism and glycine, serine and threonine metabolism. Unsaturated fatty acids (PUFA) are very important in lipid metabolism and are closely related to the transport and circulation between peroxidase and endoplasmic reticulum. People currently pay great attention to dietary fats that are concerned about nutrition and health (Lee et al., 2014). Many studies have found that unsaturated fatty acids have good therapeutic value in preventing oxidative stress, inflammation, cardiovascular and cerebrovascular diseases (Liu et al., 2023).

Thiamine is absorbed in the small intestine and converted to its active form, thiamine diphosphate (TPP). TPP is a cofactor for enzymes in pathways such as the pyruvate dehydrogenase complex and transketolase, which are essential for energy production and biosynthesis of amino acids, fatty acids, and nucleic acids (Zastre et al., 2013).

The prebiotic vegetable protein hydrolysate-soya group significantly affected glycine, serine, and threonine metabolism, just like the probiotic *Bacillus* strain group. This was also reflected in the significantly enriched pathways in the comparative analysis of its synbiotic group, with the most enriched being glycine, serine, and threonine metabolism. It was also easy to observe that the significantly enriched pathways of its synbiotic group were almost a collection of the prebiotic vegetable protein hydrolysate-soya group and the probiotic *Bacillus* strain group. Table 8 summarizes the relative levels of key metabolites in the

prebiotic vegetable protein hydrolysate-soya group, the probiotic *Bacillus* strain group, and their synbiotic combination, and classifies them by functional category, briefly describing the significance of the relevant metabolic pathways. Among them, "+" indicates relative level, and the more "+" indicates the higher the level. It was found that the commonly affected metabolic pathways include glycine, serine and threonine metabolism, primary bile acid biosynthesis, nitrogen metabolism, glycine, serine and threonine metabolism, glutathione metabolism, etc.

Table 8. Metabolic characteristics of probiotic *Bacillus* strain, prebiotic soya-based vegetable protein hydrolysate and their synbiotic combination

Metabolite Class	Metabolite	Probiotic (*Bacillus*.)	Prebiotic (vegetable protein hydrolysate)	Synbiotic (*Bacillus*.+vegetable protein hydrolysate)	Functional significance
Amino Acids	Glycine	++	+	+++	Important component of protein, active nerves
	Serine	++	+	+++	Precursor for the synthesis of many amino acids
Lipid metabolism	Unsaturated fatty acids	+	+++	+++	Dietary fat, good for health
Energy metabolism	Glutamate	+++	+	++	Precursor for the synthesis of GABA, nitrogen metabolism
	Thiamine	+	+++	++	Metabolic cofactor
Antioxidants	Selenium	+++	+	+++	Protected from free radical damage
	Cysteine	+	+++	++	Important component of glutathione, antioxidant
Bile Acids	Taurine	+	++	++	Maintains fluid balance

From the common significant difference metabolites and enriched metabolic pathways, it can be observed that each treatment group has different metabolic characteristics, but importantly, the synbiotic group provides the most balanced metabolic characteristics. The metabolic changes basically showed that the synbiotic is the superposition of the metabolic effects of the probiotic *Bifidobacterium* strain and the prebiotic APS, such as energy metabolism, antioxidant capacity, amino acid metabolism, and fatty acid metabolism. The most obvious was amino acid metabolism, with glutamate and serine elevated in both the probiotic and prebiotic groups, but highest in the synbiotic group, highlighting its ability to enhance cellular metabolism.

5.5. Translational model validation

Summarizing all the metabolome analysis results above, and comparing them, we found that the *in vitro* cell model and the *in ovo* model, however being substantially different models, have consistency in key metabolites and related metabolic functions. As summarized in Table 9, for example, lactate increased in both the co-culture group and the probiotic group, which supports its role as an antimicrobial agent and energy source. Similarly, glutathione (GSH) components were elevated in both models, and the content was particularly high in the synbiotic group.

Table 9. Validation of the translational model comparing results from *in vitro* and *in ovo* systems

Metabolite Class	Key Metabolites	*In Vitro* Model	*In Ovo* Model	Functional Significance
Carboxylic Acids	Lactic acid	↑ in co-culture	↑ in probiotic group	Antimicrobial, energy source
	Succinate	↑ in co-culture	↑ in probiotic & synbiotic	Energy metabolism, homeostasis
Antioxidants	GSH constituents	↑ in both treatments	↑↑ in synbiotic group	Cellular protection, detoxification
	Cysteine	↑ in both treatments	↑ in probiotic group	Host's antioxidant defense capacity
Amino Acids	Glutamine/Glutamate	↑ in both treatments	↑↑ in synbiotic group	Enterocyte energy, barrier function
	Ornithine	↑ with supernatant	↑↑ in synbiotic group	Nitrogen metabolism
Growth Factors	Polyamines	↑ in both treatments	↑ in probiotic & synbiotic	Cell growth, differentiation
	β-Alanine	↑ in both treatments	↑ in probiotic group	Carnosine synthesis

It is well known that *in vitro* models reveal direct cellular responses, immediate metabolic changes, and tight junction regulation. As a preclinical animal *in vivo* model with high attention, the *in ovo* model provides in-depth research on energy metabolism, amino acid metabolism, bile acid metabolism, microbial community interactions, and host immune regulation. The functional significance of the observed metabolic changes can identify model specificity and common effects. This consistency of metabolites, pathway conservation, model complementarity, and translational relevance validate our approach of using *in vitro* systems to predict *in vivo* results. Most importantly, we found common metabolic pathways in both models, including amino acid metabolism, TCA cycle function, antioxidant pathways,

polyamine synthesis, lactate production, and barrier function metabolites. This overlap suggests that the core mechanism of probiotic action is conserved across different biological systems.

6. SUMMARIES

In general, from the *in vitro* characterization and metabolite signatures analysis of the co-culture model, probiotics play a positive role in regulating intestinal barrier function, cell morphology and metabolism, which helps maintain intestinal health and prevent the occurrence of diseases. The *in vitro* intestinal models and analysis results of these studies provide important references for the future development of probiotic therapeutic doses to achieve better health effects.

To conclude, the research has established a translational model linking *in vitro* and *in ovo* effects of probiotics and prebiotics.

We identified key probiotic metabolic signatures, including increased carboxylic acids, GSH constituents, and polyamines, and mapped the affected pathways in amino acid metabolism, energy production, and antioxidant defense.

Functionally, these changes translate to enhanced barrier function, improved energy metabolism and redox balance, and increased microbiota balance.

Importantly, we demonstrated synergistic effects of prebiotic-probiotic combinations in the *in ovo* studies, *B. lactis* with Astragalus polysaccharides, and specifically between *Bacillus* and protein hydrolysate.

Our findings have several applications, including improved methods for probiotic screening, further validation in post-hatch chickens, and potential development of personalized probiotic formulations tailored to specific needs.

7. REFERENCES

Acehan, D., Petzold, C., Gumper, I., Sabatini, D. D., Müller, E. J., Cowin, P., & Stokes, D. L. (2008). Plakoglobin is required for effective intermediate filament anchorage to desmosomes. Journal of investigative dermatology, 128(11), 2665-2675 . doi: 10.1038/jid.2008.141

Akhavan, N., Hrynkiewicz, K., Thiem, D., Randazzo, C., Walsh, A. M., Guinan, K. J., O'Sullivan,J. T., & Stadnicka, K. (2023). Evaluation of probiotic growth stimulation using prebiotic ingredients to optimize compounds for *in ovo* delivery. Frontiers in Microbiology, 14, 1242027 . doi: 10.3389/fmicb.2023.1242027

Ali, A., Kolenda, R., Khan, M. M., Weinreich, J., Li, G., Wieler, L. H., Tedin, K., Roggenbuck, D., & Schierack, P. (2020). Novel avian pathogenic Escherichia coli genes responsible for adhesion to chicken and human cell lines. Applied and Environmental Microbiology, 86(20), e01068-20 . doi: 10.1128/AEM.01068-20

Alvarez-Martin, P., Fernández, M., O'Connell-Motherway, M., O'Connell, K. J., Sauvageot, N., Fitzgerald, G. F., MacSharry, J., Zomer, A., & van Sinderen, D. (2012). A conserved two-component signal transduction system controls the response to phosphate starvation in *Bifidobacterium breve* UCC2003. Applied and environmental microbiology, 78(15), 5258-5269 . doi: 10.1128/AEM.00804-12

Anjana, A., & Tiwari, S. K. (2022). Bacteriocin-producing probiotic lactic acid bacteria in controlling dysbiosis of the gut microbiota. Frontiers in Cellular and Infection Microbiology, 12, 851140. doi: 10.3389/fcimb.2022.851140

Attwood, P. V., Piggott, M. J., Zu, X. L., & Besant, P. G. (2007). Focus on phosphohistidine. Amino Acids, 32(1), 145–156. doi: 10.1007/s00726-006-0443-6

Averina, O. V., Poluektova, E. U., Marsova, M. V., & Danilenko, V. N. (2021). Biomarkers and Utility of the Antioxidant Potential of Probiotic Lactobacilli and Bifidobacteria as Representatives of the Human Gut Microbiota. Biomedicines, 9(10), 1340. doi: org/10.3390/biomedicines9101340

Balakrishnan, A., Tavakkolizadeh, A., & Rhoads, D. B. (2012). Circadian clock genes and implications for intestinal nutrient uptake. The Journal of nutritional biochemistry, 23(5), 417-422. doi: 10.1016/j.jnutbio.2012.01.002

Banwell, B. L. (2001). Intermediate filament-related myopathies. Pediatric neurology, 24(4), 257-263 . doi: 10.1016/S0887-8994(00)00248-4

Beacon, T. H., & Davie, J. R. (2021). The chicken model organism for epigenomic research. Genome, 64(4), 476-489. doi: 10.1139/gen-2020-0129

Beamer, M. A., Zamora, C., Nestor-Kalinoski, A. L., Fernando, V., Sharma, V., & Furuta, S. (2023). Novel 3D Flipwell system that models gut mucosal microenvironment for studying interactions between gut microbiota, epithelia and immunity. Scientific Reports, 13(1), 870 . doi: 10.1038/s41598-023-28233-8

Becker, R. (2015). US government approves transgenic chicken. Nature, 1038(18985), 10-1038. doi: 10.1038/nature.2015.18985

Bednarczyk, M., Dunislawska, A., Stadnicka, K., & Grochowska, E. (2021). Chicken embryo as a model in epigenetic research. Poultry Science, 100(7), 101164. doi: 10.1016/j.psj.2021.101164.

Belardi, B., Hamkins-Indik, T., Harris, A. R., Kim, J., Xu, K., & Fletcher, D. A. (2020). A weak link with actin organizes tight junctions to control epithelial permeability. Developmental cell, 54(6), 792-804 . doi: 10.1016/j.devcel.2020.07.022

Białkowska, K., Komorowski, P., Bryszewska, M., & Miłowska, K. (2020). Spheroids as a type of three-dimensional cell cultures—examples of methods of preparation and the most important application. International journal of molecular sciences, 21(17), 6225. doi: org/10.3390/ijms21176225

Biliavska, L., Pankivska, Y., Povnitsa, O., & Zagorodnya, S. (2019). Antiviral activity of exopolysaccharides produced by lactic acid bacteria of the genera *Pediococcus*, *Leuconostoc* and *Lactobacillus* against human adenovirus type 5. Medicina, 55(9), 519 . doi: 10.3390/medicina55090519

Bogucka, J., Dankowiakowska, A., Stanek, M., Stadnicka, K., & Kirkiłło-Stacewicz, K. (2022). Effect of synbiotics administered in ovo on microvascularization and histopathological changes in pectoral muscle and the biochemical profile of broiler chicken blood. Poultry Science, 101(3), 101628. doi: 10.1016/j.psj.2021.101628

Boraschi, D., & Dinarello, C. A. (2006). IL-18 in autoimmunity. European cytokine network, 17(4), 224-252 . doi: 10.1684/ecn.2006.0047

Branca, J. J., Gulisano, M., & Nicoletti, C. (2019). Intestinal epithelial barrier functions in ageing. Ageing research reviews, 54, 100938 . doi: 10.1016/j.arr.2019.100938

Cao, Y. N., Feng, L. J., Wang, B. M., Jiang, K., Li, S., Xu, X., Wang, W; Zhao, J; Wang, Y. M. (2018). *Lactobacillus acidophilus* and *Bifidobacterium longum* supernatants upregulate the serotonin transporter expression in intestinal epithelial cells. Saudi Journal of Gastroenterology, 24(1), 59-66. doi:10.4103/sjg.SJG_333_17

Chen, S. W., Wang, P. Y., Zhu, J., Chen, G. W., Zhang, J. L., Chen, Z. Y., Zuo, S., Liu, C. L., & Pan, Y. S. (2015). Protective effect of 1, 25-dihydroxyvitamin d3 on lipopolysaccharide-induced intestinal epithelial tight junction injury in caco-2 cell monolayers. Inflammation, 38, 375-383 . doi: 10.1007/s10753-014-0041-9

Costa, J., & Ahluwalia, A. (2019). Advances and current challenges in intestinal *in vitro* model engineering: a digest. Frontiers in bioengineering and biotechnology, 7, 144. doi: 10.3389/fbioe.2019.00144

Coulombe, P. A., & Wong, P. (2004). Cytoplasmic intermediate filaments revealed as dynamic and multipurpose scaffolds. Nature cell biology, 6(8), 699-706 . doi: 10.1038/ncb0804-699

Crespo-Piazuelo, D., Gardiner, G. E., Ranjitkar, S., Bouwhuis, M. A., Ham, R., Phelan, J. P., Marsh, A., & Lawlor, P. G. (2022). Maternal supplementation with *Bacillus altitudinis* spores improves porcine offspring growth performance and carcass weight. British Journal of Nutrition, 127(3), 403-420 . doi: 10.1017/S0007114521001203

Cronin, M., Ventura, M., Fitzgerald, G. F., & Van Sinderen, D. (2011). Progress in genomics, metabolism and biotechnology of *bifidobacteria*. International Journal of Food Microbiology, 149(1), 4-18 . doi: 10.1016/j.ijfoodmicro.2011.01.019

Dai, Z., Wu, Z., Hang, S., Zhu, W., & Wu, G. (2015). Amino acid metabolism in intestinal bacteria and its potential implications for mammalian reproduction. MHR: Basic science of reproductive medicine, 21(5), 389-409 . doi: 10.1093/molehr/gav003

Deng, L., Spencer, B. L., Holmes, J. A., Mu, R., Rego, S., Weston, T. A., Hu, K., Sanches, G. F., Yoon, G., Park, N., Nagao, P. E., Jenkinson, H. F., Thornton, J. A., Seo, K. S., Nobbs, A. H., & Doran, K. S. (2019). The Group B *Streptococca*l surface antigen I/II protein, BspC, interacts with host vimentin to promote adherence to brain endothelium and inflammation during the pathogenesis of meningitis. PLoS pathogens, 15(6), e1007848 . doi: 10.1371/journal.ppat.1007848

Diao, H., Jiao, A. R., Yu, B., Mao, X. B., & Chen, D. W. (2019). Gastric infusion of short-chain fatty acids can improve intestinal barrier function in weaned piglets. Genes & nutrition, 14, 1-16 . doi: 10.1186/s12263-019-0626-x

Dicks, L. M. (2022). Gut bacteria and neurotransmitters. Microorganisms, 10(9), 1838. doi: 10.3390/microorganisms10091838

Ding, X., Hu, X., Chen, Y., Xie, J., Ying, M., Wang, Y., & Yu, Q. (2021). Differentiated Caco-2 cell models in food-intestine interaction study: Current applications and future trends. Trends in Food Science & Technology, 107, 455-465 . doi: 10.1016/j.tifs.2020.11.015

Díaz-Garrido, N., Badia, J., & Baldomà, L. (2021). Microbiota-derived extracellular vesicles in interkingdom communication in the gut. Journal of Extracellular Vesicles, 10(13), e12161. doi: 10.1002/jev2.12161

Domingo-Almenara, X., & Siuzdak, G. (2020). Metabolomics data processing using XCMS. Computational methods and data analysis for metabolomics, 11-24 . doi: 10.1007/978-1-0716-0239-3_2

Drider, D. (2021). Gut microbiota is an important source of bacteriocins and their in situ expression can be explored for treatment of bacterial infections. Probiotics and Antimicrobial Proteins, 13(6), 1759-1765. doi: 10.1007/s12602-021-09843-y

Dupont, H. L., Jiang, Z. D., Dupont, A. W., & Utay, N. S. (2020). The intestinal microbiome in human health and disease. Transactions of the American Clinical and Climatological Association, 131, 178. PMID: 32675857; PMCID: PMC7358474.

El-Ashmawy, N. E., El-Zamarany, E. A., Khedr, E. G., & Abo-Saif, M. A. (2019). Activation of EMT in colorectal cancer by MTDH/NF-κB p65 pathway. Molecular and cellular biochemistry, 457, 83-91 . doi: 10.1007/s11010-019-03514-x

El-Sharkawy, H., Tahoun, A., Rizk, A. M., Suzuki, T., Elmonir, W., Nassef, E., Shukry, M., Germoush, M. O., Farrag, F., Bin-Jumah, M., & Mahmoud, A. M. (2020). Evaluation of *Bifidobacteria* and *Lactobacillus* probiotics as alternative therapy for Salmonella typhimurium infection in broiler chickens. Animals, 10(6), 1023. doi: org/10.3390/ani10061023

European Food Safety Authority and European Centre for Disease Prevention and Control (EFSA and ECDC). (2018). The European Union summary report on trends and sources of zoonoses, zoonotic agents and food-borne outbreaks in 2017. EFSa Journal, 16(12), e05500 . doi: 10.2903/j.efsa.2018.5500

Fedi, A., Vitale, C., Ponschin, G., Ayehunie, S., Fato, M., & Scaglione, S. (2021). In vitro models replicating the human intestinal epithelium for absorption and metabolism studies: A systematic review. Journal of Controlled Release, 335, 247-268. doi: 10.1016/j.jconrel.2021.05.028

Fusco, A., Savio, V., Cimini, D., D'Ambrosio, S., Chiaromonte, A., Schiraldi, C., & Donnarumma, G. (2023). In vitro evaluation of the most active probiotic strains able to improve the intestinal barrier functions and to prevent inflammatory diseases of the gastrointestinal system. Biomedicines, 11(3), 865. doi: 10.3390/biomedicines11030865

Garcia, M. A., Nelson, W. J., & Chavez, N. (2018). Cell–cell junctions organize structural and signaling networks. Cold Spring Harbor perspectives in biology, 10(4), a029181 . doi: 10.1101/cshperspect.a029181

Garcia, P., Wang, Y., Viallet, J., & Macek Jilkova, Z. (2021). The chicken embryo model: A novel and relevant model for immune-based studies. Frontiers in immunology, 12, 791081. doi: 10.3389/fimmu.2021.791081

Gerardi, G., Rivero-Pérez, M. D., Cavia-Saiz, M., Melero, B., Salinero-Zorita, A., González-SanJosé, M. L., & Muñiz, P. (2021). Wine Pomace Product Inhibit Listeria monocytogenes invasion of intestinal cell lines Caco-2 and SW-480. Foods, 10(7), 1485 . doi: 10.3390/foods10071485

German, J. B., Bauman, D. E., Burrin, D. G., Failla, M. L., Freake, H. C., King, J. C., Klein S., Milner J.A., Pelto G.H., Rasmussen K.M., & Zeisel, S. H. (2004). Metabolomics in the opening decade of the 21st century: building the roads to individualized health. The Journal of nutrition, 134(10), 2729-2732 . doi: 10.1093/jn/134.10.2729

Gerwig, G. J. (2019). Structural analysis of exopolysaccharides from lactic acid bacteria. Lactic acid bacteria: methods and protocols, 67-84 . doi: 10.1007/978-1-4939-8907-2_7

Ghaffari-Tabrizi-Wizsy, N., Passegger, C. A., Nebel, L., Krismer, F., Herzer-Schneidhofer, G., Schwach, G., & Pfragner, R. (2019). The avian chorioallantoic membrane as an alternative tool to study medullary thyroid cancer. Endocrine connections, 8(5), 462-467. doi: 10.1530/EC-18-0431

Ghiselli, F., Rossi, B., Felici, M., Parigi, M., Tosi, G., Fiorentini, L., Massi, P., Piva, A., & Grilli, E. (2021). Isolation, culture, and characterization of chicken intestinal epithelial cells. BMC Molecular and Cell Biology, 22, 1-14 . doi: 10.1186/s12860-021-00349-7

Gilmore, W. J., Johnston, E. L., Zavan, L., Bitto, N. J., & Kaparakis-Liaskos, M. (2021). Immunomodulatory roles and novel applications of bacterial membrane vesicles. Molecular Immunology, 134, 72–85. doi: 10.1016/j.molimm.2021.02.027

Gomes, A. P., Ilter, D., Low, V., Drapela, S., Schild, T., Mullarky, E., Han, J., Elia, I., Broekaert, D., Rosenzweig, A., Nagiec, M., Nunes, J. B., Schaffer, B. E., Mutvei, A. P., Asara, J. M., Cantley, L. C., Fendt, S. M., & Blenis, J. (2022). Altered propionate metabolism contributes to tumour progression and aggressiveness. Nature metabolism, 4(4), 435-443. doi: 10.1038/s42255-022-00553-5

González-Mariscal, L., Tapia, R., & Chamorro, D. (2008). Crosstalk of tight junction components with signaling pathways. Biochimica et Biophysica Acta (BBA)-Biomembranes, 1778(3), 729-756 . doi: 10.1016/j.bbamem.2007.08.018

Groschwitz, K. R., & Hogan, S. P. (2009). Intestinal barrier function: molecular regulation and disease pathogenesis. Journal of allergy and clinical immunology, 124(1), 3-20. doi: 10.1016/j.jaci.2009.05.038

Haas, A. J., Zihni, C., Krug, S. M., Maraspini, R., Otani, T., Furuse, M., Honigmann, A., Balda, M. S., & Matter, K. (2022). ZO-1 guides tight junction assembly and epithelial morphogenesis via cytoskeletal tension-dependent and-independent functions. Cells, 11(23), 3775 . doi: 10.3390/cells11233775

Han, M., Liang, J., Hou, M., Liu, Y., Li, H., & Gao, Z. (2024). *Bifidobacterium bifidum* Ameliorates DSS-Induced Colitis in Mice by Regulating Microbial Metabolome and Targeting Gut Microbiota. Journal of Agricultural and Food Chemistry . doi: 10.1021/acs.jafc.4c00365

Han, X., Bertzbach, L. D., & Veit, M. (2019). Mimicking the passage of avian influenza viruses through the gastrointestinal tract of chickens. Veterinary microbiology, 239, 108462 . doi: 10.1016/j.vetmic.2019.108462

Hardy, K. M., Yatskievych, T. A., Konieczka, J. H., Bobbs, A. S., & Antin, P. B. (2011). FGF signalling through RAS/MAPK and PI3K pathways regulates cell movement and gene expression in the chicken primitive streak without affecting E-cadherin expression. BMC developmental biology, 11, 1-17 . doi: 10.1186/1471-213X-11-20

Hradicka, P., Beal, J., Kassayova, M., Foey, A., & Demeckova, V. (2020). A novel lactic acid bacteria mixture: Macrophage-targeted prophylactic intervention in colorectal cancer management. Microorganisms, 8(3), 387. doi: 10.3390/microorganisms8030387

Hristov, B. D. (2022). The role of glutathione metabolism in chronic illness development and its potential use as a novel therapeutic target. Cureus, 14(9). doi: 10.7759/cureus.29696.

Hu, C. A. A., Hou, Y., Yi, D., Qiu, Y., Wu, G., Kong, X., & Yin, Y. (2015). Autophagy and tight junction proteins in the intestine and intestinal diseases. Animal Nutrition, 1(3), 123-127 . doi: 10.1016/j.aninu.2015.08.014

Hu, C. H., Gu, L. Y., Luan, Z. S., Song, J., & Zhu, K. (2012). Effects of montmorillonite–zinc oxide hybrid on performance, diarrhea, intestinal permeability and morphology of weanling pigs. Animal Feed Science and Technology, 177(1-2), 108-115 . doi: 10.1016/j.anifeedsci.2012.07.028

Hu, J., Ma, L., Zheng, W., Nie, Y., & Yan, X. (2018). *Lactobacillus gasseri* LA39 activates the oxidative phosphorylation pathway in porcine intestinal epithelial cells. Frontiers in Microbiology, 9, 423260 . doi: 10.3389/fmicb.2018.03025

Huang, X., He, H., Li, Z., Liu, C., Jiang, B., Huang, Y., Su, Y., & Li, W. (2024). Screening and effects of intestinal probiotics on growth performance, gut health, immunity, and disease resistance of Nile tilapia (Oreochromis niloticus) against Streptococcus agalactiae. Fish & Shellfish Immunology, 109668 . doi: 10.1016/j.fsi.2024.109668

Ibrahim, M., Grochowska, E., & Stadnicka, K. (2025). Primordial germ cells as a potential model for understanding (Nutri) epigenetic-metabolic interactions: a mini review. Frontiers in Cell and Developmental Biology, 13, 1576768. doi: 10.3389/fcell.2025.1576768.

Ibrahim, S., Zhu, X., Luo, X., Feng, Y., & Wang, J. (2020). PIK3R3 regulates ZO-1 expression through the NF-kB pathway in inflammatory bowel disease. International immunopharmacology, 85, 106610 . doi: 10.1016/j.intimp.2020.106610

Jing, H., Wang, S., Wang, Y., Shen, N., & Gao, X. J. (2020). Environmental contaminant ammonia triggers epithelial-to-mesenchymal transition-mediated jejunal fibrosis with the disassembly of epithelial cell-cell contacts in chicken. Science of the total environment, 726, 138686 . doi: 10.1016/j.scitotenv.2020.138686

Johnson, C. H., Ivanisevic, J., & Siuzdak, G. (2016). Metabolomics: beyond biomarkers and towards mechanisms. Nature reviews Molecular cell biology, 17(7), 451-459 . doi: 10.1038/nrm.2016.25

Kadekar, D., Udrea, A. C., Bak, S. Y., Christensen, N., Gibbs, K., Shen, C., & Bernardeau, M. (2024). Cell-free culture supernatant of *Lactobacillus acidophilus* AG01 and *Bifidobacterium animalis* subsp. lactis AG02 reduces the pathogenicity of NetB-positive Clostridium perfringens in a chicken intestinal epithelial cell line. Microorganisms, 12(4), 839 . doi: 10.3390/microorganisms12040839

Kathayat, D., Closs, G., Helmy, Y. A., Deblais, L., Srivastava, V., & Rajashekara, G. (2022). *In vitro* and *in vivo* evaluation of *Lacticaseibacillus rhamnosus* GG and *Bifidobacterium lactis* Bb12 against avian pathogenic Escherichia coli and identification of novel probiotic-derived bioactive peptides. Probiotics and Antimicrobial Proteins, 1-17. doi: org/10.1007/s12602-021-09840-1

Khodaii, Z., Ghaderian, S. M. H., & Natanzi, M. M. (2017). Probiotic bacteria and their supernatants protect enterocyte cell lines from enteroinvasive *Escherichia coli* (EIEC) invasion. International journal of molecular and cellular medicine, 6(3), 183 . doi: 10.22088/acadpub.BUMS.6.3.183

Koh, A., De Vadder, F., Kovatcheva-Datchary, P., & Bäckhed, F. (2016). From dietary fiber to host physiology: short-chain fatty acids as key bacterial metabolites. Cell, 165(6), 1332-1345. doi: 10.1016/j.cell.2016.05.041

Kolenda, R., Burdukiewicz, M., Wimonć, M., Aleksandrowicz, A., Ali, A., Szabo, I., Tedin, K., Scott, J. B., Pickard, D., & Schierack, P. (2021). Identification of natural mutations responsible for altered infection phenotypes of *Salmonella* enterica clinical isolates by using cell line infection screens. Applied and Environmental Microbiology, 87(2), e02177-20. doi: 10.1128/AEM.02177-20.

Kosobucki, P., Studziński, W. & Zuo, S. (2022). The role of analytical chemistry in poultry science . Physical Sciences Reviews, 9(2), 689-700. doi: org/10.1515/psr-2021-0126

Kunz, P., Schenker, A., Sähr, H., Lehner, B., & Fellenberg, J. (2019). Optimization of the chicken chorioallantoic membrane assay as reliable in vivo model for the analysis of osteosarcoma. PLoS One, 14(4), e0215312. doi: 10.1371/journal.pone.0215312

Lee, H., & Park, W.J. (2014). Unsaturated fatty acids, desaturases, and human health. Journal of medicinal food, 17(2), 189-197. doi: 10.1089/jmf.2013.2917.

Lerner, A., & Matthias, T. (2015). Changes in intestinal tight junction permeability associated with industrial food additives explain the rising incidence of autoimmune disease. Autoimmunity reviews, 14(6), 479-489 . doi: 10.1016/j.autrev.2015.01.009

Lewis, M. C., Merrifield, C. A., Berger, B., Cloarec, O., Duncker, S., Mercenier, A., Nicholson, J. K. Holmes, E., & Bailey, M. (2017). Early intervention with *Bifidobacterium lactis* NCC2818 modulates the host-microbe interface independent of the sustained changes induced by the neonatal environment. Scientific reports, 7(1), 5310 . doi: 10.1038/s41598-017-05689-z

Li, N., Lewis, P., Samuelson, D., Liboni, K., & Neu, J. (2004). Glutamine regulates Caco-2 cell tight junction proteins. American Journal of Physiology-Gastrointestinal and Liver Physiology, 287(3), G726-G733 . doi: 10.1152/ajpgi.00012.2004

Li, S., Wang, X. F., Ren, L. N., Li, J. L., Zhu, X. D., Xing, T., & Zhou, G. H. (2019). Protective effects of γ -irradiated Astragalus polysaccharides on intestinal development and mucosal immune function of immunosuppressed broilers. Poultry science, 98(12), 6400-6410. doi： 10.3382/ps/pez478

Li, W., Khan, M., Mao, S., Feng, S., & Lin, J. M. (2018). Advances in tumor-endothelial cells co-culture and interaction on microfluidics. Journal of pharmaceutical analysis, 8(4), 210-218 . doi: 10.1016/j.jpha.2018.07.005

Liang, H., Tao, S., Wang, Y., Zhao, J., Yan, C., Wu, Y., Liu, N., & Qin, Y. (2024). Astragalus polysaccharide: implication for intestinal barrier, anti-inflammation, and animal production. Frontiers in Nutrition, 11, 1364739. doi: 10.3389/fnut.2024.1364739

Ling, X., Linglong, P., Weixia, D., & Hong, W. (2016). Protective effects of *bifidobacterium* on intestinal barrier function in LPS-induced enterocyte barrier injury of Caco-2 monolayers and in a rat NEC model. PloS one, 11(8), e0161635. doi: org/10.1371/journal.pone.0161635

Liu, Q., Yu, Z., Tian, F., Zhao, J., Zhang, H., Zhai, Q., & Chen, W. (2020). Surface components and metabolites of probiotics for regulation of intestinal epithelial barrier. Microbial Cell Factories, 19, 1-11. Doi: 10.1186/s12934-020-1289-4

Lopez-Tello, J., Schofield, Z., Kiu, R., Dalby, M. J., van Sinderen, D., Le Gall, G., Sferruzzi-Perri, A. N., & Hall, L. J. (2022). Maternal gut microbiota *Bifidobacterium* promotes placental morphogenesis, nutrient transport and fetal growth in mice. Cellular and Molecular Life Sciences, 79(7), 386. doi： 10.1007/s00018-022-04379-y

Luo, J., Zheng, A., Meng, K., Chang, W., Bai, Y., Li, K., Cai, H., Liu, G., & Yao, B. (2013). Proteome changes in the intestinal mucosa of broiler (*Gallus gallus*) activated by probiotic Enterococcus faecium. Journal of proteomics, 91, 226-241 . doi: 10.1016/j.jprot.2013.07.017

Ma, Z., Akhtar, M., Pan, H., Liu, Q., Chen, Y., Zhou, X., You, Y., Shi, D., & Liu, H. (2023). Fecal microbiota transplantation improves chicken growth performance by balancing jejunal Th17/Treg cells. Microbiome, 11(1), 137 . doi: 10.1186/s40168-023-01569-z

Macfarlane, G. T., & Macfarlane, S. (2012). Bacteria, colonic fermentation, and gastrointestinal health. Journal of AOAC International, 95(1), 50-60 . doi: 10.5740/jaoacint.SGE_Macfarlane

Mager, L. F., Wasmer, M. H., Rau, T. T., & Krebs, P. (2016). Cytokine-induced modulation of colorectal cancer. Frontiers in oncology, 6, 96. doi: 10.3389/fonc.2016.00096

Maiorano, G., Stadnicka, K., Tavaniello, S., Abiuso, C., Bogucka, J., & Bednarczyk, M. (2017). *In ovo* validation model to assess the efficacy of commercial prebiotics on broiler performance and oxidative stability of meat. Poultry science, 96(2), 511-518. doi: 10.3382/ps/pew311

Mamas, M., Dunn, W. B., Neyses, L., & Goodacre, R. (2011). The role of metabolites and metabolomics in clinically applicable biomarkers of disease. Archives of toxicology, 85, 5-17 . doi: 10.1007/s00204-010-0609-6

Markowiak-Kopeć, P., & Śliżewska, K. (2020). The effect of probiotics on the production of short-chain fatty acid by human intestinal microbiome. Nutrients, 12(4), 1107. doi: 10.3390/nu12041107

Martin-Gallausiaux, C., Marinelli, L., Blottière, H. M., Larraufie, P., & Lapaque, N. (2021). SCFA: mechanisms and functional importance in the gut. Proceedings of the Nutrition Society, 80(1), 37-49. doi: 10.1017/S0029665120006916

Mátis, G., Mackei, M., Boomsma, B., Fébel, H., Nadolna, K., Szymański, Ł., Edwards, J. E., Neogrády, Z. & Kozłowski, K. (2022). Dietary protected butyrate supplementation of broilers modulates intestinal tight junction proteins and stimulates endogenous production of short chain fatty acids in the caecum. Animals, 12(15), 1940. doi: 10.3390/ani12151940

McKell, M. C., Crowther, R. R., Schmidt, S. M., Robillard, M. C., Cantrell, R., Lehn, M. A., Janssen, E. D., & Qualls, J. E. (2021). Promotion of anti-tuberculosis macrophage activity by L-arginine in the absence of nitric oxide. Frontiers in Immunology, 12, 653571. doi: 10.3389/fimmu.2021.653571

Meng, J., Zhang, Q. X., & Lu, R. R. (2017). Surface layer protein from *Lactobacillus acidophilus* NCFM inhibit intestinal pathogen-induced apoptosis in HT-29 cells. International journal of biological macromolecules, 96, 766-774 . doi: 10.1016/j.ijbiomac.2016.12.085

Miebach, L., Berner, J., & Bekeschus, S. (2022). *In ovo* model in cancer research and tumor immunology. Frontiers in Immunology, 13, 1006064. doi: 10.3389/fimmu.2022.1006064

Mosmann, T. (1983). Rapid colorimetric assay for cellular growth and survival: application to proliferation and cytotoxicity assays. Journal of immunological methods, 65(1-2), 55-63 . doi: 10.1016/0022-1759(83)90303-4

Neto, M. P. C., de Souza Aquino, J., Da Silva, L. D. F. R., de Oliveira Silva, R., de Lima Guimaraes, K. S., de Oliveira, Y., de Souza, E. L., Magnani, M., Vidal, H., & de Brito Alves, J. L. (2018). Gut microbiota and probiotics intervention: a potential therapeutic target for management of cardiometabolic disorders and chronic kidney disease?. Pharmacological Research, 130, 152-163 . doi: 10.1016/j.phrs.2018.01.020

Niloofar, A., Marek, B., Krzysztof, K., & Katarzyna, S. (2024). Emerging *in ovo* technologies in poultry production and the re-discovered chicken model in preclinical research. Physical Sciences Reviews, 9(2), 843-859. doi: 10.1515/psr-2021-0130

Odenwald, M. A., & Turner, J. R. (2017). The intestinal epithelial barrier: a therapeutic target?. Nature reviews Gastroenterology & hepatology, 14(1), 9-21. doi: 10.1038/nrgastro.2016.169

O'Reilly, E. L., Burchmore, R. J., Sparks, N. H., & Eckersall, P. D. (2016). The effect of microbial challenge on the intestinal proteome of broiler chickens. Proteome science, 15, 1-17 . doi: 10.1186/s12953-017-0118-0

Okumura, R., & Takeda, K. (2018). Maintenance of intestinal homeostasis by mucosal barriers. Inflammation and regeneration, 38, 1-8 . doi: 10.1186/s41232-018-0063-z

Otani, T., Nguyen, T. P., Tokuda, S., Sugihara, K., Sugawara, T., Furuse, K., Miura, T., Ebnet, K., & Furuse, M. (2019). Claudins and JAM-A coordinately regulate tight junction formation and epithelial polarity. Journal of Cell Biology, 218(10), 3372-3396 . doi: 10.1083/jcb.201812157

Pabla, D., Akhlaghi, F., & Zia, H. (2010). Intestinal permeability enhancement of levothyroxine sodium by straight chain fatty acids studied in MDCK epithelial cell line. European journal of pharmaceutical sciences, 40(5), 466-472 . doi: 10.1016/j.ejps.2010.05.002

Pfaffl, M. W. (2001). A new mathematical model for relative quantification in real-time RT–PCR. Nucleic acids research, 29(9), e45-e45 . doi: 10.1093/nar/29.9.e45

Prieto, M. L., O'Sullivan, L., Tan, S. P., McLoughlin, P., Hughes, H., Gutierrez, M., Lane J. A., Hickey R. M., Lawlor P.G., & Gardiner, G. E. (2014). *In vitro* assessment of marine *Bacillus* for use as livestock probiotics. Marine drugs, 12(5), 2422-2445 . doi: 10.3390/md12052422

Puren, A. J., Fantuzzi, G., & Dinarello, C. A. (1999). Gene expression, synthesis, and secretion of interleukin 18 and interleukin 1β are differentially regulated in human blood mononuclear cells and mouse spleen cells. Proceedings of the National Academy of Sciences, 96(5), 2256-2261 . doi: 10.1073/pnas.96.5.2256

Qiao, Y., Sun, J., Xia, S., Tang, X., Shi, Y., & Le, G. (2014). Effects of resveratrol on gut microbiota and fat storage in a mouse model with high-fat-induced obesity. Food & function, 5(6), 1241-1249 . doi: 10.1039/C3FO60630A

Rattigan, R., Lawlor, P. G., Cormican, P., Crespo-Piazuelo, D., Cullen, J., Phelan, J. P., Ranjitkar, S., Crispie, F., & Gardiner, G. E. (2023). Maternal and/or post-weaning supplementation with *Bacillus* altitudinis spores modulates the microbial composition of colostrum, digesta and faeces in pigs. Scientific Reports, 13(1), 8900 . doi: 10.1038/s41598-023-33175-2

Rei Yan, S. L., Wakasuqui, F., Du, X., Groves, M. R., & Wrenger, C. (2021). Lipoic acid metabolism as a potential chemotherapeutic target against Plasmodium falciparum and Staphylococcus aureus. Frontiers in Chemistry, 9, 742175. doi: 10.3389/fchem.2021.742175

Roberts, T., Wilson, J., Guthrie, A., Cookson, K., Vancraeynest, D., Schaeffer, J., Moodt, R., & Clark, S. (2015). New issues and science in broiler chicken intestinal health: intestinal microbial composition, shifts, and impacts. World's poultry science journal, 71(2), 259-270 . doi: 10.1017/S0043933915000276

Rovithi, M., Avan, A., Funel, N., Leon, L. G., Gomez, V. E., Wurdinger, T., Griffioen, A. W., Verheul, H. M. W., & Giovannetti, E. (2017). Development of bioluminescent chick chorioallantoic membrane (CAM) models for primary pancreatic cancer cells: A platform for drug testing. Scientific reports, 7(1), 44686. doi: 10.1038/srep44686

Roy, P., Rana, R., Neogi, S., Dutta, K., Maity, M., & Tewari, S. (2023). Postbiotics: potential applications in early life nutrition and beyond. Journal of Survey in Fisheries Sciences, 10(1S), 6161-6169. doi: 10.3390/ijms20194673

Saitou, M., Furuse, M., Sasaki, H., Schulzke, J. D., Fromm, M., Takano, H., Nado, T., & Tsukita, S. (2000). Complex phenotype of mice lacking occludin, a component of tight junction strands. Molecular biology of the cell, 11(12), 4131-4142 . doi: 10.1091/mbc.11.12.4131

Sałański, P., Kowalczyk, M., Bardowski, J. K., & Szczepankowska, A. K. (2022). Health-Promoting nature of Lactococcus lactis IBB109 and Lactococcus lactis IBB417 strains exhibiting proliferation inhibition and stimulation of interleukin-18 expression in colorectal cancer cells. Frontiers in Microbiology, 13, 822912 . doi: 10.3389/fmicb.2022.822912

Satsu, H. (2017). Molecular and cellular studies on the absorption, function, and safety of food components in intestinal epithelial cells. Bioscience, Biotechnology, and Biochemistry, 81(3), 419-425. doi: 10.1080/09168451.2016.1259552

Scott, S. A., Fu, J., & Chang, P. V. (2020). Microbial tryptophan metabolites regulate gut barrier function via the aryl hydrocarbon receptor. Proceedings of the National Academy of Sciences, 117(32), 19376-19387. doi: 10.1073/pnas.2000047117

Shafer, M., Low, V., Li, Z., & Blenis, J. (2025). The emerging role of dysregulated propionate metabolism and methylmalonic acid in metabolic disease, aging, and cancer. Cell Metabolism, 37(2), 316-329. doi: 10.1016/j.cmet.2025.01.005

Sharma, S., Tripathi, P., Sharma, J., & Dixit, A. (2020). Flavonoids modulate tight junction barrier functions in hyperglycemic human intestinal Caco-2 cells. Nutrition, 78, 110792 . doi: 10.1016/j.nut.2020.110792

Siwek, M., Slawinska, A., Stadnicka, K., Bogucka, J., Dunislawska, A., & Bednarczyk, M. (2018). Prebiotics and synbiotics–*in ovo* delivery for improved lifespan condition in chicken. BMC veterinary research, 14, 1-17 . doi: 10.1186/s12917-018-1738-z

Sivaprakasam, S., Prasad, P. D., & Singh, N. (2016). Benefits of short-chain fatty acids and their receptors in inflammation and carcinogenesis. Pharmacology & therapeutics, 164, 144-151. doi: 10.1016/j.pharmthera.2016.04.007

Sözener, Z. C., Cevhertas, L., Nadeau, K., Akdis, M., & Akdis, C. A. (2020). Environmental factors in epithelial barrier dysfunction. Journal of Allergy and Clinical Immunology, 145(6), 1517-1528. doi: 10.1016/j.jaci.2020.04.024

Stadnicka, K., Bogucka, J., Stanek, M., Graczyk, R., Krajewski, K., Maiorano, G., & Bednarczyk, M. (2020). Injection of raffinose family oligosaccharides at 12 days of egg incubation modulates the gut development and resistance to opportunistic pathogens in broiler chickens. Animals, 10(4), 592. doi: 10.3390/ani10040592

Stefely, J. A., Kwiecien, N. W., Freiberger, E. C., Richards, A. L., Jochem, A., Rush, M. J., Ulbrich, A., Robinson, K. P., Hutchins, P. D., Veling, M. T., Guo, X., Kemmerer, Z. A., Connors, K. J., Trujillo, E. A., Sokol, J., Marx, H., Westphall, M. S., Hebert, A. S., Pagliarini D. J., & Coon, J. J. (2016). Mitochondrial protein functions elucidated by multi-omic mass spectrometry profiling. Nature biotechnology, 34(11), 1191-1197 . doi: 10.1038/nbt.3683

Surayot, U., Wang, J., Seesuriyachan, P., Kuntiya, A., Tabarsa, M., Lee, Y., Kim, J., Park, W., & You, S. (2014). Exopolysaccharides from lactic acid bacteria: structural analysis, molecular weight effect on

immunomodulation. International journal of biological macromolecules, 68, 233-240 . doi: 10.1016/j.ijbiomac.2014.05.005

Takeichi, M. (2014). Dynamic contacts: rearranging adherens junctions to drive epithelial remodelling. Nature reviews Molecular cell biology, 15(6), 397-410 . doi: 10.1038/nrm3802

Tang, L., Wang, W., Zhou, W., Cheng, K., Yang, Y., Liu, M., Cheng, K., & Wang, W. (2015). Three-pathway combination for glutathione biosynthesis in Saccharomyces cerevisiae. Microbial cell factories, 14, 1-12. doi: org/10.1186/s12934-015-0327-0

Taylor, J., King, R., ltmann, T. A., & Fiehn, O. (2002). Application of metabolomics to plant genotype discrimination using statistics and machine learning. BIOINFORMATICS-OXFORD-, 18, S241-S248 . doi: 10.1093/bioinformatics/18.suppl_2.S241

Tsukita, S., Tanaka, H., & Tamura, A. (2019). The claudins: from tight junctions to biological systems. Trends in biochemical sciences, 44(2), 141-152 . doi: 10.1016/j.tibs.2018.09.008

Tsutsui, H., & Nakanishi, K. (2012). Immunotherapeutic applications of IL-18. Immunotherapy, 4(12), 1883-1894 . doi: 10.2217/imt.12.137

Van Deventer, S. J. H. (1997). Chemokine production by intestinal epithelial cells: a therapeutic target in inflammatory bowel disease?. Alimentary pharmacology & therapeutics, 11, 116-121 . doi: 10.1111/j.1365-2036.1997.tb00816.x

Van Eekelen, J. A. M., Shammas, F. V., Wee, L., Heikkilä, R., & Osland, A. (2000). Quantitative analysis of cytokeratin 20 gene expression using RT-PCR and capillary electrophoresis with fluorescent DNA detection. Clinical Biochemistry, 33(6), 457-464 . doi: 10.1016/S0009-9120(00)00155-7

Vancamelbeke, M., & Vermeire, S. (2017). The intestinal barrier: a fundamental role in health and disease. Expert review of gastroenterology & hepatology, 11(9), 821-834. doi: 10.1080/17474124.2017.1343143.

Vaz, F. M., & Ferdinandusse, S. (2017). Bile acid analysis in human disorders of bile acid biosynthesis. Molecular aspects of medicine, 56, 10-24. doi: 10.1016/j.mam.2017.03.003.

Velge, P., Bottreau, E., Quéré, P., Pardon, P., Nicolle, J. C., Morisson, M., Bout, D., & Dimier, I. (2002). Establishment and characterization of partially differentiated chicken enterocyte cell clones. European journal of cell biology, 81(4), 203-212 . doi: 10.1078/0171-9335-00237

Walker, M. C., & van der Donk, W. A. (2016). The many roles of glutamate in metabolism. Journal of Industrial Microbiology and Biotechnology, 43(2-3), 419-430. doi: 10.1007/s10295-015-1665-y.

Wang, H., Zhang, W., Zuo, L., Zhu, W., Wang, B., Li, Q., & Li, J. (2013). *Bifidobacteria* may be beneficial to intestinal microbiota and reduction of bacterial translocation in mice following ischaemia and reperfusion injury. British journal of nutrition, 109(11), 1990-1998 . doi: 10.1017/S0007114512004308

Wang, L., Mohanasundaram, P., Lindström, M., Asghar, M. N., Sultana, G., Misiorek, J. O., Jiu, Y., Chen, H., Chen, Z., Toivola, D. M., Cheng, F., & Eriksson, J. E. (2022). Vimentin suppresses inflammation and tumorigenesis in the mouse intestine. Frontiers in Cell and Developmental Biology, 10, 862237. doi: 10.3389/fcell.2022.862237

Wang, M., Zhang, X., Wang, Y., Li, Y., Chen, Y., Zheng, H., Ma, F., Ma, C. W., Lu, B., Xie, Z., & Liao, Q. (2018). Metabonomic strategy for the detection of metabolic effects of probiotics combined with prebiotic supplementation in weaned rats. RSC advances, 8(9), 5042-5057. doi: 10.1039/C7RA12067B

Wang, Y., Srinivasan, K., Siddiqui, M. R., George, S. P., Tomar, A., & Khurana, S. (2008). A novel role for villin in intestinal epithelial cell survival and homeostasis. Journal of biological chemistry, 283(14), 9454-9464 . doi: 10.1074/jbc.M707962200

Wang, Z.H., Zeng, X., Huang, W., Yang, Y., Zhang, S., Yang, M., Liu, H., Zhao, F., Li, A., Zhang, Z. & Shi, J. (2025). Bioactive nanomotor enabling efficient intestinal barrier penetration for colorectal cancer therapy. Nature Communications, 16(1), 1-19. doi: 10.1038/s41467-025-57045-9

Wolanin, P. M., Thomason, P. A., & Stock, J. B. (2002). Histidine protein kinases: key signal transducers outside the animal kingdom. doi: 10.1186/gb-2002-3-10-reviews3013

Wu, G., Fang, Y. Z., Yang, S., Lupton, J.R., & Turner, N.D. (2004). Glutathione metabolism and its implications for health. The Journal of nutrition, 134(3), 489-492. doi: 10.1093/jn/134.3.489.

Wu, M., Zuo, S., Maiorano, G., Kosobucki, P., & Stadnicka, K. (2022). How to employ metabolomic analysis to research on functions of prebiotics and probiotics in poultry gut health?. Frontiers in Microbiology, 13, 1040434. doi: 10.3389/fmicb.2022.1040434

Xie, L., Xu, C., Fan, Y., Li, Y., Wang, Y., Zhang, X., Yu, S., Wang, J., Chai, R., Zhao, Z., Jin, Y., Xu, Z., Zhao, S., & Bian, Y. (2021). Effect of fecal microbiota transplantation in patients with slow transit constipation and the relative mechanisms based on the protein digestion and absorption pathway. Journal of Translational Medicine, 19, 1-17 . doi: 10.1186/s12967-021-03152-2

Xie, S. Z., Shang, Z. Z., Li, Q. M., Zha, X. Q., Pan, L. H., & Luo, J. P. (2019). Dendrobium huoshanense polysaccharide regulates intestinal lamina propria immune response by stimulation of intestinal epithelial cells via toll-like receptor 4. Carbohydrate polymers, 222, 115028 . doi: 10.1016/j.carbpol.2019.115028

Xu, Y., Zhu, M., Feng, Y., & Xu, H. (2023). Panax notoginseng-microbiota interactions: from plant cultivation to medicinal application. Phytomedicine, 154978 . doi: 10.1016/j.phymed.2023.154978

Liu, Y., Shen, N., Xin, H., Yu, L., Xu, Q., & Cui, Y. (2023). Unsaturated fatty acids in natural edible resources, a systematic review of classification, resources, biosynthesis, biological activities and application. Food Bioscience, 53, 102790. doi: org/10.1016/j.fbio.2023.102790.

Zagato, E., Mileti, E., Massimiliano, L., Fasano, F., Budelli, A., Penna, G., & Rescigno, M. (2014). *Lactobacillus paracasei* CBA L74 metabolic products and fermented milk for infant formula have anti-inflammatory activity on dendritic cells *in vitro* and protective effects against colitis and an enteric pathogen *in vivo*. PloS one, 9(2), e87615. doi: 10.1371/journal.pone.0087615

Zastre, J. A., Sweet, R. L., Hanberry, B. S., & Ye, S. (2013). Linking vitamin B1 with cancer cell metabolism. Cancer & metabolism, 1, 1-14. doi: 10.1186/2049-3002-1-16

Zhang, D., Hua, Z., & Li, Z. (2024). The role of glutamate and glutamine metabolism and related transporters in nerve cells. CNS neuroscience & therapeutics, 30(2), e14617. doi: 10.1111/cns.14617.

Zhang, G., Wang, H., Zhang, J., Tang, X., Raheem, A., Wang, M., Lin, W., Liang, L., Qi, Y., Zhu, Y., Jia, Y., Cui, S., & Qin, T. (2021). Modulatory effects of *Bacillus subtilis* on the performance, morphology, cecal microbiota and gut barrier function of laying hens. Animals, 11(6), 1523. doi: org/10.3390/ani11061523

Zhang, H., Chen, F., Liang, Z. H., Wu, Y., & Pi, J. S. (2019). Isolation, culture, and identification of duck intestinal epithelial cells and oxidative stress model constructed. *In Vitro* Cellular & Developmental Biology-Animal, 55, 733-740. doi: 10.1007/s11626-019-00388-7

Zhang, Q., Eicher, S. D., Ajuwon, K. M., & Applegate, T. J. (2017). Development of a chicken ileal explant culture model for measurement of gut inflammation induced by lipopolysaccharide. Poultry science, 96(9), 3096-3103 . doi: 10.3382/ps/pex160

Zhang, X., Akhtar, M., Chen, Y., Ma, Z., Liang, Y., Shi, D., Cheng, R., Cui, L., Hu, Y., Nafady, A. A., Ansari, A. R., Abdel-Kafy, E. M., & Liu, H. (2022). Chicken jejunal microbiota improves growth performance by mitigating intestinal inflammation. Microbiome, 10(1), 107 . doi: 10.1186/s40168-022-01299-8

Zhong, L., Zhang, X., & Covasa, M. (2014). Emerging roles of lactic acid bacteria in protection against colorectal cancer. World J. Gastroenterol. 20, 7878–7886. doi: 10.3748/wjg.v20.i24.7878

Zhou, B., Yuan, Y., Zhang, S., Guo, C., Li, X., Li, G., & Zeng, Z. (2020). Intestinal flora and disease mutually shape the regional immunity in the intestinal tract. Frontiers in immunology, 11, 575. doi: 10.3389/fimmu.2020.00575

Zhou, Q., Toivola, D. M., Feng, N., Greenberg, H. B., Franke, W. W., & Omary, M. B. (2003). Keratin 20 helps maintain intermediate filament organization in intestinal epithelia. Molecular biology of the cell, 14(7), 2959-2971 . doi: 10.1091/mbc.e03-02-0059

Zhu La, A. L. T., Wen, Q., Xiao, Y., Hu, D., Liu, D., Guo, Y., & Hu, Y. (2024). A New *Bacillus velezensis* Strain CML532 Improves Chicken Growth Performance and Reduces Intestinal Clostridium perfringens Colonization. Microorganisms, 12(4), 771 . doi: 10.3390/microorganisms12040771

8. APPENDIX

8.1. List of Tables

8.2. List of Figures

8.3. List of Abbreviations

Abbreviation	Full Name
2CRS	Two-component regulatory system
2D	Two-dimensional
3D	Three-dimensional
AA	Amino acids
AJC	Apical junctional complex
AJs	Adherens junctions
APEC	Avian pathogenic *Escherichia coli*
ATP	Adenosine triphosphate
BEV	Bacterial extracellular vesicles
BT	Bacterial translocation
CFS	Cell-free supernatant
CHD1	E-cadherin
cIEC	Chicken intestinal epithelial cell cultures
CK18	Cytokeratin 18
CK20	Cytokeratin 20
CLDN	Claudin-1
CRC	Colorectal cancer
DES	Desmosomes
DMEM	Dulbecco's Modified Eagle Medium
DMPK	Desmoplakin
DMSO	Dimethyl sulfoxide
DPBS	Dulbecco's phosphate buffered saline

EPS	Extracellular polysaccharides
EV	Extracellular vesicles
FBS	Fetal bovine serum
FC	Fold Change
FIA-MS/MS	Flow injection analysis- tandem mass spectrometry
GALT	Gut-associated lymphoid tissue
GC-MS	Gas chromatography-mass spectrometry
GJ	Gap junctions
GSH	Glutathione
HS	Hydrogen sulfide
I/R	Ischemia and reperfusion
IBD	Inflammatory bowel disease
IEC	Intestinal epithelial cells
IFN-γ	Interferon γ
IL-18	Interleukin 18
JAM	Junctional adhesion molecule
LC- MS/MS	Liquid chromatography -tandem mass spectrometry
LDH	Lactate dehydrogenase
LPS	Lipopolysaccharides
MAPK	Mitogen-activated protein kinase
MEM	Minimum Essential Medium Eagle
MLCK	Myosin light chain kinase
NE	Necrotizing enteritis
NEC	Necrotizing enterocolitis

NO	Nitric oxide
OCCL	Occludin
OD	Optical density
OPLS-DA	Orthogonal partial least squares-discriminant analysis
PBS	Phosphate buffered saline
PCA	Principal Component Analysis
PEPT1	Peptide transporter 1
PES	Polyethersulfone
PGM	Porcine stomach type III
PKC	Protein kinase C
PUFA	Unsaturated fatty acids
RPT	Response permutation testing
SCFAs	Short-chain fatty acids
SERT	Serotonin transporter
T test	Student's t test
TCA	Tricarboxylic acid cycle
TICs	Total ion chromatograms
TJs	Tight junctions
TPP	Thiamine diphosphate
VILL	Villin
VIM	Vimentin
VIP	Variable important in projection
ZO	Zonula occludens
ZO-1	Zonula occludens-1